CHARACTERISATION OF M23-DOMAIN ACTIVATORS OF PEPTIDOGLYCAN DEGRADING AMIDASES IN *MYCOBACTERIUM TUBERCULOSIS*

A thesis submitted to the Faculty of Health Sciences, University of the Witwatersrand, Johannesburg, in fulfilment of the requirements for the degree of Doctor of Philosophy.

Andrea Olga Papadopoulos
Student. no. 0713551A
Supervisor: Bavesh Kana

Johannesburg, 2020

Declaration

I, Andrea Olga Papadopoulos, declare that this Thesis is my own, unaided work. It is being submitted for the Degree of Doctorate of Philosophy at the University of the Witwatersrand, Johannesburg. It has not been submitted before for any degree or examination at any other University.

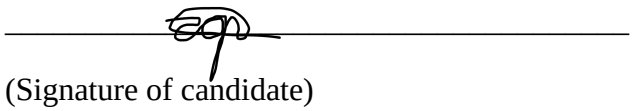

(Signature of candidate)

10th day of September 2020 in Johannesburg

“Since you are surrounded by such a great cloud of witnesses, run with perseverance the race marked out for you”

Hebrews 12:1

Dedication

To my Grandmother, Noreen Olga Pienaar (1934-2010), the first woman in her family to graduate and without whose tireless love and support I could not have reached this far.

Presentations arising from this research project

1. Papadopoulos, A.O and Kana, B.D. *In silico* Analysis of M23-Domain Activators of Peptidoglycan Degrading Amidases in *Mycobacterium tuberculosis*. Poster presentation, Molecular Biosciences Research Thrust Postgraduate Research Day, Wits University, Johannesburg. 3 December, 2015.
2. Papadopoulos, A.O and Kana, B.D. Characterisation Of M23-Domain Activators of Peptidoglycan Degrading Amidases in *Mycobacterium tuberculosis*. Poster presentation, 7th Cross-faculty Postgraduate Symposium, Wits University, Johannesburg. 1-2 March 2016.
3. Papadopoulos, A.O and Kana, B.D. A Novel Family Of Proteins in *Mycobacterium tuberculosis* With Putative, Differential Roles in Bacterial Cell Wall Degradation. Poster presentation, Faculty of Health Sciences Biennial Research Day, Wits University, Johannesburg. 1 September 2016.
4. Papadopoulos, A.O and Kana B.D. Breaking Down Walls! How Do Mycobacteria Remodel Their Cell Surface? Oral presentation, Molecular Biosciences Research Thrust, Wits University, Johannesburg. **2nd Prize for PhD/Post-doc category**. 8 December 2016.
5. Papadopoulos, A.O and Kana B.D. The Ins And Outs of Mycobacterial Lytm Endopeptidases. Seminar presentation, Molecular Medicine and Haematology Wednesday Seminar, Faculty of Health Sciences, Wits University, Johannesburg. 6 September 2017.
6. Papadopoulos, A.O and Kana B.D. LytM Endopeptidases Contrast Cell Division Regulation Between Slow-Growing *M. tuberculosis* and Rapidly-growing Model Organisms. Poster presentation, Molecular Biosciences Research Thrust Postgraduate Research Day, Wits University, Johannesburg. 30 November, 2017.
7. Papadopoulos, A.O and Kana B.D. A Novel Metallo-Endopeptidase Required for Peptidoglycan Remodelling During Osmolarity Changes in *M. tuberculosis*. National Oral presentation. South African Society for Biochemistry and Molecular Biology, North West University, Potchefstroom Campus, Potchefstroom. 9 July 2018.
8. Papadopoulos, A.O and Kana B.D. A Novel Metallo-Endopeptidase Required for Peptidoglycan Remodelling During Osmolarity Changes in *M. tuberculosis*. Oral presentation, Faculty of Health Sciences Biennial Research day, Wits University, Johannesburg. 6 September 2018.

9. Papadopoulos, A.O and Kana, B.D. A Putative M23-Domain Containing Endopeptidase is Required for Maintenance of Cell Length in *M. tuberculosis*. International Poster presentation, 2nd Bacterial Morphogenesis, Survival and Virulence congress, Cape Town. 24-28 November 2019.

Abstract

Mycobacterium tuberculosis, the causative agent of Tuberculosis (TB), continues to claim a substantial number of human lives globally, a situation that has continued for centuries. South Africa is one of the designated high burdened countries where the high number of people with HIV are most vulnerable to TB infection and disease. Although TB is curable with 6 months of chemotherapy, this outcome can be thwarted by the emergence of drug resistance. Multiple and extensive drug resistant TB are harder to treat, take longer to cure using drugs associated with severe side-effects. New, faster-curing drugs are urgently needed against targets in *M. tuberculosis* that are not targeted by current drugs. The broader objective of this research was to explore the peptidoglycan core of the *M. tuberculosis* cell wall for novel drug targets. Since mycobacterial growth depends on the synthesis, degradation and maintenance of the cell wall, enzymes involved in these processes are promising drug targets. Various enzymes required for remodelling of the cell wall, at the stem-peptide of the peptidoglycan core, have been shown to be necessary for mycobacterial growth, division and virulence. Peptidoglycan M23 endopeptidases are necessary for growth and virulence in numerous bacteria but have not been identified in *M. tuberculosis*. This research focused on identifying M23 endopeptidase-encoding genes in *M. tuberculosis* and to characterise a potential role for these genes in *M. tuberculosis* growth. Three putative endopeptidase domain containing genes, encoded at Rv0950c, Rv2891 and Rv3786c were identified. Rv0950c is the most conserved among the three homologues, with a predicted, hydrolytic active-site and was therefore the focus of further study. A deletion mutant strain of *M. tuberculosis* lacking Rv0950c was generated and studied. Loss of Rv0950c caused cell shortening and modulated incorporation of mono-peptide and di-peptide fluorescent peptidoglycan probes at the side-wall of cells during axenic growth and following cell wall damage. These phenotypes were reversed upon genetic complementation and suggest a role for Rv0950c in cell length maintenance and peptidoglycan stem-peptide formation, likely for maturation of peptidoglycan at the *M. tuberculosis* side wall. Transcriptomic analyses further demonstrated that Rv0950c is expressed at exponential growth under axenic conditions, and further upregulated under nutrient-limited stress. A Rv2891 deletion mutant strain was also generated and studied. The loss of Rv2891 did not alter cell morphology but patterns of fluorescent mono-peptide and Vancomycin labelling point to a role for Rv2891 in nascent, 4-3 cross-link remodelling, which needs to be confirmed by genetic complementation. The work

therefore presents foundational characterisation of novel M23 endopeptidases in *M. tuberculosis*.

Acknowledgements

My supervisor, Prof. Bavesh Kana. It is an honour and privilege to be at the receiving end of your excellent supervision and mentorship through this steep learning curve. Thank-you also for encouraging and permitting time outside the lab to be part of various TB awareness activities. The humanitarian attitude with which you approach TB research is exemplary.

The staff and students at the CBTBR. Thank-you for all your support, assistance, encouragement, check-ups, cheerleading and all that you do beyond your own research to keep the lab going. You are all admirably brave, persevering individuals. A special thank-you to Dr. Bhavna Gordhan and Dr. Chris Ealand (among many other responsibilities) for overseeing the maintenance and safety of the BSL3 facilities. Without your hard-work this research could not be possible. Thank-you Astika, for the patience, friendliness and sensitivity with which you juggle the immense responsibilities of an administrator.

The South African Medical Research Council, Research and Development Unit, for personal funding under the National Health Scholars Programme. Thank-you for vital living support and highly insightful training via numerous workshops and exquisite conferencing. A special thank-you to Dr. Thabi Maitin for the passion and enthusiasm that you have poured into your role.

The Faculty of Health Sciences Research Office, for research funding under the Medical Research Endowment grant: 001.283.8468202.5121105.5151

The National Research Foundation and Howard Hughes Medical Institute for research funding provided to the CBTBR.

To the following researchers for contributing materials:

Dr. Sloan Siegrist, University of Massachusetts, Amherst for the gift of alk DADA.

Prof. Tom Bernhardt, Department of Microbiology and Immunobiology, Harvard Medical School, for the gift of the *E. coli* Δ*envC*,Δ*nlpD* strain.

Prof. Joel Glasgow, Department of Microbiology, University of Alabama at Birmingham for the gift of pUAB400.

Dr. Gavin Owen, HIV Pathogenesis Research Unit, Department of Molecular Medicine and Haematology, Wits University, for the gift of *E. coli* BL21Star.

Prof. Michael VanNieuwenhze, Department of Chemistry, Indiana University Bloomington, for the gift of TADA.

To my pillars of strength, my close friends: Ezio Fok, my designated wingman, photography guru, incredible friend, ingenious molecular biologist. Nobantu Modise, thank-you for being an incredible prayer partner, for your honesty and wise perspective, your own work-ethic and perseverance has inspired me to stay focused in this PhD. Hazel Bomba, thanks for over 10 years of loyally staying in touch, always being there with godly wisdom and your awesome sense of humour. Dr. Flavia Zita, thanks for journeying with me, your faith is inspirational and contagious; thanks for being a safe-space (usually involving coffee and cake). Dr. Brenda Milner, thanks for endless laughs and your example of strength and courage in the way you finished your PhD. The "snowman", I've been really blessed by your care, understanding and positivity in these last stages of writing up.

Claire, Adam, Neli, Fulufelo, Sarah Katherine, Pumz, Zah, Stacey and others who have stood by me. My Rivers connect group: thank-you Cherie, Shenalle, and my prayer partner Seanene, for your incredible leadership. My LBC cell group, Byron, Zah, the Morris', aunt Mercy, aunt Susie, uncle Mel, Justice and Zama. If you see Dr. uncle Edo, please tell him I said thank-you for continued mentorship, support and prayers. My amazing running family in The Pack and Run-tell-that: Zonke, Hlasi, and all of you who consistently show up.

Uncle Hans, Corné, Mia, Clara and James. I really could not have reached this milestone without all you have practically shared with me, from as early as I can remember to this day.

Auntie Di, thank-you for your love and kindness, for your constant open door and warm heart.

To Nic, thank-you for being the best brother in the world, for supplying memes and for helping me out so much.

Mom, thank-you for persevering with me, for always being there, for all you still do for me, for always modelling a big and generous heart. Thank-you for brilliant proof-reading.

My late Gran, Noreen Olga, thank-you for everything. I wish you could have seen what became of all you did for me, and your unwavering belief in me.

Lastly, our angel scientist, Thandiwe Peace Msibi (1987-2016), “it’s been a long day without you my friend, I’ll tell you all about it when I see you again.” (Wiz Khalifa and Charlie Puth).

Table of contents

List of Figures

List of tables

Nomenclature

2XTY: 2x Tryptone-Yeast
Ag85: Antigen 85
alk DADA: alkyne D-Alanine-D-Alanine dipeptide
ANOVA: Analysis of variance
ART: Anti-Retroviral Therapy
ATP: Adenosine triphosphate
BCG: Bacille Calmette Guerin
BLAST: Basic Local Alignment Search Tool
BODIPY: Boron dipyrromethane
bp: base pairs
BSA: Bovine Serum Albumin
C': C-terminus
cDNA: complementary DNA
CFU: colony forming unit
CTAB: Cetyl Trimethyl Ammonium Bromide
CTP: Cytidine triphosphate
CuACC: copper-catalysed azide alkyne cycloaddition
Dat: D amino transaminase
DCO: double cross over
dH_2O: distilled water
DIC: differential interference contrast
DIG: Digoxygenin
DMSO: Dimethyl sulphoxide
DNA: Deoxyribonucleic Acid
dNTPs: dinucleotide triphosphates
DR: Drug Resistant
DS: Drug susceptible
EDTA: Ethylene Diamine tetra acetic acid
EP: Enol pyruvate
EtBr: Ethidium Bromide
EtOH: Ethanol
FAD: Flavin Adenine Dinucleotide
FDAA: fluorescent D amino acid
gDNA: genomic DNA
GlcNac: *N*-acetyl glucosamine
HIV/AIDS: Human Immuno-deficiency virus/Acquired Immuno-deficiency syndrome
IGRA: Interferon γ Release Assay
INH: Isoniazid
IPTG: Isopropyl β- d-1-thiogalactopyranoside
LB: Luria Bertani
Ldt: L,D transpeptidase
LED: light emitting diode
mDAP: *meso* diaminopimelic acid
MDR: Multiple Drug Resistant
MGIT: Mycobacterial Growth Indicator Tube
MIC: minimum inhibitory concentration
min: minute
MPFC: Mycobacterial Protein Fragment Complementation
MurNac: *N*-acetyl muramic acid
N': N-terminus
NADH: Nicotinamide Adenine dinucleotide dehydrogenase
NTHI: Non-typable *Haemophilus influenzae*
OADC: Oleic acid Albumin Dextrose Catalase

OD: optical density
ORF: open reading frame
PAGE: poly-acrylamide gel electrophoresis
PBD: Pyrolbenzodiazepine
PBP: Penicillin Binding Protein
PBS: Phosphate buffered saline
PBSTB: PBS Tween BSA
PCR: Polymerase Chain Reaction
PEP: Phosphoenol pyruvate
PG: Peptidoglycan
PHMMER: Profile Hidden Markov Model
RNA: Ribonucleic Acid
Rpf: Resuscitation promoting factor
rpm: revolutions per minute
RR: Rate Ratio
R-R: Rif resistant including mono-resistant
RT qPCR: Reverse Transcription quantitative PCR
SCO: single cross over
sdH_2O: sterile/nuclease-free distilled water
SDS: Sodium Dodecyl Sulphate
SEM: scanning electron microscopy
TADA: tetramethylrhodamine-3-amino-d-alanine
TAE: Tris Acetic acid EDTA
TB: Tuberculosis
TBE: Tris Boric acid EDTA
temp.: temperature
TST: Tuberculin Skin Test
UDP: Uridine diphosphate
UTP: Uridine triphosphate
UV: ultraviolet
Van-FL: fluorescence conjugated Vancomycin
vol: volume
WHO: World Health Organization
WT: wild type
XDR: Extensively Drug Resistant
XGal: 5- bromo-4-chloro-3-indolyl-β-D-galactopyranoside

1 Introduction

1.1 The Tuberculosis epidemic

Tuberculosis (TB), primarily caused by infection with *Mycobacterium tuberculosis* has surpassed HIV/AIDS as the leading cause of death globally by an infectious disease (WHO, 2019) and is the leading cause of death in South Africa. Africa and South East Asia jointly account for ~80% of the global TB mortality (WHO, 2019). The TB epidemic is composed of three major TB components: drug-susceptible TB (DS), drug-resistant TB (DR-TB) and HIV-TB co-infection. In 2018, around 10 million people contracted TB (WHO, 2019) (Fig. 1.1). South Africa is among the 30 highest burden countries for all three of these categories (WHO, 2019). The overall incidence reported for South Africa in 2018 was 301 000 (Fig. 1.1), representing one of eight countries constituting two-thirds of the global incidence (WHO, 2019). The majority of South Africans with TB in 2018 were in the age group where they were most likely able to contribute to economic growth (WHO, 2019).

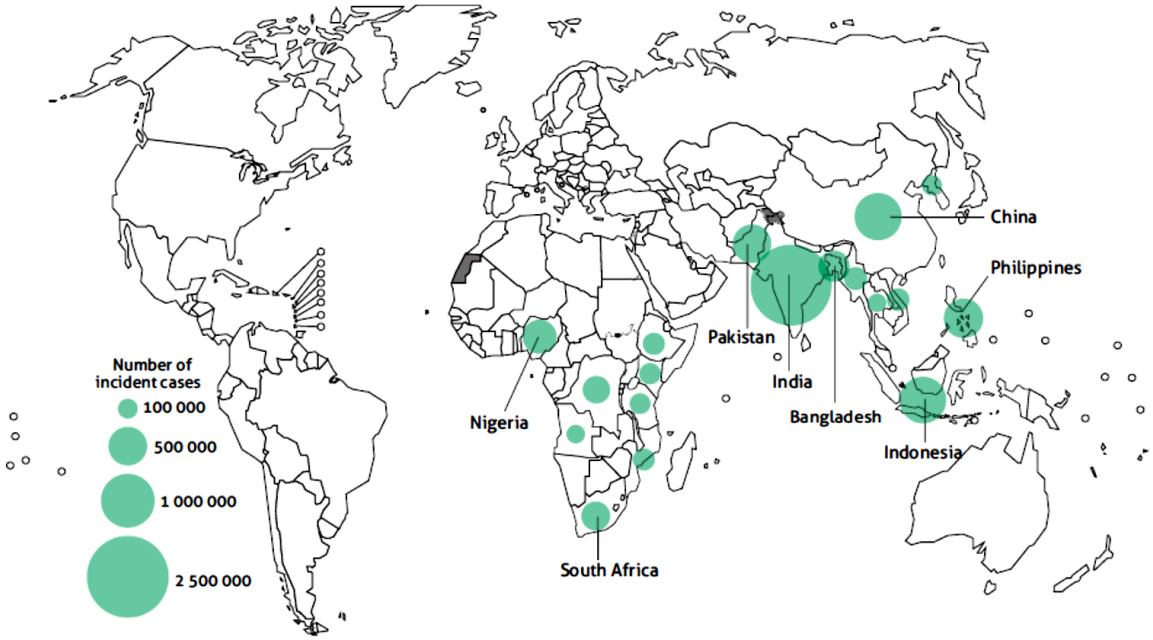

Figure 1.1 "Estimated TB incidence in 2018.
Highlighted countries have at least 100 000 incident cases. (WHO, 2019).

Although the rate of decline in TB incidence is increasing year-on-year, it is still too slow to achieve the End TB goal of eliminating TB by 2030 (WHO, 2019). New and relapse cases steadily accounted for ~ half the TB incidence in South Africa over the period of 2000 to 2018 (WHO, 2019). Multifaceted strategies need to be accelerated, including basic research, to rapidly expand options for treating and curing TB in difficult-to-cure population groups. Compared to mortality in untreated individuals with TB, treatment

alone was associated with preventing 48 million deaths between 2000 and 2018 (WHO, 2019).

1.2 Drivers of the TB epidemic: Drug resistance, HIV and diagnostic challenges

The End TB Strategy is a commitment by WHO members to reduce global TB mortality and incidence by 90% and 80% respectively by 2030 (WHO, 2019). Reaching these goals will rely on improving treatment coverage, ensuring better treatment success as well as providing appropriate therapeutic options for TB-HIV co-infection (WHO, 2019). New treatments for DRTB and limiting the emergence of further resistance are also important goals.

1.2.1 Drug resistance

In 2018, ~500 000 new cases of Rifampicin-resistant (R-R) cases were reported, of which 78% had multi drug resistance (MDR) (WHO, 2019). Concurrently, 214 000 individuals succumbed to R-R or MDR TB (WHO, 2019). While drug resistance can occur in treatment-naive patients, it is more prevalent in those previously treated for TB (Lukoye et al., 2015). Furthermore, a study of transmission among household contacts revealed that contacts were at increased risk for infection when exposed to INH-mono-resistant TB or MDR TB compared to exposure to drug-susceptible TB (Becerra et al., 2019). These data suggest that in certain settings, DRTB may be more transmissible.

According to the WHO Tuberculosis report for 2019, only half of global MDR cases achieve a successful treatment outcome (WHO, 2019). A meta-analysis of data pertaining to approx. 12000 adult MDR patients spanning 2009 to 2016 revealed a treatment success rate of 65%, a mortality rate of 11% and treatment failure rate of 6% (Ahmad et al., 2018). The outcome of MDR TB in children was observably better, for which 78% were successfully treated, but the mortality rate was approximately the same as the adults (Harausz et al., 2018). In both populations, the numbers of MDR patients not experiencing a successful outcome were attributed to death or loss-to-follow up (Ahmad et al., 2018; Harausz et al., 2018). Among the MDR patients, 10% were further identified as extensively drug resistant, for which only half could be cured by MDR treatment, while 16% succumbed during treatment (Ahmad et al., 2018).

Only 55% of South Africans who were initiated on treatment for MDR and Rifampin mono-resistant (R-R) TB in 2015 were reported to achieve treatment success (WHO, 2018). Resistance to pyrazinamide or the fluoroquinolone - Levofloxacin was more common in Rif-resistant South Africans, when compared to those who were Rif-susceptible (WHO, 2019).

When second-line MDR treatment fails, the outcomes are worse as there are far fewer drugs available to treat extensively drug resistant (XDR) TB. Treatment success is 39% for global XDR TB patients (WHO, 2019). MDR patients who develop resistance to ethionamide, pyrazinamide or ethambutol are more likely to relapse or succumb after short-term treatment for 6-9 months (Abidi et al., 2019). Although a 20-month treatment regimen improves the outcome of these patients, such long-term regimens are harder to complete and associated with a greater rate of non-compliance (Abidi et al., 2019). Adverse drug reactions were reported for 56% of a XDR TB cohort based in South Africa, of which 34% required modifications to the drug regimen to circumvent the adverse reactions (Shean et al., 2013). In a Johannesburg-based cohort, only 21% of the XDR-TB patients had a successful outcome, either cure or treatment completion, whereas 26% of patients succumbed (Nkurunziza et al., 2018). Pre-XDR TB patients, defined as MDR TB with additional resistance to the fluoroquinolones, had almost identical outcomes as the aforementioned XDR-TB patients (Nkurunziza et al., 2018). In a XDR TB South African retrospective cohort study, only 22% experienced culture conversion to negative while 26% of these patients succumbed (Shean et al., 2013). Treatment failure or default was reported in 36% of a Johannesburg XDR TB cohort (Nkurunziza et al., 2018). Another retrospective study of XDR TB patients treated in Cape Town, Kimberley, Port Elizabeth and Johannesburg (all in South Africa) reported a mortality rate of 36% and sputum conversion of only 19% (Dheda et al., 2010). A long-term prospective study, following XDR TB patients in the Western Cape, Northern Cape and Gauteng regions in South Africa for more than 60 months after treatment initiation, reported even poorer outcomes: 73% of the patients succumbed, only 5% were reported to be cured and 10% who reported treatment failure were released back into the community (Pietersen et al., 2014). Collectively, these poor treatment outcomes suggest that TB treatment programmes are losing the battle with DR TB, creating an urgent need for new TB drugs that can shorten treatment duration, with limited side-effects.

The inability to treat and cure XDR TB also drives transmission, as patients who cannot be treated are released from care (Pietersen et al., 2014). In Kwa-Zulu Natal (KZN – South Africa) alone, over 1000 individuals were diagnosed with XDR TB in the space of three years (2011-2014) (Auld et al., 2018; Peterson et al., 2019). An average of seven close contacts per individual was estimated for each of the 1000 infected individuals (Auld et al., 2018). A large proportion of the KZN cohort were based in urban and sub-urban parts of Durban (Peterson et al., 2019). A small proportion (15%) of these patients were linked epidemiologically, mainly by close contact or through hospitalisation but 60% of the patients for whom the route of transmission was vague had genotypically-related isolates of XDR TB that differed by only five or less SNPs (Auld et al., 2018), suggesting high transmissibility of this deadly form of TB. A mathematical model, incorporating TB and HIV transmission and treatment outcome, activation of latent TB, adverse reactions to drugs and population growth, predicted increases in MDR and XDR TB incidence in South Africa and other high-burden countries by 2040 (Sharma et al., 2017). Urgent interventions are required to subvert this.

1.2.2 The HIV epidemic

The risk for contracting TB is 19 times higher in the HIV positive population than HIV negative individuals, with an associated treatment success rate that is only 10% lower (WHO, 2019). As a result, HIV infection is currently the strongest risk factor for contracting TB in Southern Africa, compared to other risk factors which stand out in other countries such as smoking and alcohol-use (WHO, 2019). South Africa contributed the highest proportion of HIV-TB coinfected individuals of the global estimate for 2018 (WHO, 2019). Only 8.6% of the global TB burden is HIV positive, just over half of this burden is carried by South Africa (WHO, 2019). HIV infection was the greatest risk factor for mortality in adult MDR TB patients (Ahmad et al., 2018). In a cohort based in the Free-State province of South Africa, HIV-infected individuals were at higher risk for mortality than their HIV-negative counterparts (Heunis et al., 2017).

With the increase in ART roll-out in South Africa, the high rate of TB mortality in the HIV-positive population is on the decline (WHO, 2018a). Treating MDR-TB infected children with ARTs significantly improved TB outcome when compared to children who were not on ART (Harausz et al., 2018). In a mouse model of TB infection and disease,

immunodeficient mice were more susceptible to TB treatment failure and the development of drug resistance (Park et al., 2017). A fully constituted immune system functions synergistically with TB treatment to clear the bacterial infection. ART appears to little effect the outcomes in XDR-TB – HIV co-infected patients. Most of the patients of a XDR and pre-XDR cohort (65%) were HIV-infected of which 95% were on ART, yet treatment was only successful in under 30% of these patients (Nkurunziza et al., 2018). In a long-term prospective study, wherein 74% of the XDR-TB patients succumbed, 41% were HIV positive of which 80% were on ART (Pietersen et al., 2014). The incidence of TB mortality among HIV-negative individuals remains consistent at around fifty per hundred thousand every year since 2010 (WHO, 2018). Expanding the current set of TB treatment options, by developing new drugs, is important for improving the prognosis of HIV as well as eradicating TB disease in the HIV negative population.

1.2.3 Diagnostic challenges

Detection of TB is the most important means to reduce TB mortality, when one considers the 85% treatment success rate for DS TB (WHO, 2019). There are multiple means of diagnosing TB including GeneXpert, sputum smear microscopy, chest X-rays, the Tuberculin Skin Test (TST) and the Interferon γ release assay (IGRA) (Davids et al., 2015). Apart from GeneXpert and TST, the other tests require sophisticated infrastructure, which is usually not available at Primary healthcare sites (Davids et al., 2015). This means that samples such as sputum, blood or urine are sent to centralised facilities, increasing the turn-around-time for test results (Davids et al., 2015). With regards to culture-based TB diagnostics, these delays are exacerbated due to the slow-growing nature of *M. tuberculosis*. The BACTEC MGIT test is considered negative if no growth is observed after 42 days, although rarely, growth has been observed thereafter (Mahomed et al., 2017). Modified IGRA tests known as TSPOT and TSPOT.TB are able to detect TB in smear-negative culture (Li et al., 2017), emphasising how a successful TB diagnosis requires multiple tests, increasing the cost and resource burden of diagnosing TB. Another challenge to diagnosing TB is the difficulty in obtaining good quality sputum for testing (Davids et al. 2015). Although the GeneXpert can rapidly diagnose Rif-resistant *M. tuberculosis*, other susceptibility tests rely on culture, which delays treatment of DR TB. Even with the technology for rapid testing for Rif-resistance, this was only performed in 51% of TB cases around the world, among whom most were previously treated (WHO,

2019). This suggests that it is easier to monitor patients once they have been initially identified, and that the diagnostic gap lies in detecting new cases of TB. Additional rapid testing for resistance to other first line drugs is needed as INH resistance was observed in Rif-susceptible individuals at an average rate of 18% per year (WHO, 2019).

1.3 Critical gaps for epidemic control

1.3.1 Treatment shortening

Treatment of DS and DR TB is hampered by the difficulty in adhering to a long treatment period: on average six months for DS TB and 20 months for MDR. A shorter regimen will be easier for National TB programme to implement and will also be more acceptable to patients. However, simply shortening the existing Rif-INH-Ethambutol-Pyrizinamide regimen from six-months to four months was associated with a significantly greater risk of relapse (Johnson et al., 2009; Ammerman et al., 2018). Instead, current experimental four-month regimens differ to the standard six-month DST treatment by replacing one of the four first-line drugs with alternatives such as Moxifloxacin and Gatafloxicin, or replacing Rifampicin with Rifapentine for example. In a clinical trial including South African patients, a three-drug regimen consisting of Moxifloxacin, Pretomanid and Pyrazinamide showed significantly higher bactericidal activity and rate of culture conversion after just 8 weeks of treatment compared to standard first-line therapy for the same duration (Dawson et al., 2015). A pooled analysis of DST patients comparing four-month experimental regimens containing a fluoroquinolone to standard, first-line six month treatment revealed a 23% rate of unfavourable outcome for the four month regimen compared to only 16% for the six month regimen (Imperial et al., 2018). In a systematic review, four-month experimental regimens were associated with a higher rate of relapse than the standard six-month regimens, but in other respects (death, treatment failure, development of drug resistance), the four month regimens performed just as well (Grace et al., 2019). Not all patients require six months of treatment, but a large number of patients cannot be treated effectively after four months. A careful set of selection criteria must be determined for selecting patients for four-month treatment. In particular, DS TB patients diagnosed with higher smear grade and/or HIV-infection or those who were observably less likely to experience favourable outcomes from a four-month regimen compared to patients with low smear grade and/or HIV-negative (Imperial et al., 2018). Adherence is a very important

factor in the four-month regimens as missing only one or two doses per week significantly increased risk for treatment failure (Imperial et al., 2018).

An MDR regimen consisting of six or more drugs showed a similar likelihood of sputum conversion (from culture positive to culture negative) at 18 and 24 months after treatment initiation (Yuen et al., 2015) A current, standardised treatment shortening regimen, on average for 12 months as opposed to 20 months produced excellent outcomes in MDR patients susceptible to fluoroquinolones (Ahmad Khan et al., 2017). Treatment shortening however significantly worsened the outcome of fluoroquinolone-resistant MDR patients (Ahmad Khan et al., 2017; Abidi et al., 2019).

These data suggest that treatment shortening using currently available drugs is feasible for improved TB control for certain patients and is centred around substituting the standard Rif-Ethambutol-INH-Pyrizinamide regimen with different drugs. However, expanding the spectrum of drugs available for TB treatment can create more opportunities for shorter treatment which is optimised for all types of patients.

1.3.2 New vaccines

There is currently only one approved vaccine available for the prevention of TB in exposed individuals, the BCG vaccine. BCG is an attenuated strain of *Mycobacterium bovis* Bacille Calmette Guerin which currently confers variable protection against *M. tuberculosis* infection (Fine, 1995). BCG can also protect against TB meningitis (Colditz et al., 1994). A meta-analysis of thirteen previous trials testing, the effect of BCG administration on protection and TB mortality only reported 51% protection for prevention of pulmonary TB (Colditz et al., 1994). A more recent systematic review of 21 randomised trials, compared rate ratios (RR) of BCG once-vaccinated and non-vaccinated individuals with TB, which should be less than 1 for a highly efficacious vaccine (lower rate for vaccinated/higher rate for non-vaccinated) (Mangtani et al., 2014). The review revealed hypervariability in BCG efficacy ranging from highly efficacious (RR=0.22) to lowprotection (RR=1.3) across the 21 studies based all around the world (Mangtani et al., 2014). A recent trial suggests that revaccination of adolescent individuals vaccinated with BCG as infants enhances BCG immunogenicity (Nemes et al., 2018). The efficacy of revaccination with BCG was 48%, compared to ~30% for revaccination with a placebo

(Nemes et al., 2018). In the absence of an approved alternative vaccine, BCG is a necessity in high TB burden countries and also recommended in low burden regions (WHO, 2018b).

Fortunately, numerous vaccine candidates are undergoing various clinical trials. The most promising candidate is M72/AS01$_E$, which expresses recombinant *M. tuberculosis* antigens, 32a and 39a, and an AS01$_E$ adjuvant (Van Der Meeren et al., 2018; Tait et al., 2019). Preliminary results of a phase 2b clinical trial, involving 2 years of follow up of individuals with latent *M. tuberculosis* infection, reported 57% efficacy for M72/AS01$_E$ (Van Der Meeren et al., 2018). Accordingly, the number of cases reporting activation to pulmonary TB in the vaccinated group was almost half of those observed for the placebo control group (Van Der Meeren et al., 2018). M72/AS01$_E$ is efficiently immunogenic, for which antibodies were detected in 100% of those eligible to form part of the immunogenicity analyses 2 months after vaccination, and seropositivity was sustained for 12 months (Van Der Meeren et al., 2018). After 3 years of follow up, on completion of the phase 2b trial, the rate of TB incidence increased proportionally for each group, wherein the incidence in the vaccinated group was still half that of the control group, and the vaccine efficacy was 49% (Tait et al., 2019). Seropositivity was maintained after 36 months of vaccination in all of the immunogenicity participants, which translated into CD4 cell responses in 54% (Tait et al., 2019). The safety of M72/AS01$_E$ was excellent: the numbers of adverse events were negligible (1%) or not related to vaccination, encouraging further trials (Tait et al., 2019).

The MVA85A vaccine consists of immunogenic Modified Vacinia virus Ankara (MVA) expressing highly conserved, *M. tuberculosis* antigen 85 (85A). An MVA85A booster reduced TB pathology and bacterial burden in monkeys compared to those vaccinated with BCG alone (Verreck et al., 2009). In a Rhesus Macaque model, MVA85A was well tolerated and immunogenic by either intradermal injection or aerosol delivery (White et al., 2013). Aerosol delivery would be highly favourable against pulmonary TB, priming the site of primary infection. A study following individuals vaccinated with MVA85A for phase II clinical trials showed that MVA85A can elicit long-term persisting memory CD4 cells specific to Ag85, but unfortunately did not improve protection against TB infection above that of BCG (Tameris et al., 2014). In an attempt to enhance the MVA85A response, different homogenous boosting delivery methods were tested in a phase I trial: switching between intravenous and aerosol delivery of repeated MVA85A compared to repeated

intravenous boosts (Manjaly Thomas et al., 2019). Here, aerosol delivery of the first dose of MV85A (priming step) was well tolerated but aerosol delivery of boosters was not tolerated in the participants (Manjaly Thomas et al., 2019). Although well tolerated, intravenous boosting after aerosol priming did not result in actual immunogenic boost, thereby not improving the previously observed low efficacy of MV85A (Manjaly Thomas et al., 2019).

Another vaccine candidate, AERAS-402, consisting of an adenovirus expressing three *M. tuberculosis* antigens, was combined with MVA85A in a "prime-boost" strategy, wherein the AERAS-402 is hypothesised to prime the immune-system which is boosted with the MVA85A vaccine (Sheehan et al., 2015). AERAS-402 alone in a prior study produced little protection in a macaque model even though the cellular response was promising (Darrah et al., 2014). The prime-boost vaccine proved to be moderately tolerated in a phase I trial, with most of the reported adverse reactions fortunately clearing within 2-days (Sheehan et al., 2015). The trial compared three different boosting strategies over four months, each starting with AERAS-402 and either boosted with MVA85A followed by AERAS-402; boosted just with MVA85A; or boosted twice with AERAS-402 (Sheehan et al., 2015). Boosting with MVA85A was more immunogenic than in the group boosted with multiple doses of AERAS-402 alone, but the group in which MVA85A boosting was followed by an AERAS-402 boost was superior (Sheehan et al., 2015). A similar trend was observed for Ag85-specific, interferon γ (IFN γ) response, for which the best strategy seemed to be the boost of the initial AERAS-402 vaccination with MVA85A and additional AERAS-402 (Sheehan et al., 2015).

More recently, a heterologous prime-boost strategy has been tested in a mouse model with a novel Sendai virus vector expressing Ag85A (SeV85AB or Se' hereon) and B in combination with a recombinant DNA vaccine (Hu et al., 2019). The mice were either vaccinated with each individual vaccine alone or by prime-boost either starting with Se' and boosted with DNA or vice versa (Hu et al., 2019). As seen in the AERAS-402 trial (Sheehan et al., 2015), the heterologous prime-boost strategy outweighed once-off vaccination, but was dependent on the order of prime-boosting: first with Se' and boosted with DNA (Hu et al., 2019). The Se'-DNA strategy reduced bacterial load in mice subsequently exposed to TB, which was associated with a strong production of Ag85-specific IFNγ response (Hu et al., 2019). These preliminary outcomes highlight the

complexity and unpredictability of vaccine development, which could be assumed for other immune-based therapeutic strategies.

1.3.3 New drugs

Within the recent decade, three entirely novel drugs were approved for treatment of extensively drug resistant TB: Bedaquiline, Delamanid and Pretomanid. The use of Bedaquiline and Pretomanid alongside Pyrazinamide (B-Pa-Z) as an 8 week treatment regimen produced superior bacterial clearance in DS TB patients compared to those on standard, first-line RHEZ in a phase IIb clinical trial (Tweed et al., 2019). Similarly, the bactericidal activity of a B-Pa-Z regimen was stronger than standard first-line treatment (Diacon et al., 2015). In a study comparing MDR TB patients either treated with regimens of Delamanid or Bedaquiline, Bedaquiline performed better in terms of culture conversion and was associated with lower rates of further drug resistance development (Kempker et al., 2019). When MDR-TB patients from a Western-Cape cohort were treated with a regimen including both Bedaquiline and Delamanid, the outcome was fairly similar to regimens containing Bedaquiline and not Delamanid (Bed-based): a culture conversion rate after 6 months of treatment of 93.8% for both v.s 92.5% for Bed-based; and the rate of favourable outcomes was 67.5% for both compared to 63.4% for Bed-based (Olayanju et al., 2019). The incidence of adverse events was similarly high in either regimen: 92.5% for both compared to 89% for Bed-based (Olayanju et al., 2019). In a multicentre cohort of MDR-TB patients, Bedaquiline-Delamanid combination regimens led to 79% culture conversion, with 25% reported adverse reactions to treatment (Ferlazzo et al., 2018). A prior published systematic review of seven studies across the world also reported good efficacy of regimens including both drugs: culture conversion in 81% and a successful treatment outcome in 71.4% (Pontali et al., 2018).

When Delamanid (but not Bedaquiline) was added to a regimen for treating Rif-resistant patients in Khayalitsha (South Africa), the culture conversion rate after 12 months was only 45% for those still on treatment; a further 15% successfully completed treatment, while 31% experienced an unfavourable outcome (Mohr et al., 2018). In the same cohort, the incidence of adverse reactions to treatment was 86%, for whom an average of four adverse events were reported per patient (Hughes et al., 2019). MDR-TB patients of the EndTB observational cohort treated with a Delamanid-containing regiment exhibited

culture conversion in 80% after 6 months of treatment, while 4% experienced a confirmed unfavourable outcome (Seung et al., in press).

To prevent emergence of resistance to these new drugs, the WHO recommends addition of Bedaquiline or Delamanid only after three prior sub-groups of drug-resistant treatment regimens have been attempted (Falzon et al., 2017). Combining both Bedaquiline and Delamanid in a regimen is only recommended as a "salvage" treatment when alternative regimens are not expected to work in a specific patient. This approach is expected to avoid the opportunity for the emergence of strains resistant to both drugs. One such case has been reported in an XDR TB patient (Polsfuss et al., 2019). Although the increase in Delamanid MIC was small in this patient, it still translated into clinical resistance (Polsfuss et al., 2019).

1.4 Research aimed at developing new drugs

Recent technological advances have accelerated antitubercular drug development, since all 3 recently approved drugs were approved in the previous decade, roughly 30-40 years after other antitubercular drugs. The next possible candidate under clinical trial, Q203, targets *M. tuberculosis* respiration (Pethe et al., 2013). The flexibility of the mycobacterial electron respiratory chain allows the bacteria to continue to grow in the presence of Q203, by which electrons can still reach terminal oxidases (Lamprecht et al., 2016; Kalia et al., 2017). Whilst this approach is promising, other avenues need to be explored.

Targeting DNA and RNA biosynthetic processes inhibits replicating and non-replicating *M. tuberculosis* (Mori et al., 2015). A thiophene carboxyamide derivative, and the metabolite thereof, inhibit conversion of UTP to CTP by competing for the ATP-binding site of PyrG (Mori et al., 2015). Pyridin-thiazole derivatives inhibit PyrG in the same way, and in so doing revealed that disrupting CTP synthesis affects global processes in the *M. tuberculosis* cell (Esposito et al., 2017). Targeting nucleotide-dependent processes poses a risk for host drug tolerance and compliance to treatment, since there is conservation between enzyme targets in eukaryotes and prokaryotes. PyrG inhibitors can bind human CTP synthetases (Esposito et al., 2017). Pyrrolobenzodiazepines (PBDs) are naturally occurring, DNA-binding antibacterials produced by streptomyces which are being explored as anti-cancer therapeutics, due to the eukaryotic cytotoxicity of these molecules (Rahman et al., 2013). To avert this, a strategy was tested by conjugating a bulky

fluoroquinolone to a PBD to reduce binding to eukaryotic DNA (Picconi et al., 2019). Although PBDs alone were highly inhibitive of *M. tuberculosis*, conjugates were significantly less effective albeit significantly less cytotoxic than PBDs alone (Picconi et al., 2019), suggesting that drugs targeting DNA share similar mechanisms between Prokaryotes and Eukaryotes. Further, cytoplasmic drugs, such as Q203 are susceptible to export out of the cell via efflux systems (Jang et al., 2017). Targeting the prokaryote-specific mycobacterial cell wall is an attractive strategy due to the lack of homology of cell wall structures and biosynthetic enzymes with eukaryotes, the essentiality of the cell wall and the location of these targets away from efflux systems.

1.4.1 The structure of the mycobacterial cell wall and the peptidoglycan core

The cell wall of *M. tuberculosis* consists of a multi-layer, highly complex structure made up of a peptidoglycan (PG) core linked to Arabinogalactan, linked to a Mycolic acid layer. This heteropolymer is referred to as the MAPc complex (Fig. 1.2) (Bhamidi et al., 2011). The PG core is made up of a repeating disaccharide of *N*-acetyl glucosamine (GlcNac) and *N*-acetyl muramic acid (MurNac) or *N*-glycolyl muramic acid (MurNGlyc) linked to a stem-peptide beginning with L-Alanine, D-Glutamate, *meso* diaminopimelic acid and a terminal di D-Alanine (Fig. 1.2) (Lavollay et al., 2008; Mahapatra et al., 2008). PG is typically stabilised by cross-links between the 4th D-Alanine and 3rd *m*DAP (4-3) of the stem-peptide (Fig. 1.2). In addition, mycobacterial PG has a characteristically high proportion of 3-3 cross-linking that is especially high at stationary phase (Lavollay et al., 2008). Cross-bridges, consisting of glycine residues were also found to link PG between *m*DAP residues (Lavollay et al., 2008).

1.4.2 Current drugs that target the *M. tuberculosis* cell wall

There are several drugs that target the mycobacterial cell wall. The novel drugs, Delamanid and Pretomanid are hypothesised to inhibit mycolic acid synthesis (Bhat et al., 2017). Ethambutol inhibits synthesis of the arabinogalactan layer, but a recent study suggests that ethambutol also inhibits the PG synthesis enzyme, Glutamate racemase, MurI (Pawar et al., 2019). Isoniazid is known to inhibit mycolic acid synthesis and treatment of mycobacteria with both Ethambutol and INH weakens the cell and modulates how the cell wall is synthesised (Rodriguez-Rivera et al., 2018). Ethionamide inhibits mycolic acid synthesis and the Benzothiazinones interfere with Arabinogalactan synthesis (Bhat et al.,

2017). Cycloserine inhibits PG synthesis (Halouska et al., 2014). Carbapenems were shown to bind to the PG remodelling enzyme, L,D transpeptidase wherein the catalytic site interacts with the β-lactam ring of the drug (Cordillot et al., 2013).

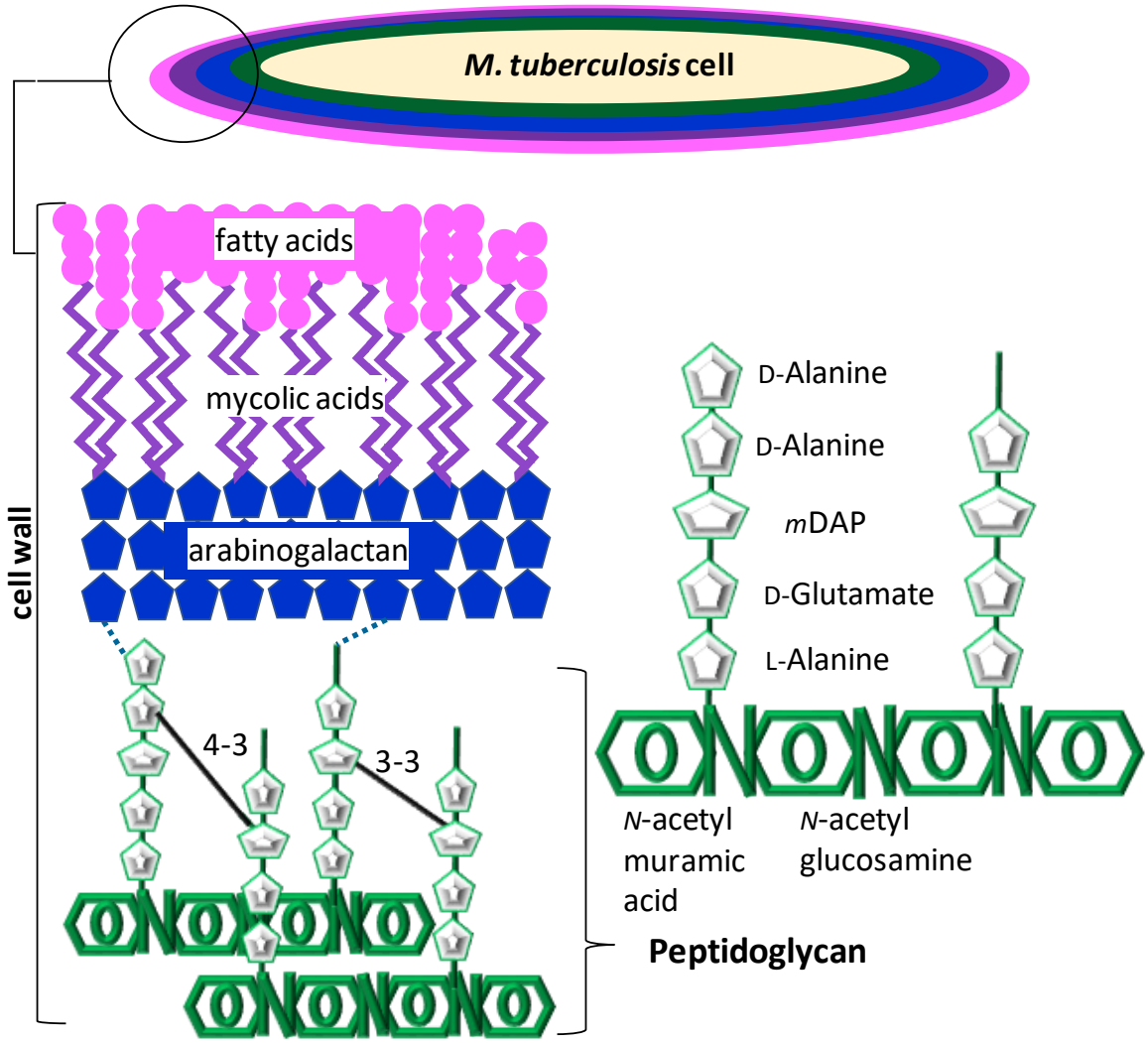

Figure 1.2 Components of the *M. tuberculosis* cell wall.
Outer layers consist of fatty and mycolic acids. The peptidoglycan (PG) core is covalently linked (blue, dashed lines) to the aribinogalactan layer. Stem-peptides of PG are cross-linked (black lines) between the 4th D-Alanine and the 3rd *m*DAP (4-3) or both *m*DAP (3-3).

1.4.3 Targeting PG synthesis

1.4.3.1 The PG biosynthetic pathway

The canonical pathway of PG biosynthesis begins with the generation of the *N*-acetyl muramic acid (MurNAc) precursors in the cytosol (Fig. 1.3). MurNAc results from MurA-catalysed transfer of enolpyruval onto uridine diphosphate (UDP) *N*-acetyl glucosamine (GlcNAc) (Fig. 1.3). MurA is essential for mycobacterial growth (Xu et al., 2014) and is expressed at all stages of growth (Gonzalez V Merchand, Colston & Cox, 1999). Conditional deletion of *M. smegmatis murA* produces a crumpled, irregular cell surface

and obscure cell wall structure, emphasising the role of UDP-MurNac in cell wall integrity (Xu et al., 2014). The protein consists of 2 active, globular domains: a transferase domain and a 3-phosphoshikimate-1-carboxyvinyltransferase (EPSP-synthase) domain (Babajan et al., 2011; Xu et al., 2014). MurA activity was confirmed in purified derivatives of *M. tuberculosis* and *M. smegmatis* by observing depletion of the catalytic substrates, phosphoenol pyruvate (PEP) and UDP-GlcNAc using HPLC (Xu et al., 2014). Further, *M. tuberculosis* and *M. smegmatis* MurA displayed differential affinity for substrates based on slower processivity than the corresponding enzyme from *E. coli* (Xu et al., 2014). The *M. tuberculosis* orthologue also performed slower than that of *M. smegmatis,* despite conservation across predicted catalytic residues including those occurring in *E. coli* MurA (Xu et al., 2014) this may be related to the comparable slow-growth of *M. tuberculosis*. Unlike *E. coli* MurA, which has a cysteine residue in position 117, essential for EP-UNAG product release, *M. tuberculosis murA* has an aspartate residue which confers resistance to the common MurA inhibitor, Fosfomycin (De Smet et al., 1999; Eschenburg, Priestman & Schönbrunn, 2005).

Following the activity of MurA, MurB catalyses the NADPH-dependent conversion of enolpyruval UDP-GlcNAc to UDP-MurNAc (Fig. 1.3). MurB catalyses the 2-step reduction of enolpyruval UDP-GlcNAc, the first step involving electron transfer between NADH and FAD (Benson et al., 1993). The *M. tuberculosis* orthologue is a type I MurB consisting of 3 domains, all of which associate with the cofactor FAD (Kumar et al., 2011). Formation of hydrogen-bonds between FAD and glycine residues at the FAD binding site is conserved between *E. coli* and *S. aureus* MurB enzymes in which the gly-X-gly motif is generally found (Kumar et al., 2011). The 'X' residue of this motif is not present in *M. tuberculosis* MurB, and in comparison, FAD-binding is tighter than that of the *S. aureus* homologue (Kumar et al., 2011). In terms of drug design, MurB is a promising target for competitive inhibitors due to flexibility in electrostatic charge distribution across the catalytic surface (Kumar et al., 2011). For example, the 3,5-dioxypyrazolidine derivatives bind potently *in silico,* optimally in the presence of the Tyr155 and Ser237 residues (Kumar et al., 2011).

The UDP-MurNAc pentapeptide, consisting of [L-Ala, D-Glu, *m*DAP, D-Ala, D-Ala] is subsequently formed step-wise by concerted action of 4 ATP-dependent amino-acid ligases: MurC, MurD, MurE and MurF (Fig. 1.3). This requires conversion of L-Glu to D-

Glu and L-Ala to D-Ala catalysed by Glutamate racemase (murI) and D-Ala racemase (Alr) respectively (Fig. 1.3). MurI interacts with MurD (Munshi et al., 2013) and catalyses the conversion of L-Glu to D-Glu. The *murI* gene is essential for *M. tuberculosis* and *M. smegmatis* growth in the absence of D-Glu, as it is encoded by a single gene, and no orthologue exists for the isoenzyme D-amino acid transaminase (Dat) which aids L-glutamate conversion in other *murI* deficient bacteria (Li et al., 2014; Morayya et al., 2015). Disruption of *M. smegmatis murI* produces a pear-shape morphology (Li et al., 2014). The essentiality of *murI* is growth-condition dependent underscoring the importance of *in vivo* studies to further unravel the utility of this enzyme for drug development. Alr is a dimeric protein which catalyses conversion of L-Ala to D-Ala and vice-versa (Lee et al., 2013; Halouska et al., 2014). This is the primary means of D-Ala acquisition, evident in attenuation of growth and survival of mycobacteria in the absence of exogenous D-Ala when Alr is deleted (Milligan et al., 2007; Chacon et al., 2009; Anthony et al., 2011; Awasthy et al., 2012; Halouska et al., 2014). The generation of an Alr insertion mutant, TAM23, has proved useful in determining the mechanism through which growth and survival of mycobacteria is impacted by Alr inactivation (Chacon et al., 2009). Attempts to delete the *alr* gene have proved that it is essential for growth in *M. smegmatis* (Milligan et al., 2007), while the TAM23 insertion mutant displays residual racemase activity in a manner that permits low levels of growth enough to analyse the impact of disruption D-Ala dipeptide synthesis (Halouska et al., 2007; Chacon et al., 2009). In *M. smegmatis*, *alr* disruption results in general compromise of cell wall integrity (Halouska et al., 2007; Milligan et al., 2007; Chacon et al., 2009). Intracellular survival in macrophages is impeded as a result of hypersensitivity to reactive oxygen and reactive nitrogen intermediates in the absence of *alr* (Halouska et al., 2007; Chacon et al., 2009). This is likely due to defects in PG synthesis and integrity, evident from the hypersensitivity to the PG-targeting antibiotics, imipenem and vancomycin (Chacon et al., 2009), and extended cell length, which is indicative of the inability to form septal PG prior to cell separation (Milligan et al., 2007) as well as markedly smoother colony morphology (Halouska et al., 2007). Similar effects are seen in *M. tuberculosis*, wherein *alr* proves to be essential for growth and establishment of murine lung infection (Awasthy et al., 2012).

Multiple proteins are required to produce the stem pentapeptide of PG (Fig. 1.3). Of these, the ATP-dependent ligases, also annotated as synthetases, MurC-MurF are co-transcribed downstream from a single promoter within the *dcw* operon, beginning with transcription of

MurE (Munshi et al., 2013). Each ligase is a 3-domain monomeric protein in which the UDP-portion of the substrate binds to domain 1, the peptide portion and ATP to domain 2 and the incoming amino acid to domain 3 (Basavannacharya et al., 2010; Arvind et al., 2012). MurC is versatile given that it is conserved in *M. leprae*, where it is predicted to catalyse addition of glycine instead of L-Alanine, for which an alternative ligase has not been identified (Vissa & Brennan, 2001). Each ligase displays high substrate specificity, with exception of MurC which also binds Gly and L-Ser apart from L-Ala, UDP-MurNAc and ATP (Munshi et al., 2013); and MurE which can accommodate *N*-glycolmuramic acid instead of *N*-acetylmuramic acid (Basavannacharya et al., 2010). It remains to be determined if L-Ser and/or Gly is incorporated into the stem peptide or what prevents this if not (Munshi et al., 2013).

Lack of evident interaction between the ligases suggests that stem-peptide synthesis takes place via a cascade of enzymatic reactions whereby each reaction product becomes a subsequent substrate (Munshi et al., 2013). The only interacting partners observed are specific to each phase of pentapeptide production: MurD interacts with the glutamate racemase MurI to obtain the D-Glu substrate to add to the pentapeptide; similarly, MurE interacts with DapF; and MurF with DdlA and NamH, which ligate D-Ala residues and convert *N*-acetyl UDP to *N*-glycol respectively (Munshi et al., 2013). Interruption of the cascade results in the accumulation of prior substrates (Halouska et al., 2007; Halouska et al., 2014). The 2nd line drug, Cycloserine inhibits the latter stage of pentapeptide synthesis causing accumulation of the early pre-cursor UDP (Halouska et al., 2014). Inhibition of enzyme activity is achieved above threshold substrate concentration which may be evidence of a regulatory negative-feedback loop (Munshi et al., 2013; Halouska et al., 2014).

After stem-peptide formation, MraY then catalyses the addition of the UDP-MurNAc pentapeptide to an undecaprenyl phosphate (UP) to form lipid I (Fig. 1.3). MurG then converts Lipid I to Lipid II which is flipped over to the outer membrane via a flippase, Mvin (Fig. 1.3). In the outer membrane, lipid II is polymerised to form the NAM-NAG repeating units, catalysed by the action of glycosyl transferase penicillin binding proteins (PBPs) (Fig. 1.3). The transpeptidase and carboxypeptidase activities of PBPs are critical for cross-link formation between the stem-peptides and form part of the PG remodelling enzymes.

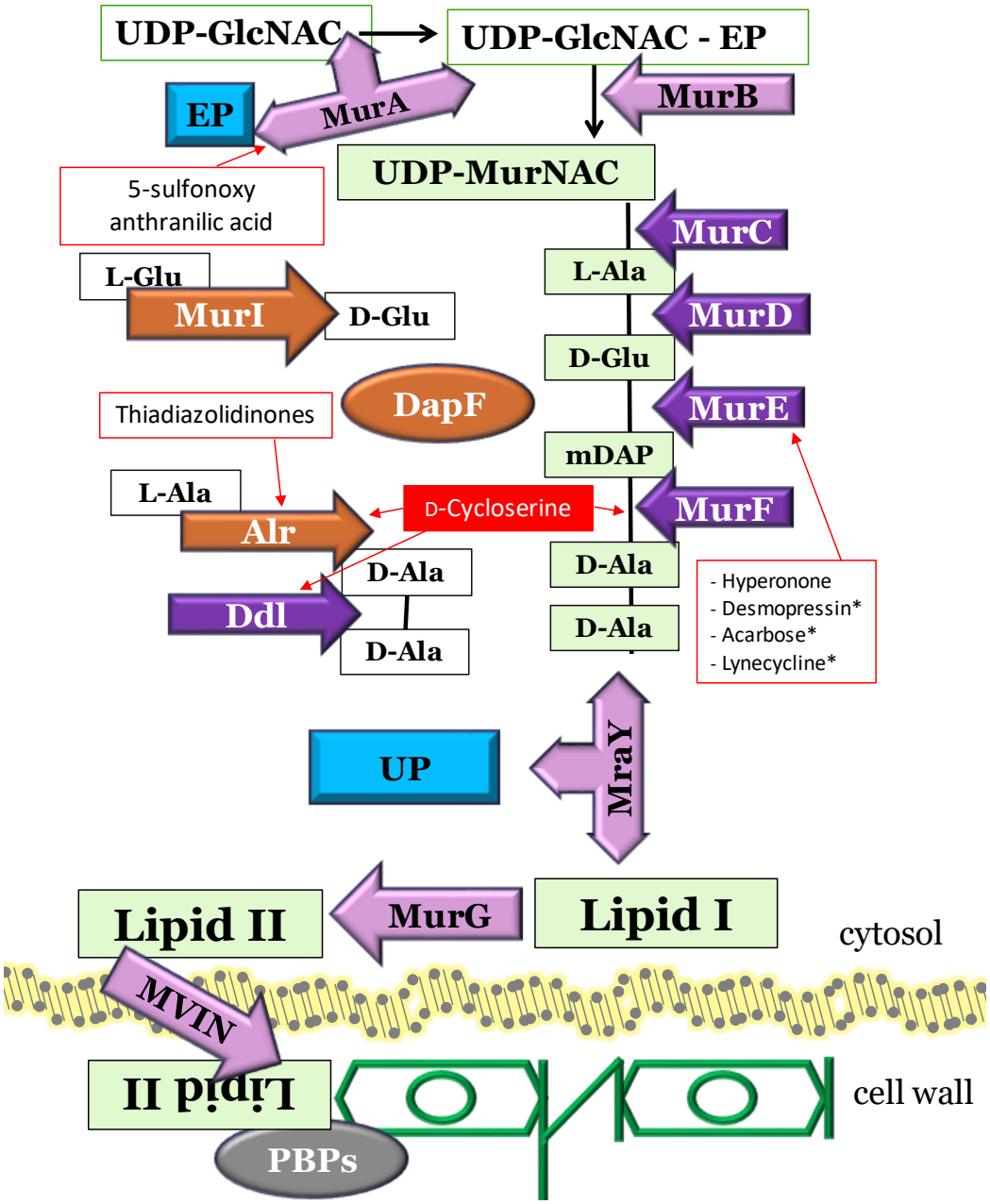

Figure 1.3 The general bacterial PG biosynthesis pathway.
PG biosynthesis begins in the cytosol with production of the sugar backbone precursors, followed by stepwise addition of amino-acids to form the stem pentapeptide. This structure is flipped across the membrane and incorporated into existing cell wall. Precursors and individual residues of the stem-pentapeptide are indicated in white. Various ligases are indicated in dark purple. Racemases are indicated in orange and other important enzymes are indicated in light purple. EP: enolpyruvate; UP: undecaprenyl phosphate; UDP: uridine diphosphate; MurNAc: *N*-acetyl muramic acid; GlcNAc: *N*-acetyl glucosamine; PBPs: penicillin binding proteins. Red boxes indicate inhibitory compounds targeting PG biosynthesis: solid red: current, approved drugs; red outline: novel compounds not yet purposed for TB treatment; *drugs approved for treating other conditions.

1.4.3.2 Novel compounds and strategies targeting PG

Enzymes for the synthesis of PG are essential for *M. tuberculosis* growth. Therefore, targeting drugs against these enzymes is a good strategy for inhibiting the growth of *M.*

tuberculosis (Moraes et al., 2015). Binding of MurA by 5'sulphonoxy-anthranilic acid analogs has been demonstrated *in silico* (Babajan et al., 2011) (Fig. 1.3) but inhibition and mammalian cytotoxicity has not yet tested *in vitro* or *in vivo.* MurC is the target of INH (Anuradha et al., 2010).

MurE can be targeted by Hyperenone, which is produced by the plant species *Hypericum acmosepalum*, reducing growth with an MIC at 75 mg/L and fully inhibiting growth at 100 mg/L (Osman et al., 2012) (Fig. 1.3). An *in silico* screen identified fifty compounds with binding affinity to the PG synthesis enzymes MurA and MurE important for stem-peptide synthesis (Eniyan et al., 2020). The *in vitro* activity of these compounds was tested by measuring inhibition of PG stem-peptide synthesis with purified Mur enzymes, where seven of the fifty compounds were found to inhibit > 50% of Mur enzyme activity (Eniyan et al., 2020). After determination of MICs, one compound successfully inhibited MurE at an IC_{50} of ~28 µM (Eniyan et al., 2020). MurE is also a promising target of repurposed drugs, for which two diabetes therapeutics, Desmopressin and Acarbose, as well as the antibacterial Lymecycline have a high binding affinity determined using an *in silico* screen (Brindha et al., 2016) (Fig. 1.3).

A high-throughput screen of multiple compound libraries was performed to identify inhibitors of the PG synthesis enzyme, Alanine racemase (Alr) (Anthony et al., 2011). Seven compounds were found to inhibit Alr activity and *M. tuberculosis* growth at very low MIC concentrations ranging from 1.5-12.5 µg/ml (Anthony et al., 2011). However, supplementation of *M. tuberculosis* growth with D-Alanine did not confer resistance to any of the compounds tested, suggesting they may have other targets as well (Anthony et al., 2011). Cycloserine targets multiple features of the PG biosynthesis pathway, including binding to Ddl and potentially MurF in competition with D-Ala and ATP (Halouska et al., 2014) (Fig. 1.3). Cycloserine has also been shown to inhibit Alr activity (Halouska et al., 2007; Awasthy et al., 2012) (Fig. 1.3). Accumulation of exogenous of D-Ala and D-Ala-D-Ala, therefore, leads to resistance to Cycloserine (Awasthy et al., 2012; Halouska at al., 2014), suggesting it may be more feasible to target alanine uptake. However, D-Ala levels do not affect Alr inhibition by thiadiazolidinones (Lee et al., 2013) (Fig. 1.3) as excess D-Ala may be converted back to L-Ala for earlier incorporation into the stem (Halouska et al., 2014). Thiadiazolidinones act at a very low MIC of 6.25 µg/ml and 1.56 µ/ml for DS

and DR strains respectively (Lee et al., 2013). At these dosages, toxicity in a murine model was circumvented (Lee et al., 2013).

Because of the highly impenetrable nature of the mycobacterial cell wall, a potential therapeutic route could be to combine cell wall degrading agents with other drugs to enhance access of drugs to other intracellular targets (Gustine et al., 2019). Combining the PG hydrolase, lysozyme with first-line and/or other antibiotics enhanced inhibition of *M. smegmatis* culture growth and colony formation compared to treating either with the antibiotics or lysozyme alone (Gustine et al., 2019). Recombinant forms of *M. tuberculosis* RipA or RpfE, which also hydrolyse PG were bactericidal to *M. smegmatis* evident as a significantly lower OD_{600} after 32 hours of growth compared to untreated control cultures grown for the same duration (Gustine et al., 2019). As such, innate PG hydrolases could be exploited as anti-tubercular therapeutics.

Beyond PG synthesis, the processes of PG maturation and remodelling are also important targets. Compounds potentially inhibiting L,D transpeptidases (LDt), which catalyses 3-3 cross-linking between stem-peptides of mature PG, were screened by molecular docking based on binding of the carbapenem, meropenem (Billones et al., 2016). One compound, filtered through molecular docking and a toxicity assay provided over 90% inhibition of *M. tuberculosis* H37Ra through hypothesised binding to LDt (Billones et al., 2016).

1.4.4 PG remodelling enzymes

Growth and persistence of mycobacteria relies on the synergistic synthesis and hydrolysis of the PG core (Machowski et al., 2014; Baranowski et al., 2018; García-Heredia et al., 2018; Shaku & Kana, 2018). The enzymes required for PG remodelling are summarised in figure 1.4 and represent an area that is rich for the development of new TB drugs.

1.4.4.1 *N*-acetylmuramyl-L-alanine amidases

Amidases are classified as enzymes which hydrolyse the amide bond between the L-Alanine of the stem peptide and muramic acid of the sugar backbone to degrade PG. In *E. coli*, amidase_3 family amidases particularly degrade septal PG to complete cellular constriction before dividing daughter cells can separate (Heidrich et al., 2001, 2002; Bernhardt & De Boer, 2003; Priyadarshini, De Pedro & Young, 2007). *E. coli amiABC*

deletion strains form long chains of cells bearing rings of thickened PG at sites of early cell division septum formation and sites of cell constriction (Bernhardt & De Boer, 2003; Priyadarshini, De Pedro & Young, 2007). Amidase_2 family amidases, such as AmpD and AmiD are required to cleave the stem-peptide of PG for PG recycling (Uehara & Park, 2007; Kerff et al., 2010; Rivera et al., 2016).

Mycobacteria encode multiple homologues of both amidase_2 and amidase_3 domain amidases (Machowski et al., 2014). The mycobacterial amidases are phylogenically divergent from *E. coli* AmiABC (Prigozhin et al., 2013a). Amidases of the Amidase_3 domain family are more conserved than those of the amidase_2 family (Machowski et al., 2014). Among five homologues in *M. smegmatis*, loss of either of Ami1-4 increases cell wall permeability (Wu et al., 2019). Ami4 (MSMEG_5315/Rv3594) has not been characterised but Ami1-3 are discussed further.

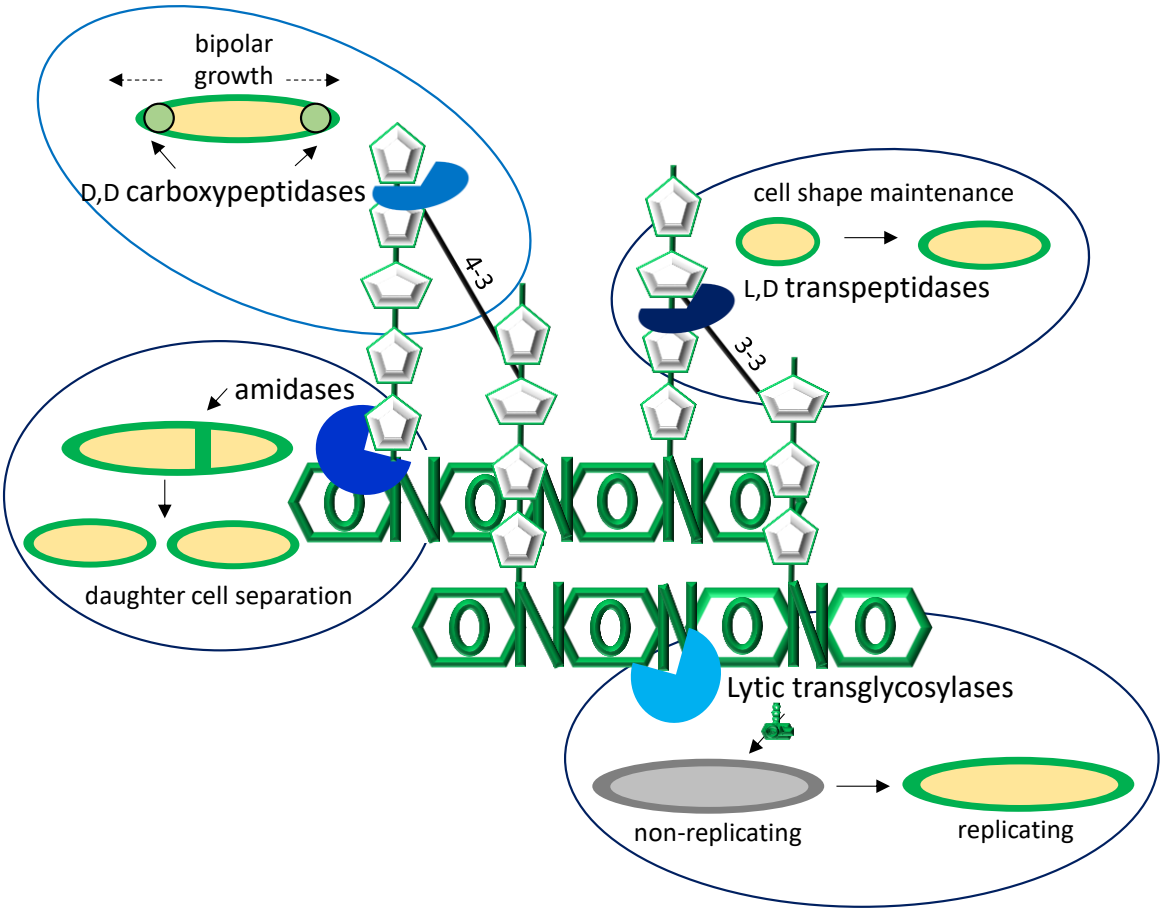

Figure 1.4 PG remodelling enzymes required for mycobacterial growth.
The complex structure of PG requires a variety of hydrolases to catalyse degradation necessary for mycobacterial physiology. D,D carboxypeptidases catalyse 4-3 cross-link formation between stem-peptides for bipolar growth. L,D transpeptidases catalyse 3-3 cross-link formation to maintain mycobacterial cell shape. Amidases cleave the stem-peptide from the glycan backbone to degrade septal PG during cell division. Lytic transglycosylases release PG products which trigger resuscitation of dormant bacteria.

Ami1 encoded by MSMEG_6281 is a cell division amidase (Senzani et al., 2017; He et al., 2019) of the amidase_3 family, in common with *E. coli* cell separation amidases (Heidrich et al., 2002). *M. smegmatis* Ami1 was demonstrated to be required for septum hydrolysis which in turn is required to regulate the relationship between cell division and elongation (Senzani et al., 2017). Loss of *ami*1 results in chains of cells and induces ectopic, lateral growth, evident as branching and budding, yet this enzyme is dispensable for growth (Senzani et al., 2017; He et al., 2019). As observed for the *E. coli* amidases (Priyadarshini, De Pedro & Young, 2007), loss of *M. smegmatis ami*1 does not prevent initiation of septal PG biosynthesis but prevents the septum hydrolysis required for mycobacterial cell separation, an effect that destabilises DivIVA and FtsZ at the septum leading to malformed septa in some cells within the division-defective chains (Senzani et al., 2017).

M. tuberculosis encodes four putative amidases, two Amidase_3 domain and two Amidase_2 domain homologues (Machowski et al., 2014). A role for the *M. tuberculosis* Ami1 homologue, Rv3717, in cell division has not yet been demonstrated. Instead, Rv3717 appears to lack the N-terminal AMIN domain that directs *E. coli* AmiC to the periplasm (Kumar et al., 2013). When *M. smegmatis* was treated with purified Rv3717, lytic activity higher than lysozyme was observed (Kumar et al., 2013) suggesting that MSMEG_6281 and Rv3717 function differentially or are differentially regulated. Although complementation of *M. smegmatis* Δ6281 with Rv3717 reduced cell length (He et al., 2019), it is not then clear if this is due to the global lytic activity of Rv3717 or septum hydrolysis. While the physiological role of Rv3717 is not clear at this point, multiple studies have confirmed the PG amidase activity (Kumar et al., 2013; Prigozhin et al., 2013a).

M. smegmatis CwlM or Ami2, encoded by MSMEG_6935 is an essential amidase which plays a regulatory interacting role in cell wall synthesis (Boutte et al., 2016). Complete depletion of *M. smegmatis* CwlM is lethal, while partial depletion causes cell shortening demonstrated to be due to inability of the cells to elongate (Boutte et al., 2016). Although recombinant CwlM demonstrated hydrolytic activity against PG (Deng et al., 2005), the amidase catalytic site is dispensable for *M. smegmatis* elongation (Boutte et al., 2016). Heterologous complementation of the *E. coli* Δ*ami*C short chains, subtly defective for cell division, with *M. smegmatis* and *M. tuberculosis* CwlM (Rv3915) restored these cells to

wild-type (Gaiwala Sharma, Kishore & Raghunand, 2016), even though this amidase lacks canonical catalytic residues. Instead, an interactory role of CwlM to activate the PG biosynthesis enzyme, MurA, depends on a phosphorylation site at the CwlM C-terminus, not involving the amidase active site (Boutte et al., 2016). As such, the phosphorylation site at the C-terminus is required for elongation and growth of *M. smegmatis* (Boutte et al., 2016). CwlM is phosphorylated by the serine-threonine protein kinase (STPK) PknB in both *M. smegmatis* and *M. tuberculosis* (Boutte et al., 2016; Turapov et al., 2018). Phosphorylation of CwlM acts as a nutrient sensor as it is less phosphorylated during starvation conditions (Boutte et al., 2016). When *M. smegmatis* CwlM is phosphorylated, it activates the first enzyme in PG biosynthesis, MurA, the activity of which is reduced with reduced CwlM phosphorylation thereby reducing PG biosynthesis during starvation conditions (Boutte et al., 2016). In *M. tuberculosis*, CwlM is encoded by Rv3915. Similar to *M. smegmatis*, phospho-regulation of Rv3915 is essential for PG biosynthesis and therefore growth (Turapov et al., 2018). Although MSMEG_6935 appears to act only in the cytoplasm (Boutte et al., 2016), the *M. tuberculosis* homologue plays two different phospho-regulatory roles in the cytoplasm as well as the membrane (Turapov et al., 2018). In agreement with the role of *M. smegmatis* CwlM in elongation (Boutte et al., 2016), cytoplasmic, phosphorylated *M. tuberculosis* CwlM primarily interacts with FhaA (Turapov et al., 2018), a protein required for mycobacterial elongation (Viswanathan et al., 2017). Other elongation proteins were also identified in the cytoplasmic CwlM-FhaA interactome, including DivIVA, FtsZ and DnaA (Turapov et al., 2018). In the *M. tuberculosis* membrane, unphosphorylated CwlM interacts with the putative lipid II flipase MVIN (MurJ), as well as FtsE and CwsA (Turapov et al., 2018).

It is not completely clear what role Ami3 plays in mycobacterial cell biology but there is growing evidence that it may function during *M. smegmatis* growth. MSMEG_6406 localises to the poles and septum, and overexpression causes cell shortening (Wu et al., 2019). There is also strong evidence that it is an active cell wall hydrolase since overexpression also causes *M. smegmatis* lysis but only in the presence of naturally occurring zinc co-ordinating catalytic residues and a potential mannosylation site which is hypothesised to activate Ami3 activity via a mannosyl-transferase, Pmt (Wu et al., 2019). The absence of Pmt phenocopies the loss of the Ami3 mannosylation site, as Ami3

overexpression in a *M. smegmatis* Δ*pmt* background is less destructive than WT (Wu et al., 2019).

1.4.4.2 Lytic transglycosylases

M. tuberculosis encodes five homologues of the lytic transglycosylase, termed resuscitation promoting factor (Rpf) originally identified in *Micrococcus luteus* (Tufariello, Jacobs & Chan, 2004; Mukamolova et al., 2006). Rpfs have a lysozyme-like, lytic transglycosylase domain hypothesised to hydrolyse the glycosidic bonds of PG (Mukamolova et al., 2006; Telkov et al., 2006). *M. tuberculosis* RpfB actively degrades the mycobacterial cell wall in the presence of an interacting-partner, RipA (Hett et al., 2007, 2008). Although depletion of *rpfB* alone does not result in defective growth of *M. tuberculosis* (Tufariello, Jacobs & Chan, 2004), the interaction partner, RipA, is required for cell division in *M. smegmatis* (Hett et al., 2008) and co-localises with RpfB at the mycobacterial septum (Hett et al., 2007). Loss of the five *rpf* genes is associated with delayed colony formation in *M. tuberculosis*, which was only restored by complementation with RpfB or RpfE (Kana et al., 2008). Combinatorial mutant strains of *M. tuberculosis* lacking *rpfB* or *rpfE* were more sensitive to SDS than mutants in which either of these genes were still present (Kana et al., 2008), also observed in *M. smegmatis* (Ealand et al., 2018). RpfE, like RpfB, interacts with the cell division factor RipA (Hett et al., 2007). Importantly, *M. tuberculosis* quadruple mutant strains, either lacking *rpfE* or *rpfD*, were defective for infection in a mouse model (Kana et al., 2008).

1.4.4.3 Carboxypeptidases

The D,D carboxypeptidases cleave the PG stem-peptide at the terminal D-Alanine, remodelling the stem to a tetrapeptide, which precludes 3-3 cross-link formation (Bansal et al., 2015; Pandey et al., 2018). Carboxypeptidases have either an S13 or S11 peptidase domain for which four *M. smegmatis* and three *M. tuberculosis* homologues exist (Ealand et al., 2019). An essential carboxypeptidase homologue, MSMEG_6113, an orthologue of the essential *M. tuberculosis dacB* gene, is required for *M. smegmatis* growth, in particular bipolar PG synthesis (Ealand et al., 2019). The *M. tuberculosis* homologue, Rv3627c exhibits carboxypeptidase activity *in vitro* (Zhang et al., 2019). Two genomic neighbouring, but not operonic, carboxypeptidase genes, MSMEG_2433 and 2432 are collectively required for 3-3 cross-link formation in *M. smegmatis* as deletion of both

genes resulted in *M. smegmatis* PG composed of a greater proportion of 4-3 cross-links to 3-3 cross-links (Pandey et al., 2018). Furthermore, recombinant MSMEG_2433 displayed pentapeptide hydrolysis activity (Bansal et al., 2015). Deletion of both these genes also caused growth defects, defects in biofilm formation and produced longer cells (Pandey et al., 2018), which could suggest a role for carboxypeptidases in cell division. Similarly, deletion of Rv2911, the *M. tuberculosis* homologue of MSMEG_2433 caused a reduced growth rate under acidic conditions (Bourai, Jacobs & Narayanan, 2012). Carboxypeptidases are classed as low-molecular weight penicillin binding proteins, and evidence points to a role for these enzymes in β-lactam resistance via β-lactamase activity (Bansal et al., 2015; Pandey et al., 2018). Recombinant MSMEG_2433 restored the β-lactam resistance of an *E. coli* Δ6PBP mutant strain, and exhibited *in vitro* β-lactamase activity (Bansal et al., 2015). Consistent with this, the *M. smegmatis* Δ2433, Δ2432 double mutant exhibited increased susceptibility to β-lactams (Pandey et al., 2018).

1.4.4.4 L,D transpeptidases

L,D transpeptidases (LDts) catalyse the formation of 3-3 cross-links between a tetrapeptide and tripeptide stem of PG (Lavollay et al., 2008). *M. tuberculosis* encodes five LDts, designated LDt_{MT1}-LDt_{MT5}. Recombinant *M. tuberculosis* Ldt_{MT1} and Ldt_{MT2} catalysed 3-3 cross-link formation between Corynebacterium tetrapeptides (Lavollay et al., 2008; Gupta et al., 2010). The *ldt_{MT2}* gene, encoded by Rv2518c, was identified by transposon mutagenesis screening for genes required for *M. tuberculosis* growth (Gupta et al., 2010). Ldt_{MT2} consists of an N-terminal transmembrane domain and C-terminal transpeptidase domain with a catalytic SHGC motif (Gupta et al., 2010). *M. tuberculosis* cells lacking both *ldt_{MT1}* and *ldt_{MT2}* are significantly shorter than wild-type and display altered cell morphology (Schoonmaker, Bishai & Lamichhane, 2014). The loss of *ldt_{MT1}* and *ldt_{MT2}* also reduced infectivity of *M. tuberculosis* in a mouse-model (Schoonmaker, Bishai & Lamichhane, 2014). Ldt_{MT5} has distinct structural differences when compared to MT1 and MT2 (Brammer Basta et al., 2015). LdtMt1-4 can be inactivated by binding of carbapenems, but not LdtMt5 (Cordillot et al., 2013)

1.4.5 Regulation of PG remodelling enzymes

The most well-studied example of PG hydrolase regulation is arguably the model of amidase activation. The crystal structure of *E. coli* AmiC revealed multiple mechanisms of AmiC regulation that limits hydrolytic activity to septal PG (Rocaboy et al., 2013). It is

important to regulate these activities as dysregulated septal hydrolysis can result in cell lysis. The N-terminal AMIN domain regulates localisation of the amidase to the septum (Peters, Dinh & Bernhardt, 2011) (Fig. 1.5) and is also a PG binding domain (Rocaboy et al., 2013). The C-terminal amidase-3 domain houses a catalytic centre bearing an auto-inhibitory α-helix (Rocaboy et al., 2013). The α-helix prevents amidase activity in three ways, the first is through steric hinderance leading to blockage of substrate entry (Fig. 1.5); the second is through the formation of stable interactions with the catalytic site; and the third is through the ability to chelate zinc ions before these can reach the catalytic site (Rocaboy et al., 2013). Only expression of an α-helix-5 (H5) mutant resulted in an independently active amidase with PG degrading activity equivalent to lysozyme (Rocaboy et al., 2013).

Purified wild-type *E. coli* amidases cannot degrade PG independently – only in the presence of the M23 endopeptidase EnvC or NlpD, can these enzymes degrade PG (Uehara et al., 2010) (Fig. 1.5). This suggests EnvC and NlpD are activators of *E. coli* amidases however, these activators are degenerate and retain no hydrolytic activity by themselves. The loss of degenerate M23 endopeptidase, *envC* causes filamentation in *E. coli* and conditional lethality when the MinCDE division regulation system is depleted (Bernhardt & De Boer, 2004). The cell division defect in *envC*-disrupted cells, which phenocopies loss of cell division amidases, also causes delayed septal ring formation (Bernhardt & De Boer, 2004). Loss of the M23 endopeptidase, *nlpD* in addition to *envC* further exacerbated the cell division defect in *E. coli* and was most severe when a further two M23 endopeptidases, YebA and YgeR were deleted (Uehara, Dinh & Bernhardt, 2009). In this quadruple mutant, cell separation is prevented by the presence of unresolved septal PG, which in turn inhibits outer membrane constriction (Uehara, Dinh & Bernhardt, 2009). Preventing septal hydrolysis delays ampicillin-induced lysis of *E. coli* (Uehara, Dinh & Bernhardt, 2009). The timing of amidase-mediated septal hydrolysis is also regulated in that recruitment of amidases to the division site only coincides with the presence of an intact Z-ring (Peters, Dinh & Bernhardt, 2011) (Fig. 1.5).

Although, YebA and YgeR appear to play a role in cell separation, EnvC and NlpD are the main amidase activators. *E. coli* also utilises YebA, for PG cross-link cleavage (Singh et al., 2012). The cross-link activity of YebA together with two NlpC/p60 proteins, is essential for *E. coli* growth (Singh et al., 2012) (Fig. 1.5). Recombinant YebA was shown

to degrade intact PG and convert cross-linked tetrapeptide residues into monomeric tetrapeptides (Singh et al., 2012).

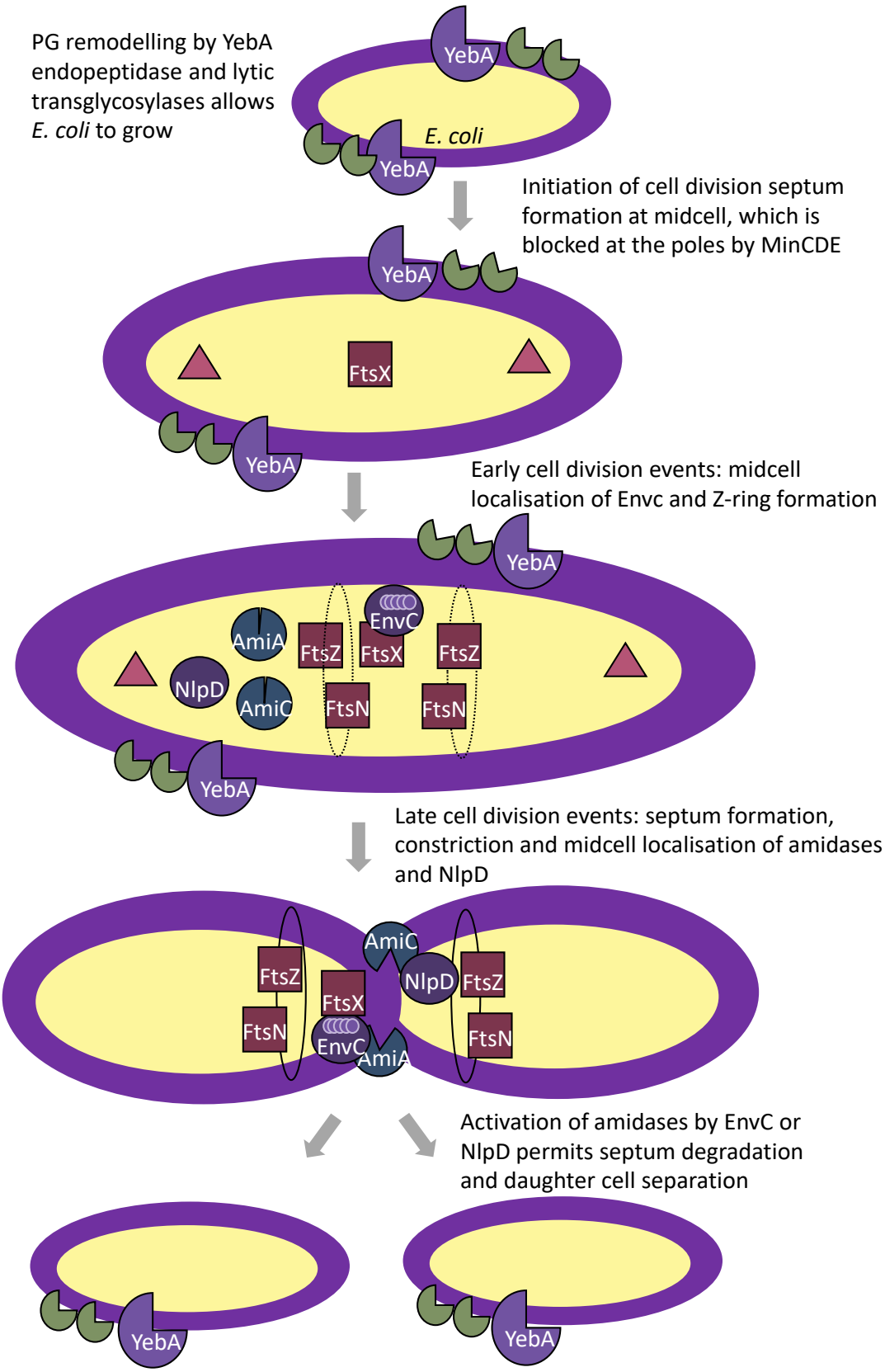

Figure 1.5 The role of M23 endopeptidases in growth and cell division regulation of *E. coli*.

(Figure 1.5 continued) YebA M23 endopeptidase activity mediates *E. coli* growth, eventually leading to cytokinesis and daughter cell separation. Cell division is regulated via the interaction between degenerate M23 endopeptidases and septum-degrading amidases. Purple: M23 endopeptidases; olive: lytic transglycosylases; red: cell division factors; blue: amidases; triangles: MinCDE complex. Partial circle: active enzyme; closed circle: inactive or degenerate.

Combining purified EnvC or NlpD with purified AmiB or AmiC released the stem-peptides of PG (Uehara et al., 2010). EnvC lacks zinc-coordinating residues required for classical M23 endopeptidase PG hydrolysis (Peters et al., 2013a). Consistent with this, when EnvC and NlpD were provided alone, no hydrolysis activity was observed, confirming that these proteins lack activity but instead activate the conformationally inactive amidases (Uehara et al., 2010) (Fig. 1.5). Amidase inactivation or the loss of EnvC is synthetically lethal in a PBP1b-depleted strain (Yang et al., 2011). The cell separation defect in any of the M23 endopeptidases mutants of *E. coli* was negligible in the presence of wild-type *envC*, suggesting that EnvC is the primary amidase activator, needed to activate both AmiA and AmiB (Uehara et al., 2010) (Fig. 1.5).

EnvC and NlpD can cause lysis if not localised to sites of cell division via an N-terminal coiled-coil or LysM domain (Fig. 1.5), unless the cognate amidase which it activates is absent (Uehara et al., 2010; Peters et al., 2013a; Tsang, Yakhnina & Bernhardt, 2017). Both EnvC and NlpD localise to sites of *E. coli* cell division, though it is evident that EnvC localises early during division, via FtsEX recruitment before the amidases are recruited, whereas NlpD localises at sites of constriction and lacks the coiled-coil domain directing EnvC localisation (Uehara, Dinh & Bernhardt, 2009; Uehara et al., 2010; Peters, Dinh & Bernhardt, 2011; Yang et al., 2011) (Fig. 1.5). A signal sequence and N-terminal LysM domain direct NlpD to the site of division (Tsang, Yakhnina & Bernhardt, 2017). If NlpD is not transported to the septal ring when *envC* is absent, cell separation cannot take place (Tsang, Yakhnina & Bernhardt, 2017). The amidases and NlpD require the presence of FtsN and Z-ring formation in order to localise at the septum, whereas EnvC localises at midcell in an FtsN-independent manner (Peters, Dinh & Bernhardt, 2011) (Fig. 1.5). NlpD is particularly associated with outer membrane invagination (Tsang, Yakhnina & Bernhardt, 2017). Amidase and activator localisation occurs independent of each other (Peters, Dinh & Bernhardt, 2011).

M. tuberculosis Rv3717 (Ami1), on the other hand, does not carry a similar autoinhibitory α-helix (Kumar et al., 2013; Prigozhin et al., 2013b). Two different purified forms of

Rv3717 exhibited zinc-dependent hydrolytic activity: the form purified by Kumar et al (2013) was lytic to *M. smegmatis* and degraded a variety of bacterial PG preparations in a zymogram assay independent of the presence of a putative activator. A form of Rv3717 purified by Prigozhin et al (2013) also produced zinc-dependent activity against a murein-dipeptide product but in contrast appears to only access non-cross-linked PG. Still, both studies of the biochemical characterisations of Rv3717 suggest it is not auto-regulated like *E. coli* AmiABC. The function of *M. tuberculosis* Ami2, commonly termed CwlM is regulated via PknB phosphorylation as the phosphorylated form of this amidase is required in the cytoplasm while the non-phosphorylated form functions in the membrane (Turapov et al., 2018).

Ami3 (Rv3811) is putatively regulated by a cytoplasmic protease, HtrA (Wu et al., 2019). HtrA is essential for *M. smegmatis* growth and cannot be depleted under stress conditions (Wu et al., 2019). When *ami*3 is deleted, HtrA is no longer required, alluding to the putative toxicity of Ami3 amidase activity (Wu et al., 2019). Reduced growth rate coincident with increased susceptibility to cell wall antibiotics in the HtrA-depleted cells suggests that dysregulated hydrolases weaken the cell wall, likely as a result of cell wall hydrolysis taking place faster than the required rate of cell wall synthesis to achieve cell growth homeostasis (Wu et al., 2019).

1.5 M23 endopeptidases: to be active or to activate?

Endopeptidases catalyse the hydrolysis of peptide bonds. Hydrolysis of peptide bonds within the stem peptide of PG or cross-links and cross-bridges between the stem peptide can be catalysed by M23 endopeptidases to remodel PG for a variety of physiological purposes (Firczuk, Mucha & Bochtler, 2005; Bardelang et al., 2009; Bonis, Ecobichon, Guadagnini, Prevost, et al., 2010; Sycuro et al., 2010; Stohl et al., 2012; Dörr et al., 2013; Stohl et al., 2013; Raulinaitis et al., 2017a). Structurally the M23 domain within an M23 endopeptidase protein is made up of antiparallel β-sheets with zinc-coordinating motifs which classes these enzymes as metallo-proteases (Firczuk, Mucha & Bochtler, 2005). A small group of M23 endopeptidases diverged with degenerate M23 domains, such as the *E. coli* amidase activators (Uehara, Dinh & Bernhardt, 2009; Uehara et al., 2010). Degenerate M23 endopeptidases have conserved the overall β-sheet structure of the domain but have amino acid substitutions within the zinc-binding residues causing these proteins to be catalytically inert (Uehara, Dinh & Bernhardt, 2009; Uehara et al., 2010; Peters et al.,

2013b). Instead, degenerate M23 endopeptidases interact with other proteins for regulatory purposes (Meisner et al., 2012; Peters et al., 2013a; Möll et al., 2014; Lenz et al., 2016a; Stohl et al., 2016). Characterisation of numerous M23 endopeptidases point to a trend by where these proteins are functionally polarised into degenerate cell division regulators or active PG hydrolases. Both groups are further customised for their respective functions in combining the M23 domain with accessory interactory, hydrolytic or substrate-binding domains, which often direct these proteins to positions of required function in the bacterial cell. Select examples, as discussed further can encode both active and degenerate M23 endopeptidases, highlighting these proteins as highly dynamic tools across a spectrum of bacterial physiology.

1.5.1 Lysostaphin and LytM are important, secreted M23 endopeptidases of staphylococci

Staphylococcal PG is linked by pentaglycine cross-bridges between the stem peptides. *Staphylococcus simulans* exports a M23 endopeptidase autolysin, lysostaphin, which hydrolyses the PG of competing bacteria at the pentaglycine cross-bridge. Hence this enzyme is a glycil, glycine endopeptidase. The autolytic activity of lysostaphin has been harnessed as anti-staphylococcul agent, in the context of life-threatening infection with multiple drug resistant *S. aureus* (MRSA) infection (Wu et al., 2003). Lysostaphin is highly dynamic, active within a broad pH range between 4.5 to 9, optimally active in a neutral environment (Firczuk, Mucha & Bochtler, 2005) and is also resistant to environmental protease degradation (Sabala et al., 2012). Treatment of *S. aureus* infection with Lysostaphin was highly efficient in a mouse-eczema model (Sabala et al., 2012). *S. aureus* is able to form biofilms on human skin and medical devices. Biofilm formation contributes to antimicrobial resistance but Lysostaphin effectively disrupts biofilms of drug susceptible *S. aureus* and MRSA strains (Wu et al., 2003). MRSA biofilms require more lysostaphin than drug susceptible *S. aureus*, yet in both instances lysostaphin was observably faster acting at a lower MIC than other biofilm-disrupting antimicrobials, oxacillin and vancomycin (Wu et al., 2003). However, staphylococci can overcome lysostaphin hydrolysis by replacing glycine residues with serine in the cross-bridges, known as a Lysostaphin immunity factor (lif) (Bardelang et al., 2009).

LytM is a lysostaphin orthologue produced by *S. aureus*. LytM bears the canonical HxGxD...HxH zinc-binding motifs in the M23 endopeptidase C-terminal domain (Bochtler et al., 2004; Odintsov et al., 2004). LytM primarily requires zinc chelation for activity but can also utilise other divalent metals albeit with reduced activity (Firczuk, Mucha & Bochtler, 2005). Although the first Histidine of the HxH motif does not directly chelate zinc, it is still required for catalysis as site-directed mutagenesis of this residue to an alanine prevented pentaglycine hydrolysis. Similarly, mutations to the Histidine and Aspartate of the first motif, or either of Histidines of the second motif all prevented hydrolytic activity of Lysostaphin (Bardelang et al., 2009). Like amidases, LytM activity appears to be auto-regulated bearing an auto-inhibitory, zinc-chelating asparagine residue upstream of the hydrolytic site and an occluding, disordered N-terminus (Fig. 1.6) (Bochtler et al., 2004; Odintsov et al., 2004). Loss of the N-terminus and metal-chelating asparagine freed the catalytic site for penta-glycine degradation (Odintsov et al., 2004).

S. aureus LytM is also regulated transcriptionally, where two different sized transcripts are produced, in a growth phase-dependent, inversely proportional manner (Fig. 1.6) (Lioliou et al., 2016). The longer transcript is upregulated at stationary phase and displays a lower translational efficiency than the shorter transcript, leading to a reduction in LytM protein abundance at stationary phase (Lioliou et al., 2016). This is due to the upregulation of a repressor, RNAIII, at stationary phase, which binds the untranslated region of the longer LytM transcript (Fig. 1.6) (Lioliou et al., 2016). Growth-phase dependent transcription regulation of LytM is required to maintain cell wall integrity during stationary phase, where the absence of the RNAIII repressor causes *S. aureus* cell wall weakening, a phenotype which is reversed by deleting *lytM* (Lioliou et al., 2016). The shorter transcript which produces LytM is induced by the two-component system WalKR, made up of the Histidine kinase WalK and response regulator WalR that binds to the promoter of *lytM* (Fig. 1.6) (Peng et al., 2017). A *walK* mutation (S221P) was identified as a genetic determinant of Vancomycin resistance in the highly-virulent VISA strain of *S. aureus* (Peng et al., 2017). Serine residues are sites of phospho-regulation, and the mutation of Serine221 to Proline causes reduced autophosphorylation of WalK, which in turn reduces binding of WalR at the *lytM* promoter (Peng et al., 2017). Such strains exhibit cell wall thickening and reduced autolysis (Peng et al., 2017). WalKR also induces the signal transduction protein SpdC (Fig. 1.6) (Poupel et al., 2018). SpdC downregulates *lytM* in a negative-feedback loop (Fig. 1.6) (Poupel et al., 2018). Interestingly, although LytM does

not appear to have a direct role in cell division, both WalKR and SpdC co-localise at the *S. aureus* cell division septum (Poupel et al., 2018).

Although *S. simulans* lysostaphin and *S. aureus* LytM are close orthologues, native LytM, even without the inhibitory N-terminus, is not a successful *S. aureus* treatment (Sabala et al., 2012; Osipovitch & Griswold, 2015). While lysostaphin successfully disrupts *S. aureus* biofilms (Wu et al., 2003), endogenous LytM was identified within *S. aureus* biofilms (Den Reijer et al., 2016). The process of autolysis appears to be required for *S. aureus* growth, since Targocil, which prevents the translocation of LytM to the *S. aureus* cell wall, successfully inhibits *S. aureus* growth (Tiwari et al., 2018). The lack of LytM treatment efficiency is associated with intrinsic biochemical characteristics that differ between the two orthologues (Sabala et al., 2012). *S. aureus* LytM is less stable to proteolytic degradation than *S. simulans* Lysostaphin (Sabala et al., 2012). Lysostaphin also binds to crude cell wall more effectively than LytM, the latter binding only to washed or purified PG (Sabala et al., 2012), suggesting that *S. aureus* may employ other cell wall hydrolases to make PG accessible to LytM. *S. simulans* Lysotaphin encodes a cell-wall-binding domain in addition to the M23 endopeptidase domain, whereas the occluding N-terminus of *S. aureus* LytM cannot bind PG at all (Sabala et al., 2012). When the M23 endopeptidase of *S. simulans* Lysostaphin was replaced with that of *S. aureus* LytM, the resultant chimeric protein produced activity on par with native Lysostaphin (Osipovitch & Griswold, 2015; Jagielska, Chojnacka & Sabała, 2016).

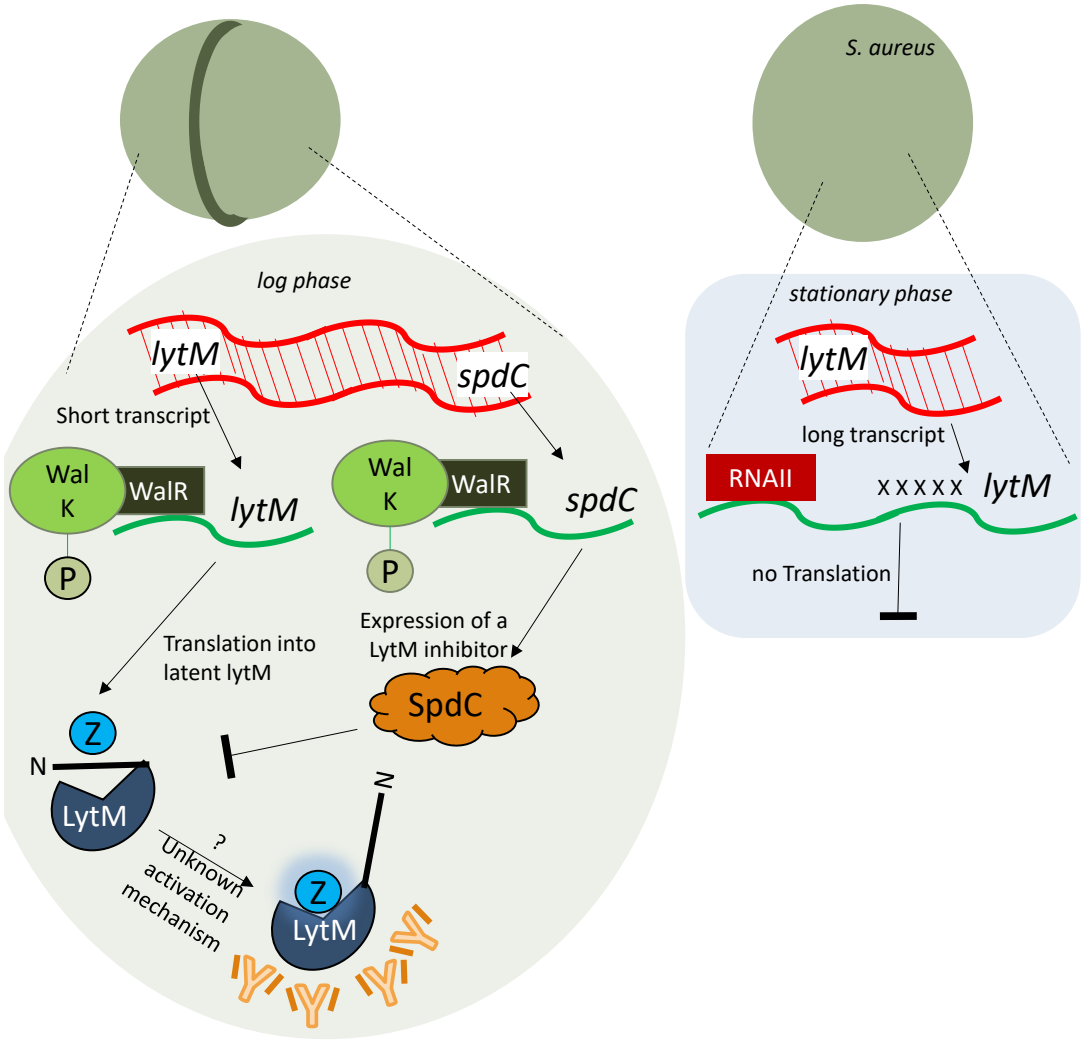

Figure 1.6 Regulation of the highly immunogenic, M23 autolysin, LytM of *S. aureus*.
The expression of lytM is upregulated by the two-component WalKR system from a short transcript during log phase. LytM is expressed in a latent, inactive form, due to occlusion of the endopeptidase active site by an N-terminal loop which scavanges zinc co-factors. For autolysis, which is required with cell wall maintenance during log phase, the endopeptidase must co-ordinate a zinc co-factor. Two mechanisms downregulate LytM activity: 1) the expression of SpdC, also via WalKR; 2) the transcription of a longer *lytM* transcript with an upstream RNAII-repressor binding site during stationary phase, at which LytM activity is toxic. P: phosphate; Z: Zinc; N: N-terminus.

Given that *S. aureus* LytM is a highly-conserved, secreted protein, it is an important antigen in *S. aureus* infection (Fig. 1.6) (Van Der Kooi-Pol et al., 2013; Liew et al., 2015; Van Den Berg et al., 2015). Multiple antibodies elicited against LytM were identified in patients who are vulnerable to *S. aureus* skin exposure by a genetic blistering disease, Epidermolysis bullosa (Van Der Kooi-Pol et al., 2013; Van Den Berg et al., 2015). Another study also reported that LytM-specific antibodies correlated to skin and soft-tissue *S. aureus* infections (Liew et al., 2015). Antibodies to LytM were also identified in an *S. aureus* biofilm adherent to an epidermal model of human skin (Den Reijer et al., 2016). Attempts to translate the antigenicity of LytM in combination with other common *S.*

aureus antigens into an *S. aureus* vaccine did not prove successful in an animal model (Van Den Berg et al., 2015). Although the size of *S. aureus* skin lesions were reduced by vaccination, this neither lead to a reduction in bacterial load nor improved mortality (Van Den Berg et al., 2015). Still, the high availability of secreted LytM in patient samples highlights the importance of M23 endopeptidases in virulence and pathogenesis which is currently the focus of research in a number of bacterial pathogens.

As with *E. coli*, a cell division M23 endopeptidase was also identified in *S. aureus* known as LytU (Raulinaitis et al., 2017b). Loss of *S. aureus lytU* leaves intact septa between divided daughter cells but this does not inhibit cell growth (Raulinaitis et al., 2017b). Overexpression of *lytU* inhibits *S. aureus* growth and causes cell lysis (Raulinaitis et al., 2017b). Adding exogenous, purified LytU to *S. aureus* cells also caused cell lysis (Raulinaitis et al., 2017b), an effect not observed for the LytM autolysin, suggesting that LytU and LytM are regulated differently. Accordingly, full length and C-terminal LytU were able to hydrolyse pentaglycine at the same rate, suggesting that LytU lacks the auto-inhibitory N-terminus found in LytM (Raulinaitis et al., 2017b). The N-terminus of LytU consists of a transmembrane domain and disordered region (Raulinaitis et al., 2017b). Unlike *E. coli* amidase activators which are degenerate proteins, *S. aureus* LytU has conserved zinc-binding motifs in the C-terminal M23 endopeptidase domain (Raulinaitis et al., 2017b). LytU is regulated by zinc concentration: up to a threshold level, LytU binds one zinc molecule as a cofactor to the active site like most active M23 endopeptidase; above this threshold LytU binds a second zinc which become inhibitory to activity (Raulinaitis et al., 2017b).

1.5.2 The cell-shape determining M23 endopeptidases of *Helicobacter pylori*

Helicobacter pylori encodes multiple cell shape determining (csd) M23 endopeptidases required for virulence (Bonis, Ecobichon, Guadagnini, Prévost, et al., 2010; Sycuro et al., 2010). Gut colonization by *H. pylori* relies on a helical bacterial morphology which is altered by modifying the expression of the M23 endopeptidase-encoding gene *csd3* also referred to as *hdpA* (Fig. 1.7) (Bonis, Ecobichon, Guadagnini, Prévost, et al., 2010; Sycuro et al., 2010). Disruption of the *csd3* gene both shortens cells and inhibits gut colonization whereas, *csd3* overexpression converts rods to cocci (Fig. 1.7) (Bonis, Ecobichon, Guadagnini, Prévost, et al., 2010). PG cleavage with purified Csd3 confirmed both

terminal Alanine (carboxypeptidase activity) and cross link cleavage (endopeptidase activity) (Bonis, Ecobichon, Guadagnini, Prévost, et al., 2010). PG analyses further revealed a direct association between morphology and peptidase activity, evident as increased intact pentapeptides and decreased 4-4 cross-links in the absence of *csd3* (Bonis, Ecobichon, Guadagnini, Prévost, et al., 2010; Sycuro et al., 2010). Further, point mutations to zinc-coordinating residues of the endopeptidase domain phenocopied cell shortening (Bonis, Ecobichon, Guadagnini, Prévost, et al., 2010). Overexpression of *csd3* increased the abundance of tri- and tetrapeptides (Bonis, Ecobichon, Guadagnini, Prévost, et al., 2010). Loss of the other two homologues, *csd1* or *csd2* also resulted in reduced cross-links and impaired gut colonisation in a mouse model (Fig. 1.7), but did not affect *H. pylori* motility (Sycuro et al., 2010). Notably, Csd1 has a conserved catalytic M23 endopeptidase domain while Csd2 is degenerate, but the two proteins form a heterodimer (An et al., 2016), which may explain the matching phenotypes of *csd1* and *csd2* deletion.

1.5.3 Neisseria species

In *Neisseria gonorrhoeae*, periplasmic NG1686, encoding M23 active against PG (*mpg)* is required for pilin production (Fig. 1.8) (Stohl et al., 2012, 2013). Piliation is a characteristic of clinical isolates of *N. gonorrhoeae.* The *mpg* mutant strains are attenuated for pilin production and exhibit pilin-deficient phenotypes such as susceptibility to hydrogen peroxide reduced capacity for DNA transformation and susceptibility to host bactericidal peptides (Fig. 1.8) (Stohl et al., 2012, 2013). Site-directed mutagenesis attributed hydrogen peroxide resistance directly to the aspartate and third histidine of the HxGxD-HLH zinc-binding motif in the NG1686 M23 domain (Stohl et al., 2012). Multiple PG degradation experiments also confirmed these 2 residues were indispensable for PG hydrolysis of 3-3 or 3-4 cross-links, whereas the first or second histidine were not required (Stohl et al., 2012). This implies that Mpg endopeptidase activity contributes to survival and adaptation within the host (Fig. 1.8). Endopeptidase activity is dependent on the Aspartate and third histidine of the zinc-binding motif, although the other Histidines are highly conserved in M23 endopeptidases. This may be due to different types of cross linking in bacterial PG: *S. aureus* PG is cross-linked by a pentaglycine crossbridge, different to the cross-links present in Neisseria, mycobacteria or *E. coli* PG.

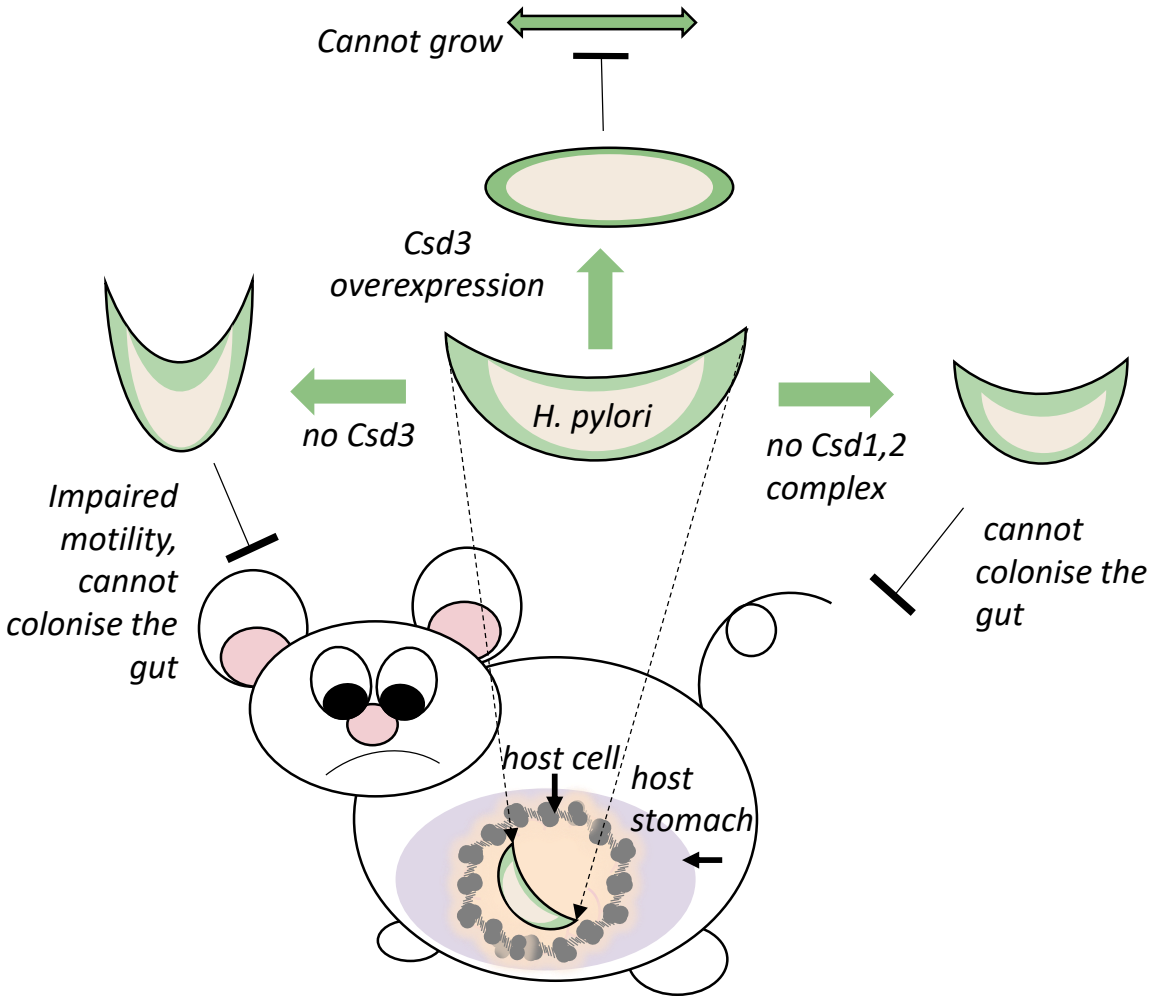

Figure 1.7 The role of M23 endopeptidase-mediated cell shape maintenance in *H. pylori* growth and virulence.
M23 endopeptidases, Csd1,2 and 3 *H. pylori* deletion mutants and overexpression strains have grossly-altered cell morphology represented here as alternatives to the central *H. pylori* cell. These changes impair host gut colonisation associating M23 endopeptidases with pathogenesis.

N. gonorrhoeae also encodes a degenerate M23 endopeptidase, NlpD which has no catalytic activity of its own but enhances the activity of the sole *N. gonorrhoeae* cell separation amidase, AmiC (Fig. 1.8) (Lenz et al., 2016b; Stohl et al., 2016). The domain architecture of *N. gonorrhoeae* NlpD, matches that of *E. coli*, including a LysM domain which exhibits PG binding capacity, demonstrated *in vitro* in a PG pull down assay (Stohl et al., 2016). Unlike *E. coli*, *N. gonorrhoeae* NlpD is non-redundant and loss of the single gene leads to a severe growth and cell separation defect (Fig. 1.8) (Stohl et al., 2016). Given that *N. gonorrhoeae* forms coccoid cells, the cell separation phenotype appears as clusters of cocci (Stohl et al., 2016), unlike the chains of rod-shaped *E. coli* Δ*envC*,Δ*nlpD* (Uehara, Dinh & Bernhardt, 2009).

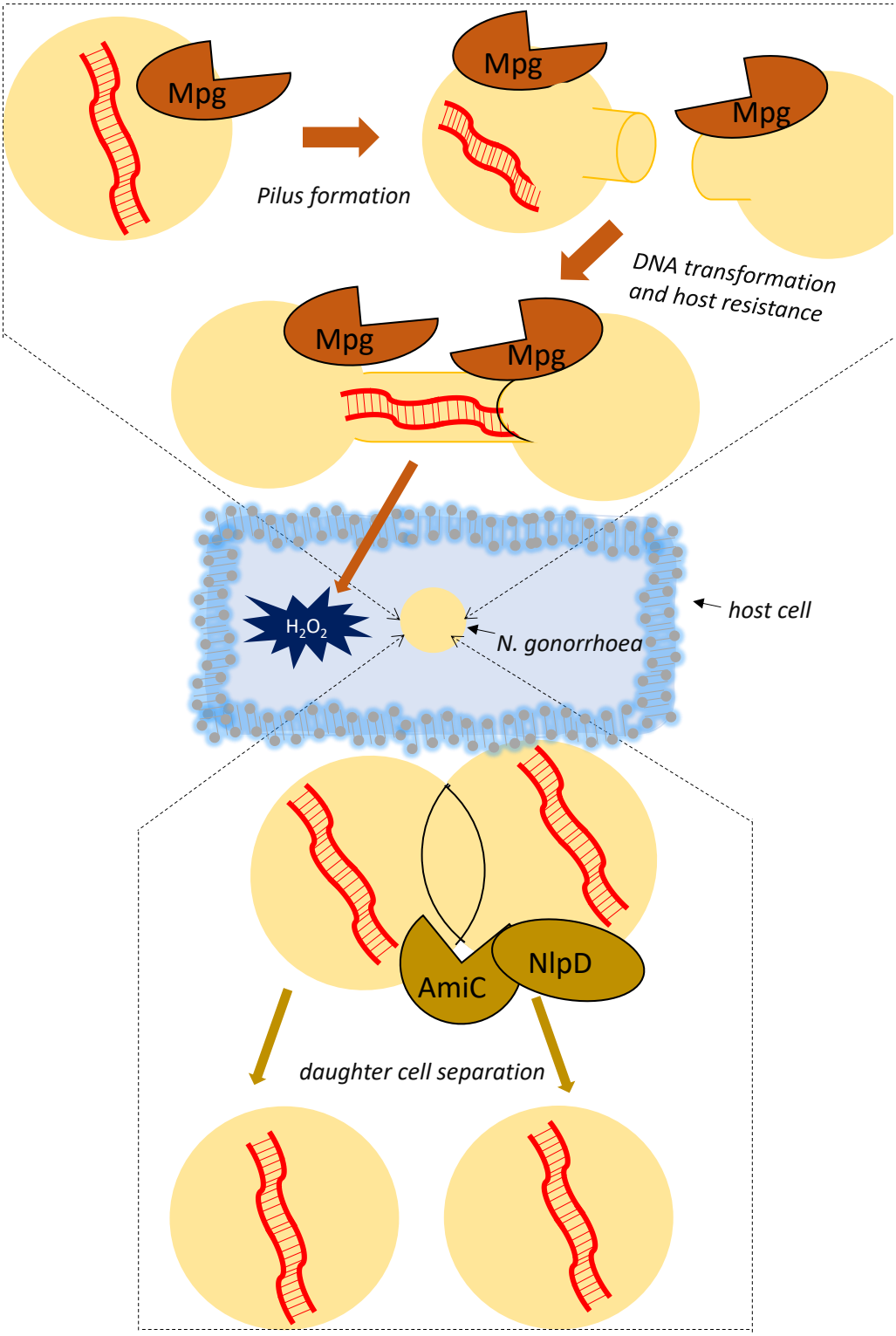

Figure 1.8 *N. gonorrhoea* encodes both active and degenerate M23 endopeptidases.
Active Mpg is required for pilin formation, which is necessary for virulence, DNA transformation and resistance to host defences such as hydrogen peroxide. Degenerate NlpD classically activates AmiC which degrades the septal PG of dividing cells for cell separation.

1.5.4 *Vibrio cholerae* encodes a zinc-independent M23 endopeptidase

The water-borne entero-pathogen, *Vibrio cholerae*, encodes multiple active and degenerate M23 endopeptidases, including the three side-wall hydrolases (Shy) and orthologues of cell division factors EnvC and NlpD. The Shy homologues consist of putative PG binding domains known as Opacity-Associated domain (OapA) in addition to the C-terminal M23 endopeptidase domain (Dörr et al., 2013). ShyA is involved in *V. cholerae* cell elongation (Fig. 1.9), and becomes essential for growth in the absence of the degenerate homologue, ShyC (Dörr et al., 2013). ShyA localises to the periplasm where it cleaves the cross-links of *V. cholerae* PG via zinc-dependent D,D-endopeptidase activity catalysed by the M23 domain (Dörr et al., 2013). In addition to elongation, ShyA activity is also required to transform *V. cholerae* into a sphere shape which is protective against β-lactam lysis (Fig. 1.9) (Dörr, Davis & Waldor, 2015). Like *S. aureus* LytU (Raulinaitis et al., 2017b), ShyA is inactivated by excess zinc (Dörr et al., 2013).

The zinc-dependence of ShyA prevents the activity of this protein under zinc-starvation conditions. Since Shy activity is so important for growth, *V. cholerae* encodes a zinc-independent homologue, ShyB, which substitutes for ShyA activity during zinc-starvation (Fig. 1.9) (Murphy, Alvarez, Adams, Liu, Chappie, Cava & Dörra, 2019). ShyB exhibits D,D endopeptidase activity in the presence of zinc or the metal-chelator EDTA, while ShyA is inhibited by EDTA (Murphy, Alvarez, Adams, Liu, Chappie, Cava & Dörra, 2019). The activity of ShyA during nutrient rich conditions is sufficient, therefore ShyB is repressed to prevent excess hydrolysis of the *V. cholerae* cell wall (Murphy, Alvarez, Adams, Liu, Chappie, Cava & Dörra, 2019). ShyB repression is brought about by the Zinc uptake repressor (Zur) which uses zinc to bind to the *shyB* promoter (Fig. 1.9) (Murphy, Alvarez, Adams, Liu, Chappie, Cava & Dörra, 2019). When the concentration of free zinc is reduced in the cell, Zur binding affinity is reduced, freeing the *shyB* promoter, leading to ShyB transcription (Fig. 1.9) (Murphy, Alvarez, Adams, Liu, Chappie, Cava & Dörra, 2019). ShyB further bears autoinhibitory structures orthologous to *S. aureus* LytM (Ragumani et al., 2008).

ShyC is a degenerate homologue of ShyAB which localises to the *V. cholerae* septum, the functional consequence of which is not clear (Dörr et al., 2013). *V. cholerae* encodes further degenerate M23 endopeptidases which are orthologues of *E. coli* amidase

activators EnvC and NlpD (Möll et al., 2014). *V. cholerae* activators are structurally similar to the *E. coli* orthologues whereby EnvC has a N-terminal coiled-coil domain and

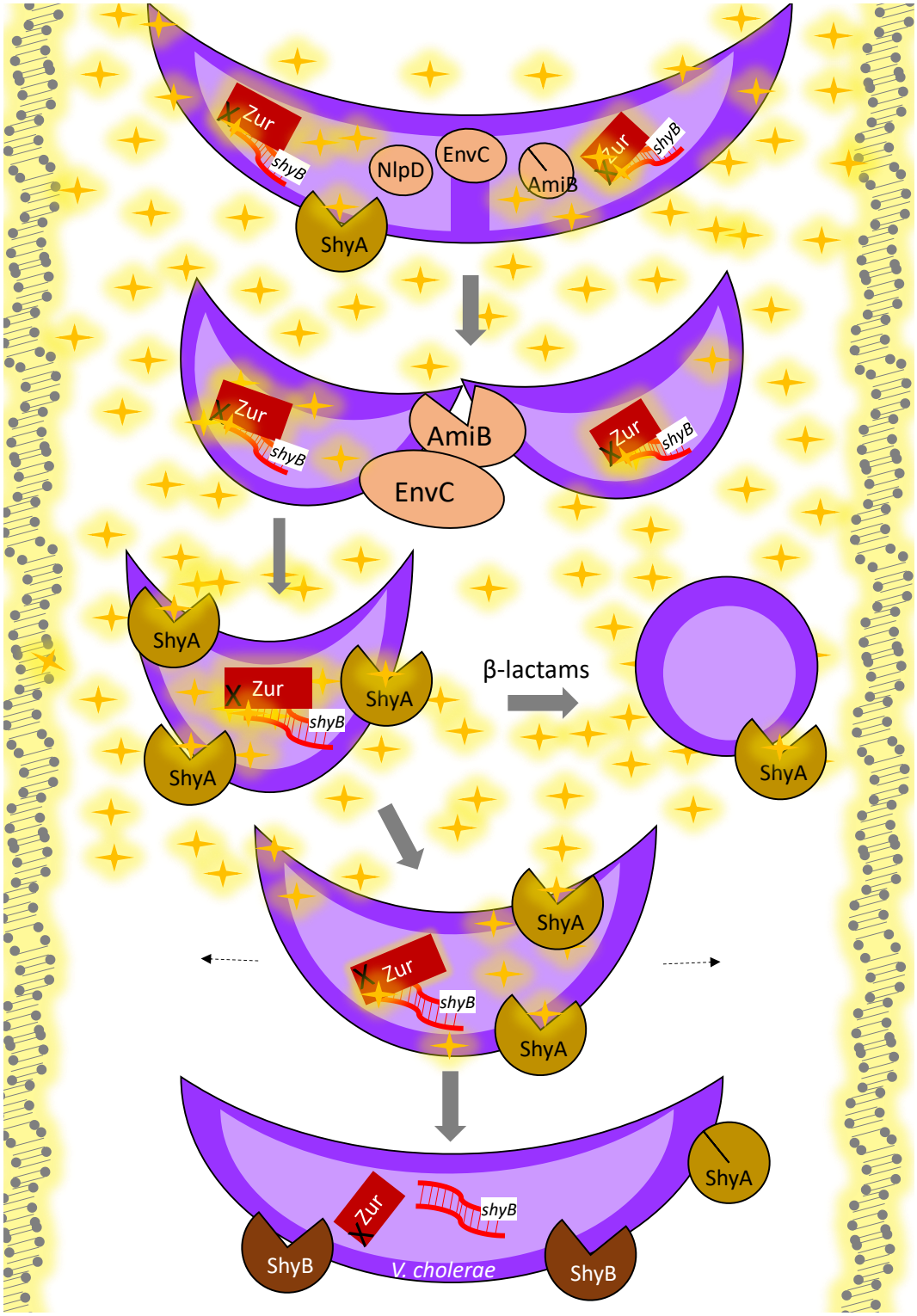

Figure 1.9 Differential M23 endopeptidases assist with *V. cholerae* elongation and cell division. When cells are ready to divide, the degenerate endopeptidase EnvC localises to the septum, where it later binds and activates AmiB. NlpD can also activate AmiB at late cell division. Active AmiB then cleaves the septal PG, allowing *V. cholerae* daughter cells to separate. Under zinc-rich conditions (stars), the active M23 endopeptidase, ShyA cleaves the *V. cholerae* side wall for cellular elongation (dashed arrows), or transition to sphere morphology in response to β-lactam

treatment. Zinc allows the Zur repressor to remain bound to the promoter of a zinc-independent endopeptidase, ShyB. During zinc-starvation, via host nutritional immunity, the Zur repressor falls off the *shyB* promoter, allowing ShyB activity which substitutes for inactive ShyA so that *V. cholerae* continues to grow.

NlpD has a N-terminal LysM domain (Möll et al., 2014). *V. cholerae* encodes one cell division amidase, AmiB which is activated by partially redundant EnvC and NlpD, since deletion of both these factors phenocopies the cell division defect of the Δ*amiB* strain (Fig. 1.9) (Möll et al., 2014). *V. cholerae* AmiB localises midcell at late division whereas the activator, EnvC is able to localise earlier, prior to cell constriction (Fig. 1.9) (Möll et al., 2014). AmiB midcell localisation is dependent on the presence of EnvC or NlpD (Fig. 1.9) (Möll et al., 2014). While EnvC appears to be the predominant activator *in vitro*, NlpD plays a non-redundant role in *V. cholerae* fitness during intestinal colonisation in a mouse model, adding to the evidence that M23 endopeptidases can contribute multifunctional roles in bacterial virulence (Möll et al., 2014).

1.5.5 *Bacillus subtilis* sporulation relies on the degenerate, M23 endopeptidase SpoIIQ

Bacteria are classically unicellular organisms, but spore-forming bacteria can transition between unicellular and bicellular states, the latter referring to the forespore "cell" within the mother (spore-forming) cell, reverting to unicellularity once the mother cell is lysed to release a mature spore. This requires a form of intercellular communication that does not take place in non-spore-forming bacteria. In *Bacillus subtilis*, the M23 endopeptidase SpoIIQ, assists in signalling between the mother cell and internal forespore particularly in production of a Type III secretion system spanning the membranes of the mother cell and forespore (Fig. 1.10) (Meisner & Moran, 2011; Meisner et al., 2012). Expression of the *spoIIQ* gene is necessary for localisation of SpoIIIAH on the mother cell membrane, at the conjuncture between the mother and spore cell (Doan, Marquis & Rudner, 2005). SigF regulates the expression of both SpoIIQ in the forespore and SigE in the mother cell, which in turn regulates the expression of SpoIIIAH (Fig. 1.10) (Doan, Marquis & Rudner, 2005). Like amidase activators, SpoIIQ utilises a degenerate M23 domain for protein-protein interaction with the SpoIIIAH scaffolding protein to assist construction of an intermembrane channel (Meisner & Moran, 2011; Meisner et al., 2012). Specifically, SpoIIQ is produced by the forespore, positioned across the membrane via the N-terminal transmembrane domain, protruding the M23 domain extracellularly where it can interact with SpoIIIAH spanning the mother cell membrane, thus connecting the two cells (Fig.

1.10) (Meisner & Moran, 2011; Meisner et al., 2012). A stable interaction is formed by hydrogen bonding between the β-sheets of the SpoIIQ M23 domain paired with those of SpoIIIAH (Fig. 1.10) (Meisner et al., 2012). In this instance, the function of the SpoIIQ M23 domain is conferred by the characteristic β-sheets of the domain. SpoIIQ cannot bind to PG (Meisner & Moran, 2011).

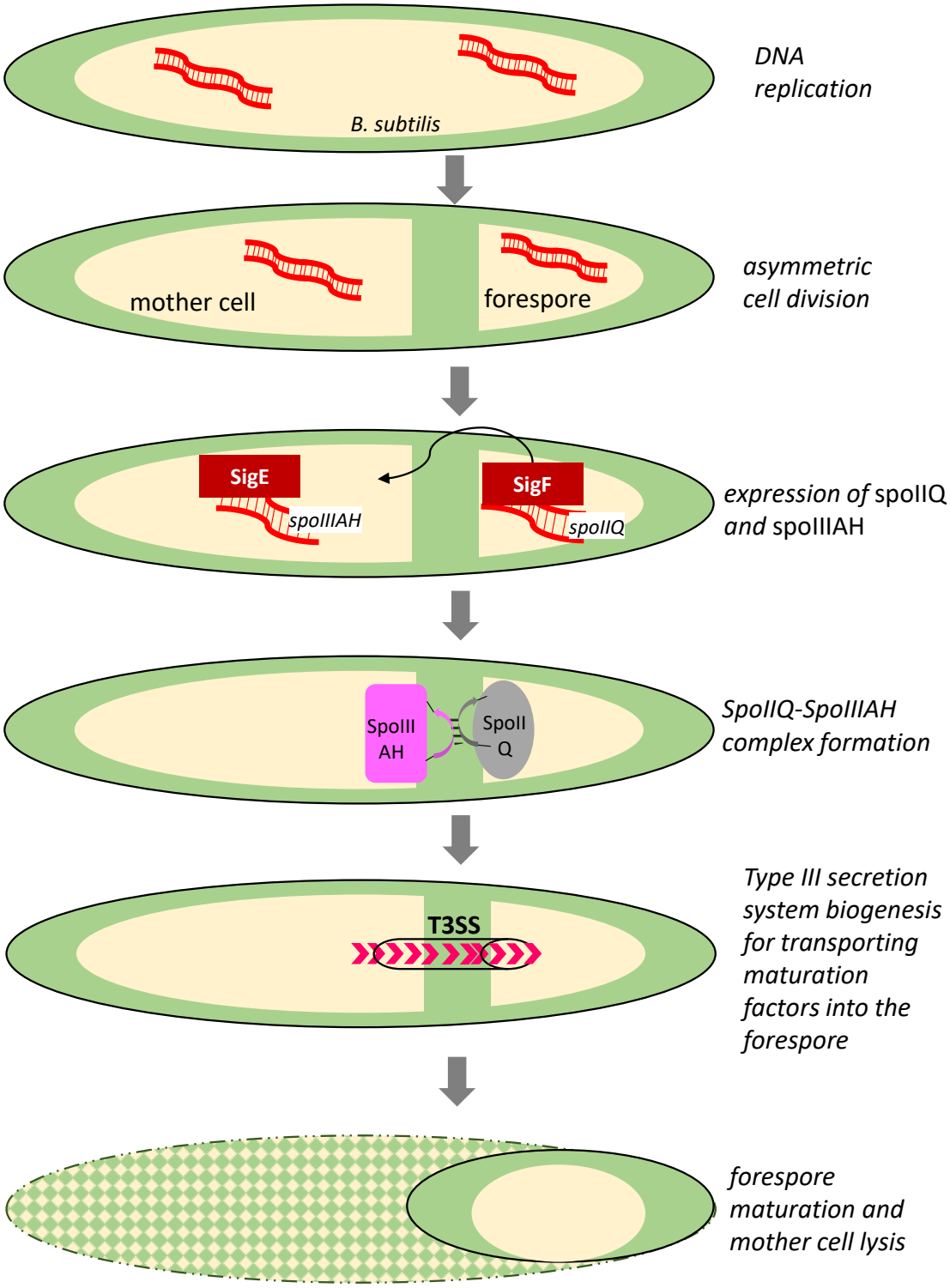

Figure 1.10 M23 endopeptidase-mediated spore maturation in *Bacillus subtilis*.

(Figure 1.10 continued) The M23 endopeptidase gene, *spoII*Q is expressed via SigF in the forespore, where it spans the forespore membrane. SpoIIQ (purple) forms hydrogen bonds with SpoIIIAH expressed via SigE in the mother cell. SigF also regulates SigE. The SpoIIQ-SpoIIIAH complex assists with scaffold formation for a type III secretion system that allows translocation (chevrons) of factors from the mother cell required for spore development.

Like *V. cholerae*, *Bacillus subtilis* encodes an M23 endopeptidase, Cell-wall-lytic enzyme P (CwlP), with zinc-independent activity (Sudiarta, Fukushima & Sekiguchi, 2010). The M23 domain of CwlP has D,D endopeptidase activity to degrade 4-3 cross-links in *B. subtilis* PG (Sudiarta, Fukushima & Sekiguchi, 2010). In addition, CwlP bears a soluble lytic transglycosylase (SLT) domain with muramidase activity against the *B. subtilis* PG backbone (Sudiarta, Fukushima & Sekiguchi, 2010). Although the CwlP M23 domain has the conserved HxGxD and HLH zinc-binding motifs, it does not require zinc for catalysis (Sudiarta, Fukushima & Sekiguchi, 2010). Site-directed mutagenesis also revealed that only the first Histidine in the HLH motif and a Histidine occurring in the sixth β-sheet are required for CwlP endopeptidase activity, although substitutions within the HxGxD motif weakened activity (Sudiarta, Fukushima & Sekiguchi, 2010). Instead, *B. subtilis* CwlP appears to be co-ordinated by Calcium and Cobalt co-factors (Sudiarta, Fukushima & Sekiguchi, 2010).

1.5.6 *Haemophilus influenzae* encodes a non-classical homologue of EnvC

Non-typable *Haemophilus influenzae* (NTHI) is an opportunistic pathogen for which three M23 endopeptidases were recently identified, two of these are putatively degenerate orthologues of *E. coli* EnvC and NlpD with corresponding domain architecture (Ercoli et al., 2015). These bacteria also carry an additional putatively active endopeptidase, YebA with an N-terminal trans-membrane and LysM domain in addition to a zinc-binding, M23 endopeptidase domain (Ercoli et al., 2015). As observed for other NlpD orthologues, NTHI NlpD localises near the division septum outside of the cell, YebA occurs in the outer membrane fraction, likely anchored by the transmembrane domain, EnvC is found in the periplasm (Ercoli et al., 2015). Although YebA lacks features of a cell division M23 endopeptidase, having intact zinc-binding motifs, deletion of *yebA* caused a cell separation defect which phenocopied that of NTHI *nlpD* deletion (Fig. 1.11) (Ercoli et al., 2015). Single *yebA* or *nlpD* deletion caused NTHI cell separation defects (Fig. 1.11) (Ercoli et al., 2015), though this only occurred in *E. coli* or *V. cholerae* when multiple activators were deleted collectively (Uehara, Dinh & Bernhardt, 2009; Möll et al., 2014) Also, NTHI EnvC appears to play a completely different physiological role than other EnvC

orthologues, as deletion had no effect on NTHI cell division but rather disrupted outer membrane vesicle transportation of proteins forming part of the outer membrane protein chaperone complex (Fig. 1.11) (Ercoli et al., 2015). Loss of NTHI *envC* further negatively impacted NTHI virulence via reducing adhesion to host cells, impairing biofilm formation and increasing susceptibility to host serum, indicative of weakened persistence against host defences (Fig. 1.11) (Ercoli et al., 2015).

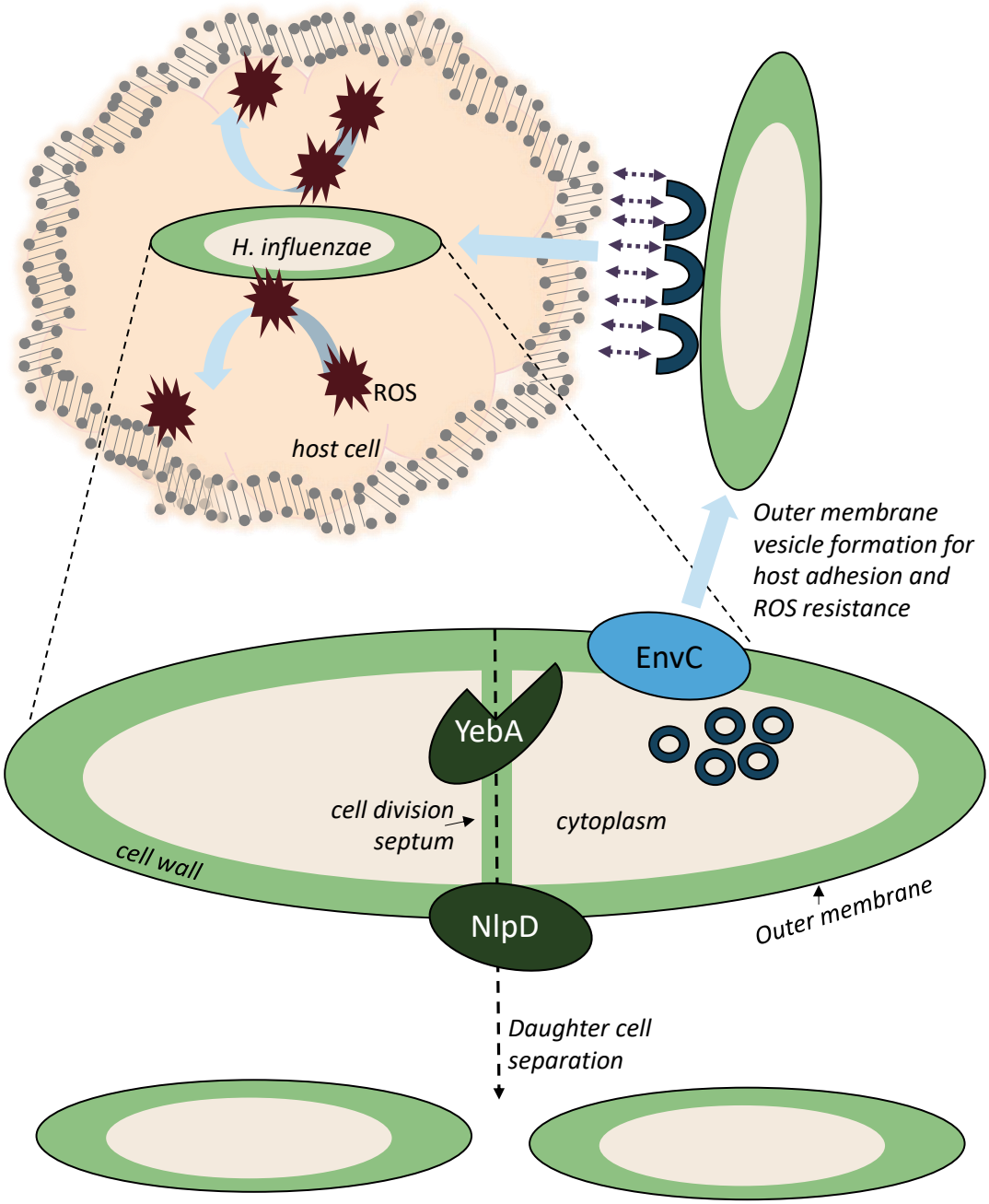

Figure 1.11 M23 endopeptidases required for cell division and virulence in *H. influenzae*. Degenerate NlpD and active YebA are required for cell separation. The EnvC homologue is non-classically important for outer membrane vesicle formation (teal) which is associated with adherence to host cells (purple arrows) and resistance to host defence (maroon).

1.5.7 *Yersinia pestis* NlpD is required for pathogenesis in mice

Yersinia pestis is the causal agent of bubonic plague which rapidly caused mortality in millions in global outbreaks throughout history. The M23 endopeptidase NlpD is encoded within *pcm* locus required for virulence, but *nlpD* appears to be the only gene in the locus to contribute to virulence (Tidhar et al., 2009). Instead, deletions of the neighbouring genes, *pcm* and *rpoS* caused hypervirulence (Tidhar et al., 2009). A *Y. pestis* Δ*nlpD* mutant, despite being defective in cell separation like many of the NlpD orthologues, could successfully infect mice but failed to cause disease, making a *nlpD*-depleted strain promising as a vaccine candidate (Fig. 1.12) (Tidhar et al., 2009). Similar to other M23 endopeptidases, *Y. pestis* NlpD is required for protein translocation, in particular, the twin-arginine transport (TAT) system (Fig. 1.12) (Tidhar et al., 2019).

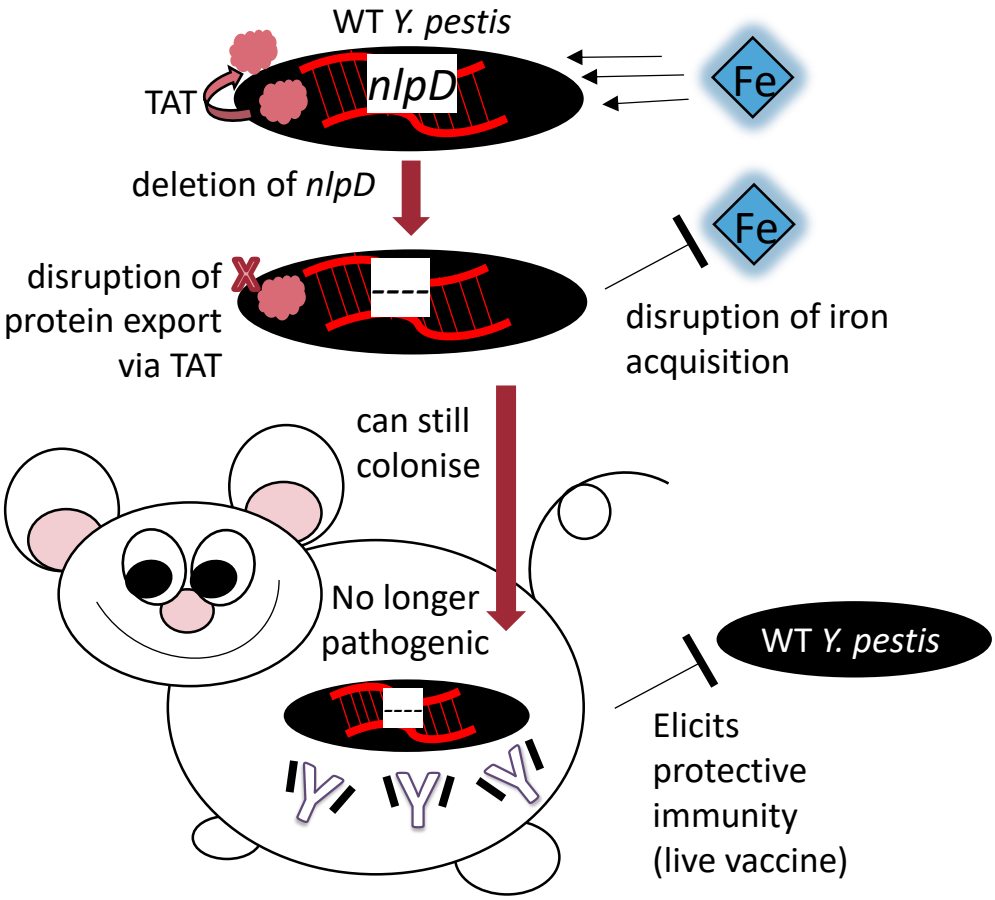

Figure 1.12 The M23 endopeptidase encoding gene, *nlpD* for development of a novel *Yersinia pestis* vaccine in a Bubonic plague mouse model.
A *Y. pestis nlpD* deletion mutant is impaired in iron acquisition, TAT export and pathogenesis but is still infective, serving as a highly immunogenic, live vaccine candidate for prevention of Bubonic Plague.

The lack of NlpD prevents development of bubonic plague through inefficient colonisation and dissemination in mouse organs, but allows *Y. pestis* to persist in the mouse host long

enough to elicit an immune response (Fig. 1.12) (Tidhar et al., 2009). As such, mice previously infected with *Y. pestis* Δ*nlpD* could survive subsequent infection with wild-type *Y. pestis* (Fig. 1.12) (Tidhar et al., 2009). Protective efficiency against wild-type increased with increasing Δ*nlpD* load (Tidhar et al., 2009). NlpD is also associated with gene modulation for iron acquisition (Fig. 1.12) (Tidhar et al., 2019). This correlated with the highly protective efficacy of a vaccine candidate, EV76, which is a live vaccine consisting of *Y. pestis* without the *pcm* locus, where vaccination was associated with enhanced antibacterial, iron limitation (Zauberman et al., 2017).

1.6 Hypothesis

Drugs targeting PG, the core of the *M. tuberculosis* cell wall, are promising as PG provides an impenetrable layer limiting other drugs from reaching targets and does not occur in humans. To identify novel drug targets, research is required to better understand PG as a structure, and how it is maintained and remodelled during growth, division and stress. The M23 endopeptidases required for PG remodelling and maintenance in multiple bacterial pathogens remain unexplored in *M. tuberculosis* as these homologues have never been characterised before. It is hypothesised here that *M. tuberculosis* encodes M23 endopeptidases that function in PG remodelling, processes that are important for cell division.

1.7 Aims

The aim of this study is to identify and functionally characterise M23-endopeptidase encoding genes in *M. tuberculosis*.

1.8 Objectives

- Identify putative genes encoding an M23 endopeptidase domain in the *M. tuberculosis* H37Rv genome based on homology to the well-characterised *E. coli* amidase activators
- Determine growth phase dependent transcription profiles of M23-endopeptidase encoding genes as prediction of *M. tuberculosis* M23 endopeptidase function
- Deletion of putative M23 endopeptidase-encoding genes from the *M. tuberculosis* genome and phenotyping cell wall and PG alterations in the deletion strains

2 Materials and methods

Various *in silico* databases and *in vitro* molecular techniques were employed to characterise the M23 endopeptidases of *M. tuberculosis*. The research approach is outlined in Figure 2.1.

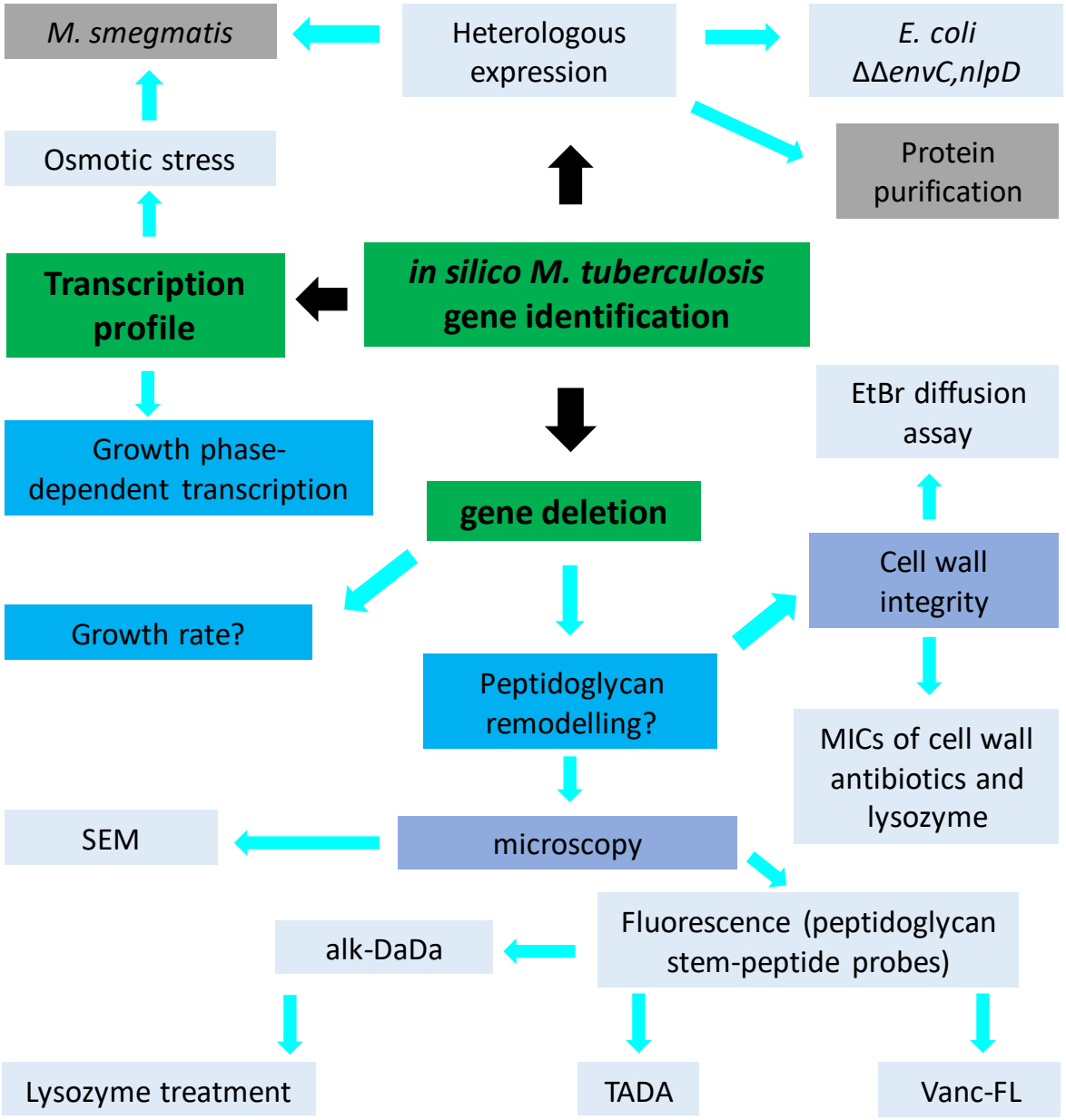

Figure 2.1 Outline of research approach and methods for characterisation of putative M23 endopeptidase genes in *M. tuberculosis.*
The main approach is emphasised in bold, key experiments are indicated in blue, additional experiments of interest are indicated in grey.

2.1 *in silico* analyses

Starting with BLAST identification of putative M23 endopeptidase genes in the *M. tuberculosis* genome, various databases and tools (Table 2.1) were used for further structural and functional predictions, for which the workflow is summarised in Figure 2.2.

Table 2.1 Citations for databases, software and online tools contributing to bioinformatics analyses.

Title	Website	citation
BLAST	http://blast.ncbi.nlm.nih.gov/Blast.cgi	(Altschul et al., 1990)
Tuberculist	http://tuberculist.epfl.ch/	(Kapopoulou, Lew & Cole, 2011)
PHMMER	http://www.ebi.ac.uk/Tools/hmmer	(Eddy, 1998)
Uniprot	http://www.uniprot.org/uniprot/	(Bateman et al., 2015)
PFAM	http://pfam.xfam.org/	(Finn et al., 2014)
SignalP 3.0	http://www.cbs.dtu.dk/services/SignalP-3.0/	(Bendtsen et al., 2004)
Clustal Omega	http://www.ebi.ac.uk/Tools/msa/clustalo/	(Sievers et al., 2011)
Swiss Model PDB	http://swissmodel.expasy.org/repository/	(Kiefer et al., 2009)
Swiss PDB Viewer	http://www.expasy.org/spdbv/	(Guex & Peitsch, 1997)
T-Rex online	http://www.trex.uqam.ca/	(Alix, Boubacar & Vladimir, 2012)

2.1.1 BLAST analysis and M23-endopeptidase gene identification

The tBLASTn database hosted by NCBI was used to identify genes in the *M. tuberculosis* H37Rv genome putatively encoding M23 endopeptidases. Template protein sequences used were either *E. coli* amidase activator EnvC (NP_418070.6) or NlpD (NP_417222.1), and the nucleotide query database was specified as Bacterial and sub-specified as *M. tuberculosis* H37Rv. Hits from tBLASTn were then cross-checked in the Tuberculist genome to study any pre-existing annotations for the identified genes. Tuberculist provides a link to the pFAM secondary structure database for the respective gene, which was used to confirm if the hits identified had predicted M23-endopeptidase domains and any accessory domains. Tuberculist also provides the protein sequences for any gene queried. The protein sequences of the tBLASTn hits were used for subsequent *in silico* analyses described below, as well as to perform a second tBLASTn to cross-check the hits orthologous to *E. coli*. This cross-reference tBLASTn step helped to confirm the initially identified targets and to identify any further putative *M. tuberculosis* M23 endopeptidases not homologous to the *E. coli* amidase activators.

2.1.2 Homology modelling

To confirm the presence of a putative M23 endopeptidase domain in the tBLASTn-identified homologues, homology modelling was performed, which predicts the secondary structure of an amino-acid sequence of a protein, for which no crystal structure is available, based on highest sequence homology to previously crystalised proteins uploaded to the Swiss Protein Database (Guex, Peitsch & Schwede, 2009; Bertoni et al., 2017; Bienert et al., 2017; Waterhouse et al., 2018; Studer et al., 2020). The model could be viewed and analysed thereafter using the Swiss PDB viewer. For this amino-acid

sequences obtained from Tuberculist for each of the putative M23 endopeptidases was used as the template sequence. A graphic model for each homologue was generated in Swiss PDB viewer.

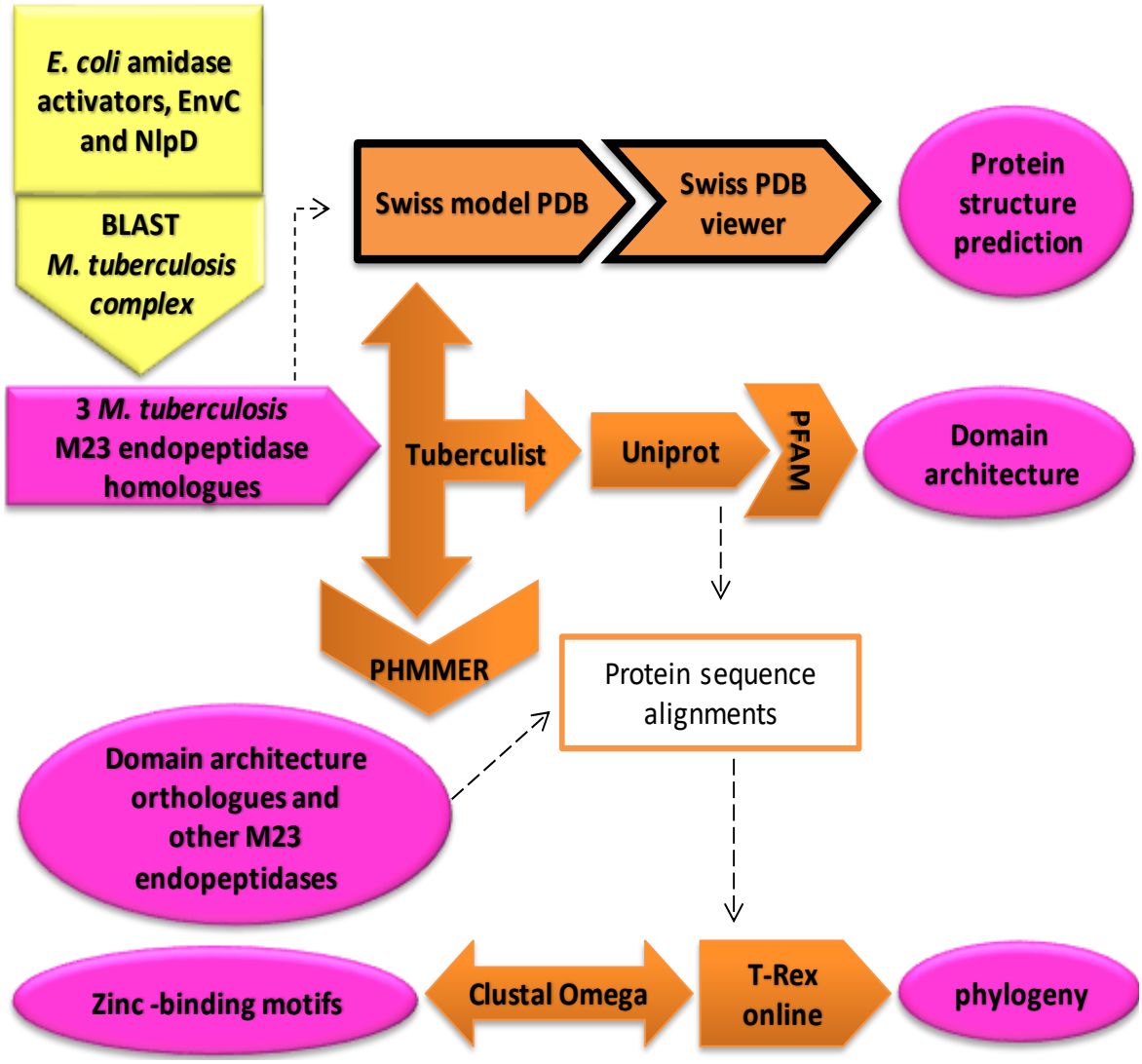

Figure 2.2 Schematic diagram of online tools (orange) used in identification and analysis of *M. tuberculosis* M23 endopeptidase homologues. Information garnered from the various tools is outlined in pink. Yellow indicates input sequences.

2.1.3 Signal peptide prediction

The *E. coli* EnvC and NlpD amidase activators function in cell division via signal peptide-directed localisation to the cell division stem peptide. Prediction of signal peptides was compared for the *M. tuberculosis* homologues using the pFAM annotations linked to Tuberculist and using the SignalP 3.0 database. SignalP 3.0 uses multiple algorithms, specific to either Gram-positive or Gram-negative bacteria, to predict the likelihood of a signal peptide, peptide cleavage site and/or transmembrane domain for an amino-acid query sequence. All algorithms for both Gram positive and Gram negative were compared

for the *M. tuberculosis* homologues, since the complex cell wall structure of mycobacteria equates to gram-variability.

2.1.4 Characterisation of the zinc-binding motifs in the putative *M. tuberculosis* M23 endopeptidases

Reviewing the literature of previously characterised M23 endopeptidases suggests that the presence or lack of zinc co-ordination amino-acids, HxGxD and HxH, in the catalytic site of the M23 endopeptidase domain appears to polarise the function of these proteins as active PG remodelling enzymes or degenerate, regulatory proteins. Multiple amino-acid sequence alignment was performed, using Clustal Omega between the putative M23 endopeptidase domains of the *M. tuberculosis* homologues and various characterised M23 endopeptidases to determine which *M. tuberculosis* residues align with the HxGxD and HLH motif of *S. aureus* LytM. Amino-acid sequences of non-mycobacterial M23 endopeptidase domains were obtained from NCBI.

2.1.5 Phylogeny of bacterial PG remodelling enzymes

The mechanism of M23 endopeptidase catalysis, as reviewed in the literature, relies on zinc co-ordination, necessitating the presence of conserved zinc-residues between M23 endopeptidases and other PG remodelling enzymes, which could amount to overlapping structural homology between different PG hydrolases. In addition, some M23 endopeptidases are co-opted to function like other hydrolases, for example, the observed carboxypeptidase activity of *B. subtilis* CwlP (Sudiarta, Fukushima & Sekiguchi, 2010) or *V. cholerae* ShyA (Dörr et al., 2013). As such, multiple sequence analysis was performed between proteins of various mycobacterial PG remodelling enzymes, various characterised M23 endopeptidases and the putative M23 endopeptidases of *M. tuberculosis*. The multiple sequence alignment was then processed into a cladogram to study structure-function relatedness of the various enzymes as a prediction of *M. tuberculosis* M23 endopeptidase function. The various bacterial M23 endopeptidase proteins were selected from published literature or based on orthologues identified in the PHMMER database. To obtain PHMMER orthologues, the amino-acid sequence of the most conserved putative *M. tuberculosis* M23 endopeptidase was entered as the template sequence. Protein sequences of the various enzymes were obtained from NCBI Protein linked to literature in PubMed, or the UniProt database.

2.1.6 Patterns of conservation of M23 endopeptidases in mycobacteria

Tuberculist and the PHMMER database was used to identify homologues of the putative *M. tuberculosis* M23 endopeptidases in other mycobacterial species. PFAM was used to predict the protein domain architecture of the identified homologues.

2.2 General techniques

2.2.1 Bacterial growth

Bacterial strains used and generated in this study are described in Table 2.2, 2.3 and 2.4 and were grown as described below.

2.2.1.1 *Mycobacterium tuberculosis*

In a pressure-regulated, BSLIII facility, strains of *M. tuberculosis* H37Rv(s) (Table 2.2) were grown in vented, sealed-cap culture flasks or 9 mm petri dishes containing either Middlebrook 7H9 (Appendix A1) broth supplemented with oleic acid-albumin-dextrose-catalase (OADC) (10%), glycerol (0.2%) and Tween-80 (0.2%) or Middelebrook 7H11 solid media (Appendix A1) supplemented with OADC (10%), and glycerol (0.5%). 7H9 and 7H11 were further supplemented with antibiotics [Kanamycin Sulphate (25 µg/ml) and/or Hygromycin B (50 µg/ml)] where applicable (Table 2.2). Cultures were grown at 37°C. Aliquots of broth (1 ml) were cryostored in o-ring, cryotubes at -80°C.

Table 2.2 Strains of *M. tuberculosis* used and generated in this study.

Strain	Description	Reference
H37Rv(s)	*M. tuberculosis* wild-type parent strain	Common lab stock
H37Rv(s)ΔRv0950c	Derivative of H37Rv(s) carrying an unmarked, in-frame deletion of region 1060692-1061627 of Rv0950c	This study
H37Rv(s)ΔRv0950c *lysU*::pTTp1b-^{NP}Rv0950c	Derivative of the Rv0950c deletion mutant strain complemented with Rv0950c and putative native promoter off the pTTp1b backbone at the *attB* region of *M. tuberculosis lysU*, Km^R	This study
H37Rv(s)ΔRv0950c *lysU*::pTTp1b	Derivative of the Rv0950c deletion mutant strain complemented with empty pTTp1b backbone, Km^R	This study
H37Rv(s)ΔRv0950c, Rv2891::p2NilΔRv2891	Derivative of the Rv0950c deletion mutant strain carrying a single cross-over with p2NilΔRv2891 at the Rv2891 locus in the Rv0950c deletion mutant strain, Km^R	This study
H37Rv(s)ΔRv2891	Derivative of H37Rv(s) carrying an unmarked, in-frame deletion of region 3200382-3200789 of Rv2891	This study

^{R} antibiotic resistance cassette, Km: Kanamycin, Hyg: Hygromycin, ^{NP}native promoter

2.2.1.2 *Mycobacterium smegmatis*

In a BSLII facility, strains of *M. smegmatis* mc^2155 (Table 2.3) were grown in Erlenmeyer flasks or 9 mm petri dishes containing either Middlebrook 7H9 broth (Appendix A1) supplemented with glucose salts (0.5%), glycerol (0.2%) and Tween-80 (0.2%) or Middlebrook 7H10 solid media (Appendix A1) supplemented with glycerol (0.5%) and glucose-salts (0.5%). 7H9 and 7H10 were further supplemented with antibiotics [Kanamycin Sulphate (25 µg/ml) and/or Hygromycin B (50 µg/ml)] where applicable (Table 2.3). Cultures were grown at 37°C with/and shaking (100 rpm). For heterologous overexpression studies, 7H10 was replaced with 7H11 maintaining the same supplements according to the mycobacterial protein fragment complementation (MPFC) assay protocol (Singh et al., 2006). Aliquots of broth (1 ml) were cryostored in cryotubes at -80°C.

Table 2.3 Strains of *M. smegmatis* used and generated in this study.

Strain	Description	Reference
mc^2155	Wild-type parent strain	Common lab stock
mc^2155::pUB400	Derivative of mc^2155 carrying empty, integrating, Hsp60 promoter vector pUAB400, Km^R	This study
mc^2155::pUB400-Rv0950c FL	Derivative of mc^2155 carrying full length *M. tuberculosis* Rv0950c in the pUAB400 backbone, Km^R	This study
mc^2155::pUB400-Rv0950c N'	Derivative of mc^2155 carrying the Rv0950c N terminus in the pUAB400 backbone, Km^R	This study
::pUB400-Rv0950c C'	Derivative of mc^2155 carrying the Rv0950c C-terminal M23 endopeptidase domain in the pUAB400 backbone, Km^R	This study

^{R} antibiotic resistance cassette, Km: kanamycin, Hyg: Hygromycin

2.2.1.3 *Escherichia coli*

In a BSLII facility, strains of *E. coli* DH5α (Table 2.4) were grown in Erlenmeyer flasks or 9 mm petri dishes containing Luria-Bertani (LB) broth (Appendix A1) or solid agar (LA) (Appendix A1) respectively supplemented with antibiotics [Kanamycin Sulphate (50 µg/ml), Hygromycin B (200 µg/ml), and/or Ampicillin (100 µg/ml)] where applicable (Table 2.4). Wild-type or transformants carrying vectors <5 kbps were grown at 37°C, with/and shaking (100-250 rpm). Transformants carrying vectors >5kbps were grown at 30°C, with/and shaking (100-250 rpm). Aliquots of broth (1 ml) were cryostored in 33% glycerol in cryotubes at -80°C.

Table 2.4 Strains of *E. coli* used and generated in this study.

Strain	Description	Reference
DH5α	Host strain for cloning and vector propagation	Common lab stock
DH5α BL21Star	IPTG-inducible derivative of DH5α lacking *ion* and *ompT* proteases for enhanced protein expression (gentoype F-ompT hsdSB (rB-, mB-) galdcmrne131 (DE3))	ThermoFisher
DH5α BL21Star::pET29a-Rv0950c	Derivative of BL21Star carrying C-terminal His-tagged Rv0950c in the pET29a vector, Km^R.	This study
DH5α BL21Star::pET24a-Rv0950c	Derivative of BL21Star carrying *E. coli* codon-harmonised, C-terminal His-tagged Rv0950c in the pET24 vector, Km^R.	This study
K12Δ*lacizya*::Δ*envC*, Δ*nlpD*	*E. coli* cell division-defective strain lacking *envC* and *nlpD* genes, Km^R.	Uehara et al., 2009
K12Δ*lacizya*::Δ*envC*, Δ*nlpD*::pSE100-Rv0950c	*E. coli* cell division-defective strain lacking *envC* and *nlpD* genes complemented with *M. tuberculosis* Rv0950c in the pSE100 high-copy vector backbone, Km^R, Hyg^R.	This study
K12Δ*lacizya*::Δ*envC*, Δ*nlpD*::pSE100	*E. coli* cell division-defective strain lacking *envC* and *nlpD* genes complemented with the empty pSE100 high-copy vector backbone, Km^R, Hyg^R.	This study

^{R} antibiotic resistance cassette, Amp: Ampicillin, Km: Kanamycin, Hyg: Hygromycin

2.2.2 DNA isolation

2.2.2.1 Large-scale genomic DNA extraction

The Cetyl Trimethyl Ammonium Bromide (CTAB) method was used for extraction of high quality, high yeild DNA from mycobacteria. For this, the liquid culture of the required strain of *M. tuberculosis* was grown to stationary phase. The culture was separated into 10 ml aliquots and cells harvested by centrifugation at 4000 rpm for 10 min. The supernatant was discarded, and cell pellets were resuspended in 1X Tris-EDTA (TE) buffer (500 µl). Suspended cells were heat killed at 80°C for 60 min. Heat killed cells were cooled on ice and mixed with 10 mg/ml lysozyme (Roche) (70 µl). Lysozyme treatment was performed at 37°C, for 60 min. The lysate was incubated with 10 mg/ml Proteinase K (Roche) (50 µl) and 10% SDS (70 µl) at 65°C for 2 hours. Prewarmed 5M NaCl (100 µl) was added, followed by a prewarmed mixture of CTAB-NaCl (80 µl), mixed and incubated at 65°C, for 10 min. Following CTAB treatment, Chloroform:isoamyl alcohol (24:1) was added to an equal volume and the suspension was centrifuged for phase separation at 13 000 rpm for 5 min. The aqueous DNA layer (up to 650 µl) was carefully pipetted into a clean tube containing isopropanol (100%, 650 µl) to precipitate the DNA. The precipitate was centrifuged at 13000 rpm, for 20 min, the supernatant was discarded, and the pellet gently washed in 70% EtOH. The precipitate was centrifuged again at 13

000 rpm for two min, the supernatant discarded, and the pellet was dried by SpeedVac at 65°C. The dried pellet was stored at -20°C before use or immediately resuspended in TE buffer at 65°C. Intact quality of the resuspended DNA was confirmed by agarose gel electrophoresis, with 0.8% agarose at 80V, appearing as a single, bright band of ~20 Kbp, as opposed to smearing or laddering, indicative of fragmented or degraded genomic DNA.

2.2.2.2 Small-scale genomic DNA extraction

The colony boil DNA extraction method was used for procedures requiring small amounts of template DNA, such as genotyping transformants by PCR. For this, all or part of a respective colony was scraped off the agar and homogenised in sterile-distilled H_2O (sdH_2O) (100 µl). The homogenate was centrifuged at 13 000 rpm for 1 min, the supernatant discarded, and the pellet resuspended in 100% chloroform (50 µl) and sdH_2O (50 µl). The suspension was heated at 95°C for 5 min. The heated suspension was centrifuged for phase separation at 13 000 rpm for 5 min. The aqueous DNA phase was carefully transferred to a new tube and stored at 4°C or -20°C for short term, or long term respectively.

2.2.2.3 Large-scale plasmid DNA extraction

2.2.2.3.1 Large-scale, manual, plasmid isolation for cloning.

Broth culture (20-50 ml) was centrifuged at 4000 rpm for 10 min and resuspended in Solution I [Tris-HCl, EDTA and glucose] (1 ml) and 10 mg/ml RNase A (5 µl) by vortexing to homogeneity. Solution II [SDS, NaOH] (2 ml) was added and mixed by inverting 6-8 times, followed by incubation at room temperature for up to 3 min. Ice-cold Solution III [KCH_3COOH + acetic acid] (1.5 ml) was added and mixed by inverting. Following addition of the 3 buffers, the preparation was centrifuged at 4000 rpm for 10 min. The clear supernatant was added to an equal volume of isopropanol, split into 1.5 ml aliquots and the DNA harvested at 13 000 rpm for 20 min. The supernatant was gently discarded and washed in 70% EtOH, followed by centrifugation at 13 000 rpm for 2 min. The precipitate was dried using a vacuum concentrator for 10 min. The DNA pellet was stored at -20°C until required. Once required, the DNA was resuspended in sdH_2O (90 µl) and quality and quantity assessed by EtBr-agarose gel electrophoresis. Poor quality plasmid DNA was further purified by salt-EtOH precipitation (2.2.5).

2.2.2.3.2 Large-scale, column affinity plasmid isolation for cloning and electroporation

Plasmid DNA required for sensitive procedures, such as electroporations and sequencing, in which high salt contamination can inhibit efficiency, was extracted using the Nucleobond Xtra Maxi column affinity extraction procedure, according to the manufacturer's recommendations (MN). In summary, *E. coli* liquid culture transformed with the required plasmid was grown for two days at 30°C. The liquid culture (50 ml) was centrifuged at 4000 rpm, 4°C for 10 min, and resulting cell pellet resuspended in RES buffer (12 ml) pre-supplemented with provided RNase A. Buffer LYS (12 ml) was added and inverted, incubated at Room temperature for 5 min. Buffer NEU (12 ml) was added and mixed by inversion. The suspension was centrifuged at 4000 rpm, 4°C for 10 min. Buffer EQU (25 ml) was applied to the Nucleobond Xtra Column followed by loading the supernatant. The column was washed twice with WASH buffer (8 ml). The column was placed over a 50 ml falcon tube of 100% isopropanol (5 ml), Buffer ELU (5 ml) was added to column to elute plasmid DNA into isopropanol. The eluate was then aliquoted into ~6 x 1.5 ml Eppendorf tubes and centrifuged at 13 000 rpm for 20 mins. The supernatant was poured off and the precipitate was washed in 70% Ethanol (1 ml) followed by centrifugation at 13 000 rpm for 2 min. The supernatant was discarded, and the pellet vacuum dried in a SpeedVac. To resuspend the plasmid DNA, each pellet was resuspended in sdH_2O (~15 ul) pre-warmed to 65°C, pooled (~90 µl). The extract was checked by DNA electrophoresis to detect the 3 conformations of plasmid DNA (coiled, linear and super-coiled) with a linear band at the expected size alongside a DNA molecular weight marker (Roche) and further purified by salt-EtOH precipitation where necessary.

2.2.2.4 Small-scale plasmid DNA extraction

2.2.2.4.1 Small-scale, manual, plasmid isolation for screening putative, recombinant plasmids.

Broth culture (1-2 ml) was centrifuged at 13000 rpm, 1 min and resuspended in solution I [Tris-HCl, EDTA and glucose] (100 µl), by vortexing to homogeneity. Solution II [SDS, NaOH] (200 µl) was added and mixed by inverting 6-8 times, incubated at room temperature for up to 3 min. Ice-cold Solution III [KCH_3COOH + acetic acid] (150 µl) was added and mixed by inverting. Preparations were kept on ice for 10 min while inverting at intervals before spinning down at 13 000 rpm for 10 min. The clear supernatant was

transferred to a 1.5 ml test tube containing 10 mg/ml RNase A (2 µl) and incubated at 42°C for 20 min. RNase activity was inactivated by addition of isopropanol (630 µl) and spun at 13000 rpm for 20 min. The supernatant was gently discarded, and the pellet washed in 70% EtOH and centrifuged again at 13000 rpm for 2 min. The supernatant was discarded, and the pellet dried using a vacuum concentrator for 10 min. The DNA was stored at -20°C until required. Once required, the DNA was resuspended in sdH_2O (30 µl) and quality and quantity assessed by EtBr-agarose gel electrophoresis as described in section 2.2.2.3.2.

2.2.2.4.2 Small-scale, column-affinity plasmid isolation for cloning and sequencing.

Broth culture (4-10 ml) was split into 2 ml aliquots and processed using the Qiagen mini-plasmid isolation kit according to the instructions provided. Briefly, cultures were centrifuged at 13 000 rpm for 1 min and resuspended in buffer P1. Lysis buffer P2 was added to the suspension before inverting tubes and incubated at room temperature for 2-3 min. Buffer N3 was then added and mixed by inverting. The suspension was centrifuged at 13 000 rpm for 10 min and the supernatant applied to the spin column and centrifuged at 13000 rpm for 1 min. The column was washed twice with buffer PE. Plasmid was eluted in TE buffer supplied with the kit and quality and quantity assessed by EtBr-agarose gel electrophoresis as before.

2.2.2.5 Salt-EtOH precipitation

Sodium acetate, 1/10 vol (3M, pH 5.2) and ice-cold 100% Ethanol (3.5X vol.) was added to the DNA and incubated either at -80°C for 10 min.; -20°C for 30-60 min. or 4°C O/N. DNA was centrifuged at 13 000 rpm for 15 min. and washed in 70% EtOH at 13000 rpm for 1 min. The precipitate was dried using a vacuum concentrator for 10 min and stored/resuspended as described previously.

2.2.3 Molecular cloning

Generally, genetic manipulations were performed by cloning one or two DNA fragments of interest into a suitable plasmid backbone (Appendix A2). Plasmids used in this study are described in Table 2.5. DNA fragments were generally obtained by PCR amplification using primers designed with flanking restriction recognition sites plus clamp sequence, which correspond to the selected restriction sites encoded in the plasmid backbone. After

PCR amplification, the amplicon was purified from PCR reaction components by salt-EtOH precipitation and resuspended in a volume of sdH_2O suitable for subsequent restriction digestion. Concurrently, suitable vector DNA was extracted, and further purified by salt-EtOH precipitation. Plasmid DNA and fragments were appropriately digested using the selected restriction enzymes (section 2.2.4). Digestion was confirmed by agarose gel electrophoresis. Digested plasmid DNA was then dephosphorylated as follows: in a final volume of 25 µl, to the plasmid DNA restriction digestion reaction, Antarctic Phosphatase buffer (NEB) was added to a 1X concentration as well as sdH_2O and mixed before adding Antarctic Phosphatase (NEB) (5 U) followed by incubation at 37°C, for 30 min. After 30 min of digestion, additional Phosphatase was added (5 U) for a further 30 min. The phosphatase reaction was inactivated at 65°C for 20 min. Digested fragments and dephosphorylated vector were separately purified by salt-EtOH precipitation and resuspended in sdH_2O (10-30 µl). The quantity of purified vector and fragment was estimated from agarose gel electrophoresis alongside an appropriate DNA molecular weight marker (Roche).

For ligation of vector and fragments, vector and DNA fragments were added at molecular equivalent ratios of 1:1; 1:3 and/or 1:5. Molecular equivalent of 1:1 was calculated as follows:

$$I(ng) = \frac{I(bp) \times V\ (ng)}{V\ (bp)}$$

where I refers to insert (fragment), V refers to Vector, bp refers to the base pair size and ng refers to weight in nanograms. Vector weight is generally accepted as 50 – 100 ng. For three-way ligation, each insert was calculated separately.

The above-determined amounts of vector and insert DNA were mixed together with sdH_2O in a final ligation reaction volume of 20 – 30 µl. T4 ligase buffer (NEB) was added to a final concentration of 1X and the reaction mixed again. T4 Ligase (NEB) (200-400 U) was added and the ligation incubated for 60 min at 16-25°C. Inactivation of ligation was performed at 72°C for 10 min and cooled on ice before transformation into *E. coli* DH5α (section 2.2.6). Control ligation reactions excluding insert DNA included (I) "vector only" control, which indicates the efficiency of the phosphatase reaction and predicts how many transformants may not contain inserts; and (II) where sufficient vector was available, a "cut and ligate" control, for phosphorylated, linearised vector, indicating the efficiency of the ligation reaction. Transformation controls are described under bacterial transformation of *E. coli* (section 2.2.6.1).

Following plating and incubation of transformants, colonies, displaying phenotypes for selectable markers (selected antibiotic resistance and/or *lacZ* expression) were inoculated into microculture tubes (5 ml) in LB broth (1.5 ml) supplemented with appropriate antibiotics for selection and incubated for 2 days at 30°C. Inoculations (1 ml) were prepared for small-scale DNA extraction, while the remainder of the culture was stored at 4°C for bulk sub-culture upon confirmation of the correct construct. Plasmid extracts of putative constructs were mapped by restriction digestion analysis to confirm successful cloning.

2.2.4 Restriction endonuclease digestion

A maximum of 1 µg DNA was mixed with the appropriate volume of sdH_2O and the specified restriction buffer to a final concentration of 1X. The mixture was cooled on ice before adding the restriction enzyme (NEB and Roche Biosciences) (0.5 – 1 µl). The restriction digestion reaction was incubated for at least 60 min at 37°C (unless otherwise specified by the manufacturer) and inactivated either by heat (at the temperature specified by the manufacturer) or by inactivation of the restriction enzyme with loading dye to a final concentration of 1X. Restriction digestions were mapped by agarose gel electrophoresis alongside undigested DNA as a negative control.

2.2.5 PCR

Two general methods were used depending on the subsequent application. Primers for PCR were designed with the aid of Primer3, specifying optimal GC content of 50-80% as mycobacterial DNA is GC rich. Primers were synthesised by Inqaba Biotechnologies (Pretoria, South Africa). All PCR reactions were performed using the BioRad T100 thermal cycler.

2.2.5.1 Amplification of inserts for cloning

The high-fidelity polymerase, Q5 (NEB) was used to amplify cloning inserts for genetic manipulation of *M. tuberculosis*. In a final reaction volume of 50 µl, sdH_2O, Q5 Reaction buffer (NEB) (1X), GC Rich solution (NEB) (1X), DMSO (2.5%), dNTPs (200 µM), Forward and Reverse primer (0.3 µM), was combined as a master mix. DNA (1-2 µl) was added on ice, followed by Q5 polymerase (0.2 µl).

Table 2.5 List of bacterial plasmid vectors used in this study.

Vector	Description	Selection	Reference
pBlueScript	Cloning vector with multiple cloning site inside *lacZ* for blue-white selection	Amp^R, *lacZ*	Alting-Mees & Short, 1989
pBlue09US	Rv0950c Upstream region blunt cloned into pBlueScript at *Sma*I	Amp^R, *lacZ*	This study
pBlue28US	Rv2891 Upstream region blunt cloned into pBlueScript at *Sma*I	Amp^R, *lacZ*	This study
pBlue28DS	Rv2891 Downstream region blunt cloned into pBlueScript at *Sma*I	Amp^R, *lacZ*	This study
p2Nil	Vector lacking a mycobacterial *ori*	Km^R	Parish et al., 2000
p2NilΔRv0950c	p2Nil with fusion of Rv0950c upstream and downstream regions for suicide vector-mediated Rv0950c deletion	Km^R	This study
p2NilΔRv2891	p2Nil with fusion of Rv2891 upstream and downstream regions for suicide vector-mediated Rv2891 deletion	Km^R	This study
pGOAL17	vector carrying *Pac*I-flanked *lac_sac* selectable markers to be sub-cloned into p2Nil vectors	Amp^R, *lacZ*, *sacB*	Parish et al., 2000
p2NilΔ09SV	p2NilΔRv0950c suicide vector with pGOAL-17 derived *lac_sac* genes	Km^R, *lacZ*, *sacB*	This study
p2NilΔ28SV	p2NilΔRv2891 suicide vector with pGOAL-17 derived *lac_sac* genes	Km^R, *lacZ*, *sacB*	This study
pTweety (pTTP1b)	Mycobacterial, phage derived, integration vector for genetic complementation at the *attB* region of *M. tuberculosis lysU*	Km^R	Pham et al., 2007
pT09	pTweety with Rv0950c and putative native promoter for genetic complementation	Km^R	This study
pUAB400	Mycobacterial, integrating, hsp60 overexpression vector	Km^R	Singh et al., 2006
pUB09FL	pUAB400 with full length Rv0950c	Km^R	This study
pUB09N'	pUAB400 with Rv0950c N terminus (lacking M23 endopeptidase domain)	Km^R	This study
pUB09C'	pUAB400 with Rv0950c C-terminal M23 endopeptidase domain	Km^R	This study
pSE100	High copy replicating vector with tetracycline operator	Hyg^R	Guo et al., 2007
pSE09	pSE100 with Rv0950c open reading frame and putative ribosome binding site	Hyg^R	This study
pET29a	Vector for S-tagged or His-tagged protein expression in *E. coli* with *lacI* repressor	Km^R	EMD Bioscience
pET09P	pET29a with Rv0950c open reading frame with C-terminal fusion to Hepta-His tag, for Rv0950c expression and purification in *E. coli*	Km^R	This study
pET2409	pET24 expression vector with *E. coli* codon-harmonised, Rv0950c open-reading frame synthesised and cloned as a C-terminal fusion to Hepta-His, for Rv0950c expression and purification	Km^R	This study & GenScript
pMV306H	Mycobacterial, phage-derived integration vector for genetic complementation	Hyg^R	Andreu et al., 2010
pMVRv2891	pMV306 with Rv2891 and putative native promoter for genetic complementation	Hyg^R	This study

^{R} antibiotic resistance cassette. Amp: Ampicillin, Km: kanamycin, Hyg: Hygromycin

For primer optimisation, primer control reactions were included, which exclude either the forward or the reverse primer, for which no product is expected. All runs were performed alongside a No Template Control (NTC) for which DNA was substituted with the same volume of sdH_2O. The thermocycling programme is specified in Figure 2.3. Amplification products were confirmed by agarose gel electrophoresis, based on expected amplicon size, for which PCR reaction (5 µl) was mixed with 6X loading dye (1 µl), and added to the appropriate concentration gel. Amplicons were purified from reaction components by salt-EtOH precipitation.

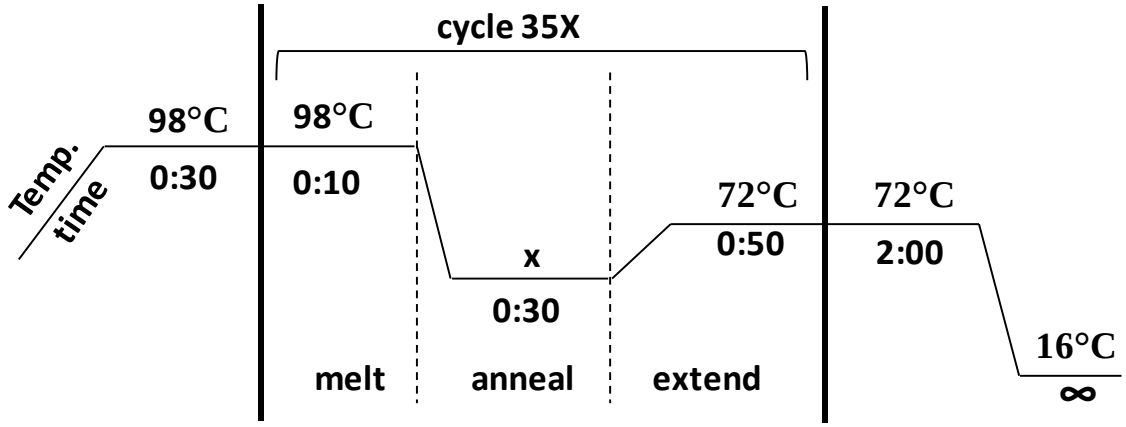

Figure 2.3 Thermocycling parameters for Q5 polymerase (NEB).
x refers to primer pair-specific annealing temperature.

2.2.5.2 PCR for genotyping

Faststart Taq polymerase (Roche Biosciences) was used for large scale (> 10 reactions) genotyping of transformed *M. tuberculosis* or *M. smegmatis*. Based on a reaction volume of 25 µl per reaction, sdH_2O, Faststart PCR buffer (1x) (Roche), GC enhancer (1X) (Roche), $MgCl_2$ (2 mM), dNTPs (200 µM), Fw and Reverse primers (0.4 µm), combined in a master mix based on the number of total reactions. Colony boil DNA (2 µl) was added to master mix (22.8 µl) on ice. Finally, Faststart (1 U) was added to the reaction. All reactions were performed alongside the NTC. Where available, control reactions were included alongside screening reactions. For example, screening for mutant alleles was done alongside reactions with wild-type DNA as a control. The thermocycling programme is outlined in Figure 2.4. Products were screened based on expected amplicon size determined by agarose gel electrophoresis as described below.

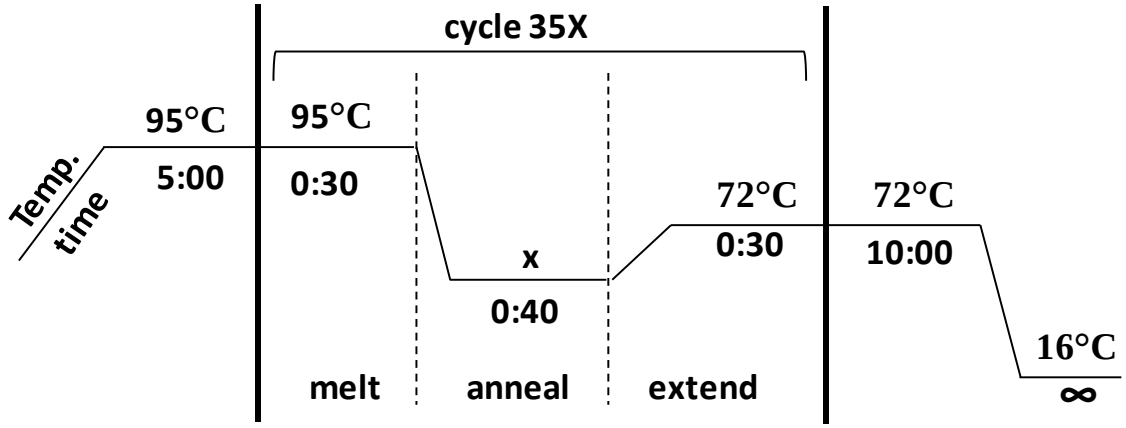

Figure 2.4 Thermocycling parameters for FastStart Taq polymerase (Roche).
x refers to primer pair-specific annealing temperature.

2.2.6 Bacterial transformation

2.2.6.1 *E. coli* ($CaCl_2$ chemical competence)

An *E. coli* freezer stock (1 ml) was inoculated in 5 ml of LB broth overnight, with or without antibiotic (see Table 2.4 for parental strains), at 37°C, with/and shaking at 200 rpm. The pre-culture was sub-cultured into LB (1 ml:100 ml) and incubated for a further 2-3 hours to an OD_{600} 0.4-0.6. The culture was split into aliquots (2x50 ml) and harvested in a pre-cooled centrifuge, at 4000 rpm for 6 min. The supernatant was discarded, and cells were resuspended, gently, in a cool environment, on ice with 100 mM $CaCl_2$ (Appendix A1) (10 ml per pellet) and kept on ice for 20 min. The suspension was centrifuged at 4000 rpm, 4°C, for 6 min. The supernatant was discarded, and the cells resuspended in multiples of 100 µl per transformation, rounded up to the nearest millilitre. DNA (up to 20 µl) was placed in an Eppendorf tube on ice, to which chemically-competent *E. coli* (100 µl) was added, and incubated on ice for 10 min. Heat shock transformation was performed by incubating the mixture at 42°C for 90 seconds, followed by recovery on ice for 5 min. Transformations were rescued in 2XTY (800 µl) (Appendix A1) and incubated at 37°C for 60 min to accommodate one round of *E. coli* DNA replication, before plating a 10 fold dilution series on LB agar supplemented with the appropriate antibiotic and, where necessary, X-Gal (0.004%). Plates were incubated at 30°C or 37°C (see bacterial growth, section 2.2.1.3).

2.2.6.2 *M. tuberculosis* and *M. smegmatis* electroporation

A pre-culture of *M. tuberculosis* was prepared by inoculation of a freezer stock (1 ml) in 7H9 media (7 ml), incubated at 37°C for 3 days (to an OD_{600} of 1.0). The log phase pre-

culture (4 ml) was sub-cultured in duplicate into 46 ml of 7H9 and grown to an OD_{600} of 1.0 for ~ 2-3 days. Glycine (Appendix A1) was added to the sub-culture at a final concentration of 0.25% for ~ 18 hours prior to electroporation. Glycerol washes were then performed, starting with harvesting the culture (2 x 40 ml) at 4000 rpm, for 10 min. The supernatant was discarded, and the cell pellet was washed in 10% glycerol (Appendix A1). The washes were performed as follows: 2 rounds of 40 ml glycerol for each pellet; followed by 20 ml each pooled into 40 ml; followed by 20 ml and then 10 ml; finally resuspending in a maximum of 4 ml 10% glycerol, depending on the number of electroporations, each requiring 200 µl of cells. Washed cells (200 µl) without DNA (no DNA control) were added to a 2 mm GenePulser Cuvette (BioRad) and pulsed using the GenePulser XCell system (BioRad) at 2500 V, 25 µF, 1000 Ω. The time-constant (msec), which should be the highest for the no-DNA control, was noted as a guide for the efficiency of experimental electroporations. Vector DNA was adjusted to aliquots of 1, 3 and 5 µg added to a 1.5 ml tube to a maximum volume of 10 µl. Starting with the lowest concentration of DNA, washed Cells (200 µl) were added to the DNA, mixed by gentle pipetting and transferred to GenePulser cuvette and pulsed as described above. The time-constant was recorded, and cells were immediately rescued by transferring to 800 µl 7H9 in 2 ml, O-ring tubes, incubated at 37°C, overnight to allow for one division cycle. Thereafter, transformations were centrifuged at 4000 rpm, for 5 min and resuspended in 1 ml 7H9. Transformations were then serially diluted, 10-fold (100 µl cells + 900 µl), and the entire 900 µl were plated on 7H11 supplemented with the required antibiotic for selection. Plates were allowed to dry overnight before incubating at 37°C. Colony forming units (CFUs) were monitored at 14 days and once a week thereafter until single colonies, large enough to harvest for genotyping, emerged. Colonies exhibiting the appropriate phenotype for selectable markers encoded by the transformation vector were harvested and homogenised in 1 ml 7H9 to form an inoculum which was pre-cultured in 5 ml 7H9 for ~ 7 days, at 37°C. Thereafter, 100 µl of pre-culture was sampled for colony boil extraction for genotyping by PCR while the remaining culture was transferred to 2 ml O-ring cryovials in 1 ml aliquots and stored at -80°C for later bulk-culture for CTAB genomic DNA extraction and Southern blotting.

For preparation of *M. smegmatis* cells, the same procedure was followed with the following exceptions: 1) Pre-cultures were grown overnight and sub-cultured in 100 ml at 3 different dilutions, in order to harvest cells at OD_{600} = 0.6-0.8 after 3 hours incubation at

37°C, with/and shaking at 100 rpm; 2) cultures were not pre-treated with glycine before glycerol washes; 3) all glycerol washes were performed on ice, centrifugation was at 4°C, and washed cells were kept on ice prior to electroporations; 4) 400 µl of cells were used per electroporation; 5) electroporations were rescued with 2XTY (Appendix A1) and incubated at 37°C for 3 hours or overnight before plating on 7H10; 6) CFUs were monitored after 4 and 7 days of plate incubation at 37°C; 7) Colonies were harvested by scraping half for colony boil extraction, while the other half was concurrently used for pre-culture inoculation.

2.2.7 DNA electrophoresis

Agarose gels were prepared by dissolving agarose to a final concentration of 0.8, 1 or 1.8% in 1X TAE (30 ml) (Appendix A1), boiled to dissolve for ~ 5 min. Once lukewarm, EtBr was added to a final concentration of 0.5 µg/ml (Appendix A1), the solution was mixed by swirling and poured into a gel mould and tray (BioRad). Once set, the gel was placed in a horizontal electrophoresis tank (BioRad) containing pre-cooled 1X TAE. DNA was mixed with 6X loading dye (Appendix A1) to a final concentration of 1X and added to gel lanes alongside the appropriate Lambda phage molecular weight marker (Roche Biosciences) (Appendix A3). Electrophoresis was performed at 90V till the loading dye reached an appropriate migration point. Gels were viewed and captured under UV light using the SynGene G:Box and GeneSnap software (v7.12).

2.2.8 Genotyping by Southern Blotting

Southern-blotting is a method of genotyping DNA by sequence-specific detection of DNA following electrophoresis, by which a chemiluminescent probe of a desired sequence is synthesised and allowed to hybridise to complementary DNA transferred from agarose to a nitrocellulose membrane . Here, Southern blotting via the High Prime DIG probe labelling system (Roche) was used to genotype mutant and genetically complemented strains of *M. tuberculosis*.

2.2.8.1 DIG-probe design and synthesis

Probes were synthesised using a modified PCR reaction using a DIG probe synthesis kit (Roche) by which DIG labelled nucleotides were incorporated into the amplicon during extension. Details of probe design are included in section 2.3.2. The reaction was made up

to a final volume of 50 µl and consisted of Probe synthesis buffer (1X), DIG probe synthesis mix (1X), dNTP stock solution (1X), Fw and Rev primers (1 µM each), template DNA (1 µl) and Enzyme mix (2.6 U). The thermal cycling programme is outlined in Figure 2.5. Successful probe-labelling and yield was confirmed by agarose gel electrophoresis of reaction product (2 µl) combined with loading dye to a final concentration of 1X. Labelling was evident as an upshift in electrophoretic migration compared to the unlabelled control as the DIG nucleotides are larger than unlabelled nucleotides. The probe was stored on ice prior to hybridisation.

2.2.8.2 Southern blotting

Strains were differentiated based on differential positioning of restriction recognition sites within the gene region to be genotyped. Therefore, genomic DNA (2-5 µg) was digested overnight with the appropriate restriction endonuclease in a final reaction volume of 24 µl. The complete reaction product was combined with commercial 6X Loading dye (ThermoScientific) (5 µl), and loaded onto an agarose gel (0.8%), alongside Lambda phage DNA marker IV, which carries a DIG-labelled, 3.1 Kbp fragment. Electrophoresis was carried out at 80V for ~2 hours. The gel was viewed and captured alongside a UV fluorescent ruler to determine the expected migration distance (cm) of DIG-labelled fragments. The agarose gel was then incubated in depurination solution, with/and shaking for 15 min and then rinsed twice in dH_2O. The gel was then incubated in denaturation solution, with/and shaking for 30 min followed by brief storage in 1x TBE (Sigma). While submersed in 1X TBE (Sigma), nitrocellulose membrane (Amersham) (9.0 cm x 4.5 cm) was on top of the gel sandwiched between Whatman paper and sponges. The sandwich was slotted into an electroblotting chamber (BioRad) filled with 1X TBE (Sigma). Electroblotting was thus performed at 500 mA for 2 hours.

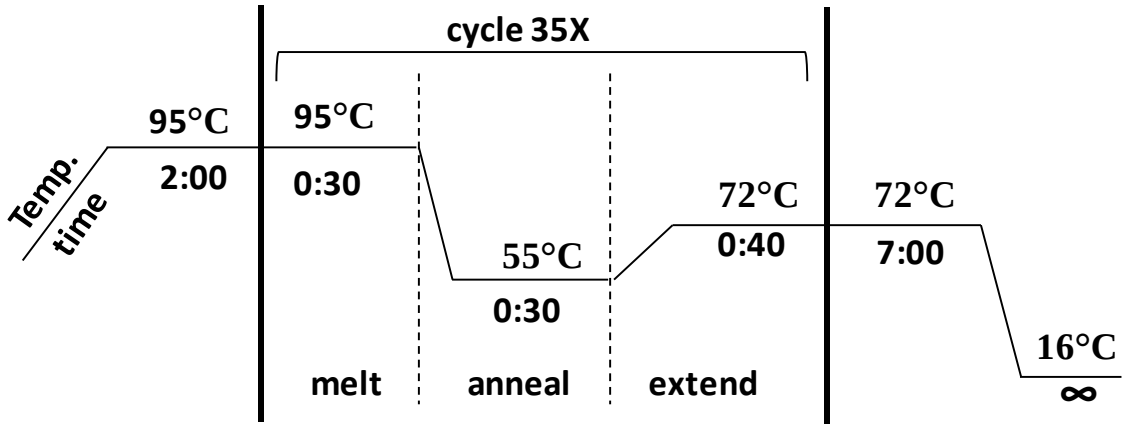

Figure 2.5 Thermocycling parameters for High Prime DIG probe synthesis (Roche).

The membrane was carefully detached from the gel and cross-linked at 2500 mJ/cm^2 before placing in a hybridisation jar with Hybridisation buffer (Hyb) (Roche). Hyb buffer was pre-warmed in a hybridisation jar and Hybaid Micro-4 hybridisation chamber to the appropriate hybridisation temperature at which DIG-labelled probe was melted partially to permit annealing to complementary sequences in the DNA. Hybridisation temperature (T_{opt}) was calculated as follows:

$$Topt = Tm - 20\ to\ 25°C$$

$$\text{and } Tm = 49.82 + 0.41(\%GC) - \frac{600}{L}$$

where %GC is the percentage of G and C nucleotides for the probe sequence, and *L* is the length of the probe sequence (bp).

Once the Hyb buffer was prewarmed to T_{opt} for ~ 20 min, the membrane was added to the hybridisation jar and chamber and incubated for 20 min. For the latter 10 min, the DIG labelled probe was denatured at 95°C for 10 min and cooled on ice before addition to the Hyb buffer in the hybridisation jar. The membrane and probe were co-incubated at T_{opt} overnight.

2.2.8.3 Chemiluminescent detection and capture of DIG-labelled hybrids

Subsequent to hybridisation, the membrane was washed twice in Solution 1 (Appendix A1) for 5 min each, with/and shaking at room temperature, followed by a further 2 washes in Solution 2 (Appendix A1) for 15 min each, at 68°C. Prior to incubation with antibody, the membrane was washed in wash buffer (Appendix A1) for 5 min at room temperature. Thereafter, the membrane was incubated in blocking buffer (Appendix A1) for 30 min, with/and shaking at room temperature. Anti-DIG antibody conjugated to alkaline phosphatase (0.9 U) (Roche) was added to the membrane in blocking solution (Roche) (12 ml) and incubated for 30 min, with/and shaking at room temperature. The DIG antibody would bind to DIG-labelled DNA which is detected when the alkaline phosphatase conjugated to the antibody releases a luminescent phenolate anion from Disodium 3-(4-methoxyspiro {l,2-dioxetane-3,2'-(5'-chloro)tricyclo[3.3.1.13,7]decan}-4-yl) phenyl phosphate (CSPD) (Roche). For the phosphatase reaction, the membrane was placed in a hybridisation bag to which 0.25 mM CSPD (1 ml) was added and incubated at 37°C for 10 min. The luminescence was captured by exposing CL-Xposure X-Ray film (Thermo Scientific) to the membrane, sealed in an X-Ray cassette for at least 60 min. The X-Ray film was developed manually in a dark room, by briefly passing the film through Developer solution (Axim), dH_2O, Fixer solution (Axim) followed by a rinse in dH_2O.

2.3 Specific techniques

2.3.1 Growth phase-dependent transcription analysis

Transcription profiles of putative M23 endopeptidase genes of *M. tuberculosis* were studied in relation to growth phase. For this, RNA was sampled from wild-type *M. tuberculosis* H37Rv(s) during lag phase, early exponential phase, late exponential phase and stationary phase. RNA was converted to cDNA using gene specific reverse primers (Table 2.6), cDNA was quantified using Sybr Green-based qPCR alongside a 10-fold genome equivalent standard dilution. This multi-step analysis is described in detail below.

Table 2.6 Primer sequences for qPCR.

Target	Sequence	Co-ordinates	Product size
Rv0950c	F: TTATCGATGGGGTGTACTGCA	1060990-1061010	
	R1: CAGCAGCTTGACCCACATTC	1060878-1060897	133
	R2: AGCTTGACCCACATTCCGTA	1060882-1060901	129
Rv2891	F: CTGAAGTCCACACCGATAC	3200764-3200782	94
	R: CGGCTTCGTTCACAAATAC	3200839-3200857	
Rv3786c	F: GAGCTCGACGTTGTCTATG	4232637-4232655	139
	R: GGACCTCGAAATGCAGATAA	4232517-4232536	
sigA	F: TGCAGTCGGTGCTGGACAC	3019213-3019231	195
	R: CGCGCAGGACCTGTGAGCGG	3019388- 3019407	

Co-ordinates and sizes in base pairs.

2.3.1.1 RNA extraction

M. tuberculosis cultures were pre-cultured and sub-cultured into 50 ml 7H9 as previously described. At OD_{600} = 0.4, 0.8, 1.2, and 2.0, 10 ml of cells were harvested by centrifuging at 4000 rpm, for 10 min at 4°C. The cell pellets were resuspended in 1 ml Trizol reagent (Sigma) spiked with poly-Aryl carrier (10 µl), transferred to lysing matrix B tubes (MP Bio) and rybolysed three times for 1 min intervals with incubation on ice for two min in between. The lysates were stored at -80°C until harvesting of each growth phase sample was complete. The lysates were thawed and briefly centrifuged, and the aqueous phase was transferred to 1-Bromo-3-Chloropropane (BCP) (Sigma) (150 µl) and mixed by rapid inversion for 10 min at room temperature. For phase separation, the mixture was centrifuged at 13 000 rpm, for 5 min and the clear aqueous phase was transferred to 24:1 chloroform: isoamyl alcohol (100 µl) and mixed by rapid inversion. The mixture was centrifuged at 13 000 rpm, for 5 min and the previous step repeated. The aqueous phase was next added to an equal volume 100% isopropanol, mixed by inversion and incubated at room temperature for 10 min. The mixture was centrifuged at 13 000 rpm, for 10 min to pellet the RNA. The RNA was then washed in 70% Ethanol (1 ml) and centrifuged at 13 000 rpm for 5 min. The pellet was air-dried and resuspended in pre-warmed nuclease-

free sdH_2O (90 µl). To remove residual genomic DNA, DNase I buffer (10 µl) and DNase I (1 µl) (Ambion) was added twice at 30 min intervals at 37°C. To remove the DNase, Trizol (500 µl) spiked with poly-aryl carrier (1 µl) was added to the DNase reaction and gently mixed. The mixture was added to BCP (150 µl), and the same phase separation process was repeated as above. The final RNA was resuspended in nuclease-free sdH_2O (~30 µl). The RNA was quantified by spectrophotometry using the Nanodrop ND1000 (Thermo Scientific) and stored in 1 µg aliquots at -80°C or converted to cDNA immediately.

2.3.1.2 Reverse Transcription

Prior to first-strand synthesis, to convert M23-endopeptidase mRNA to cDNA, total RNA (500 ng) was treated with Turbo DNase (Ambion) (1 µl) twice, at 30 min intervals in a total reaction volume of 25 – 50 µl including 1X Turbo DNase buffer at 37°C. The reaction was inactivated by addition of Inactivation Reagent resin (2 µl) (Ambion), incubated at room temperature for 5 min. The reaction was centrifuged at 13 000 rpm for 5 min and the aqueous phase was transferred to new tubes on ice. For cDNA synthesis using the SuperScript III kit (Invitrogen), a primer annealing reaction was setup containing RNA (500 ng), a mixture of reverse primers specific to M23 endopeptidase genes and *sigA* (2.5 µM) (Table 2.6) up to 25 µl. The reaction was heat treated at 94°C, for 1.5 min.; 65°C, 3 min and 57°C for 3 min. During this time, 2 Reverse transcription (RT) master mixes were prepared: with (RT+) or without (RT-) RT. The RT reaction was made up of 1X buffer, $MgCl_2$ (4 mM), Dithiothreitol (DTT) (8 mM), dNTPs (0.4 mM) and SuperScript RT III (200 U/reaction) or sdH_2O, according to the manufacturer's recommendations (Invitrogen). The primer-RNA mix was split between the RT+ and RT- reactions to make up a final volume of 25 µl each. The reaction was incubated at 55°C for 50 min and inactivated at 85°C for 5 min and stored at -20°C or kept on ice for immediate use.

2.3.1.3 qPCR

Using the SsoFast Sybr Green mastermix (BioRad), a qPCR mastermix was prepared in optical strip-qPCR tubes (BioRad) consisting of SsoFast Sybr Green mix (10 µl), 10 µM Fw and Reverse primer (0.75 µl each) (Table 2.6), and template consisting either of RT+ reaction mix (1 µl) RT- reaction mix (1 µl), gDNA standard (2 µl) or sdH_2O (NTC) (1 µl). gDNA standards were prepared as a dilution series of 10^1-10^6 genomic equivalents. For

this, CTAB-extracted *M. tuberculosis* gDNA was quantified by spectrophotometry using a Nanodrop (Thermo Scientific) and diluted to a stock of 25 ng/µl (10^7 equivalents) in a 20 µl volume. From there, a 10-fold dilution series of 2 µl of gDNA in 18 µl sdH_2O was prepared fresh for each qPCR run. The qPCR reactions were performed using the BioRad Cfx96 Real-Time thermocycler according to the programme described in Figure 2.6.

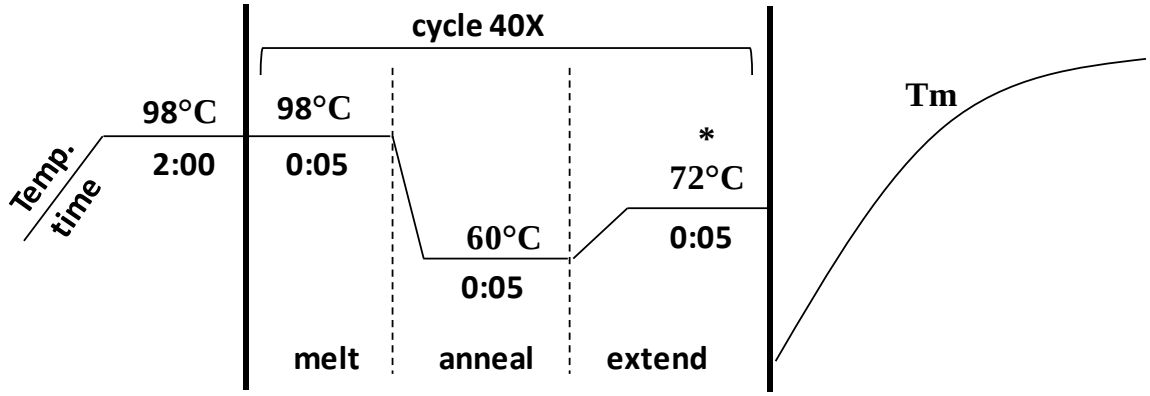

Figure 2.6 Thermocycling parameters for qPCR.
*Point at which Sybr Green fluorescence was recorded for each cycle. Tm: Melt curve.

2.3.1.4 Calculation of gene expression

Using BioRad CFX manager, groups for reactions specific to each gene were annotated. The threshold was set to a position where the R^2 value for the standard curve was 0.99-1.00. The amplification curves were inspected by eye and the melting curves for each reaction were studied to make sure products pertained to double-stranded DNA of the same temperature for the same primer pair. The calculated concentration (Sq) values for each reaction were copied into Excel. To normalise the calculated expression to that of *sigA* the following formula was used

$$\frac{Sq\ of\ GOI}{Sq\ of\ sigA}$$

GOI: gene of interest

2.3.2 Gene deletion via suicide vector-mediated homologous recombination

Unmarked deletion mutants of two M23 endopeptidase genes, Rv0950c and Rv2891 were generated via suicide vector-mediated 2-step allelic exchange between the WT gene and a deletion allele (Parish & Stoker, 2000).

2.3.2.1 Suicide vector construction

Tuberculist (Kapopoulou, Lew & Cole, 2011) was used to acquire the open-reading frames (ORF) of Rv0950c and Rv2891 with additional upstream and downstream sequences.

Clone Manager 9.0 (CM9) was used to select upstream and downstream homology regions (1300-1500 bp) which could be fused together for in-frame deletion of the ORF without disrupting potential neighbouring genes and/or their putative promoter regions. The homology sequences were further analysed in CM9 for existing or non-existing restriction sites that were compatible for cloning into the p2Nil suicide vector multiple cloning site (Appendix A2). Primers were then designed in Primer3 (http://primer3.ut.ee/) for amplification of the upstream and downstream arms with flanking restriction sites and GC-repeat hexamers (Table 2.7). Gradient PCR was performed as described above for Q5 high-fidelity polymerase to optimise the annealing temperatures for bulk amplification of the upstream and downstream cloning inserts. After performing replicate PCR of the inserts, PCR products were confirmed by DNA electrophoresis and pooled (200 µl) for purification by salt-Ethanol precipitation. The inserts were resuspended in ~ 30 µl sdH_2O and added to sequential, double restriction digestion reactions using the appropriate endonucleases for sticky-end ligation into p2Nil. Concurrently, bulk extraction of p2NIl was performed using the Nucleobond extraction protocol. Replicate, sequential double digests of p2Nil DNA (1 µg each) were performed and confirmed after each digest by DNA electrophoresis. Insert or vector DNA was purified from pooled replicate restriction digests using the Nucleospin PCR reaction affinity column purification kit (MN) according to the manufacturer's recommendations. Purified DNA was eluted from the column using buffer NE (30 µl), quantified by DNA electrophoresis and added to a ligation reaction as described above. Ligations were transformed into *E. coli* DH5α and plated onto Kanamycin-supplemented LA. Kanamycin resistant colonies were inoculated into LB for small-scale plasmid extraction. Plasmid DNA was screened for successful inclusion of both inserts by restriction mapping. Constructs with the correct restriction map were further confirmed by sequencing using primers flanking the p2Nil multiple cloning site and complementary to the upstream and downstream homology arms. The pGOAL17 vector (Appendix A2) was then prepared and digested with *Pac*I for sub-cloning of the *lac_sac* cassette into the *Pac*I sites of p2Nil deletion constructs to complete the suicide vector (Parish & Stoker, 2000). Successful *lac_sac* clones were selected as Kanamycin-resistant, blue *E. coli* colonies in the presence of 0.004% XGal, propagated and isolated for confirmation by restriction digestion mapping and sequencing. Correct suicide vectors were further tested for sucrose sensitivity conferred by the *sacB* gene by comparing CFU counts of *E. coli* on untreated and 5% sucrose-supplemented LA.

2.3.2.2 Single-cross over strain generation

Suicide vectors were bulk extracted using the Nucleobond procedure and stringently purified of excess extraction buffer salts before electroporation into WT *M. tuberculosis* H37Rv(s). Electroporations were performed as described above and plated on 7H11 supplemented with Kanamycin (25 µg/ml) and 0.004% X-Gal. CFU formation was monitored between 2-6 weeks of incubation at 37°C. Blue, Kanamycin-resistant *M. tuberculosis* colonies were then inoculated into 7H9 supplemented with Kanamycin (25 µg/ml) and grown for a week at 37°C. Liquid culture (100 µl) was harvested for colony-boil DNA extraction. DNA was genotyped by PCR to confirm single-cross overs which consist of both the WT and deletion allele using primers flanking the upstream and downstream homology arms and a primer which is only complementary to the WT allele (Table 2.8).

2.3.2.3 Double-cross over strain generation

M. tuberculosis transformants for which the single-cross over (SCO) genotype was confirmed were sub-cultured into 7H9 without kanamycin prior to screening double-cross overs (DCO) and release of the p2Nil backbone from the *M. tuberculosis* genome preferably retaining the deletion allele. Sub-cultures were subjected to a 10-fold dilution series and plated on 7H11 supplemented with 0.004% X-Gal and 2% sucrose to select for white, sucrose-resistant colonies representative of successful DCOs. DCO colonies were pre-cultured in 7H9 for genotyping by PCR. Cultures for which only the mutant allele could be amplified were sub-cultured for propagation and for genomic DNA extraction by CTAB for Southern blot confirmation.

2.3.2.4 Confirmation of gene deletion

Deletion mutant strains of Rv0950c and Rv2891 were genotyped by Southern blotting and loss of gene expression was determined by RT-qPCR.

Table 2.7 Primers for amplification of cloning inserts

Target	Sequence	Restriction site	Genomic co-ordinates	T_A	Product size
Rv0950c upstream	F: gccgcc*aagctt*TTGACGAACACGCTCTTGAC	*Hin*DIII	1062885-1062904	64	1301
	R: gcgcgc*agatct*ATCGCGAGGTGTGCGAAT	*Bgl*II	1061628-1061645		
Rv0950c downstream	F: gcgcgc*agatct*AAGCGGGGACTTAGCGTCGGCAATTA	*Bgl*II	1060666-1060691	76	1423
	R: gccgccc*tgcag*GCTATGTCGCCGACAACGAGCAC	*Pst*I	1059293-1059315		
Rv2891 upstream	F: gccgcc*ggtacc*TCGCCATATCAGCCTTTC	*Acc65*I	3199101-3199118	70	1305
	R: gcgcgc*tctaga*GAGTCGTCGGCATGG	*Xba*I	3200367-3200381		
Rv2891 downstream	F: gccgcc*tctaga*GCCGCTATCCAGCGA	*Xba*I	3200790-3200804	60	1275
	R: gcgcgc*ctgcag*GTAACCACGCCGTGATCC	*Pst*I	3202045-3202062		
Rv0950c complement	F: gcgcgc*tctaga*GTCTTCGCTCGGCTTACT	*Xba*I	1061937-1061954	65	1360
	R: gccgcc*ggtacc*TTCTCGCCCTGAGAACAC	*Acc65*I	1060619-1060636		
Rv2891 complement	F: cgcgcg*acgcgt*GCTTCATGGTGACTACGGCCA	*Mlu*I	3199961-3199981	72	1085
	R: ccgccg*cgatcg*GCTGGTTCATTGTCGGTGCC	*Pvu*I	3201002-3201021		
Rv0950c protein purification	F: ccgccg*catATG*GCAGCGATT	*Nde*I	1061643-1061654	68	1017
	R: cgcgcg*ctcgag*ACCGGTGTAATTG	*Xho*I	1060659-1060671		
Rv0950c FL for overexpression	F: ctctct*gaattc*tGCAGCaATTCGtACACCTC	*Eco*RI	1061633-1061651	72	1016
	R: agga*gg**aagctt*caGGTGTAATTGCCGA	*Hin*DIII	1060662-1060675		
Rv0950c N' for overexpression	F: ctctct*gaattc*tGCAGCaATTCGtACACCTC	*Eco*RI	1061633-1061651	64	644
	R: gttgtgt*aagctt*acCTTCGTaGGCATGACA	*Hin*DIII	1061034-1061049		
Rv0950c C' for overexpression	F: gctgct*gaattc*GGGCATCTTCACGTC	*Eco*RI	1061020-1061034	72	399
	R: agga*gg**aagctt*caGGTGTAATTGCCGA	*Hin*DIII	1060662-1060675		
Rv0950c *E. coli* complement	F: gcgcgc*ggatcc*GTATCGCCCGTTCTGCT	*BamH*I	1061658-1061674	70	1080
	R: gccgcc*aagctt*TTCTCGCCCTGAGAACAC	*Hin*DIII	1060619-1060636		

T_A: optimal annealing temperature (°C) when using Q5 polymerase. Co-ordinates and products in base pairs. Uppercase indicates wild-type sequence, restriction recognition sites in italics. FL: Full length Rv0950c, N': Rv0950c excluding the C-terminus (M23 endopeptidase domain), C': Rv0950c M23 endopeptidase C-terminal domain.

Table 2.8 Primer sequences for genotyping gene deletion and complementation.

Target	Sequence	T_A	co-ordinates
ΔRv0950c	ScF1: CTTGGCCCAGACGACGAAGA	64	1059925-1059944
	ScF2: CAGGAGCTCATCGACTGGC		1060288-1060306
	ScR1: TTGGCACCCTCGGCTGTGTC		1062039-1062058
	ScR2: ACCCCGATTTATGCGGTGTCC		1060938-1060958
ΔRv2891	F1: ATTCCAGCGACGGGTCTGATGCCC	72	3199911-3199934
	R1: CCGAGATGTGGGCCCAAGACGCTG		3201576-3201599
	R2: GCAGGCCCAGCGGATCGACA		3200745-3200764
pTweety Km^R	F: ATTCAACGGGAAACGTCTTG	55	
	R: ATTCCGACTCGTCCAACATC		
ΔRv0950c ::Rv0950c	F1: gcgcgc*tctaga*GTCTTCGCTCGGCTTACT	60	1061937-1061954
	R1: gccgcc*actagt*ACCGGTGTAATTGCCGAC		1060659-1060676
	R2: gccgcc*ggtacc*TTCTCGCCCTGAGAACAC		1060619-1060636

T_A: optimal annealing temperature (°C) when using Taq polymerase. Co-ordinates in base pairs. Km^R: Kanamycin resistance gene. Uppercase indicates wild-type sequence, restriction recognition sites in italics.

2.3.2.4.1 Southern blot genotyping of deletion mutant strains.

The general procedure for Southern blotting is described above. Specifically, gDNA was extracted using the CTAB procedure from WT and deletion mutant strains of *M. tuberculosis*. For gDNA digestion, restriction sites were chosen which occurred within the WT ORF which were expected to be lost in the deletion genotype, creating fragments which could be differentiated between WT and mutant strains based on a size difference, big enough to produce measurable electrophoretic migration differences. Digested gDNA was separated by DNA electrophoresis and the gel was electroblotted onto nitrocellulose. DIG-labelled probes were synthesised using the same primers used to amplify the upstream and downstream inserts for initial cloning. This produced DIG-labelled probes which were complementary to the upstream and downstream regions of the deleted gene, which could be detected in both strains.

2.3.2.4.2 RT-qPCR to detect loss of gene expression

Total RNA was extracted from 50 ml cultures of wild-type and deletion mutant *M. tuberculosis* using the Nucleospin RNA column-affinity extraction method, according to the manufacturer's recommendations. Briefly, the harvested cells were resuspended in buffer RA1 combined with β-mercaptoethanol (BDH). The suspension was lysed using Lysing matrix B (MP Bio) as described above, the aqueous phase was filtered through a Nucleospin filter column and the eluate combined with 70% Ethanol. After binding RNA to the column, on-column DNA digestion was performed as prescribed by manufacturer (MN). After the prescribed wash steps, RNA was eluted with nuclease-free sdH_2O (60 µl).

The eluate was reapplied for a second and final elution. RNA was quantified by spectrophotometry using a Nanodrop. RNA (1µg) was DNase treated as described earlier and converted to cDNA using a combination of reverse primers specific to either Rv0950c or Rv2891 and *sigA*. The same methodology for qPCR and expression analysis was used here as for growth-phase-dependent transcription profiling.

2.3.2.5 Double deletion of Rv0950c and Rv2891 from *M. tuberculosis* genome

The Rv0950c suicide vector was electroporated into the *M. tuberculosis* ΔRv2891 single deletion mutant strain (Table 2.2) and plated on 7H11 supplemented with Kanamycin (25 µg/ml) and 0.004% X-Gal. A single, blue, Kanamycin-resistant colony was genotyped by PCR using the same primers used previously to genotype Rv0950c single deletions. The SCO was sub-cultured in 7H9 and plated on 7H11 supplemented with 2% sucrose and 0.004% X-Gal as described previously for DCO strain generation.

2.3.3 Genetic complementation

To confirm that any observed phenotypes of gene deletion were directly due to loss of gene function and not due to polar effects of altering the *M. tuberculosis* genome, the gene of interest was reintroduced via Mycobacteriophage integration machinery expressed on integrating vectors pTTP1b (pTweety) or pMV306H which integrate the vector backbone at fixed *attB* phage recognition sites in the *M. tuberculosis* genome (Pham et al., 2007).

2.3.3.1 Construction of complementation vector

The complementation cassette consisted of the Rv0950c or Rv2891 ORF and additional upstream sequence of up to 400 bp representing the putative native promoter. The complementation cassette was amplified by PCR with restriction sites (Table 2.7) for directional, sticky-end cloning into pTTP1b (Rv0950c) or pMV306H (Rv2891) (Table 2.5). Gradient PCR was performed as described above for Q5 high-fidelity polymerase to optimise the annealing temperatures for bulk amplification of the insert. After performing replicate PCR of the inserts, PCR products were confirmed by DNA electrophoresis and pooled (200 µl) for purification by salt-Ethanol precipitation. The inserts were resuspended in ~ 30 µl sdH_2O and added to sequential, double restriction digestion reactions using the appropriate endonucleases. Concurrently, bulk extraction of vectors was performed using the Nucleobond extraction protocol. Replicate, sequential double digests of vector DNA (1

µg each) were performed and confirmed after each digest by DNA electrophoresis. Insert or vector DNA was purified from pooled replicate restriction digests using the Nucleospin PCR reaction affinity column purification kit (MN) according to the manufacturer's recommendations. Purified DNA was eluted from the column using buffer NE (30 µl), quantified by DNA electrophoresis and added to a ligation reaction as described above. Ligations were transformed into *E. coli* DH5α and plated onto Kanamycin (pTTP1b) or Hygromycin (pMV306)-supplemented LA (Table 2.5). Marked colonies were inoculated into LB for small-scale plasmid extraction. Plasmid DNA was screened for successful inclusion of inserts by restriction mapping. Constructs with the correct restriction map were further confirmed by sequencing using primers flanking the vector multiple cloning site.

2.3.3.2 Complement strain generation and confirmation

The pTweety-Rv0950c complement vector or empty vector (pTweety) was bulk extracted using the Nucleobond procedure and stringently purified to remove excess extraction buffer salts before electroporation into wild-type *M. tuberculosis* H37Rv(s)ΔRv0950c. Electroporations were performed as described above and plated on 7H11 supplemented with Kanamycin (25 µg/ml). CFU formation was monitored between 2-6 weeks of incubation at 37°C. Kanamycin-resistant *M. tuberculosis* colonies were then inoculated into 7H9 supplemented with Kanamycin (25 µg/ml) and grown for a week at 37°C. Liquid culture (100 µl) was harvested for colony-boil DNA extraction. DNA was genotyped by PCR using a combination of primers targeted to the promoter region and the 3' of Rv0950c (Table 2.8), for which both binding sites should be present in the deletion, complement and WT alleles, distinguishable by a size difference of ~1Kbp. Complement strains were expected to produce both mutant and WT alleles, whereas mutant strains with spontaneous Kanamycin resistance would lack the larger PCR products. None of the strains were expected to solely display WT alleles since the parent strain was the deletion mutant. Strains displaying all the correct alleles were further genotyped by Southern blotting as described previously. DIG-labelled probes were amplified from WT *M. tuberculosis* H37Rv(s) gDNA using the same primers used for generating the complement insert. *Bgl*II was selected for generating differentially-sized fragments in the different strains as a *Bgl*II site was introduced as a cloning scar in the deletion allele, not present in the WT allele, and also due to the presence of a *Bgl*II site in the pTweety backbone. A *Bgl*II site was also

present in the the expected integration site at the *attB* region of *lysU* (Pham et al., 2007). This equated to differentially-sized fragments for WT, ΔRv0950c and $lysU_{attB}$::Rv0950c, each detected by Southern blotting. Lastly, complementation of Rv0950c was confirmed by measuring restoration of gene expression by RT-qPCR as described for deletion confirmation (Section 2.3.2.4.2). Further, *M. tuberculosis* ΔRv0950c transformed with empty pTweety was genotyped by PCR using primers targeting the pTweety Kanamycin resistance cassette (Table 2.8).

2.3.4 Growth kinetics assay

Pre-cultures of *M. tuberculosis* were sub-cultured to OD_{600} = 0.02 in 7H9 (50 ml). A 10-fold dilution series was prepared from 1 ml culture. Dilutions (100 µl) were plated in duplicate on 7H11 quarter-90 mm agar plates and incubated at 37°C for at least 3 weeks for CFU enumeration. Subsequently, liquid cultures were sampled for OD_{600}, measured with a portable WPA Cell Density Meter and CFU dilution series at days 2, 4, 7, 9, 11, 14, 16 and 18. Data points and error bars were prepared in Excel. Experiments were carried out for at least 2 independent replicates.

2.3.5 Microscopy

2.3.5.1 Scanning Electron Microscopy

Pre-cultures of *M. tuberculosis* were sub-cultured and grown to $O.D_{600}$ = 0.6 - 0.8 to capture cells at exponential growth phase, washed in 1X PBS and fixed overnight in 2.5% glutaraldehyde at 4°C. Cells were washed in 1X PBS and resuspended in 2% osmium tetroxide for 60 min at room temperature. Cells were centrifuged and washed in an alcohol dehydration series with 30, 50, 70 and 100% EtOH incubating in each EtOH resuspension for 5 min at room temperature before centrifugation for two min at 13 000 rpm. The 100% EtOH step was repeated and pellets were stored at 4°C before transfer to the Electron Microscopy Imaging Unit at the University of Cape Town for imaging. Images were prepared at 20X magnification.

2.3.5.2 Slide preparation for fluorescence microscopy

Fixed cells (5-10 µl) were washed in 1X PBS (Lonza) and spotted onto 1% agarose on glass slides, covered with a cover slip and sealed with Cutex.

2.3.5.3 Tetramethylrhodamine-3-amino-d-alanine (TADA) fluorescence microscopy

An axenic culture (5 ml) was grown to OD_{600} = 0.6-0.7. TADA (2.5 µl) was added to culture (500 µl), incubated at 37°C, for 30 min. Cells were harvested and washed in 1X PBS (Lonza) twice before fixing overnight in 2.5% glutaraldehyde (Sigma) (250 µl) at room temperature. Slides were prepared as described above and images were captured using the Nikon Eclipse T12 and PE4000 LED light source, in the TL DIC channel (exposed 200 msec) and TADA channel (exposed 2 sec; exc. 550 nm, 50%; emm. 598 nm).

2.3.5.4 Copper-catalysed azide alkyne cycloaddition (CuACC) detection of alkyne-DADA and fluorescence microscopy

An axenic culture (5 ml) was grown to OD_{600} = 0.6-0.7. Cells were harvested and resuspended in 7H9 (100 µl) and labelled with alk-DADA (2.5 µl) at 37°C for 60 min. Cells were centrifuged, washed in 1X PBS (Lonza) and fixed overnight in glutaraldehyde (Sigma) (2.5%, 250 µl) at room temperature. Fixed cells were centrifuged at 13 000 rpm for 2 min and resuspended in PBSTB buffer (250 µl) and centrifuged at 13 000 rpm for 2 min. Pellets were resuspended in PBSTB (230 µl) to which CuACC reaction components were added in the following order: 10 mM $CuSO_4$ (5 µl), 6.4 mM TBTA (5 µl), 60 mM fresh Sodium Ascorbate (5 µl), 1 mM azido-probe (5 µl). The CuACC reaction was incubated at room temperature for 30 min and inactivated by centrifuging the cells at 13 000 rpm for 2 min. The cells were washed three times in 1X PBS and added to an agarose pad as described for slide preparation. Images were captured using the Nikon Eclipse T12 and PE4000 LED light source, in the TL DIC channel (exposed 200 msec) and azo488 channel (exposed 3 sec; exc. 490 nm, 50%; emm. 512 nm).

2.3.5.5 Lysozyme-Mutanolysin digestion prior to alk-DADA fluorescence microscopy

An axenic culture (5 ml) was grown to OD_{600} = 0.6-0.7, harvested and resuspended in 7H9 (188 µl). Lysozyme (Roche) and Mutanolysin (Sigma) were added in 10-fold increasing concentrations (5 – 500 µg/ml lysozyme and 0.5 – 50U Mutanolysin) to a final volume of 250 µl, incubated at 37°C for 120 min. Cells were centrifuged and resuspended in 7H9 (100 µl) and labelled with alk-DADA (2.5 µl) at 37°C for 60 min. Cells were centrifuged, washed in 1X PBS (Lonza) and fixed overnight in 2.5% glutaraldehyde (250 µl) at room

temperature. Fluorescence conjugation for incorporated alk-DADA was performed by CuACC described above.

2.3.5.6 BODIPY-FL – conjugated Vancomycin fluorescence microscopy

Axenic culture (5 ml) was grown to OD_{600} = 0.6-0.7. Vancomycin and Vancomycin BODIPY-FL (Invitrogen) were each added to a final concentration of 1 µg/ml to culture (1 ml) and incubated at 37°C overnight. Cells were washed twice in 1X PBS and fixed overnight in 2.5 % glutaraldehyde (250 µl) at room temperature. Slides were prepared as described previously and images were captured using the Nikon Eclipse T12 and PE4000 LED light source, in the TL DIC channel (exposed 200 msec) and BODIPY channel (exposed 5 sec; exc. 490 nm, 50%; emm. 512 nm). For Rv2891 characterisation, WT and ΔRv2891 were captured using the Zeiss Observer Z.1 in the TL DIC (exposed +/-30 msec.) and BODIPY FL (exposed 2.65 msec; exc. filter 450-490 nm; emm. filter 500-550 nm) channels and analysed in ZEN Blue 2.3 lite software.

2.3.5.7 Fluorescence intensity analyses

Images were exported from Nikon Elements Software (unless otherwise stated) to .tif files to preserve original optical data and analysed in ImageJ. The segmented line tool was used to trace the length of the cell from the brightest pole to the dim pole, for 100 cells for each biological replicate of each strain. The intensity analysis function (ctrl+k) was applied to acquire plot co-ordinates of fluorescence intensity (grey value) across the drawn line (y) with respect to pixel length of the line (x). The x and y coordinates were copied into Excel in categories of different staining patterns, eg. polar, midcell, diffuse based on the shape of the intensity profile. In Excel, pixel length was normalised to a % of cell length and average fluorescence intensity of the cells were calculated. The spatial distribution of fluorescence between the bright pole (bp), side-wall (sw) and dim pole (dp) (Figure 2.7) was calculated based on data published by García-Heredia et al., (2018), as follows:

$$fluorescence\ of\ bp = \sum grey\ values\ from\ 0\ to\ 15\%\ of\ the\ cell\ length$$

$$fluorescence\ of\ sw = \sum grey\ values\ from\ 16\ to\ 85\ \%\ of\ the\ cell\ length$$

$$fluorescence\ of\ dp = \sum grey\ values\ from\ 86\ to\ 100\%\ of\ the\ cell\ length$$

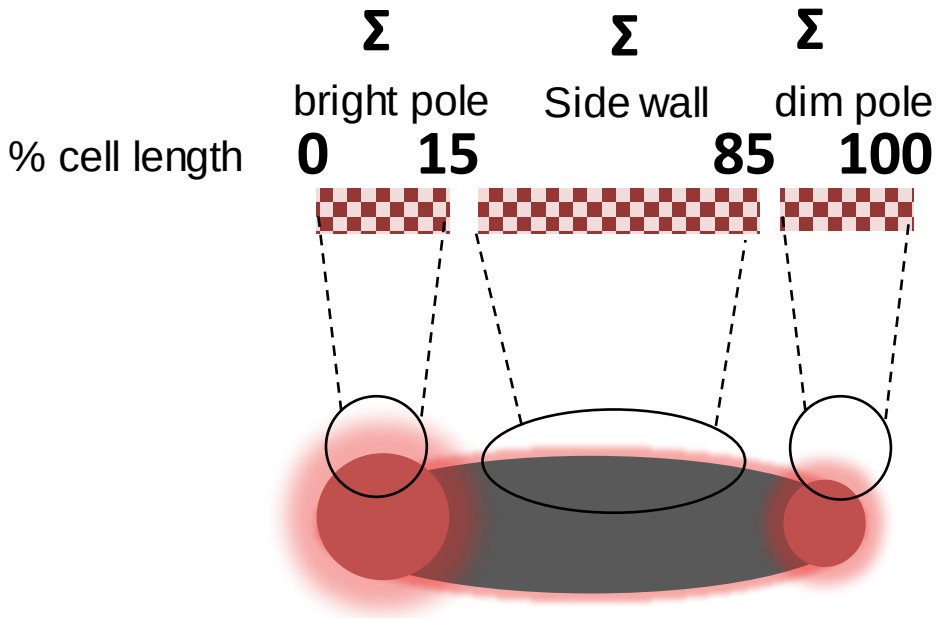

Figure 2.7 Schematic diagram describing quantification of spatial distribution of labelled PG. Distribution is quantified as percentage average fluorescence previously demonstrated by Garcia-Heredia et al., (2018): Average distribution of fluorescence between the bright pole (sum of fluorescence across the first 15% of the cell length), the side-wall (sum of fluorescence between 16-84% of the cell length) and dim pole (sum of fluorescence from 85-100% of the cell length).

2.3.5.8 Measurement of cell length

2.3.5.8.1 SEM lengths

Images (.tif) were analysed using Fiji (ImageJ) using the pixel length tool. Pixel length was converted to µm in Excel by dividing cell pixel length by the pixel length of 1 µm. The pixel length of 1 µm was determined by dividing the 2 µm scale bar pixel length by two. For accuracy, all cells in one image were normalised to the scale bar of that image. Statistical significance of cell length was compared between strains by single-factor ANOVA of cell length measured for 100 separate cells in biological triplicate (n=300), at a confidence interval of 95%.

2.3.6 Minimum Inhibitory Concentration (MIC) of antibiotics by broth microdilution

Broth microdilution was used to determine MICs of antibiotics or Lysozyme for the respective strains of *M. tuberculosis* to study how deletion of M23 endopeptidase genes impacts cell wall stability. For this, axenic pre-cultures were grown and sub-cultured to OD_{600} = 0.1. The sub-cultures were grown overnight to OD_{600} = 0.2-04. Cultures were diluted 1:20 in 7H9 media. Microbroth 2-fold dilution was setup in a clear, 96-well, round-bottom plate as follows: 7H9 (50 µl) was aliquoted into each well, except for the top row of 8 wells. Antibiotics or lysozyme was added to the top row at 128X the expected MIC in

a final volume of 100 µl (Fig. 2.8). Antibiotics were then diluted down 2-fold from the top row (row 12) to the bottom row (row 1), starting with transferring 50 µl from row 12 to row 11 containing 50 µl 7H9. For the bottom row, 50 µl was discarded, so that all wells now contained a final volume of 50 µl. After dilution of the antibiotics and controls (media only or vehicle only), 50 µl of cells were added to each well, bringing the final volume up to 100 µl. Plates were sealed and incubated at 37°C and scored visually after 4-7 days, as growth or no growth in a well. The MIC was recorded for the lowest concentration of drug at which no growth was observed.

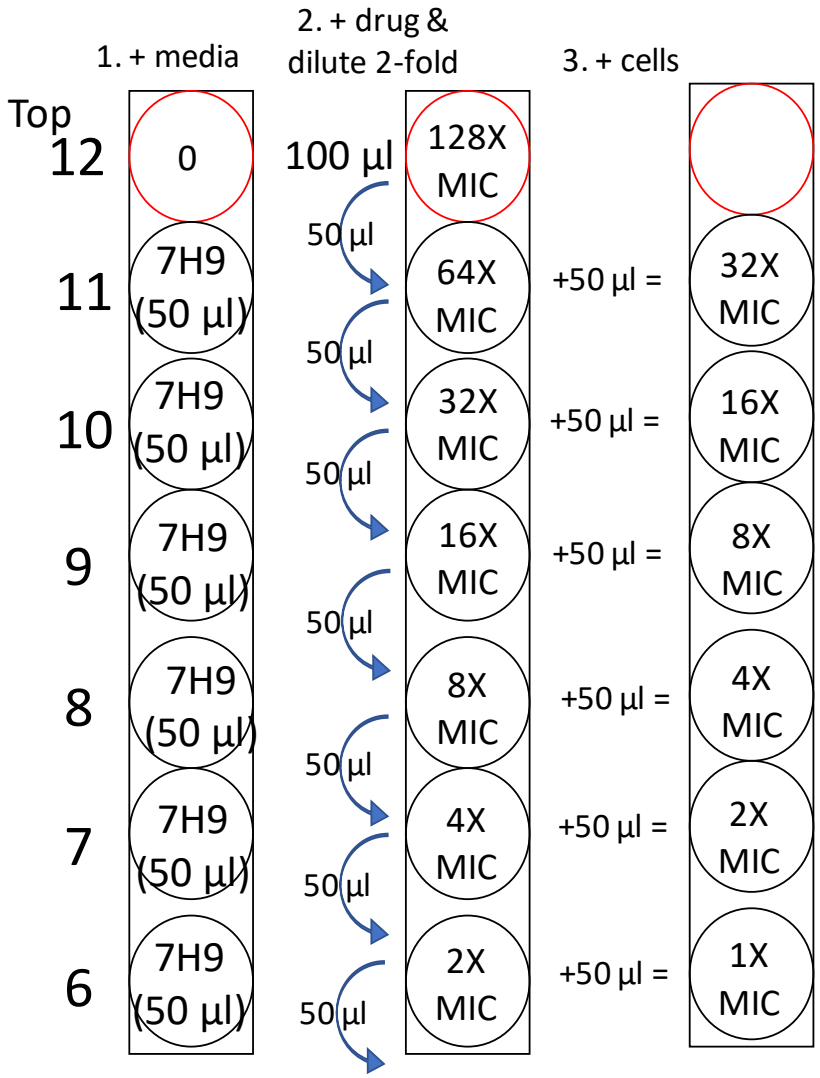

Figure 2.8 Broth microdilution for Minimum Inhibitory Concentrations of antibiotics
Calculation of antibiotic concentration to be added to the top row of the 96 well plate for 2-fold dilution, whereby the middle (row 6) should equal the expected MIC for WT *M. tuberculosis*.

2.3.7 Ethidium bromide diffusion assay

An axenic culture (20 ml) was grown to OD_{600} = 0.8, cells harvested, and washed in PBS (1 ml), and resuspended in 1X PBS and 0.5 % glucose. Cells were added to a final OD_{600} = 0.4 (50 µl) to black, flat, clear-bottom, 96-well microplates (Greiner Bio). EtBr (Appendix

A1) was added to a final concentration of 0.25, 0.5, 1 and 8 µg/ml to cells and made up to a final volume of 100 µl with nuclease-free water. EtBr fluorescence emission was measured with a Spectra Max Gemini EM microplate reader (Molecular Devices) at 1 min intervals for 60 min. Data was normalised to t0 readings. Statistical analysis was performed in Excel by one-way ANOVA.

2.3.8 Recombinant protein expression

To test the putative PG hydrolytic activity of Rv0950c *in vitro*, purification of recombinant Rv0950c was attempted.

2.3.8.1 Rv0950c expression constructs

Two expression constructs were designed for expression and purification of Rv0950c in *E. coli*. The expression cassette consisted of the Rv0950c ORF without the last three 3' nucleotides, for C'terminal fusion of a Histidine hexapeptide (Appendix A5). The cassette was amplified by PCR using primers with flanking *Nde*I and *Xho*I sites for cloning into pET29 *E. coli* expression vector (Table 2.7) (Appendix A2). Alternatively, the same cassette was codon harmonised for *E. coli* and synthesised and cloned into pET24a (GenScript) (Appendix A2).

2.3.8.2 Induction of Rv0950c expression by IPTG

The vectors were confirmed by restriction digestion mapping and transformed into *E. coli* BL21* for expression. Transformants were selected as Kanamycin-resistant colonies and inoculated into LB for overnight pre-cultures. Pre-cultures were sub-cultured and incubated at 37°C, with/and shaking to an OD_{600} = 0.8 – 1.0 before addition of IPTG (Melford) (0.8 mM- 1 mM). Induction was performed at 18°C, 30°C or 37°C, for various time intervals. At each interval, culture (1 ml) was sampled and frozen at -20°C for later protein extraction.

2.3.8.3 Protein extraction

Uninduced and induced samples were thawed on ice and centrifuged at 4000 rpm for 10 min. Cell pellets were resuspended in B-PER solution (Thermo Scientific) (250 µl) spiked with protease inhibitor (Roche) and incubated at room temperature for 10 min. The B-PER lysate was transferred to Lysing Matrix B tubes (MP Bio) and ribolysed three times for 20 seconds, at speed 6, incubating on ice for 5 min between. Cell debris was centrifuged at

13 000 rpm, briefly and the supernatant was transferred to fresh tubes and centrifuged at 13 000 rpm for 5 min for separation of the soluble and insoluble phase.

2.3.8.4 Protein electrophoresis

Protein fractions were mixed with 5X PAGE loading dye in a 20 µl volume and loaded alongside PAGE Ruler or PAGE RulerPlus molecular weight marker (5 µl) (Thermo Scientific) (Appendix A4) onto a FastCast PAGE gel prepared according to the manufacturer's instructions (Bio-Rad). PAGE was performed in 1X running buffer (Appendix A1) at 80V for ~ 2 hours. Gels were stained overnight, with/and shaking at room temperature in Coomassie blue (Appendix A1) followed by incubation overnight, with/and shaking at room temperature in Destain solution (Appendix A1). PAGE gels were captured using a Konica Minolta PS200 office scanner.

2.3.8.5 Western blotting

Duplicate unstained and stained PAGE was performed as described above. Polyvinylidene fluoride (PDVF) membrane (Amersham) was cut to the same size as the PAGE gel and incubated in methanol for 5 min at room temperature. An electroblot sandwich was prepared in 1X running buffer (Appendix A1) by placing the PVDF membrane on top of the unstained PAGE gel between Whatman filter paper and sponges as described for Southern blotting. Electroblotting was performed in 1X Transfer buffer (Appendix A1) for 45 min at 300 mA, 100V. The membrane was rinsed in dH_2O and incubated in Western Blocking buffer at 4°C overnight. Monoclonal anti-His antibody conjugated to Peroxidase (Roche) was diluted 1:10 000, 1:20 000 or 1:40 000 in Western Blocking solution (10 ml). The membrane and diluted antibody were then incubated for 45 min in Western Blocking solution at room temperature. Unbound antibody was washed off with TBST 5 times for 5 min each, with/and shaking at room temperature. Membrane was transferred to a hybridisation bag to which Chemiluminescent Peroxidase Substrate-1 (2 ml) (Sigma) was added and incubated at room temperature for 5-10 min. X-ray film was exposed to the membrane in a sealed cassette for 2 min before manual development as described for Southern blotting.

2.3.8.6 Bradford assay for protein quantification

A standard curve of dilutions of BSA (NEB) (5 – 100 µl) was made to final volume of 30 µl in sdH_2O. Bradford solution (1.5 ml) was added to BSA and incubated at room temperature for 5 min. Absorbance was measured at 595 nm and saved as a standard curve using the standard curve function for the Jenway 7200 spectrometer. Unknown protein samples were prepared as neat or diluted 10^{-1} to a final volume of 30 µl and mixed with Bradford solution (1.5 ml). The solution was incubated at room temperature for 5 min and the absorbance was measured at 595 nm which was converted to µg/ml against the previously saved BSA standard curve.

2.3.9 Heterologous complementation of *E. coli* Δ*envC,*Δ*nlpD*

Rv0950c was heterologously expressed in the cell-division defective *E. coli* Δ*envC,*Δ*nlpD* strain (Uehara, Dinh & Bernhardt, 2009) to check for restoration of cell separation. Because the double mutant is already Kanamyicin-resistance marked, the pTweety-Rv0950c complementation vector could not be used. Instead, the hygromycin-resistant, multicopy vector pSE100 (Guo et al., 2007) (Appendix A2) was used as a backbone for Rv0950c expression. The Rv0950c ORF and putative ribosome binding site was amplified by PCR using primers with flanking *BamH*I and *Hin*DIII sites for cloning into the pSE multiple cloning site (Table 2.7).

Ligations were transformed in *E. coli* DH5α. Constructs were confirmed by restriction digestion analysis and sequencing. *E. coli* Δ*envC,*Δ*nlpD* was cultured and made chemically competent for transformation with pSE100-Rv0950c or pSE100 empty vector. Transformants were selected by Hygromycin resistance and screened by restriction digestion with *Nco*I. Heterologous transformants and the parent strain were grown to log phase. Cultures (1 ml) were labelled with FM4-64 (Life Technologies) (5 µl) for 5 min at 37°C and washed once in 1X PBS before performing fluorescence microscopy. Slides were prepared as described previously and captured using the Nikon Eclipse T12 and PE4000 LED light source, in the TL DIC channel (exposed 400 msec) and TADA channel (exposed 3 sec; exc. 525 nm, 100%; emm. 640 nm).

2.3.10 Heterologous expression in *M. smegmatis*

The Rv0950c ORF was cloned full length, or just the N' terminus preceding the M23 endopeptidase domain or the C' terminal M23 endopeptidase domain, excluding stop

codon residues into a MPFC vector, pUAB400 (Singh et al., 2006) (Table 2.5) (Appendix A2). The three cloning inserts were amplified by PCR using primers with flanking restriction sites for directional cloning for C' terminal fusion with domains of Dihydrofolate Reductase (DHFR) in pUAB400 (Table 2.7). The clones were confirmed by restriction digestion analysis and sequencing before electroporation into *M. smegmatis*. Electroporations were plated on 7H11 supplemented with Glucose or Glucose salt, and CFUs were recorded after incubation at 37°C for 3-7 days. Integration of pUAB400 was genotyped in Kanamycin-resistant colonies using primers for cloning (Table 2.8).

2.3.11 Gene expression of Rv0950c in response to nutrient and osmolarity stress

Axenic pre-cultures of WT *M. tuberculosis* were prepared and sub-cultured at OD_{600} = 1.0 into 7H9 media or Sauton's media (Appendix A1) each in triplicate to OD_{600} = 0.7-0.9. Prior to RNA extraction, 14 ml was transferred to new flasks and incubated at 37°C for 60 min with or without the addition of NaCl to a final concentration of 280 mM. RNA was extracted using a column affinity kit as described previously for confirmation of gene deletion. RT and qPCR were performed as described previously.

2.4 Statistical analyses

Statistical analyses were performed using the Data Analysis Pack in Microsoft Excel, including *t-test* assuming unequal variances, single-factor ANOVA and two-way ANOVA at a 95% confidence interval. Error bars represented Standard Error of the Mean, determined using the "Descriptive statistics: summary statistics" function in Microsoft Excel.

3 Results

3.1 Bioinformatics to identify M23-endopeptidases in *M. tuberculosis*

3.1.1 BLAST against *E. coli* amidase activators and internal BLAST

Given that the M23 endopeptidases represent a highly diverse family of proteins (section 1.5), a focus was placed on searching for cell division activators on the basis of recent identification of cell division amidases in mycobacteria (section 14.4.1). Therefore, as a starting point, the *E. coli* cell division endopeptidases, EnvC (NP_418070.6) and NlpD (NP_417222.1) (Uehara, Dinh & Bernhardt, 2009) were used as template sequences for tBLASTn against the nucleotide collection database of the *M. tuberculosis* H37Rv complete genome (http://blast.ncbi.nlm.nih.gov/Blast.cgi) (Altschul et al., 1990) (Fig. 3.1.1), to identify *M. tuberculosis* genes encoding M23 endopeptidases involved in cell growth and division.

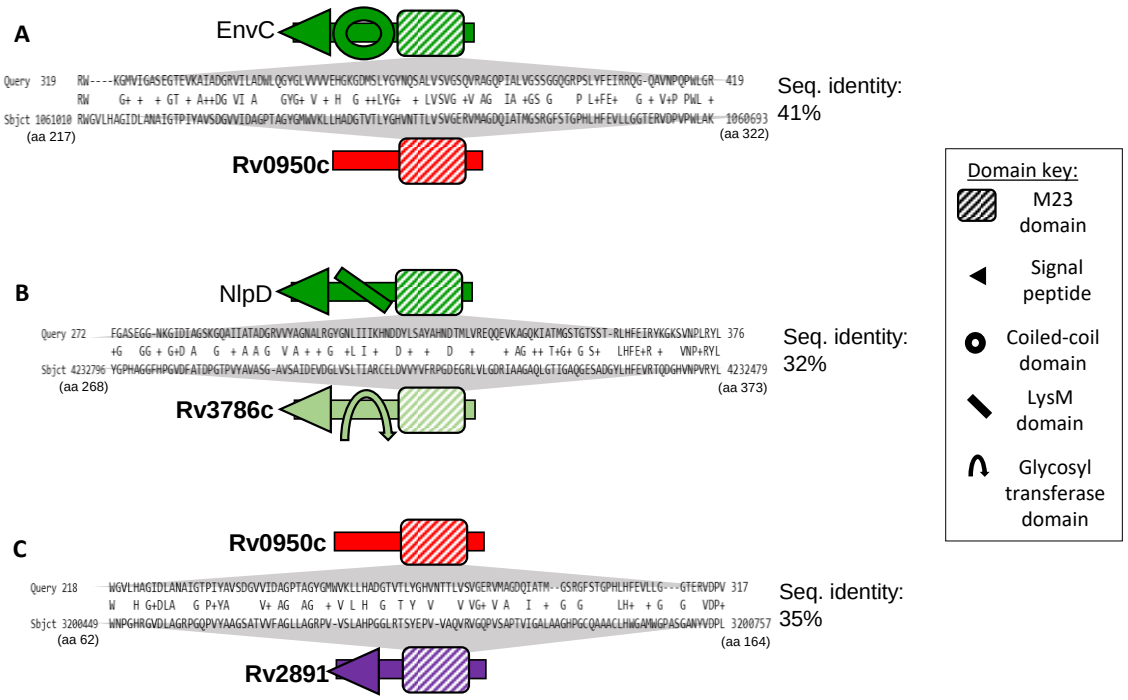

Figure 3.1.1 BLAST identification of the M23-endopeptidases of *M. tuberculosis.* (http://blast.ncbi.nlm.nih.gov/Blast.cgi) A) The *E. coli* EnvC query sequence retrieved Rv0950c; B) *E. coli* NlpD retrieved Rv3786c; C) An *M. tuberculosis* internal BLAST using Rv0950c as the query sequence retrieved Rv2891. Schematics show domain architecture defined by pFAM and confirmed for the *M. tuberculosis* homologues in Tuberculist. Grey triangles emphasise that the regions of similarity occur between the M23 domains of the orthologues.

E. coli EnvC retrieved Rv0950c (Fig. 3.1.1a) at 41% sequence identity and NlpD retrieved Rv3786c (Fig. 3.1.1b) 32% sequence identity suggesting that Rv0950c and Rv3786c are likely not direct orthologues of these proteins. Nonetheless, Tuberculist (Kapopoulou, Lew & Cole, 2011) and pFAM (Finn et al., 2014) confirmed the presence of the M23 domain,

which is where the regions of homology to *E. coli* orthologues appear (Fig. 3.1.1). To cross-check these two homologues, the Rv0950c coding sequence (NP_215465.1) was used as template for an internal BLASTp against the *M. tuberculosis* H37Rv complete genome (Altschul et al., 1990). As expected, Rv0950c and Rv3786c were retrieved along with a third putative M23-endopeptidase, Rv2891 (Fig. 3.1.1c) 35% identity. No other M23-endopeptidases were identified in these BLAST analyses or subsequent PHMMER searches (http://www.ebi.ac.uk/Tools/hmmer) (Eddy, 1998), indicating that *M. tuberculosis* encodes a total of three M23-endopeptidases, Rv0950c, Rv3786c and Rv2891.

3.1.2 Signal peptide predictions and domain architecture show divergence from *E. coli* activators

BLASTp homology between the *E. coli* and *M. tuberculosis* M23-endopeptidase orthologues were low in terms of amino-acid identity. It therefore became important to ascertain in what ways the activator homologues differ between these two organisms and what similarities are shared to better predict the role of M23-endopeptidases in *M. tuberculosis*.

3.1.2.1 Signal peptide prediction differs between the 3 homologues

The M23 domains of Rv0950c, Rv2891 and Rv3786c are highly conserved with predicted zinc-binding capacity, suggesting these are active endopeptidases. In addition, Rv0950c and Rv3786c have unique N' termini that may further differentiate the roles of these proteins in *M. tuberculosis* biology. To further study the N' termini, various databases were searched to determine if any of the M23 endopeptidases carry signal peptides. Localisation of *E. coli* EnvC and NlpD to the periplasm is directed by signal peptides in order to activate septum-degrading amidases for cell division (Uehara et al., 2010; Peters, Dinh & Bernhardt, 2011). Across the various databases within SignalP (http://www.cbs.dtu.dk/services/SignalP-3.0/) (Emanuelsson et al., 2007) and pFAM (Finn et la., 2014), Rv2891 has a predicted signal peptide, Rv0950c lacks a signal peptide, while results varied for Rv3786c (Table 3.1.1). Therefore, the three homologues appear to localise differently, but that requires experimental confirmation.

Although Rv2891 and Rv3786c have near-identical M23-domains, Rv3786c has an N'terminal, glycosyl-transferase 2_4 (GT2_4) domain. This is consistent with the earlier internal BLAST analysis, when Rv2891 was retrieved by Rv0950c but not by Rv3786c. Using a BLAST tool in Pasteurlist (Lechat et al., 2008) (http://genolist.pasteur.fr/TubercuList/) did not identify homologues to the Rv3786c GT2_4 domain, only short sequences of homology (Table 3.1.2). Clustal Omega multiple protein sequence alignment between the N' termini of Rv0950c and signal peptides or transmembrane domains of other M23 endopeptidases did not point to other domains which could have aided in characterising this region (Fig. 3.1.2).

Table 3.1.1 N-terminal variation in the M23 endopeptidases of *M. tuberculosis* based on signal peptide prediction.

***M. tuberculosis* M23 endopeptidase**	**Signal peptide prediction tool**				
	pFAM	**SignalP**			
		Neural networks		Hidden Markov Model	
		Gram+	Gram-	Gram+	Gram-
Rv0950c	x	x	x	x	x
Rv2891	✓	✓	✓	✓	✓
Rv3786c	✓	x	x	✓	x

Table 3.1.2 Tuberculist BLAST (Pasteurlist) of the glycosyl transferase domain Rv3786c showed very short regions of homology to five genes.

Locus	**Annotation**	**Homology coverage**	**similarity (%)**	**Gene Ontology**	**Domain architecture**
Rv2386c	MbtI/TrpE2	26-53	62	Chorismate synthesis	^{N}SP-Chorismate binding^{C}
Rv0549c	VapC3	1-30	60	RNase (toxin)	^{N}Metal binding – PIN nuclease^{C}
Rv1079	metB	273-295	68	Methionine biosynthesis	Cystathionine gamma synthase
Rv3232c	ppk2	185-242	47	Polyphosphate kinase	Polyphosphate kinase 2
Rv3765c	tcrx	44-74	64	transcription regulation	^{N}Response regulator receiver domain, transcriptional regulatory protein^{C}

^{N}N-terminus, ^{C}C-terminus.

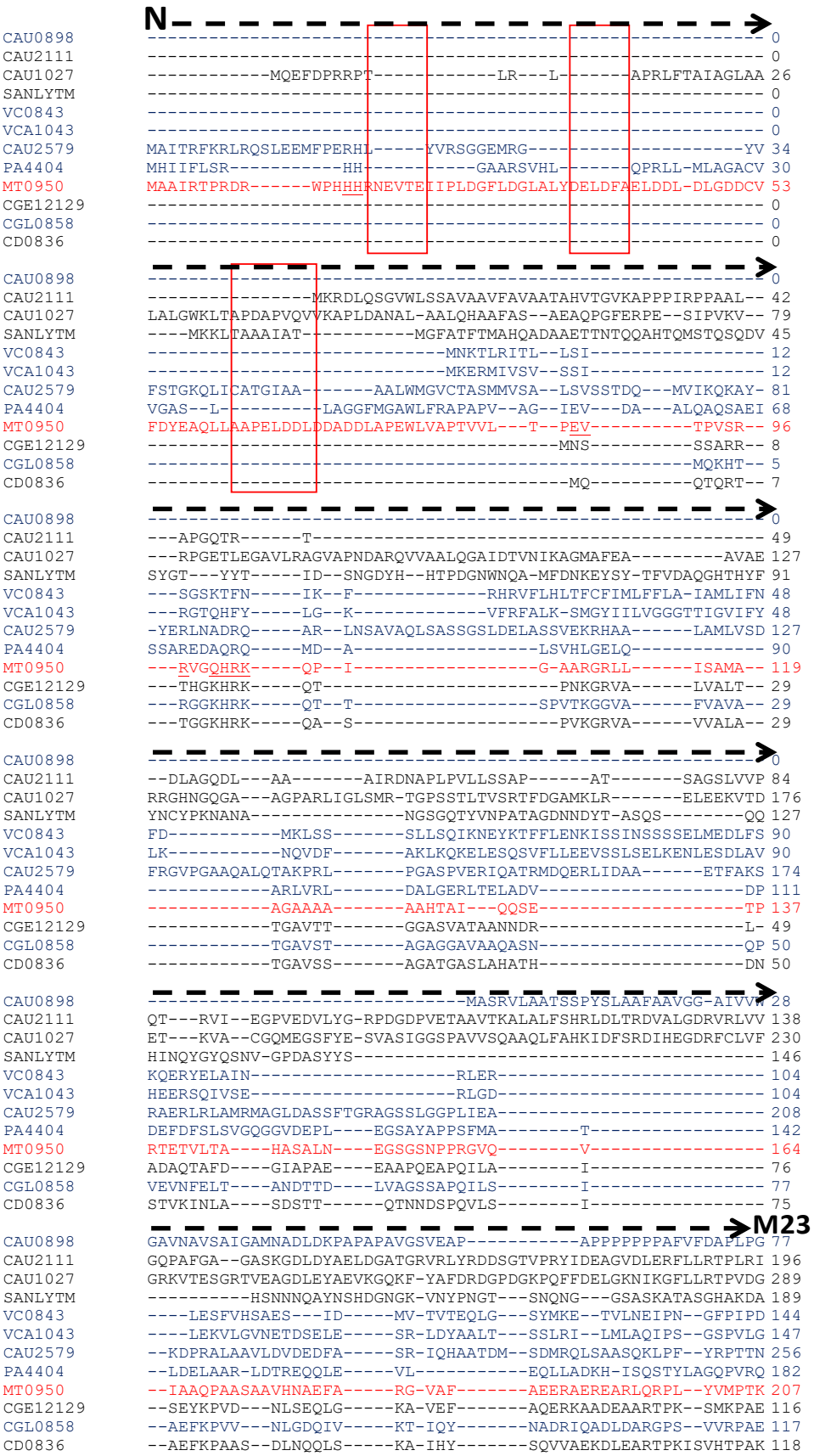

Figure 3.1.2 Clustal protein sequence alignment of the N-termini of Rv0950c (red) and M23 endopeptidases bearing either a transmembrane domain (blue) or signal peptide (black) showing alignment truncated up to the M23 domain of each protein sequence. Red boxes emphasise unique stretches (represented as gaps elsewhere) of the characteristically longer N-terminus of Rv0950c.

3.1.2.2 The *M. tuberculosis* M23 endopeptidases differ in domain architecture

Tuberculist (http://tuberculist.epfl.ch/) (Kapopoulou, Lew & Cole, 2011) annotates Rv0950c, Rv3786c and Rv2891 as conserved hypotheticals. The M23-domain, which is the main functional, yet degenerate, structure in the *E. coli* activator homologues, appears in all three *M. tuberculosis* orthologues according to the pFAM protein domain database (http://pfam.xfam.org/) (Finn et al., 2014) as well as PHMMER (Eddy et al., 1998) (Fig. 3.1.3). On closer inspection of the post-translational signals and overall domain architectures of Rv0950c, Rv3786c and Rv2891 revealed that the only commonality between *E. coli* and *M. tuberculosis* M23-endopeptidases is the M23-domain (Fig.3.1.3). It is therefore likely that these species differ in M23-endopeptidase utilisation.

Altogether, these various predictions highlight structural divergence between the *M. tuberculosis* M23 endopeptidases and the *E. coli* activators (Uehara et al., 2010), suggesting functional divergence as well (Fig. 3.1.3). In summary, the *M. tuberculosis* homologues lack either the coiled-coil or LysM accessory domains found in the *E. coli* activators and have conserved zinc-binding residues, suggesting that these are putative, active hydrolases instead of degenerate activators (Fig. 3.1.3).

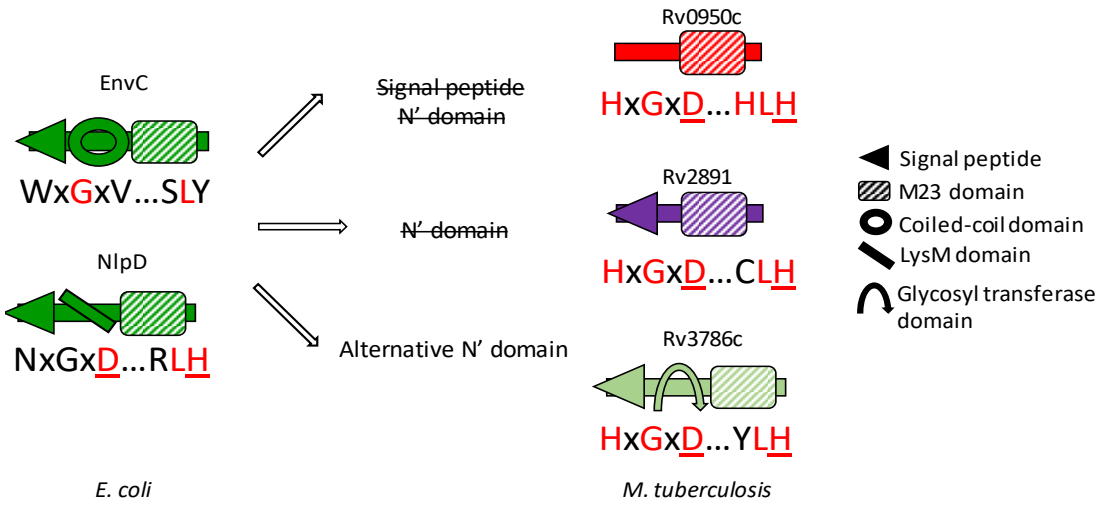

Figure 3.1.3 M23-endopeptidases of *M. tuberculosis* are structurally divergent from the *E. coli* cell division LytM factors.
Schematic diagram comparing overall domain architecture (schematics) and predicted catalytic activity of the LytM domain, based on residues of the zinc-binding motifs (indicated below structures). Conserved, zinc co-ordinating residues indicated in red, underlined residues were indispensable for activity in point-mutation studies of other bacterial M23-endopeptidases.

3.1.3 Phylogeny and functional categorisation of M23-endopeptidase orthologues

As the *E. coli* model of degenerate M23 endopeptidases is not evident in *M. tuberculosis*, an overview of orthologues occurring in other bacteria was generated to help understand the role of alternative active M23 endopeptidases, to assist in informing the choice of genes for subsequent characterisation *in vitro*. A multiple sequence alignment of characterised M23 endopeptidases, NlpC/p60 domain proteins, L,D transpeptidases and carboxypeptidases identified in the literature (Appendix B1) was performed in Clustal Omega (http://www.ebi.ac.uk/Tools/msa/clustalo) using protein sequences acquired from NCBI and UniProt (http://www.uniprot.org/uniprot/) to generate a phylogenetic tree in Trex-online (http://www.trex.uqam.ca/) (Alix, Boubacar & Vladimir, 2012). pFAM-predicted domain architecture was added as annotations (Finn et al., 2014) (Fig. 3.1.4).

M. tuberculosis Rv0950c, Rv2891 and Rv3786c all cluster together alongside direct mycobacterial orthologues in a sub-cluster with *E. coli* M23-domain YgeR and non-M23 endopeptidases, *E. coli* YcbB, AmpH, LdtD and PBP1b (Fig. 3.1.4a). *E. coli* LdtD and PBP1B play a role in 3-3 cross-link formation in PG (Kumar et al., 2012; Hugonnet et al., 2016; Morè et al., 2019). Sub-clusters neighbouring the *M. tuberculosis* M23 domain homologues also comprise PG remodelling enzymes such as *Corynebacterium jeikeium* PBP4 (Lavollay et al., 2009) , *E. coli* DacA (Nelson & Young, 2000, 2001; Chowdhury et al., 2012; Hugonnet et al., 2016) (Fig. 3.1.4b) and various SP11 or SP13-domain mycobacterial carboxypeptidases (Bansal et al., 2015; Pandey et al., 2018; Ealand et al., 2019) (Fig. 3.1.4c).

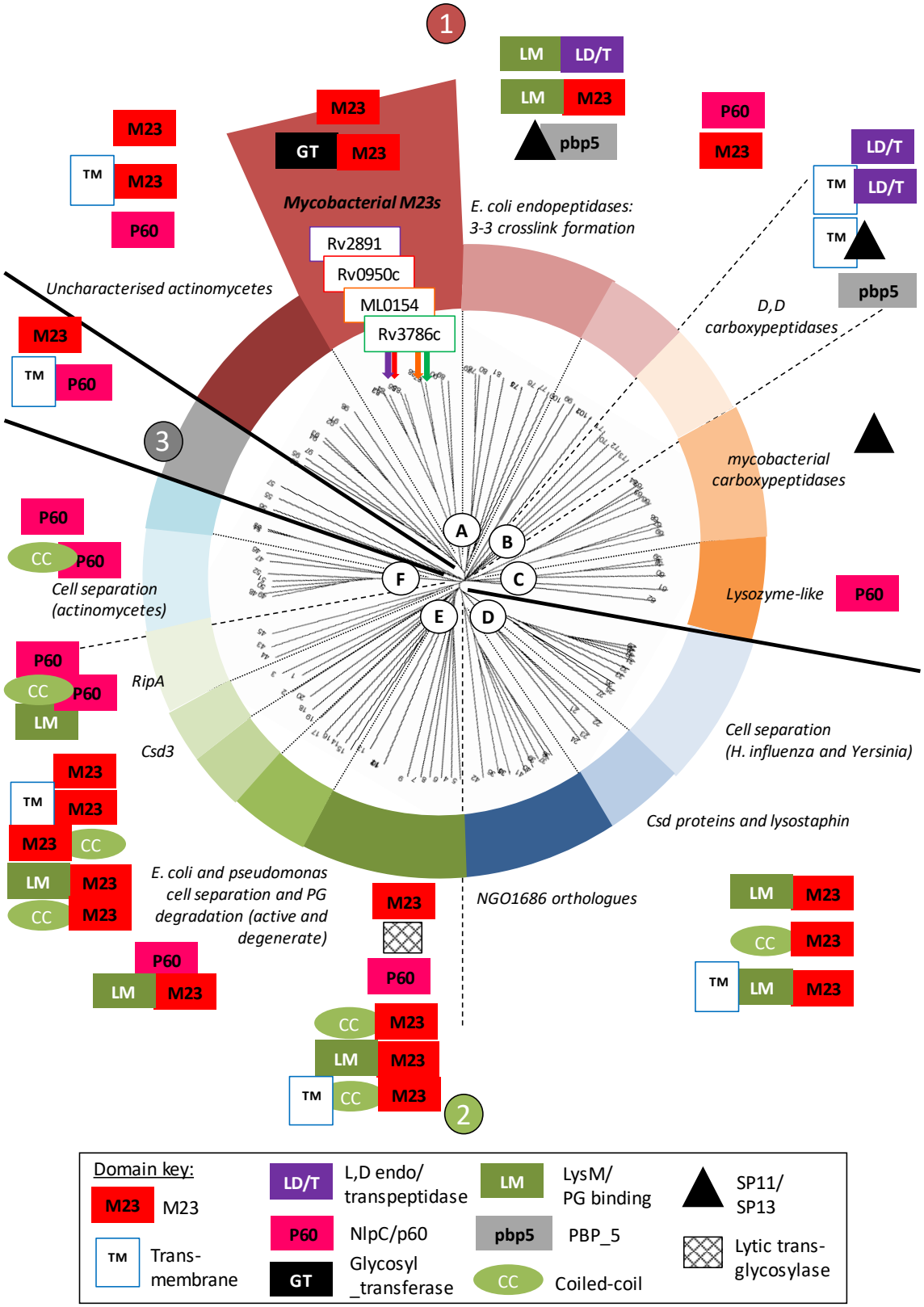

Figure 3.1.4 Phylogenetic clustering of various bacterial peptidoglycanases towards functional prediction of the *M. tuberculosis* M23 endopeptidases.
The peptidoglycanases separate into three major clusters: 1) (red to orange) comprising sub-cluster A) uncharacterised actinomycetes, mycobacterial M23 and *E. coli* L,D-transpeptidases; B) *E. coli* carboxy-peptidases; C) mycobacterial carboxypeptidases and *B. subtilis* lysozyme-like NlpC/p60 enzymes. Major cluster 2) (blue to green) comprising sub-cluster D) *Helicobacter* and *Neisseria* cell-separation M23s and *S. simulans* lysostaphin;

(Figure 3.1.4 continued) E) *E. coli* EnvC and NlpD orthologues, *M. tuberculosis* RipA and other cell separation enzymes. F) cell separation NlpC/p60 enzymes of actinomycetes. 3) an outlying cluster of three proteins: *Neisseria meningitidis* M23s of unknown function, and *M. avium paratuberculosis* MAP1272c, a PG-binding, degenerate NlpC/p60 protein.

Other bacterial M23s formed an alternative, major cluster (Fig. 3.1.4.2), including various cell division M23-endopeptidases and NlpC/p60 enzymes, such as the cell division factors, *E. coli* and *H. influenzae* EnvC, NlpD (Uehara *et al.*, 2009, 2010; Ercoli *et al*., 2015); the *H. pylori* cell shape determinant (Csd) homologues (Bonis *et al*., 2010; An *et al*., 2012) and Staphylococcal lysins, lysostaphin and LytM.

3.1.3.1 Structure homology modelling of the *M. tuberculosis* M23 endopeptidases

The *M. tuberculosis* M23 endopeptidases bear limited similarity to *E. coli* murein hydrolase activators. To search for a more functionally-predictive orthologue for the mycobacterial proteins, homology modelling was studied in the Swiss Protein Database (http://swissmodel.expasy.org/repository/) (Guex, Peitsch & Schwede, 2009; Bertoni et al., 2017; Bienert et al., 2017; Waterhouse et al., 2018; Studer et al., 2020) as the crystal structures of the *M. tuberculosis* orthologues have not been determined. Homology modelling uses protein sequence similarity to the nearest orthologue with a determined crystal structure to generate a secondary structure prediction.

For Rv0950c, the nearest structural orthologue was *N. gonorrhoea* Mpg (id. 6muk.1) (Minasov et al., 2018) at a sequence identity of 40.16%, a GMQE score of 0.27 and QMEAN score of -1.68. The GMQE estimates the quality of the model, providing a score between 0 and 1 with increasing quality, whereas the QMEAN is a multifaceted score estimates of quality relative to what would be obtained for an experimental model, whereby a positive value would equate to greater quality and a negative value, lower (Guex, Peitsch & Schwede, 2009; Bertoni et al., 2017; Bienert et al., 2017; Waterhouse et al., 2018; Studer et al., 2020). In this context, the Rv0950c model scored low with the region of homology corresponding only to the proteins' respective M23 domains (Fig. 3.1.5a, appendix B2). This supports the prior phylogeny analysis whereby the *M. tuberculosis* orthologues cluster as a unique subset of M23 endopeptidases (Fig. 3.1.4). Mpg is an active, hydrolytic M23 endopeptidase that mediates survival in the host (Stohl et al., 2012, 2013). Although both proteins have conserved residues for zinc coordination, which were important for Mpg catalytic activity (Stohl et al., 2012), the zinc atom was

excluded from the Rv0950c model (Fig. 3.1.5a) due to lack of contact. Another template, *V. cholerae* ShyA (id 6u2a.1) (Shin et al., in press), which was among the 3rd closest potential templates (appendix B2.3) produced a model wherein Rv0950c could bind zinc (Fig. 3.1.6). ShyA hydrolyses crosslinks in *V. cholerae* PG during elongation and in order to remodel cell shape for β-lactam tolerance (Dorr et al., 2013; Dörr, Davis & Waldor, 2015; Murphy, Alvarez, Adams, Liu, Chappie, Cava & Dorr, 2019). Like the Mpg model, the ShyA model scored low, at a sequence identity of 33.59%, GMQE of 0.26 and QMEAN of -0.284 also only corresponding to the M23 domain (appendix B2).

Rv2891 was modelled to *H. pylori* Csd3 (id 4rny.1) (An et al., 2015) at a sequence identity of 23.23%, GMQE of 0.41 and a QMEAN of -3.71 (appendix B2). Csd3 is a zinc-coordinating hydrolase, contributing to *H. pylori* cell shape maintenance and virulence (Bonis, Ecobichon, Guadagnini, Prevost, et al., 2010; Sycuro et al., 2010) but the zinc ligand was excluded from the model due to the presence of a Cysteine in place of the 2nd Histidine in the HxGxD...HLH motif, which is intact in Csd3 (appendix B2). Given how low scoring the first model was, a second model for zinc binding of useful quality could not be generated.

Rv3786c was modelled to *S. simulans* Lysostaphin (id 4lxc.4) (Sabala et al., 2014) at a sequence identity of 24.80%, GMQE of 0.17 and QMEAN of -2.84 (Fig. 3.1.5) (appendix B2). A low score is somewhat expected due to the highly unique N-terminus of Rv3786c, consisting of a glycosyl transferase domain. Lysostaphin is a lytic hydrolase and of the most well-characterised M23 endopeptidases (Firczuk, Mucha & Bochtler, 2005). As with the aforementioned models, zinc, which is important for Lysostaphin activity was excluded from the Rv3786c model due to lack of chelating residues (Fig. 3.1.5). Like Rv2891, the 2nd chelating Histidine is absent, replaced in Rv3786c with a Tyrosine residue. However, when Rv3786c was modelled to latent *S. aureus* LytM (2b0p.1) (Firczuk, Mucha & Bochtler, 2005), zinc binding could be predicted (Fig. 3.1.6) at a higher sequence identity than Lysostaphin (25.81%), the same GMQE (0.17) and a higher QMEAN (-2.02) despite appearing much lower on the list of potential templates. The space-fill perspective of the zinc-binding residues appears very similar in both proteins despite the substitution of a Tyrosine (Fig. 3.1.6). Still, the low scores of all the models create difficulty in detailed cross comparisons but do highlight the conserved nature of the M23 domain and yet the

uniqueness of the structures of the *M. tuberculosis* orthologues, a consistent observation throughout the above *in silico* analyses.

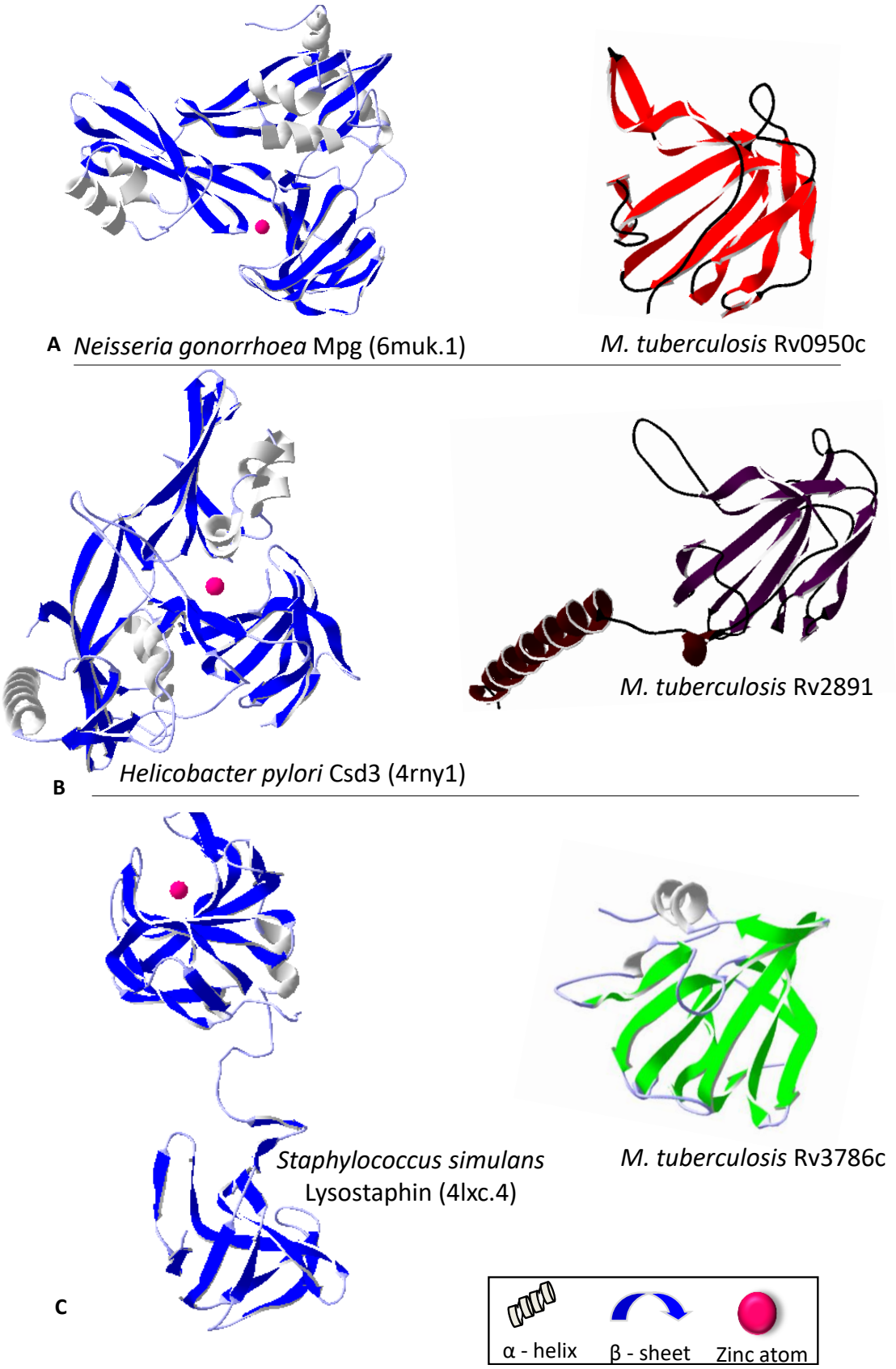

Figure 3.1.5 Swiss homology modelling (http://swissmodel.expasy.org/repository/) of the *M. tuberculosis* M23 endopeptidases

(Figure 3.1.5 continued) Left: model templates, Right: *M. tuberculosis* M23 endopeptidases which all display the canonical anti-parallel, β-sheet (colour) conformation of the M23 domain. A) Rv0950c (red) was modelled to *Neisseria gonorrhoea* Mpg; B) Rv2891 was modelled to *Helicobacter pylori* Csd3; Rv3786c was modelled to *Staphylococcus simulans* Lysostaphin. Each of the model templates were purified with a zinc atom (magenta) bound to the active site but was excluded in the models of the *M. tuberculosis* orthologues. Images were generated using Swiss PDB viewer.

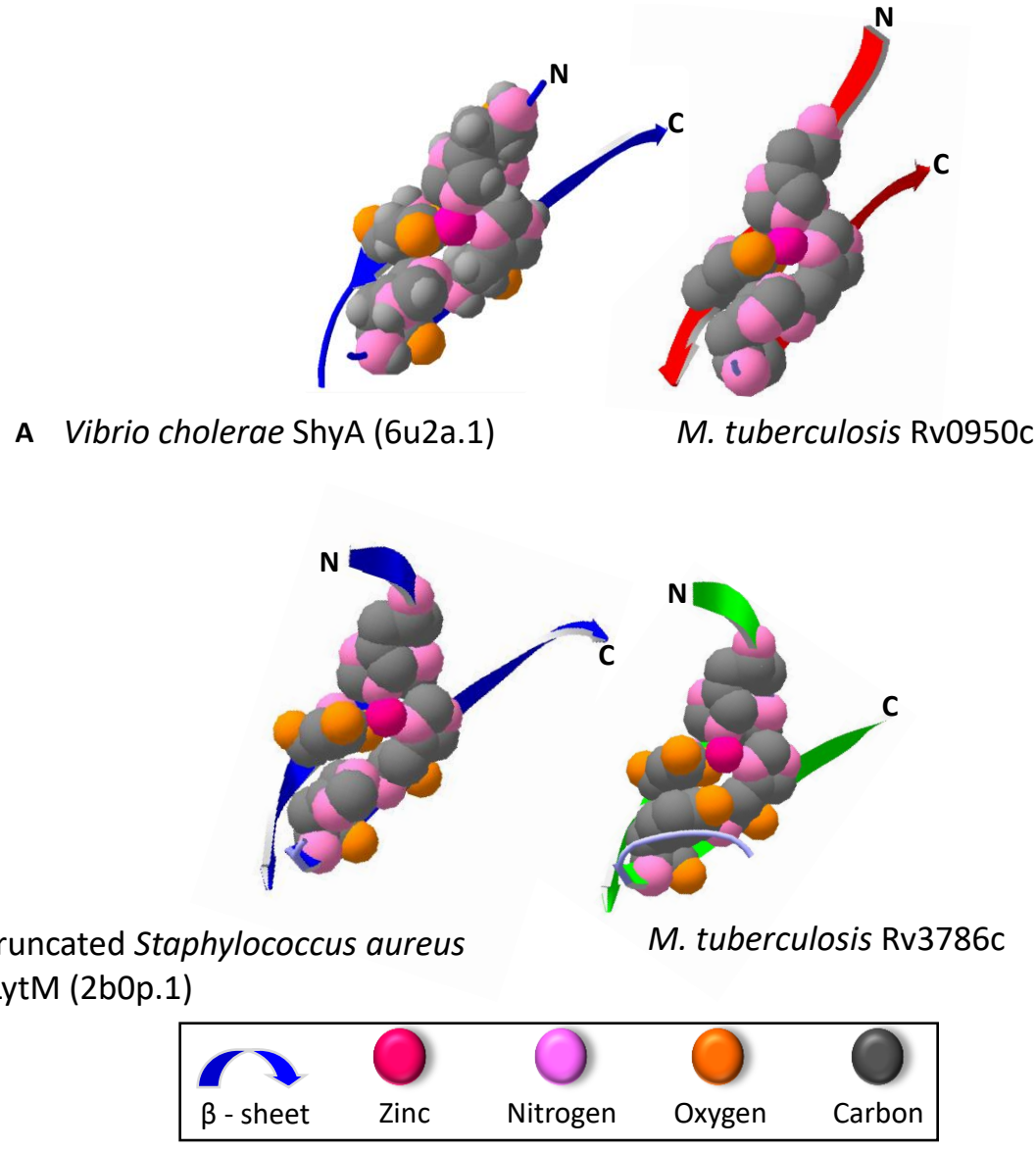

Figure 3.1.6 Space-fill models of M23 endopeptidase zinc chelation
Swiss homology modelling predicts zinc chelation for *M. tuberculosis* Rv0950c (red) when modelled to *Vibrio cholerae* ShyA (6u2a.1) (A); and Rv3786c (green) when modelled to LytM (2b0p.1) (B). The space fill model shows the amino-terminal HxGxD motif of one β-sheet lining up with the HxH motif of a carboxy-terminal β-sheet to chelate zinc. The motif is conserved in ShyA, Rv0950c and LytM, while Rv3786c has a Y substitution at the 2nd H (YxH) which does not appear to impact chelation. Images were generated using Swiss PDB viewer.

3.1.4 Summary of bioinformatics findings

The mycobacterial M23s therefore represent a functionally divergent class of M23 endopeptidases, likely required for PG remodelling. To confirm this, Rv0950c was chosen

for study (section 3.2), which appears to be the most conserved of the three homologues (Table 3.1.3).

Unpublished characterisation of the Rv0950c orthologue, MSMEG_5526 (Table 3.1.3), suggests this protein plays a role in PG remodelling for cell growth and rod shape maintenance in the non-pathogenic, model organism, *M. smegmatis* (Shaku unpublished, 2017). Loss of MSMEG_5526 caused a log phase growth defect and aberrant morphotypes such as polar and septal bulges (Shaku unpublished 2017). Cell wall weakening was also observed as hyper susceptibility to lysozyme degradation of *M. smegmatis* PG (Shaku unpublished, 2017). Two degenerate M23 endopeptidases, MSMEG_0247 and MSMEG_1192 are collectively required for *M. smegmatis* cell division (Shaku unpublished, 2017) but have no direct orthologues in *M. tuberculosis* (Table 3.1.3). Limited study of Rv2891 (Section 3.3) was also performed but could not be concluded due to time constraints.

Table 3.1.3 Mycobacterial expansion of M23 endopeptidases highlights Rv0950c as the most conserved orthologue in *M. tuberculosis*. Direct orthologues occur in the same row.

M. leprae	***M. abscessus***	***M. tuberculosis***	***M. marinum***	***M. smegmatis***
ML_0514	1055	Rv0950c	4551	5526
	3197	Rv2891	1818	2518
		Rv3786c	5347	-
			3448	-
				1192
				0247

3.2 Characterisation of Rv0950c, a putative metallo-endopeptidase required for PG maturation in *M. tuberculosis*.

3.2.1 Conservation of Rv0950c

A combination of *in silico* tools revealed a novel, putative M23-endopeptidase encoded in the genome of *M. tuberculosis* at locus Rv0950c with a possible role in PGremodelling (section 3.1). Rv0950c is the most conserved M23-endopeptidase among three putative homologues found in *M. tuberculosis* and is highly conserved in various mycobacteria (Table 3.2.1).

Table 3.2.1 Distribution of Rv0950c orthologues in mycobacterial species.

Group	Species	Locus	Domain architecture
MTB complex	*M. tuberculosis* H37Rv	Rv0950c	H...H
	M. tuberculosis H37Ra	MRa_0957	
	M. tuberculosis CDC 1551	MT0977	
	M. tuberculosis KZN 4207	TBSG_03059	
	M. africanum	RN09_1159	
	M. bovis AF122/97	MB_0975c	
	M. bovis BCG Pasteur	BCG_1004c	
Other pathogens	*M. abscessus* ATCC19977	MAB_1055c	
	M. avium	MAV_1073	
	M. avium subsp. paratuberculosis	MAP_0895c	H...H
	M. ulcerans AGY99	MUL_4721	
	M. marinum	MMAR_4551	H...H
	M. intracellularae	OCU_09440	
	M. leprae TN	ML0154c	H...H
Environmental species	*M. smegmatis*	MSMEG_5526	H...H
	M. vanbaaleni PYR-1	Mvan_4871	H...H
	M. sp KMS	Mkms_4414	H...H
	M. sp JLS	Mjls_4708; 4510	
	M. sp MCS	Mmcs_4328	
	M. gilvum PYR-GCK	Mflv_1864	H...H
		Mflv_2817	H...H

Key: m23 domain; disorder; low complexity; H...H catalytic residues; coiled-coil domain; transmembrane domain

Data obtained from Kegg SSDB ortholog (https://www.kegg.jp/kegg/kegg2.html), UniProt similar proteins (http://www.uniprot.org/uniprot/) and PHMMER (http://www.ebi.ac.uk/Tools/hmmer). Domain architecture based on pFAM (http://pfam.xfam.org/).

From the three putative M23 domain-containing peptidases identified in *M. tuberculosis*, only Rv0950c is conserved in *M. leprae*, encoded by ML_0145c (Fig. 3.2.1). *M. leprae* has been reported to retain the minimal genome required for virulence (Vissa & Brennan, 2001), and the conservation of the Rv0950c homologue suggests that this enzyme is important. The function of ML_0154c is unknown, however a closer study of the synteny between Rv0950c and ML_0154c revealed that most of the neighbouring genes of Rv0950c are conserved in a similar proximity with ML_0154c, mostly populated by genes of intermediary metabolism and cell wall processes (Fig. 3.2.1). For example, phosphoglucose isomerase (*pgi*) is required for glycerol utilisation possibly for linkage structures between PG and arabinogalactan (Tuckman et al., 1997). Rv0948c encodes a chorismate mutase involved in amino acid biosynthesis (Schneider et al., 2008). Rv0953c and Rv0954 can bind the KtsR repressor shown to regulate genes involved in lipid metabolism (Kendall et al., 2007). Rv0950c or ML_0154c may be co-regulated with these genes required for various aspects of mycobacterial growth, but this requires verification.

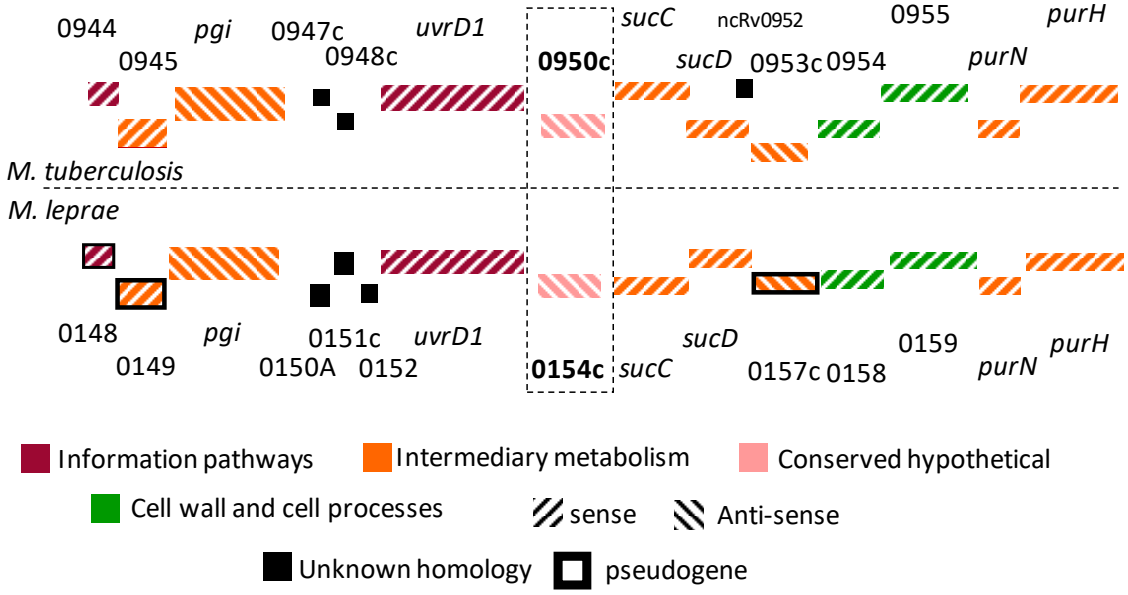

Figure 3.2.1 Conserved genetic synteny between Rv0950c and the only orthologue in *M. leprae*. *M leprae* represents the most reduced genome among the mycobacteria wherein highly conserved genes are considered important for mycobacterial growth and survival. Re-representation of genetic neighbourhoods displayed by Tuberculist (http://tuberculist.epfl.ch/).

3.2.2 Rv0950c is required during exponential growth: Growth-phase dependent transcription profile of the M23-endopeptidase encoding genes of *M. tuberculosis*

The growth phase transcription profile of the *M. tuberculosis* M23-domain genes was studied to determine the importance of these genes during cell growth. Reverse primers designed with homology to the 3' end of Rv0950c, Rv2891 Rv3786c, and a house-keeping

transcription factor *sigA* were used for cDNA conversion of RNA extracted from wild-type (WT) *M. tuberculosis* cultures at lag, early and late exponential, as well as stationary phase.

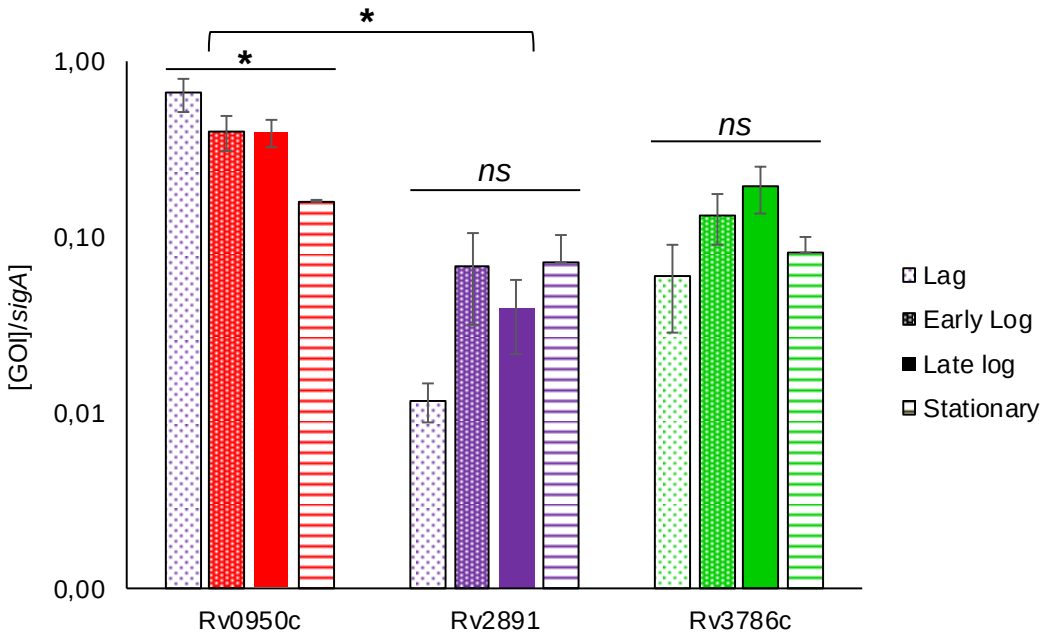

Figure 3.2.2 Growth-phase dependent transcription of the M23-endopeptidases of *M. tuberculosis.* RNA extracted from triplicate cultures of WT *M. tuberculosis*. Expression levels were measured by qPCR against gDNA standards using BioRad CFX manager and normalised to *sigA*. *p<0.02 by single-factor for Rv0950c (flat-line) or two-factor Rv0950c:Rv2891 at exponential phases (bracket) ANOVA in Excel. *ns*: not significant.

The three genes are differentially expressed related to each other across the growth phases (p = 0.02 for two-factor ANOVA and Table 3.2.2). The greatest differences were observed between Rv0950c and Rv2891, the highest and lowest abundant transcripts respectively (Fig. 3.2.2 and Table 3.2.2). Rv2891 and Rv3786c were expressed equivalently across the phases, while Rv0950c exhibited a unique growth phase dependent profile, with reducing levels upon entry into stationary phase (p = 0.025 for single-factor ANOVA between the growth phases of Rv0950c, Fig. 3.2.2). If required specifically for cell division, like the activator orthologues of *E. coli*, it was expected that Rv2891 would be upregulated at exponential phase. Instead, a non-significant increase was observed between lag and early exponential phase (Fig. 3.2.2).

Combining the data obtained from *in silico* analyses and *in vitro* transcription profiling, Rv0950c is a highly conserved, putative, active M23-endopeptidase the expression of which is modulated during growth of *M. tuberculosis*. Gene knockout studies were subsequently performed followed by phenotyping the morphological and PG composition changes upon Rv0950c deletion.

Table 3.2.2 Single factor ANOVA *p-values* for comparing growth-phase dependent expression of *M. tuberculosis* M23 endopeptidase genes.

	All genes	Rv0950c:Rv2891	Rv0950c:Rv3786c
Lag	0.002	0.0095	0.01
Early log	0.01	0.025	0.05
Late log	0.008	0.007	0.08
Stationary	0.05	ns	ns

ns: not significant.

3.2.3 Deletion of Rv0950c from the *M. tuberculosis* genome by suicide vector-mediated homologous recombination

3.2.3.1 Suicide vector construction

Rv0950c deletion was achieved using suicide vector-mediated allelic exchange of the deletion allele with the wild-type allele in the genome (Parish & Stoker, 2000). With this approach, the deletion allele consists of a fusion of 1300-1500 bp upstream and downstream regions of the gene of interest, including the first 28 and last 37 bp of the open reading frame. The majority of the gene is therefore deleted. The regions of homology will be recognised by the bacterium during recombination, thus ensuring the deletion cassette is not inserted in a non-homologous region in the genome, only disrupting the gene of interest. Rv0950c is encoded on the complement strand of the *M. tuberculosis* genome, overlapping the neighbourhood of *uvrD1* and *succC* (Fig. 3.2.3a). The upstream and downstream arms were designed in-frame so as not to disrupt these genes. The downstream homology arm overlaps a putative promoter region of *succC*, which was kept intact in the deletion allele, while ensuring deletion of the entire M23 endopeptidase domain (Fig. 3.2.3a). These homology arms were amplified by PCR from *M. tuberculosis* genomic DNA (Fig. 3.2.3). The upstream homology arm was initially blunt-cloned into pBlueScript (Alting-Mees & Short, 1989), propagated and then sub-cloned along with the digested downstream PCR product by 3-way, directional ligation into the p2nil suicide vector backbone (Fig. 3.2.4), via *Hin*DIII, *Bgl*II and *Pst*I sites incorporated on the flanks of homology arms during PCR. The resulting plasmid was confirmed by restriction digestion analysis and then sequencing (appendix B3) to ensure the integrity of the respective homology arms (to prevent additional mutation of the genome) and to ensure a functional suicide vector (Fig .3.2.4). Although digestion with *Msc*I, *Nru*I and *Nae*I did not result in complete digestion, sequencing of the upstream and downstream fusion (Fig. 3.2.4, green) confirmed the genetic integrity of the construct (appendix B3).

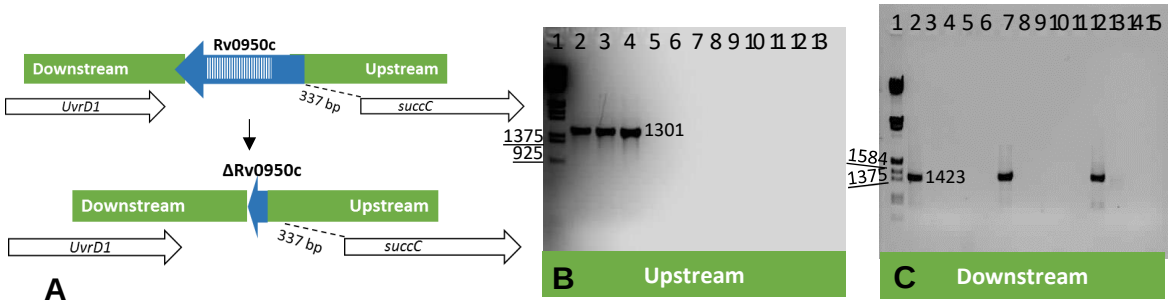

Figure 3.2.3 Cloning of p2nilΔRv0950c for suicide vector mediated deletion of Rv0950c.
A) Genomic organisation of Rv0950c showing homology regions (green) amplified for cloning into p2nil. Stripes represent the M23 domain. A small portion of the 5' end of Rv0950c was included so as not to disrupt the putative promoter region of *succC*. B) PCR amplification of 1301 bp upstream region 1) MWM III, Annealing temperature gradient of 58°C (2,5,8,11); 60°C (3,7,12) and 64°C (4,8,13). Controls excluding forward (5-7), reverse (8-10) primers and template DNA (11-13). C) PCR amplification of 1423 bp downstream 1) MWM III, Annealing temperature gradient of 76°C (2-5), 75°C (7-10) and 74°C (12-15). Controls excluding forward (3,8,13), reverse primer (4,9,14) and template DNA (5,10,15). MWM: digested Lambda phage DNA marker (underlined).

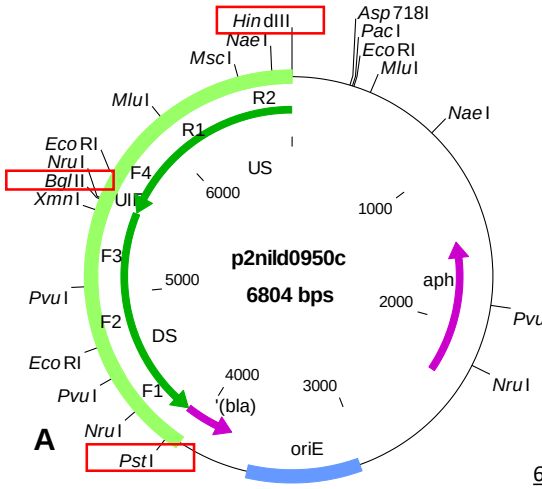

B

Enzyme	Expected sizes (bp)
MscI	6804
NruI	3476, 2130, 1198
XmnI	6804
MluI	5628, 1176
NaeI	5866, 938
PvuI	3613, 2684, 507

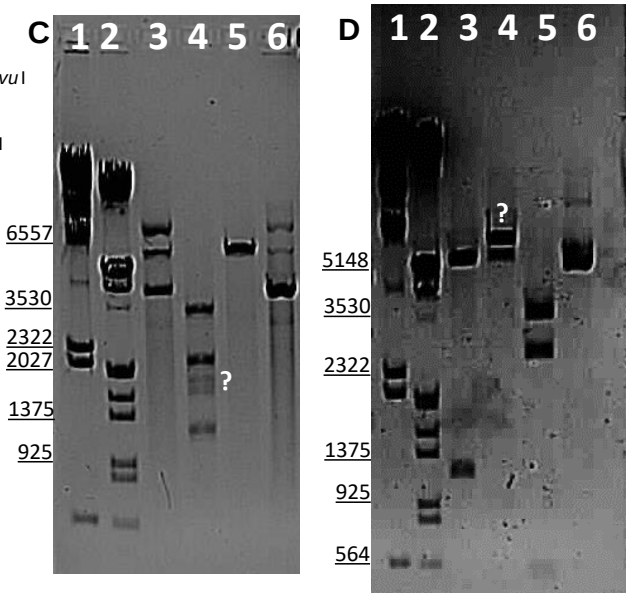

Figure 3.2.4 Restriction digestion mapping of p2nilΔRv0950c suicide vector for deletion of Rv0950c.
A) Vector map showing upstream (US) and downstream (DS) arms cloned directionally via *Hin*DIII, *Bgl*II and *Pst*I sites (red boxes) into p2Nil. Green indicates the sequenced region. B) Expected product sizes for restriction mapping. C) 1) MWM II; 2) MWM III; mapping with 3) *Msc*I; 4) *Nru*I; 5) *Xmn*I; 6) undigested control. D) 1) MWM II; 2) MWM III; 3) *Mlu*I; 4) *Nae*I; 5) *Pvu*I; 6) undigested control. MWM: digested Lambda phage DNA marker (underlined).

The p2Nil plasmid lacks a mycobacterial origin of replication for episomal maintenance and therefore can only be expressed when incorporated into the genome after the first step of allelic exchange (Parish & Stoker, 2000). This first step, referred to as a single cross over,can therefore be selected by Kanamycin resistance conferred by p2Nil. Further selective markers, *lacZ* and *sacB*, are required for selection of the second cross over step. *lacZ* allows for detection of strains carrying the p2nil backbone after single-cross-over as blue colonies, while *sacB* encodes for sucrose toxicity aiding selection after the second-step of allelic exchange, whereby the WT allele is discarded from the genome along with the p2nil backbone therefore surviving exposure to sucrose. The *lacZ* and *SacB* genes encoded by the pGOAL17 *Pac*I cassette, were sub-cloned into p2nil to complete the suicide vector construct (Fig. 3.2.5). The complete vector was confirmed again by restriction digestion analysis (Fig.3.2.5). The sucrose sensitivity of the final construct was confirmed in *E. coli* before electroporation into *M. tuberculosis* (Fig. 3.2.6).

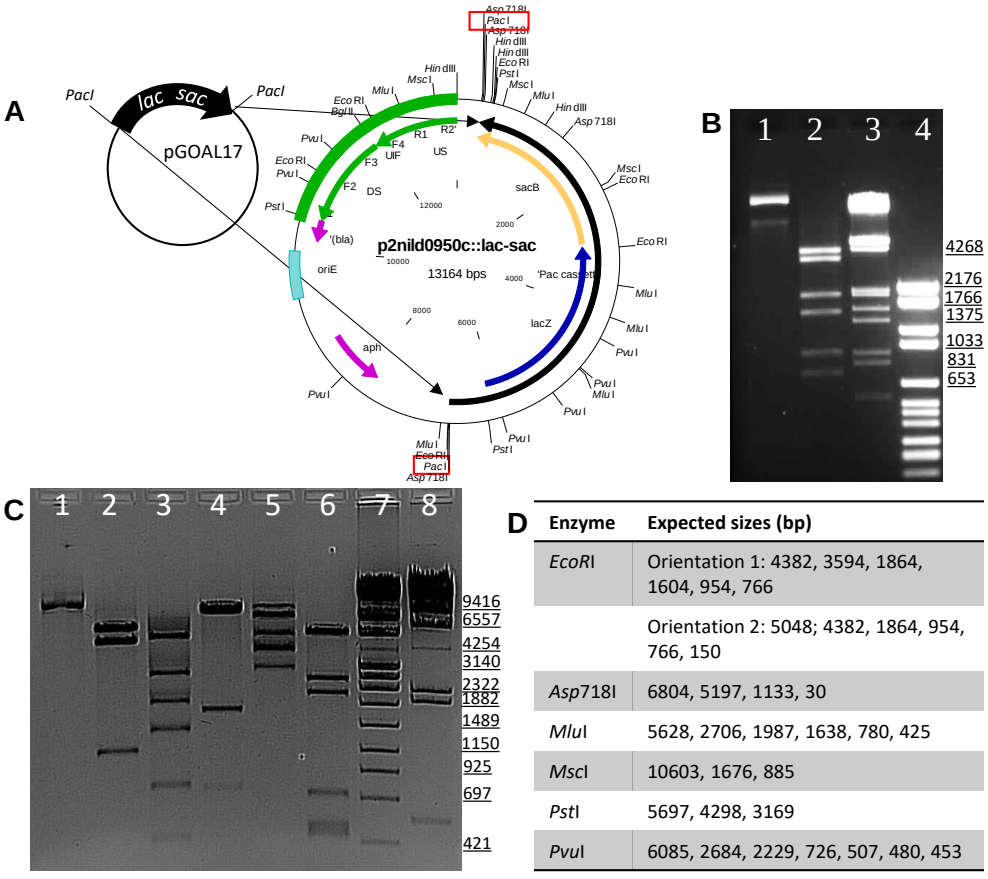

D

Enzyme	Expected sizes (bp)
*EcoR*I	Orientation 1: 4382, 3594, 1864, 1604, 954, 766
	Orientation 2: 5048; 4382, 1864, 954, 766, 150
*Asp*718I	6804, 5197, 1133, 30
*Mlu*I	5628, 2706, 1987, 1638, 780, 425
*Msc*I	10603, 1676, 885
*Pst*I	5697, 4298, 3169
*Pvu*I	6085, 2684, 2229, 726, 507, 480, 453

Figure 3.2.5 Sub-cloning of the pGOAL17 *lac_sac* cassette into p2nilΔRv0950c.
A) Schematic diagram of the sub-cloning strategy. The *lac_sac* cassette (black) was cloned into the *Pac*I site (red boxes) of p2Nil, green indicates the Rv0950c deletion cassette previously sequenced; B) Direction of *Pac*I cassette cloning determined by *EcoR*I digestion indicating orientation 1: 1) undigested control; 2) digestion with *EcoR*I; 3) MWM III; 4) MWM VI. C) Further mapping of the construct 1) undigested control; 2) *Asp*718I; 3) *Mlu*I; 4) *Msc*I; 5) *Pst*I; 6) *Pvu*I; 7) MWM IV; 8) MWM II. D) Expected products of restriction digestion of the ΔRv0950c suicide vector. MWM: digested Lambda phage DNA marker (underlined).

A

Dil. Factor (10^{-x})	0% sucrose	5% sucrose
0	TNTC	17
1	TNTC	2
2	TNTC	0
3	TNTC	0
4	19	0
5	2	0
6-11	0	0

B

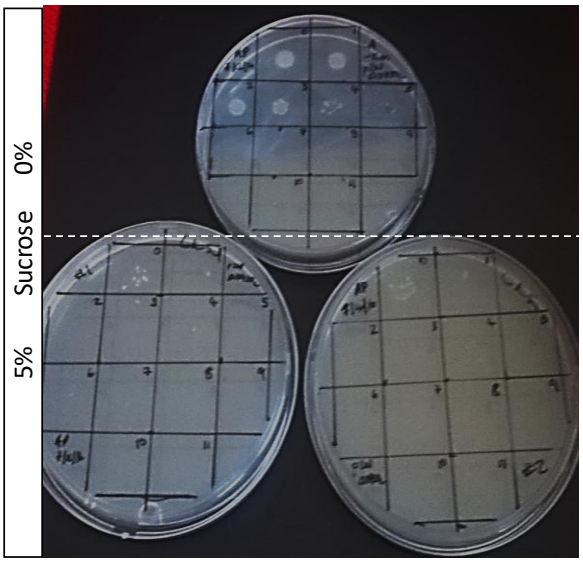

Figure 3.2.6 Sucrose sensitivity of p2nilΔRv0950c::*lac-sacB*-transformed *E. coli*.
Broth culture was diluted serially up to 10^{-11} and spotted (5 µl) on Km-supplemented LA excluding (0%) (n = 1) or including 5% sucrose (n = 2). A) No. of colony forming units shows 5-log fold killing in the presence of 5% sucrose indicating functionality of the *sacB* gene. TNTC: Too numerous to count. B) Photograph of plates showing colonies at 0% up to the fifth dilution spot vs reduced colony formation at 5% sucrose.

3.2.3.2 Screening for single cross over events

The complete ΔRv0950c suicide-vector construct, confirmed by restriction digestion, sequencing and sucrose sensitivity (Fig. 3.2.5,6), was electroporated into *M. tuberculosis* and plated on agar containing kanamycin and X-Gal to select for the single cross over event in the *M. tuberculosis* chromosome at the Rv0950c locus. This single cross over strain could then be identified as colonies with a blue, kanamycin-resistant phenotype and genotypically carrying both the WT and ΔRv0950c allele (Fig. 3.2.7). Both alleles were detected using one set of three PCR primers: ScF1 and ScR1, hybridising to the upstream and downstream homology arms, which is isogenic in both alleles but shortened in the mutant; along with ScR2 which hybridises to the coding region of Rv0950c, excluded from the deletion allele (Fig. 3.2.7a). PCR successfully detected both alleles in DNA extracted from blue colonies alongside WT genomic DNA as a control (Fig. 3.2.7b14) confirming successful single-cross over.

3.2.3.3 Double cross over events confirmed by PCR, Southern blotting and qPCR

The single-cross over strain was then passaged without kanamycin to encourage loss of the vector backbone along with the WT allele through a second cross over event. For screening, the strain was plated on sucrose, killing any remaining single-cross over events and surviving colonies were then genotyped by PCR to distinguish between WT and

ΔRv0950c strains (Fig. 3.2.8). The primers used for single-cross over events produced amplicons in the WT and mutant alleles that only differed by ~100 bp which would prove difficult to distinguish in the double-cross over strains. Primer design for DCO screening was improved on but followed the same concept as before: the second set of 3 primers amplify 1773 bp and/or 501 bp for the wild type allele, and 836 bp for the deletion allele (Fig. 3.2.8a). PCR identified mostly WT strains, a small number of mutant strains and occasional single-cross overs (Fig. 3.2.8b).

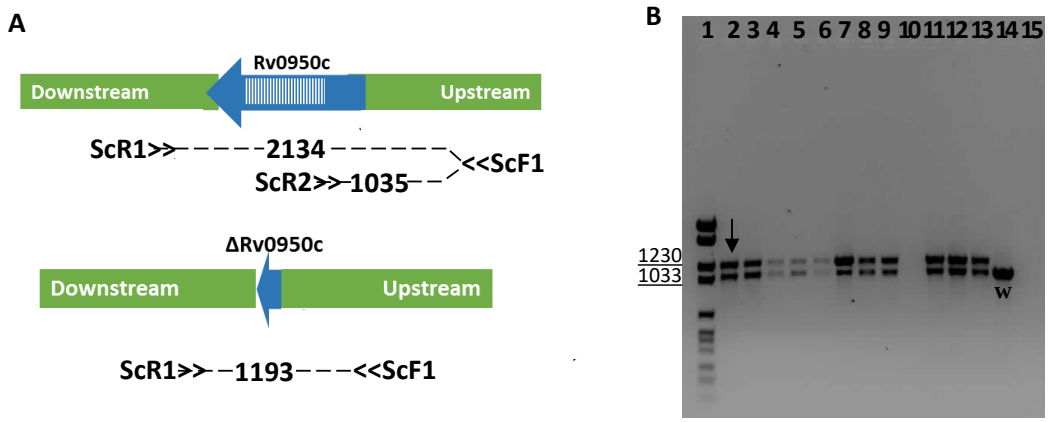

Figure 3.2.7 Genotyping of *M. tuberculosis*::p2nilΔRv0950c single cross over events by PCR. A) schematic diagram of positions of forward (F1) and reverse (R1,R2) primers and expected amplicon sizes for distinguishing between WT and mutant alleles in SCO strains; B) 1) MWM VI, 2-13) 12 blue Km^R colonies with both WT (1033) and Δ (1193) products (down arrow), 14) wild-type control (w), 15) no template control (NTC). MWM: digested Lambda phage DNA marker (underlined).

Two of the mutant strains identified by PCR were further confirmed by Southern blotting. For this, genomic DNA extracted from WT and putative mutant strains was digested with *Bgl*I for upstream genotyping. The restriction fragment size differences were due to the presence of a *Bgl*I present in the WT coding region and flanking the upstream and downstream homology arms (Fig. 3.2.8c). As such, a DIG-labelled probe complementary to the upstream homology arm hybridised to a 1949 bp fragment in the WT strain vs a 4377 bp fragment in the deletion mutant (Fig. 3.2.8c). Deletion of Rv0950c was lastly confirmed by measuring loss of Rv0950c expression (p = 0.04 for ANOVA single factor comparing all three strains; Fig. 3.2.8d). In the absence of template, mis-priming can occur and is likely the cause of the negligible Sybr Green signal in the deletion strain (Fig. 3.2.8d) which had a lower T_m than the wild-type and standard curve qPCR products (Appendix B4).

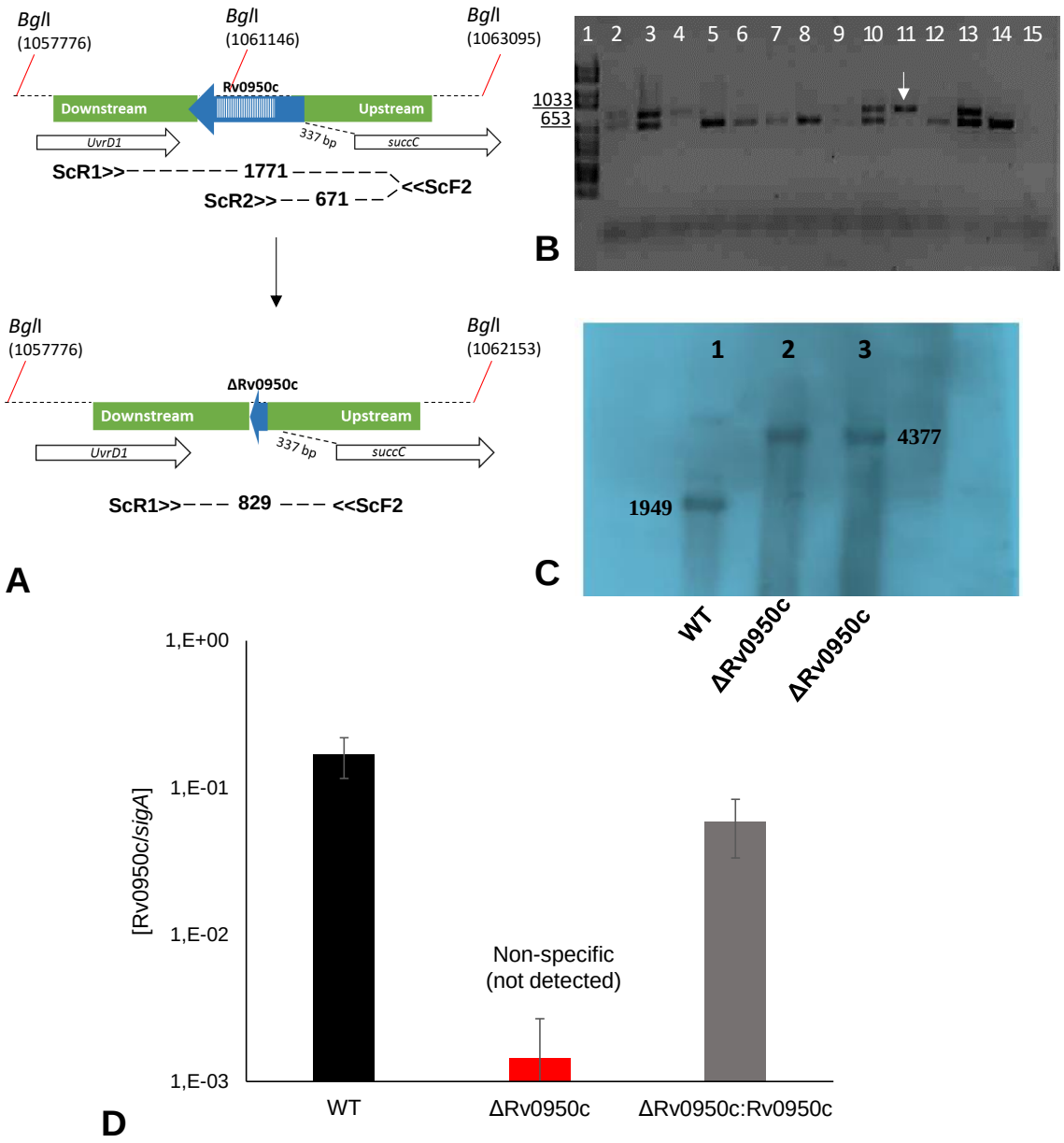

Figure 3.2.8 Genotypic confirmation of *M. tuberculosis* ΔRv0950c.
A) schematic diagram of positions of forward (F1) and reverse (R1,R2) primers and expected amplicon sizes for distinguishing between WT and mutant alleles in DCO strains, indicating sites for *Bgl*I digestion prior to Southern blotting. B) PCR genotyping of DCO strains 1) MWM VI, 2-12) products amplified from white, sucrose-resistant colonies, 11) putative DCO (down arrow) taken forward for southern blotting 13) SCO control bearing both WT and ΔRv0950c products, 14) WT control (w), 15) NTC. C) Southern blotting to confirm deletion of Rv0950c from the *M. tuberculosis* genome using a DIG-labelled probe to the upstream homology arm to detect *Bgl*I fragments: 1) WT (1949 bp); 2-3) ΔRv0950c (4377 bp). D) RT-qPCR to confirm loss of Rv0950c transcription in the ΔRv0950c strain and restoration of transcription after pTTP1b::Rv0950c complementation. MWM: digested Lambda phage DNA marker (underlined).

3.2.3.4 Genetic complementation via pTTP1B integration

To validate that subsequently observed phenotypes are as a result of the loss of Rv0950c as opposed to polar effects of genetic manipulation, it was necessary to complement the mutant strain with the wild-type allele to yield a genetically complemented strain, which should phenotypically mimic the WT strain. For this, Rv0950c was reintroduced via a vector expressing a phage integrase. Because complementation is ectopic and not at the original Rv0950c locus, the complementation allele consists of the Rv0950c coding sequence with additional 337 bp upstream sequence representing the putative promoter region of Rv0950c (Fig. 3.2.9b). The Rv0950c complementation allele was amplified by PCR and ligated into the multiple cloning site of pTweety, confirmed by restriction digestion analysis (Fig. 3.2.9) and sequencing (appendix B3). The vector was electroporated into *M. tuberculosis* and colonies were screened by kanamycin resistance. Genotyping by PCR revealed the presence of both the deletion and complement allele in transformants (Fig. 3.2.9g).

Complementation was further confirmed by southern blotting using a probe amplified from the complement allele in pTweety and restriction digestion with *Bgl*II (Fig. 3.2.10). *Bgl*II sites occurred upstream of the *lysU attB* site of pTTP1b integration (Pham et al., 2007) and within the pTTP1b backbone, while the mutant carried *Bgl*II as a cloning scar for fusion of upstream and downstream homology arms (Fig. 3.2.10b). Southern blotting revealed the expected band for complementation of Rv0950c at the *attB* site (Fig. 3.2.10c). As controls, the mutant strain produced a short band complementary to the promoter region of the probe, flanking *Bgl*II upstream; as well as a very faint band of the downstream flank that produced signal as a result of 62 bp hybridising to the 3' end of the Rv0950c probe (Fig. 3.2.10). The *lysU* homologue, *lysT* lacks *Bgl*II sites within 3000 bp flanking the locus. Therefore, based on the Southern blot products sizes (Fig. 3.2.10c), *lysT* could not have been the site for pTTP1b integration. Complementation was lastly confirmed by the return of Rv0950c expression (Fig. 3.2.8d). Although, expression levels did not match WT exactly (not significant), levels were significantly higher than the mutant parent strain (p = 0.056 for single factor ANOVA) and may be due to the ectopic position of the complement allele which may lack unknown expression-enhancing factors at the Rv0950c neighbourhood.

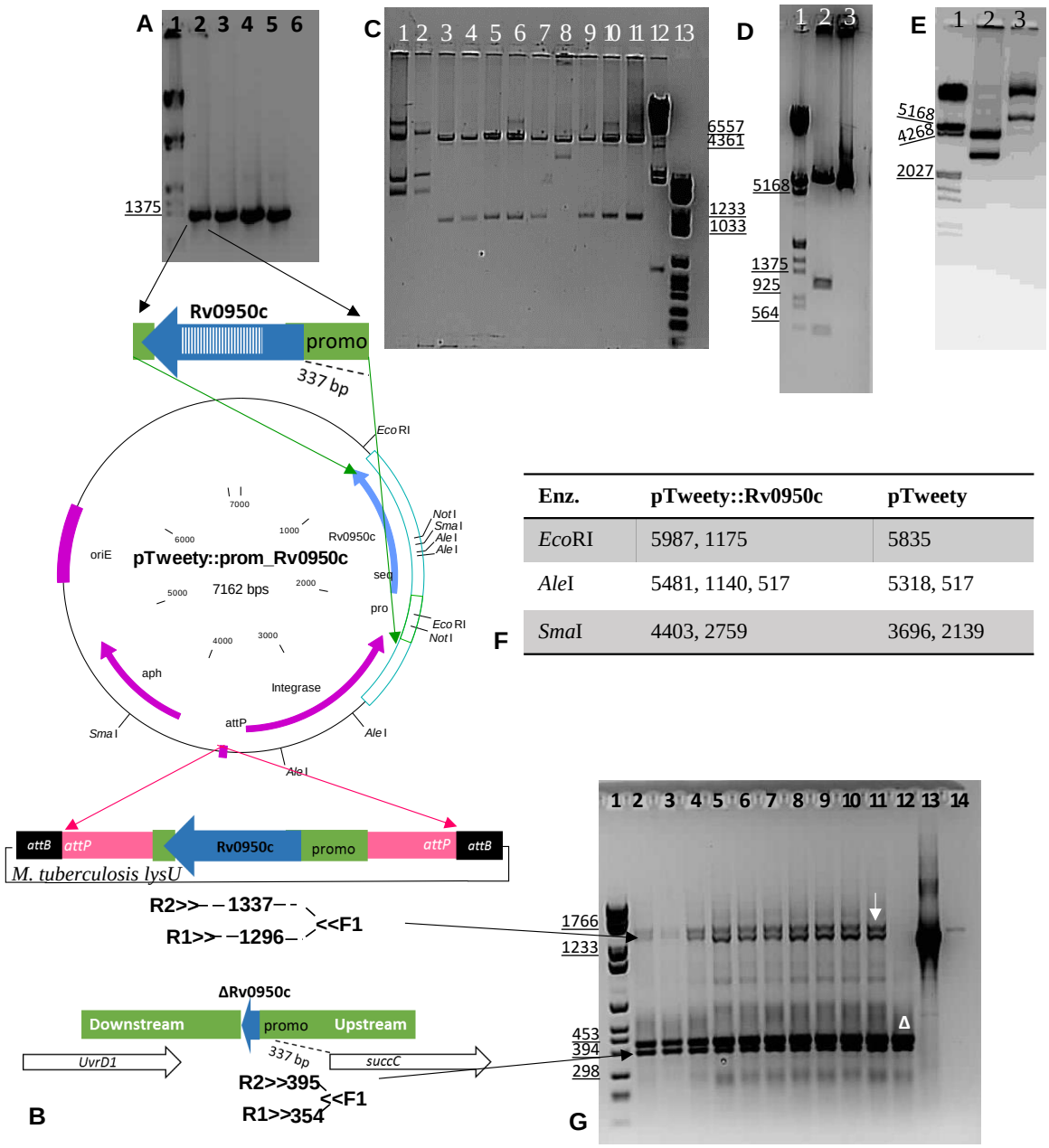

Figure 3.2.9 Cloning of the pTTP1B::Rv0950c complementation vector.
A) PCR amplification of the complementation allele for cloning into pTTP1B: 1) MWM III, 2-5) replicate amplicons (1360 bp), 6) no template control. B) Schematic diagram of complement construct design: The vector map shows the *attP* site, *integrase* gene and complement cassette which was sequenced (blue, open box). The *attP* site (pink) integrates into the *attB* region (black boxes) of homology in the *lysU* gene of the *M. tuberculosis* genome. PCR primers F1, R1 and R2 span the Rv0950c promoter region and 3' end of the open reading frame. Complement strains will therefore carry both the short mutant products and large WT products, whereas the WT or mutant strains will display either. C-E) Restriction digestion mapping of the complement construct: C) *Eco*RI digestion showing 1) empty vector uncut, 2) empty vector digested with *Eco*RI, 3-11) putative clones, 12) MWM II, 13) MWM VI. D) *Ale*I: 1) MWM III, 2) digested, 3) uncut. E) *Sma*I: 1) MWM III, 2) digested, 3) uncut. F) Table of expected restriction fragments. G) PCR confirmation of integrants 1) MWM VI, 2-11) putative complements (down arrow) displaying WT (1337 or 1296 bp) and ΔRv0950c (354, 395 bp) PCR products, 12) ΔRv0950c control (Δ) displaying only 354 and 395 bp products, 13) pTweety plasmid DNA control, 14) NTC. MWM: digested Lambda phage DNA marker (underlined).

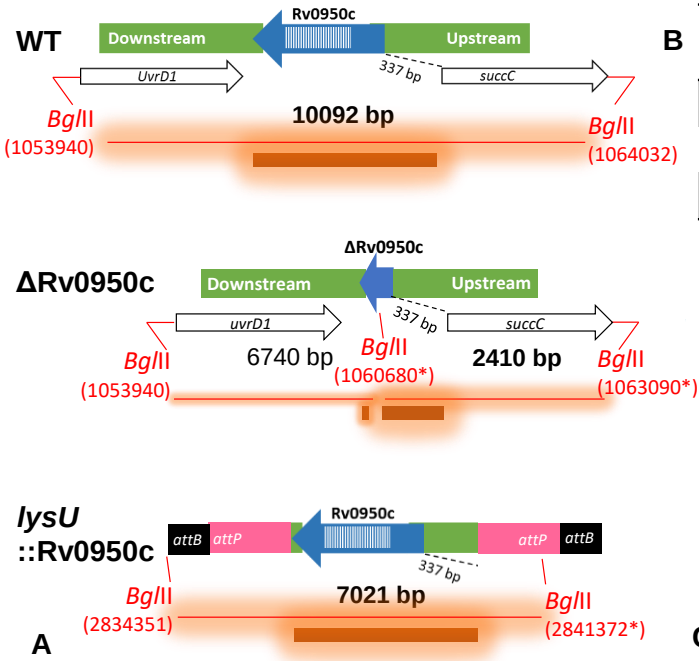

B

Strain	Expected *Bgl*II fragments (bp)
WT	10092
ΔRv0950c	2410+6740
lysU::Rv0950c	7021+2410

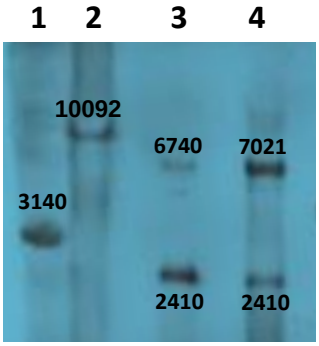

C

Figure 3.2.10 Confirmation of *M. tuberculosis* ΔRv0950c::pTweety-Rv0950c.
A) Schematic diagrams of the genomic regions of loci of interest (WT, deleted Rv0950c and *lysU-attB* integration of the complement). Sites for *Bgl*II digestion are indicated in red, the fragments generated after *Bgl*II digestion are indicated as a red glowing line with bp size indicated. The DIG-labelled probe is complementary to the Rv0950c complement cassette (orange, glowing bar). B) Expected *Bgl*II fragments complementary to the Rv0950c probe for each strain. C) Southern blot 1) MWM IV, 2) WT, 3) ΔRv0950c, 4) *lysU*::Rv0950c. MWM: digested Lambda phage DNA marker.

3.2.4 The effect of Rv0950c deletion on cellular morphology

The Rv0950c deletion mutant strain provided a system for functional characterization of Rv0950c by reverse genetics. No redundant partners are expected for Rv0950c given the *in-silico* predictions of a unique domain architecture, a unique active site and unique growth phase-dependent transcription profile among the three M23-endopeptidase genes of *M. tuberculosis*. Bioinformatics also suggested that Rv0950c is a cell-wall associated endopeptidase. Therefore, the effect of Rv0950c deletion on cell wall modification was studied firstly by scanning electron microscopy (Fig. 3.2.11). Deletion of Rv0950c did not alter the characteristic rod shape of tubercle bacilli, however cells were significantly shorter (p = 5.5E-08), an effect which was reversed by complementation (p = 2.1E-10, comparing ΔRv0950c to complement; Fig. 3.2.11). These data suggest that Rv0950c is an M23-endopeptidase required for maintenance of cell length in *M. tuberculosis*.

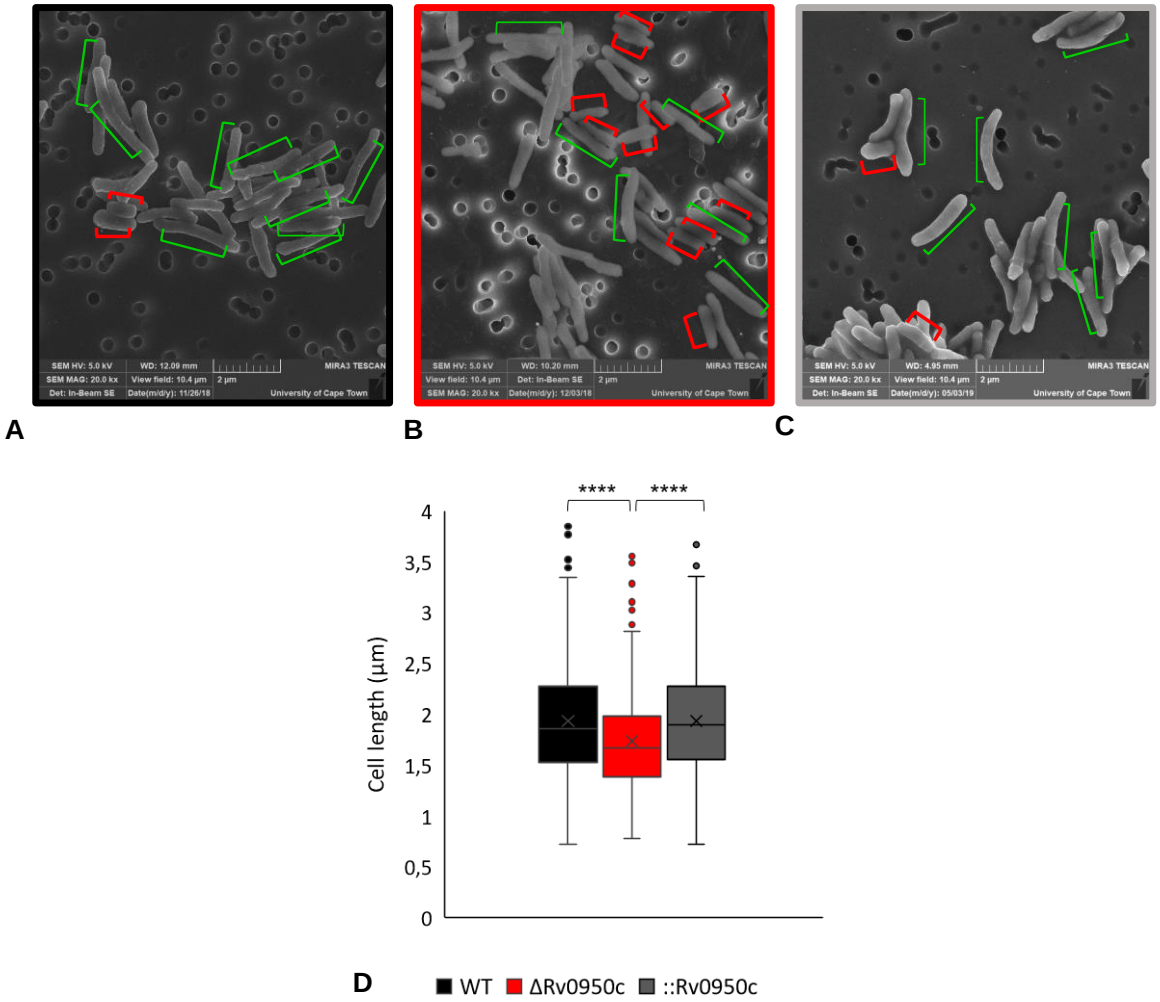

Figure 3.2.11 Scanning electron microscopy to study morphological changes to *M. tuberculosis* after Rv0950c deletion.
Representative micrographs of WT (A), ΔRv0950c (B), and ΔRv0950c::Rv0950c genetically complemented derivative (C), emphasising normal cells of ~ 2 µm (green bars) and short cells of ~ 1 µm (red bars). Scale bar = 2 µm. D) Box and whisker plot of cell lengths measured in ImageJ of 100 cells for each strain in triplicate. ****$p<0.05E^{-7}$ for t-test calculated in Excel.

3.2.5 *M. tuberculosis* growth kinetics

To study if cell shortening by loss of Rv0950c was due to a defect in elongation and growth, the growth rate of *M. tuberculosis* in the WT and mutant strain was compared both by OD at 600 nm and colony forming units sampled for 18 days under axenic conditions (Fig. 3.2.12) The growth rate was the same in both strains, showing normal progression from lag, through exponential to stationary phase (Fig. 3.2.12), suggesting that there is no relationship between cell length maintenance by Rv0950c and population growth rate.

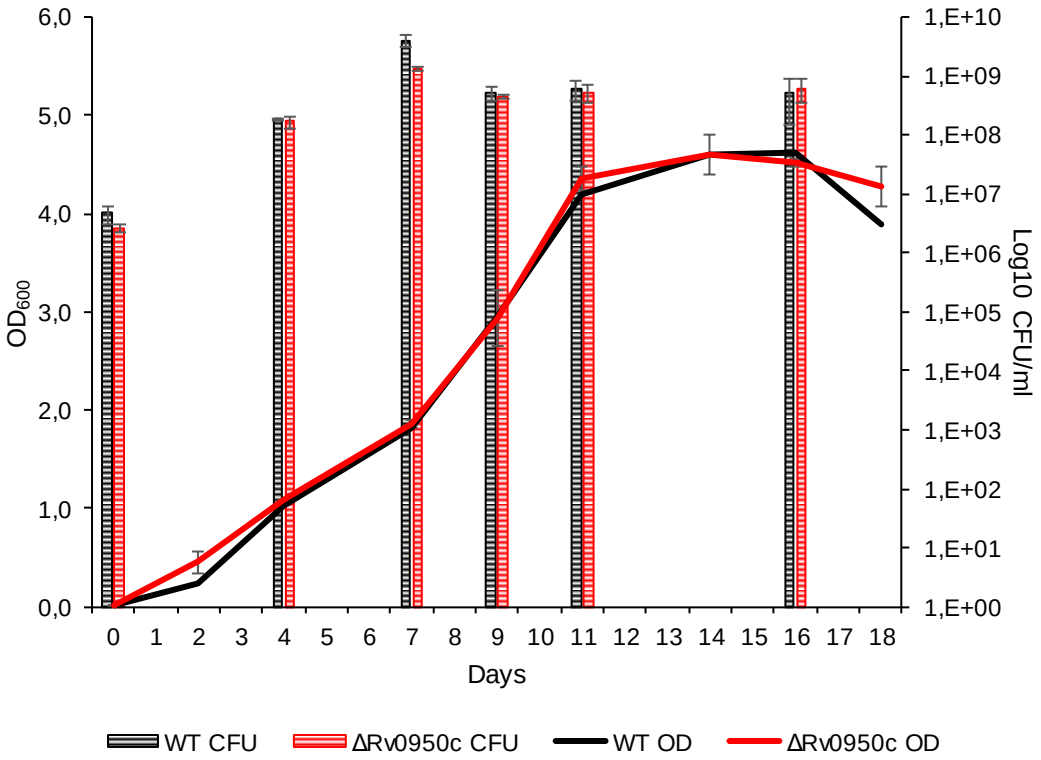

Figure 3.2.12 Growth kinetics of *M. tuberculosis* comparing optical density and colony forming units sampled over 21 days in duplicate of *M. tuberculosis* WT and ΔRv0950c grown in 7H9. CFUs scored after 2-4 weeks of incubation of 7H11 agar inoculated with serial dilutions at represented time points.

3.2.6 The use of fluorescent PG probes to study the effect of Rv0950c deletion on cell wall remodelling

M23 endopeptidases are required both for cell shape maintenance and cell wall remodelling at cross-links between stem peptides of PG (Bonis, Ecobichon, Guadagnini, Prévost, et al., 2010; Goley et al., 2010; Dörr, Davis & Waldor, 2015). In *M. smegmatis*, rod morphology relies on PG remodelling, in particular, maturation of PG along the side-wall via 3-3 cross-linkage of stem peptides (Baranowski et al., 2018). To determine if there is an association between the cell length maintenance role of Rv0950c and PG remodelling activity predicted for the M23 endopeptidase domain, the fate of fluorescent PG stem-peptide probes was studied in response to Rv0950c deletion. Recent progress in developing fluorescent probes of PG building blocks has led to enabling microscopic analysis of spatial PG synthesis and remodelling (Siegrist et al., 2013; Liechti et al., 2014; Baranowski et al., 2018; García-Heredia et al., 2018). For example, changes to PG remodelling as a result of LD transpeptidases corresponded to shifts in cellular side-wall incorporation of *M. smegmatis* by mono-peptide D-Ala probes (Baranowski et al., 2018). Di-peptide D-Ala – D-Ala (DADA) probes report on PG biosynthesis and back-bone repair

(Liechti et al., 2014; García-Heredia et al., 2018). Alternatively, conjugating a fluorescent BODIPY to a PG-binding antibiotic, Vancomycin, reveals uncross-linked PG (García-Heredia *et al*., 2018). Upon Rv0950c deletion, the fates of the mono-peptide TADA, di-peptide alk DADA, and Vancomycin-FL incorporation were studied below.

3.2.6.1 Mono-peptide labelling with TADA

Exponential phase cultures of *M. tuberculosis* WT and ΔRv0950c strains were labelled with TADA to study the role of Rv0950c in PG remodelling at the stem-peptide. Fluorescent monopeptides are incorporated into PG both during cytoplasmic biosynthesis as well as extracellularly during transpeptidation, both at the poles and laterally along the mycobacterial cell (García-Heredia et al., 2018). *M. tuberculosis* in particular exhibits a highly heterogenous manner of PG remodelling and metabolism in general from cell to cell. Asymmetric cell division in mycobacteria produces poles with differentially remodelled PG leading to heterogenous fluorescent probe incorporation (Botella, Yang, et al., 2017; Baranowski et al., 2018). After labelling *M. tuberculosis* with TADA, cells exhibited a variety of incorporation patterns (Fig. 3.2.13). For clarity, the "labelled" population below describes the entire population exposed to the respective probe while "incorporated" refers to the cells within the labelled population with a visible fluorescence signal. As such, TADA labelling produced three sub-populations of TADA incorporation: polar incorporated, cells incorporating TADA mid-cell and cells displaying diffuse fluorescence of varying intensity (Fig. 3.2.13). The polar sub-population, either monopolar or bipolar, represents actively elongating cells. The mid-cell sub-population likely displays labelled septal PG, representative of actively dividing cells. The diffuse sub-population ranges from cells incorporating little or no TADA to cells incorporating a similar amount of TADA along the side-wall as the poles. Most of the labelled cells incorporated TADA diffusely (Fig. 3.2.13a).

WT and ΔRv0950c had similar-sized diffuse sub-populations but that of the complement was significantly smaller ($p = 0.02$ comparing complement to WT or ΔRv0950c, Table in Fig. 3.2.13a). The non-diffuse sub-populations were compared separately and displayed reduced polar incorporation in the ΔRv0950c strain which was not significant when compared to WT but significant when compared to the complement strain ($p = 0.007$, Fig. 3.2.13b). It is not clear if this is directly due to loss of Rv0950c or due to the behaviour of

the complement strain, wherein the reduction in the diffused sub-population equated to an increased polar-incorporating sub-population in the complement.

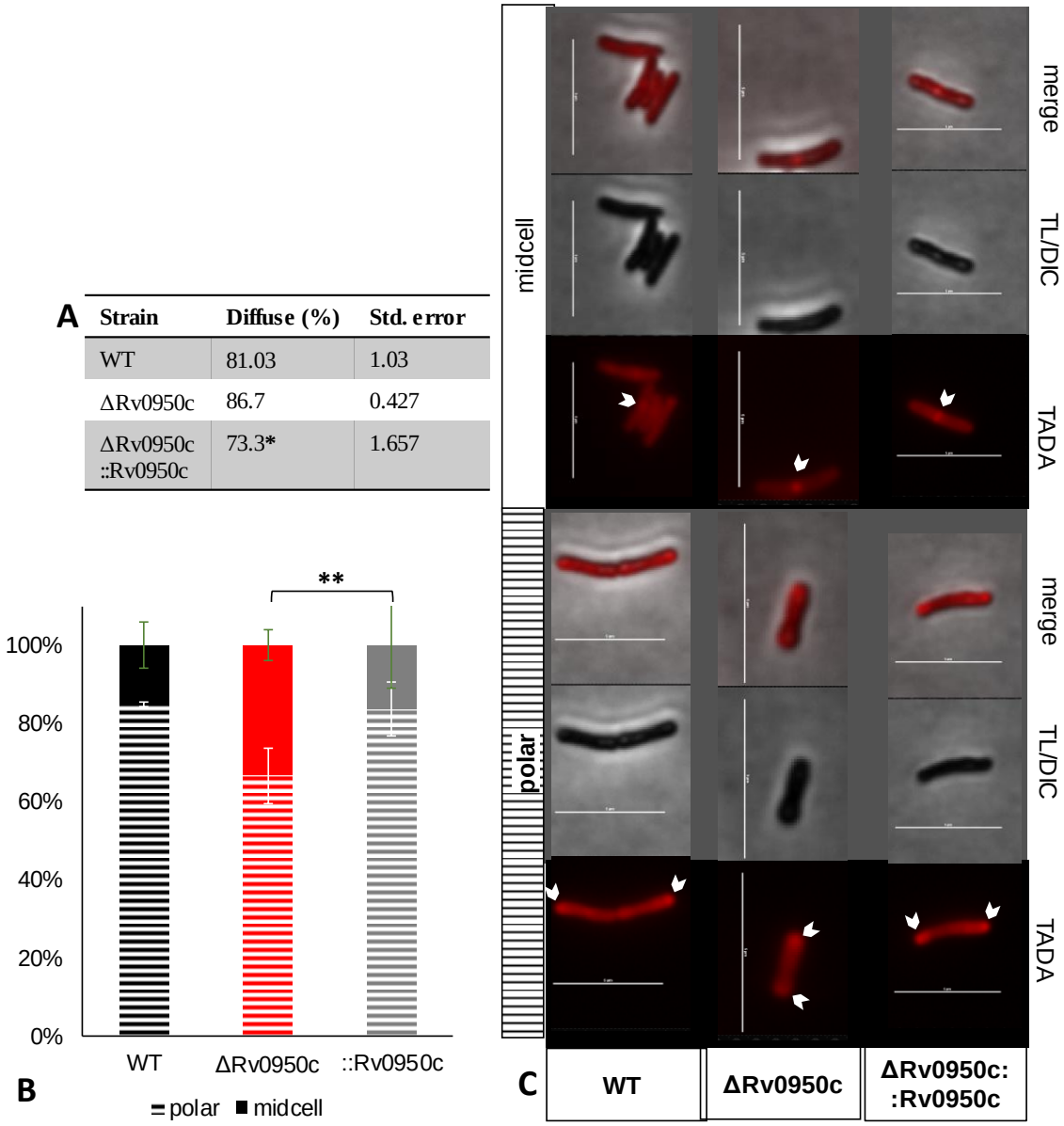

Figure 3.2.13 Incorporation of the fluorescent D-Alanine analogue, TADA in the cell wall of *M. tuberculosis*.
A) Proportions of diffusely-labelled TADA cells as a percentage of the total labelled population. Average of ~100 cells in duplicate. *p=0.02. B) Proportions of the polar or mid-cell sub-populations as percentages of the number of cells combining both sub-populations (i.e excluding the diffuse sub-population. **p = 0.007. C) Fluorescence micrographs of TADA-labelled *M. tuberculosis*. Varying fluorescence intensity between cells represents metabolic heterogeneity of *M. tuberculosis*. For each sub-population, top panel: merge; middle panel: DIC; bottom panel: TADA. White arrows point to localised incorporation or brightening at poles or midcell. Scale bar represents 5 µm. Std. error and error bars represent standard error of the mean calculated in Excel summary statistics.

Quantifying the spatial distribution of fluorescence between the bright pole, side-wall and dim pole of cells has been reported to mirror changes to PG composition (García-Heredia

et al., 2018). The bright and dim poles were defined as the first and last 15% of the cell length, with the middle 70% comprising the side wall (Fig. 3.2.14, García-Heredia et al., 2018). In the polar sub-population, loss of Rv0950c produced a significant shift to side-wall labelling (p = 0.01, Fig. 3.2.14c). Complementation produced a slight but non-significant shift back to polar labelling (Fig. 3.2.14c). The same effect did not take place in the mid-cell population, indicating the activity of Rv0950c is not required during septum formation (Fig. 3.2.14d).

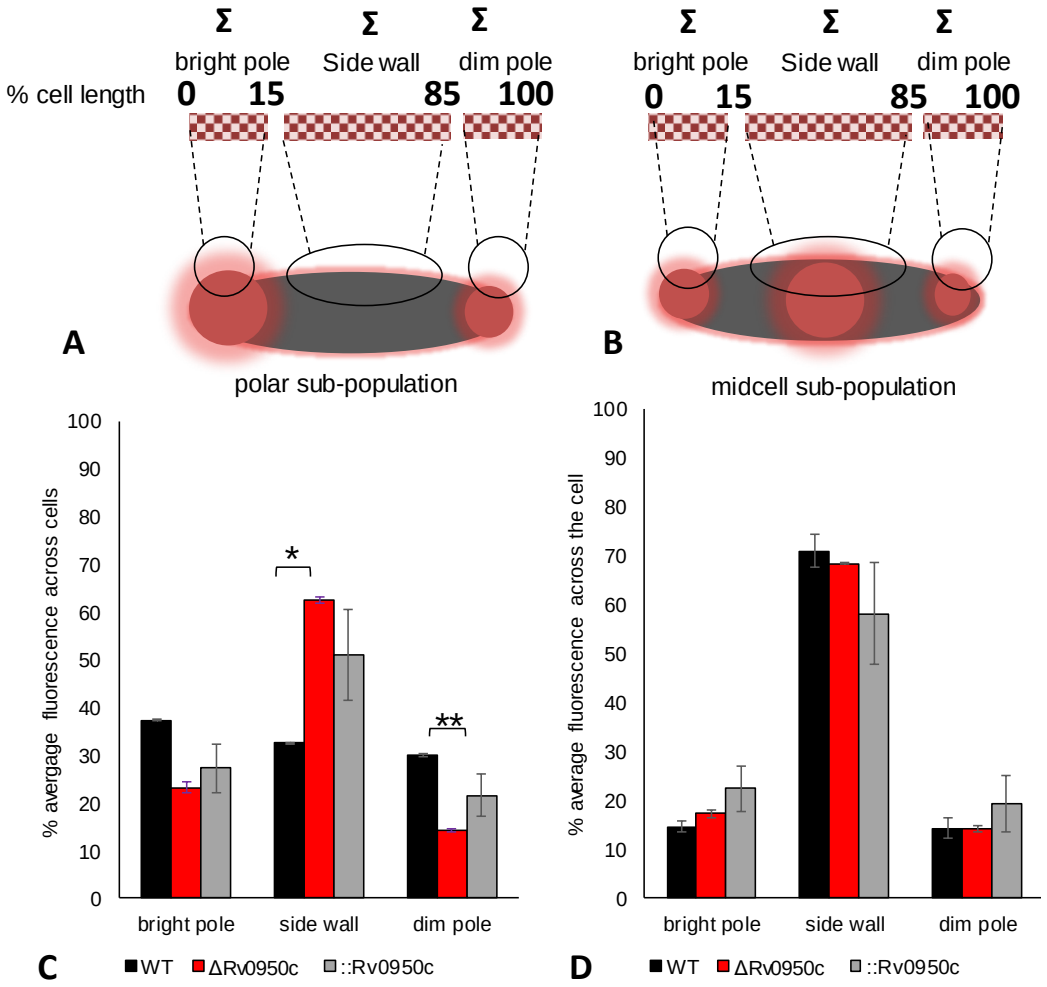

Figure 3.2.14 Spatial distribution of TADA-labelled PG in *M. tuberculosis* cells.
A-B) Schematic diagram explaining how spatial distribution is quantified as percentage average fluorescence previously demonstrated by Garcia-Heredia et al., (2018): Average distribution of fluorescence between the bright pole (sum of fluorescence across the first 15% of the cell length), the side-wall (sum of fluorescence between 16-84% of the cell length) and dim pole (sum of fluorescence from 85-100% of the cell length), measured for the polar (A) or mid-cell (B) sub-population. C) Spatial distribution in the polar sub-population. * p = 0.017, **p = 0.001 for student's t-test in Excel. D) Spatial distribution in the mid-cell sub-population.

Changes to TADA incorporation were further studied comparing the fluorescence intensity of each cell, in average and across the cell length in the different sub-populations. Fluorescence intensity of polar-incorporating cells was slightly reduced in the polar sub-

population, in agreement with the reduced frequency of polar-incorporating cells (Fig. 3.2.13) and the observed shift in spatial distribution of labelled PG away from the poles to the side-wall (Fig. 3.2.14c). Fluorescence intensity was significantly reduced in the diffuse sub-population (p = 3.E-07) after loss of Rv0950c but remained the same in the small mid-cell incorporating proportion (Fig. 3.2.15). Complementation significantly rescued TADA incorporation in the diffuse population (p = 0.0005, Fig. 3.2.15c).

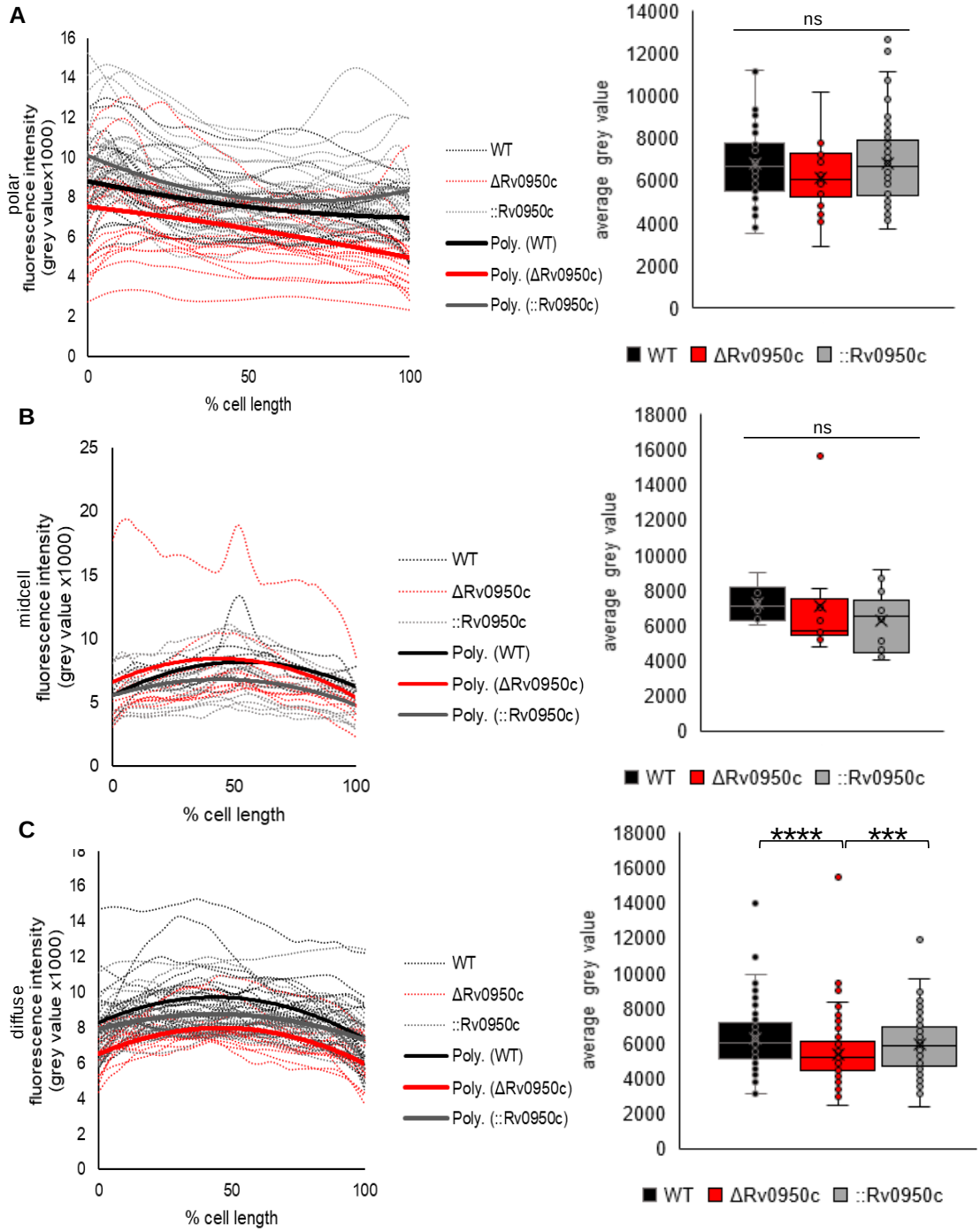

Figure 3.2.15 TADA Fluorescence intensity profiles of *M. tuberculosis* labelled with TADA. A) polar, B) midcell, C) diffuse sub-populations. Left: TADA fluorescence intensity (grey values) plotted across the length of *M. tuberculosis* cells. Right: average fluorescence intensity per cell. ****p = 3.E-07, ***p = 0.0005 for single-factor ANOVA in Excel.

Reduction in monopeptide fluorescence has been previously demonstrated in mycobacteria lacking Ldts for 3-3 cross-link formation (Baranowski et al., 2018; García-Heredia et al., 2018). By comparing TADA mono-peptide labelling between WT, ΔRv0950c and the Rv0950c complement strain, a putative role for Rv0950c in cross-link remodelling is suggested. This is based on the observation that loss of Rv0950c caused a reduction in the number of polar TADA-labelled cells (Fig. 3.2.13), a shift in spatial distribution of TADA from the poles to the side-wall (Fig. 3.2.14) and a reduction in TADA fluorescence intensity (Fig. 3.2.15c).

3.2.6.2 Incorporation of the di-peptide, alkyne-DADA, labelled by Copper-catalysed cyclo-addition (CuCCA).

Monopeptide probe incorporation is not only sensitive to changes in PG transpeptidation but can be altered by inhibition of PG biosynthesis (García-Heredia *et al*., 2018). During PG biosynthesis, the terminal D-Alanine monopeptides are ligated together to form a dipeptide, followed by MurF-catalysed addition of the di-peptide to *meso*-DAP, producing the PG pre-cursor, lipidI (Munshi et al., 2013). As such, labelling of PG with alkyne-DADA has shown incorporation in lipidI and lipidII molecules but in addition is sensitive to altered trans-peptidase activity and cell-wall damage (García-Heredia *et al*., 2018). Since monopeptides are incorporated via multiple routes (García-Heredia et al., 2018), the di-peptide incorporation response to Rv0950c deletion was studied to determine if the TADA response was as a result of disruption of PG biosynthesis or extracellular remodelling. Labelling of *M. tuberculosis* WT and ΔRv0950c was also studied in the context of PG backbone digestion. Using a combination of lysozyme and mutanolysin to digest *M. smegmatis* PG, García-Heredia et al (2018) demonstrated that PG biosynthesis in *M. smegmatis* can occur at the side-wall in addition to the poles, detected using the dipeptide alk DADA probe. Given the importance of side-wall remodelling for cell shape maintenance (Baranowski et al., 2018), reproducing this experiment in *M. tuberculosis* would provide insight into side-wall PG remodelling and the putative role of Rv0950c therein.

For untreated, dipeptide labelled *M. tuberculosis*, metabolic heterogeneity was again observed in all three strains, revealing different sub-populations (Fig. 3.2.16,17). Although alk DADA incorporation is highly efficient in *M. smegmatis*, it is detected in ~ 10% of a labelled *M. tuberculosis* population (García-Heredia *et al*., 2018) also observed here (Table

3.2.3, Fig. 3.2.16). In the untreated experiments, the percentage of cells incorporating alkDADA was non-significantly higher in the deletion mutant than the WT or complement, presented as the percentage of non-incorporating cells (Table 3.2.3). This may suggest that there is more uncross-linked PG in the Rv0950c deletion mutant.

Table 3.2.3 Average number of cells out of 100 not incorporating *alk DADA* after treating *M. tuberculosis* with lysozyme and mutanolysin.

[Lysozyme+mutanolysin]	WT	ΔRv0950c	::Rv0950c
untreated	90	78	84
5 µg/ml + 0.5 U (1X)	83	83	nd
50 µg/ml + 5 U (10X)	83	84	73
500 µg/ml + 50 U (100X)	94	85	nd

nd: not determined.

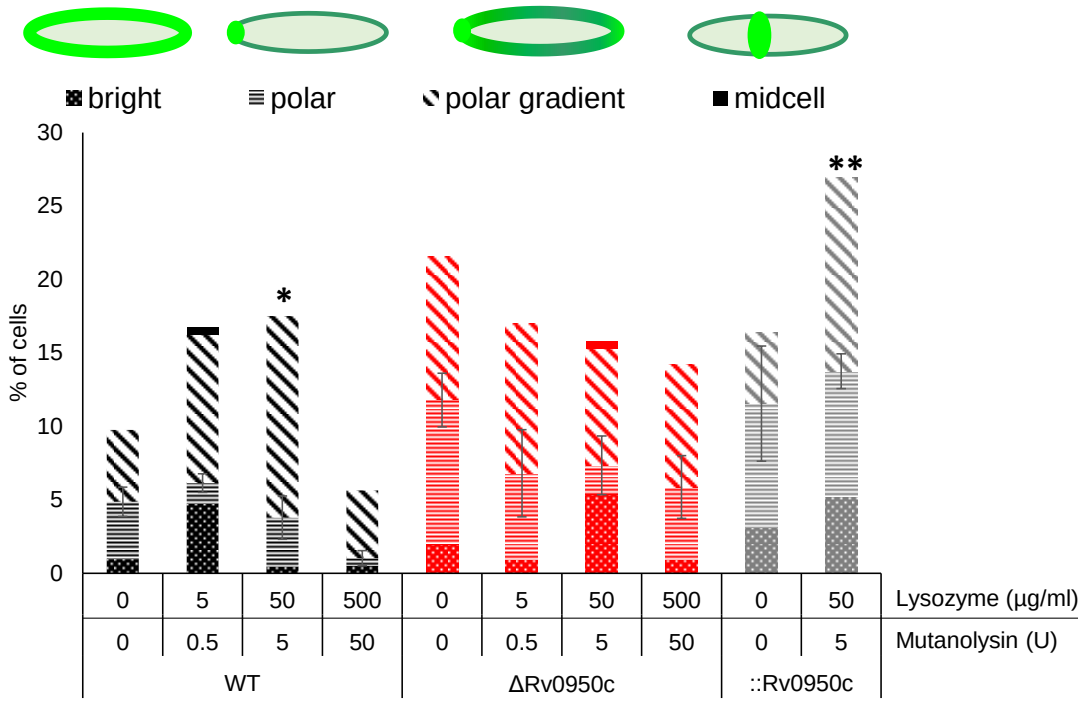

Figure 3.2.16 Percentage of *alk* DADA labelled *M. tuberculosis* cells forming different sub-populations of alk DADA incorporation (schematic), following treatment with lysozyme and mutanolysin at 10-fold increasing concentrations.
Average of ~100 cells in duplicate for each treatment, for each strain. *p = 0.045, for student's t-test comparing polar-gradient WT cells at untreated (0) vs 50 µg/ml Lysozyme + 5 U Mutanolysin treatment; **p = 0.005 for student's t-test comparing polar-gradient ::Rv0950c cells at untreated vs. 50 µg/ml Lysozyme + 5 U Mutanolysin treatment.

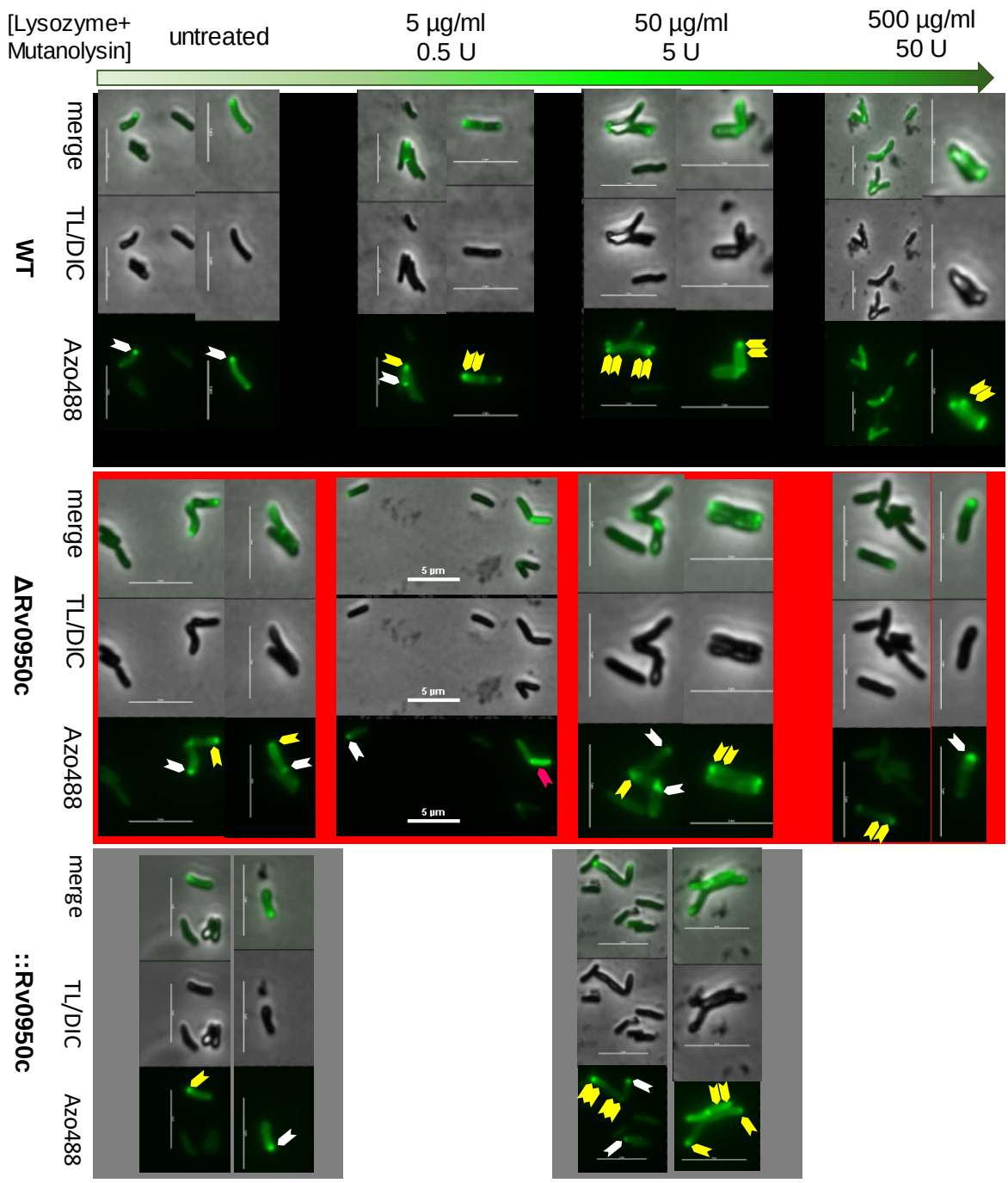

Figure 3.2.17 Micrographs of alk DADA-labelled *M. tuberculosis* showing heterogeneity in probe incorporation (variation in fluorescence intensity), indicating sub-populations of polar incorporation (white arrows), polar gradient incorporation (yellow arrows) and bright cells (pink). Left to right: increasing lysozyme-mutanolysin digestion as per schematic in green. Micrograph channel order merge (top), DIC (middle) and Azoflour488 (bottom). Strains represented: WT (black border), ΔRv0950c (red border) and ΔRv0950c::Rv0950c complement (grey border). Scale bar represents 5 µm.

When the cells were treated with 10-fold increasing concentrations of lysozyme and mutanolysin, the WT and complement strains exhibited increased side-wall dipeptide incorporation, evident as the polar-gradient sub-population, as expected, likely via MurF during PG backbone repair, also evident as an increase in the polar-gradient sub-

population (Fig. 3.2.16,17). The polar gradient describes cells in which probe incorporation is enriched at one pole and gradually decreases in intensity along the side-wall (Fig. 3.2.16,17). This sub-population increase was significant at the 50 µg/ml Lysozyme + 5 U Mutanolysin concentration (p = 0.045 and 0.005 for WT and complement respectively (Fig. 3.2.16) and recapitulated what was observed for backbone digestion of *M. smegmatis* (García-Heredia et al., 2018).

Incorporation in 500 µg/ml Lysozyme + 50 U Mutanolysin -treated WT cells was the lowest, representing a threshold over which the PG backbone could not be repaired and biogenesis delayed (Fig. 3.2.16,17). This high dose effect was negligible for ΔRv0950c treated cells compared to WT treated cells (Fig.3.2.16,17). Instead, in ΔRv0950c cells, the proportion of polar-gradient alk DADA-sub-population appeared highest in untreated cells and incorporation was reduced with increasing Lysozyme-Mutanolysin concentration, producing the opposite trend to that of WT and complement cells (Fig. 3.2.16,17). The increase in the gradient population without backbone digestion (untreated) of the ΔRv0950c strain suggests that when new fluorescent PG is incorporated into ΔRv0950c, it remains uncross-linked and the signal is therefore not lost as the PG is gradually added from the poles, suggesting that Rv0950c activity is required for PG maturation at the side-wall and not only biosynthesis, as observed with TADA labelling.

Studying the alk DADA fluorescence intensity of the polar and polar-gradient cells further indicated that untreated ΔRv0950c successfully incorporated the same amount of alk DADA in each cell as the WT and complement strain (Fig. 3.2.18b). Only at 50 µg/ml Lysozyme + 5 U Mutanolysin treatment was alk DADA intensity significantly reduced in the ΔRv0950c strain (p = 0.038) an effect reverted by complementation (p = 0.007, Fig. 3.2.18c). This is also reflected in fluorescence intensity profiles across the polar and polar gradient cells: In the WT and complement strains, the intensity trendline increased with increased PG backbone digestion, but decreased in the absence of Rv0950c (Fig. 3.2.19). The average fluorescence intensity of ΔRv0950c cells also decreased with increasing backbone digestion (p = 0.003, Fig. 3.2.19b). This suggests that the absence of Rv0950c equates to incomplete side-wall incorporation machinery and points to a spatially distinct role for Rv0950c at the *M. tuberculosis* side-wall, likely for PG maturation.

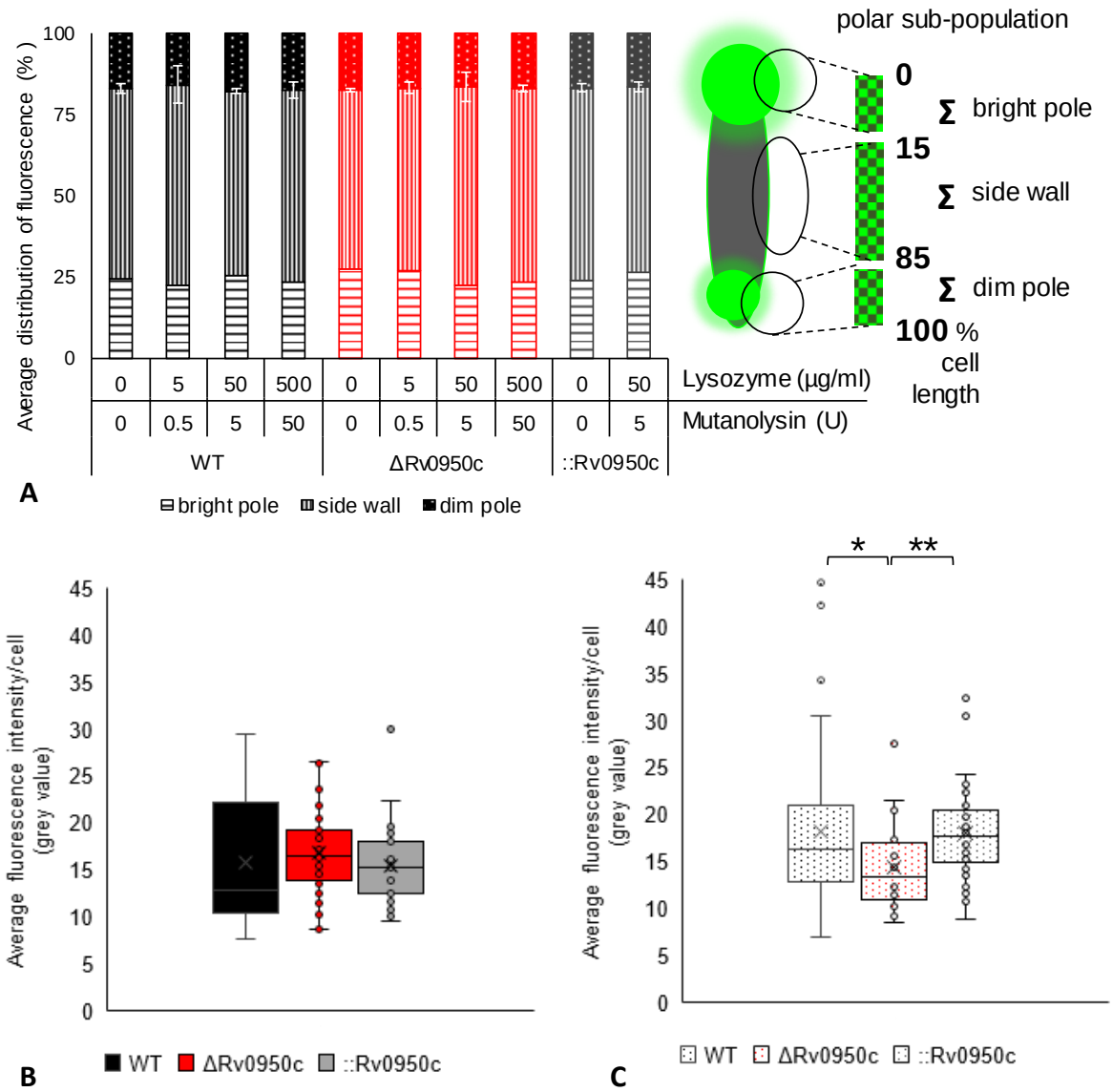

Figure 3.2.18 alk DADA fluorescence intensity of pooled polar and polar-gradient sub-populations of *M. tuberculosis.*

A) Distribution of alk DADA fluorescence between the bright pole, side-wall and dim pole after treatment with Lysozyme and Mutanolysin at 10-fold increasing concentrations. Schematic diagram shows how spatial distribution is quantified as percentage average fluorescence as previously demonstrated by Garcia-Heredia et al., (2018) B, C) average fluorescence intensity of *M. tuberculosis* polar and polar gradient sub-population for untreated (B) and 50 µg/ml Lysozyme + 5 U Mutanolysin treated (C) cells. C)**p* = 0.038 and ***p* = 0.007 for student's *t*-test.

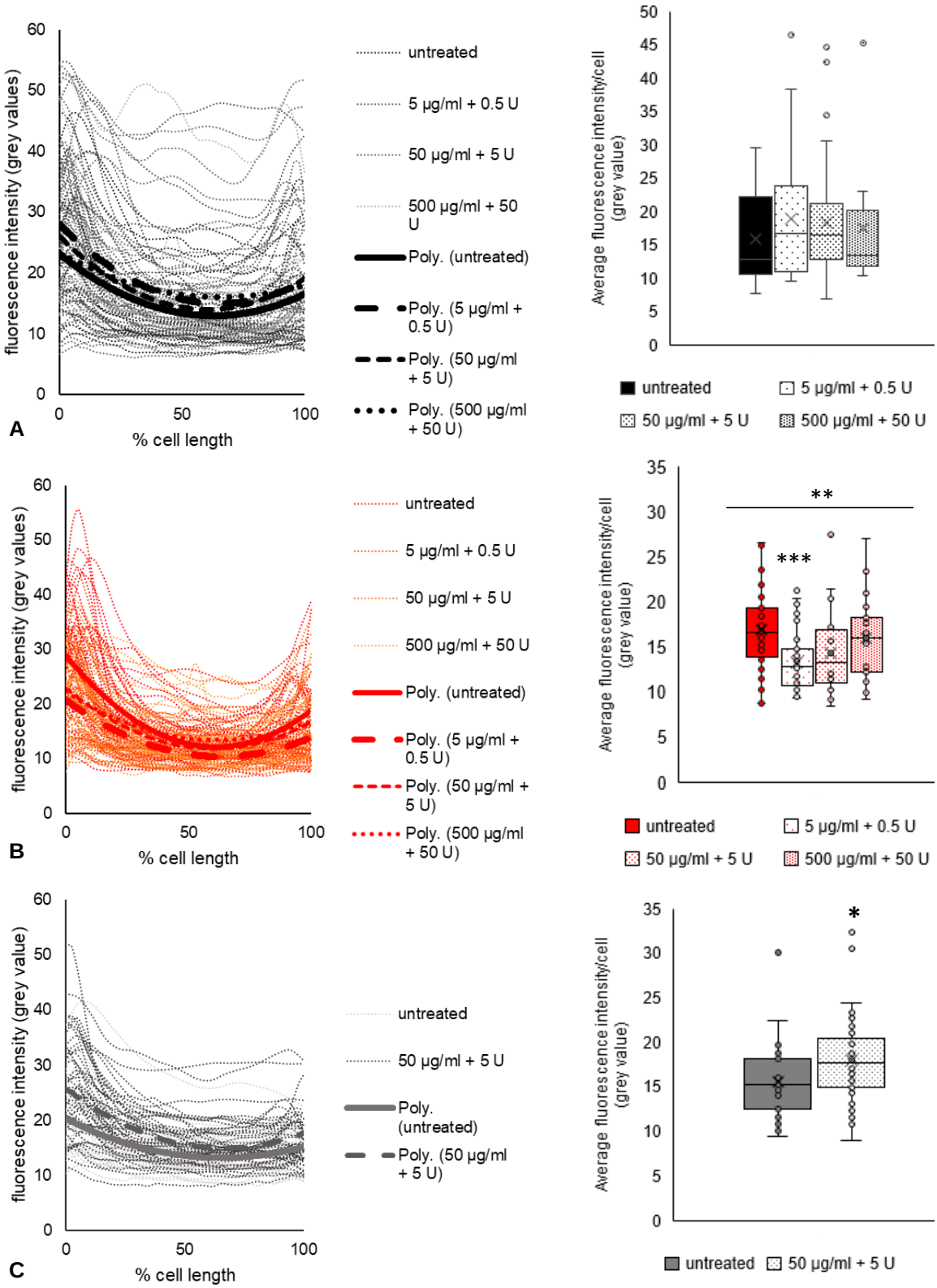

Figure 3.2.19 alk DADA fluorescence intensity profiles (left) and averages (right) of *M. tuberculosis* with 10-fold increasing lysozyme (µg/ml) + Mutanolysin (U) treatment.
A) WT; B) ΔRv0950c, $^{**}p = 0.003$ for single-factor ANOVA across all treatment points; $^{***}p = 0.0008$ for student's *t*-test of 0X vs 1X.; C) ΔRv0950c::Rv0950c, $^{*}p = 0.02$ for student's *t*-test.

3.2.6.3 Labelling of terminal D-Alanines with fluorescence-conjugated vancomycin

Vancomycin is a small molecule, glycopeptide antibiotic which inhibits PG biosynthesis by binding the terminal D-Alanines of the stem-peptide, inhibiting cross-link formation. Labelling of *M. tuberculosis* with BODIPY fluorescence-conjugated vancomycin (Van-FL), reports on polar PG biosynthesis, where it can bind uncross-linked PG pre-cursors in the cytoplasm. To further confirm that the loss of Rv0950c changes FDAA incorporation by disrupting extra-cellular PG remodelling with no effect on cytoplasmic PG biosynthesis, the fate of Van-FL was studied. In both the WT and the ΔRv0950c, Van-FL appeared predominantly at the cell poles, expected as these are the primary sites of PG biosynthesis (Fig. 3.2.20). Limited PG incorporation at the side-walls, exhibited in the bright sub-population, was also observed in both strains (Fig. 3.2.20), representative of side-wall PG biosynthesis, a recently-reported phenomenon in mycobacteria (García-Heredia *et al*., 2018). A subtle, non-significant reduction in the size of monopolar sub-population was observed after loss of Rv0950c (Fig. 3.2.20b).

Further studying Vancomycin-FL fluorescence intensity of the cells revealed a subtle, non-significant, increase in average fluorescence intensity in polar-incorporating cells after loss of Rv0950c (Fig. 3.2.21a). In addition, the trend-line of the polar sub-population revealed brighter poles of ΔRv0950c cells (Fig. 3.2.21a), consistent with our observation that there is more uncross-linked PG in ΔRv0950c cells. No differences were observed in the mid-cell sub-population (Fig. 3.2.21b) or in the distribution of fluorescence between the brighter pole, side-wall and dim pole comparing WT and ΔRv0950c (Fig. 3.2.21c). This suggests that compositional changes in ΔRv0950c reported by TADA and alk DADA labelling are more likely associated with maturation of PG, possibly at 3-3 cross-link regulation with the consequence of cell-shortening. As there were no significant changes in Vancomycin binding after Rv0950c deletion, this was not further studied in the complement strain.

3.2.7 Susceptibility to cell wall-targeted antibiotics, focusing on stem-peptide disruption by cephalosporins

M. tuberculosis ΔRv0950c cells appear to have altered PG composition and respond differently to PG backbone digestion. It was expected that the loss of Rv0950c would alter susceptibility of *M. tuberculosis* to lysozyme and cell-wall targeted antibiotics, for which

MIC was thus determined by broth-microdilution (Table 3.2.4,5). No differences in antibiotic susceptibility were observed between WT and ΔRv0950c (Table 3.2.4,5).

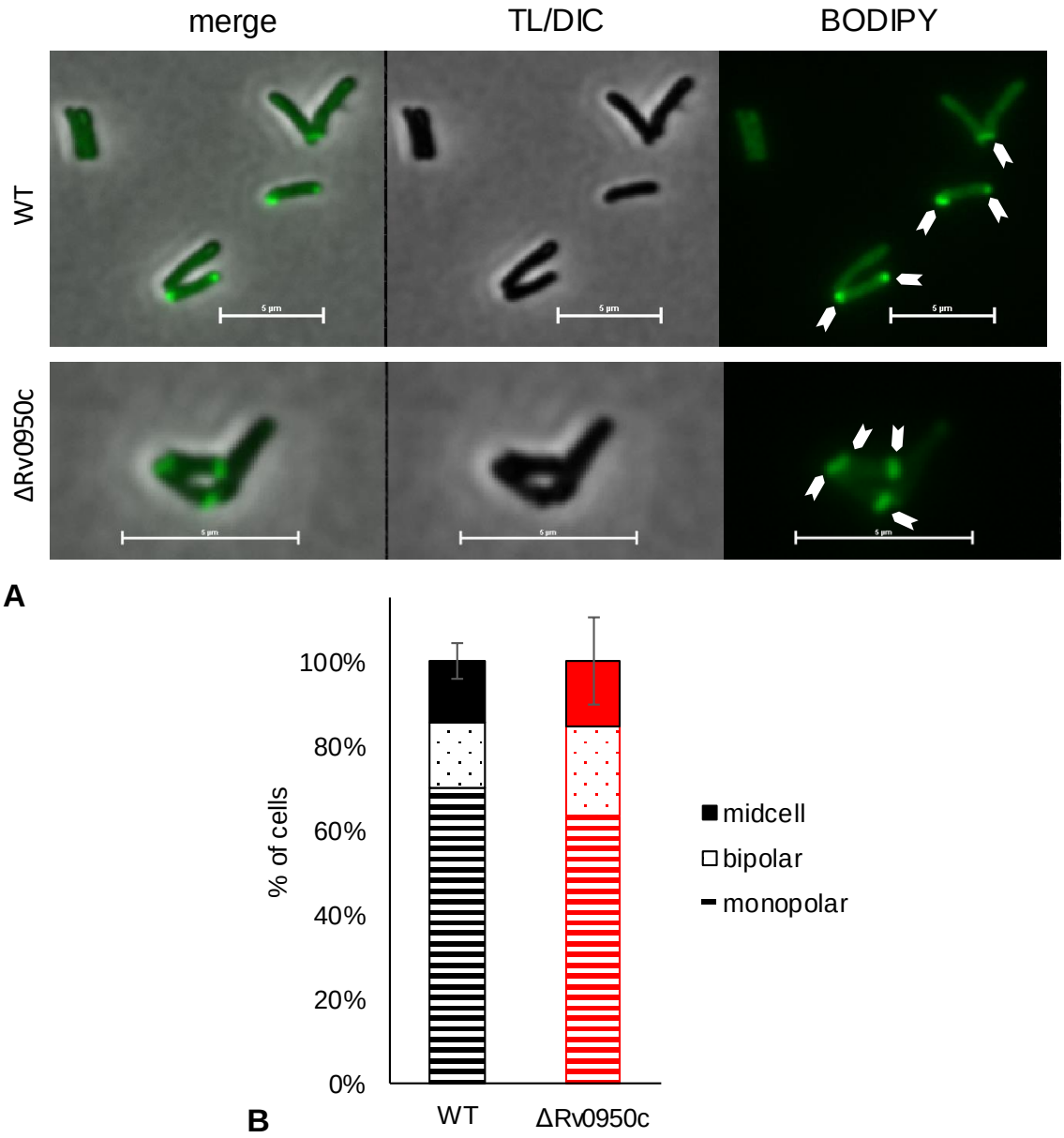

Figure 3.2.20 Labelling of the *M. tuberculosis* cell wall with fluorescence-conjugated vancomycin. A) fluorescence micrographs of *M. tuberculosis* labelled with BODIPY-Vanc. BODIPY Vanc. incorporates mainly at the poles of the cells (white arrows); Left panel: merge, middle: BODIPY-FL, right: phase. scale bar = 5 µm. B) Percentage of labelled cells forming different sub-populations of Vanc incorporation. Average of ~100 cells in triplicate.

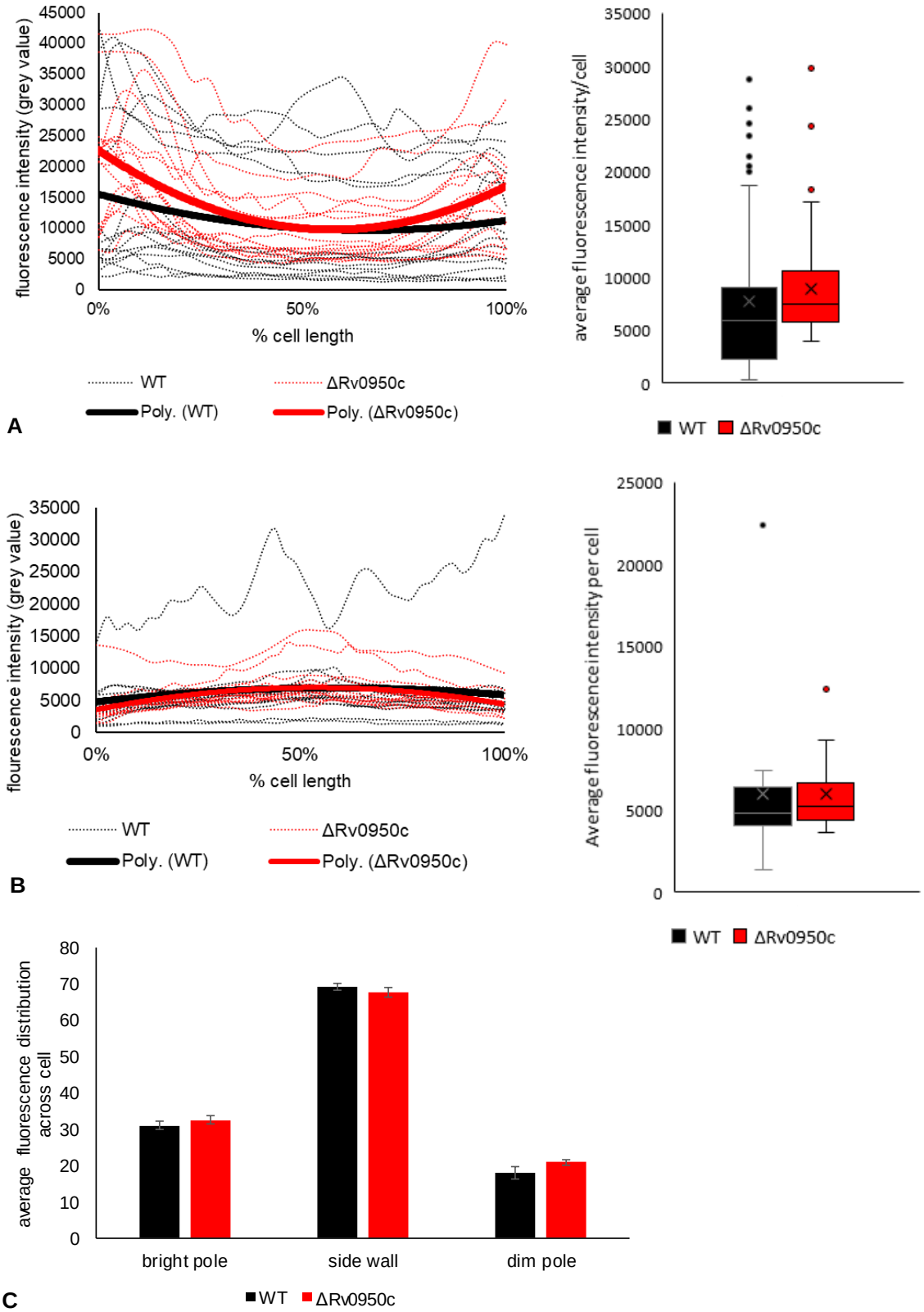

Figure 3.2.21 Vanc-FL fluorescence intensity profiles.
Left: Vanc fluorescence intensity (grey values) plotted across the length of *M. tuberculosis* cells. Right: average fluorescence intensity per cell. A) polar sub-population; B) mid-cell sub-population. Sub-populations derived from three Vanc-labelled biological replicates of each strain. C) Average distribution of fluorescence between the bright pole, side-wall and dim pole, measured for the polar sub-population.

Table 3.2.4 Broth microdilution determination of MIC (µg/ml) of cell-wall targeting antibiotics comparing wild-type *M. tuberculosis* to ΔRv0950c

Antibiotic	WT	ΔRv0950c	::Rv0950c
cefamandole	7.8	7.8	nd
cefotaxime	0.5	0.5	nd
ceftriaxone	3.9	3.9	nd
cycloserine	12.5	12.5	nd
meropenem	0.25	0.5-1	0.5-1
INH	0.015	0.015	0.015-0.03

Determined for independent, triplicate cultures grown in 7H9. nd: not determined.

Table 3.2.5 Broth microdilution determination of lysozyme MIC (µg/ml) comparing wild-type *M. tuberculosis* to ΔRv0950c across

Antibiotic	WT	ΔRv0950c	::Rv0950c
lysozyme	160	160	160-320

Determined for independent, triplicate cultures grown in 7H9

3.2.8 Permeability to Ethidium Bromide

Alterations to the cell wall of *M. tuberculosis* following Rv0950c deletion were further studied by assaying the permeability of the cell wall to ethidium bromide (Fig. 3.2.22). As observed for antibiotic susceptibility studies, Rv0950c deletion did not enhance cell wall permeability to Ethidium Bromide (EtBr).

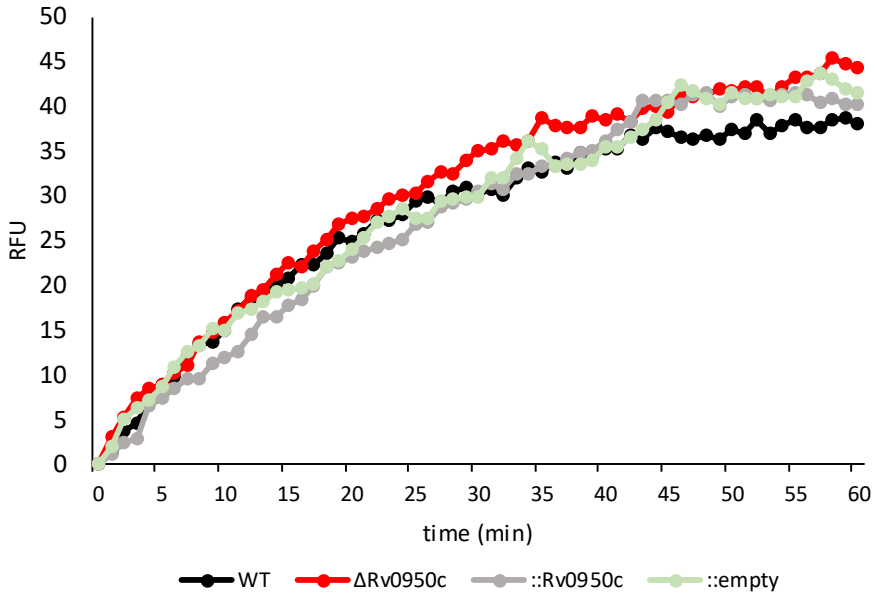

Figure 3.2.22 Permeability of *M. tuberculosis* to ethidium bromide.
Plate-based fluorescence readout over 60 min incubation of *M. tuberculosis* with EtBr (0.25 µg/ml). Data averaged from technical duplicates in biological triplicate. Empty: *M. tuberculosis* transformed with native pTTP1b as an empty vector control.

3.2.9 Summary of findings on the characterisation of Rv0950c

Using bioinformatics and various biochemical assays, namely transcriptomics, microbiological assays and microscopy, Rv0950c was identified as a metallo-endopeptidase putatively required for 3-3 cross link formation during PG maturation in *M. tuberculosis*. Bioinformatics and online annotations suggested that Rv0950c is highly conserved, with a putative zinc co-ordinating active site, and clusters phylogenetically with enzymes involved in stem-peptide and cross-link remodelling. Microscopy showed that Rv0950c regulates the cell length of *M. tuberculosis*, and side-wall incorporation of fluorescent PG probes was altered at the loss of Rv0950c, pointing to the hypothesis that Rv0950c is required for PG maturation which further regulates elongation in *M. tuberculosis*. Given the highly-conserved nature of the zinc co-ordinating site of Rv0950c, attempts were made to test the hydrolytic activity of the protein via various heterologous expression systems (Appendix B5). Induction of Rv0950c in *E. coli* was not successful and heterologous complementation of the *E. coli* Δ*envC*,Δ*nlpD* division impaired mutant was inconclusive on the hydrolytic activity of Rv0950c (Appendix B5.1,2). Instead, heterologous expression of Rv0950c in *M. smegmatis*, where the direct orthologue MSMEG_5526 was still intact, caused subtle osmotoxicity (Appendix B5.3). Exploring expression of Rv0950c during osmolarity stress instead revealed that *M. tuberculosis* upregulates Rv0950c under nutrient-limiting conditions (Appendix B5.3).

Further studies looking into the physiological role of a second M23 endopeptidase, Rv2891 are presented below (Section 3.3).

3.3 Characterisation of Rv2891, a putative secreted endopeptidase involved in septal PG remodelling.

3.3.1 Bioinformatics

A second, uncharacterised M23-endopeptidase, Rv2891 was identified *in silico* in the *M. tuberculosis* genome (section 3.1). Rv2891 has a distinctly different predicted structure to the endopeptidase Rv0950c, in that it bears a secretory signal peptide and a zinc-co-ordinating site that is both divergent from active and degenerate M23 endopeptidases. The growth phase transcription profile was constitutive across the growth phases. To study this, the process of reverse genetics was used similar to Rv0950c characterisation.

3.3.2 Deletion of Rv2891 by suicide vector-mediated homologous recombination

3.3.2.1 Suicide vector construction

As with deletion of Rv0950c, suicide vector-mediated homologous recombination was used to delete Rv2891 from the *M. tuberculosis* genome. The 5' end of Rv2891 overlaps with the 400 bp putative promoter region of *rpsBc* (Fig. 3.3.1). Therefore, the upstream homology arm was designed to include this while ensuring exclusion of the M23 domain of Rv2891 to avoid disrupting *rpsBc* expression. Similarly, the downstream homology arm was designed to include the 3' end of Rv2891 overlapping *ppe45* (Fig. 3.3.1). The two homology arms of Rv2891 were amplified by PCR (Fig. 3.3.1) and phosphorylated with PNK before separately blunt cloning each arm into pBlueScript (Alting-Mees & Short, 1989) (Fig. 3.3.1). The pBlueScript clones were confirmed by restriction analysis (Fig. 3.3.1). The two arms were then sub-cloned from pBlueScript into p2Nil, followed by sub-cloning in the pGOAL17-derived *lac_sac* cassette (described in section 3.2) to complete the ΔRv2891 suicide-vector. The ΔRv2891 vector was then confirmed by restriction analysis (Fig. 3.3.2) and sequencing (appendix B3).

3.3.2.2 Screening for single cross-over events

After confirming the sucrose-sensitivity of the ΔRv2891 deletion vector in *E. coli* (Fig. 3.3.3a,b), the vector was electroporated into *M. tuberculosis* and plated on 7H11 supplemented with kanamycin (25 µg/ml) and X-Gal (2%) for selection and identification respectively of single-cross over events. PCR was performed to genotype Km^R, blue colonies to confirm the presence of the both the wild-type and deletion alleles of Rv2891 using a combination of three primers, two which hybridise to the upstream and

downstream arms of Rv2891 and one which hybridises to the wild-type M23 domain of Rv2891 (Fig. 3.3.3c).

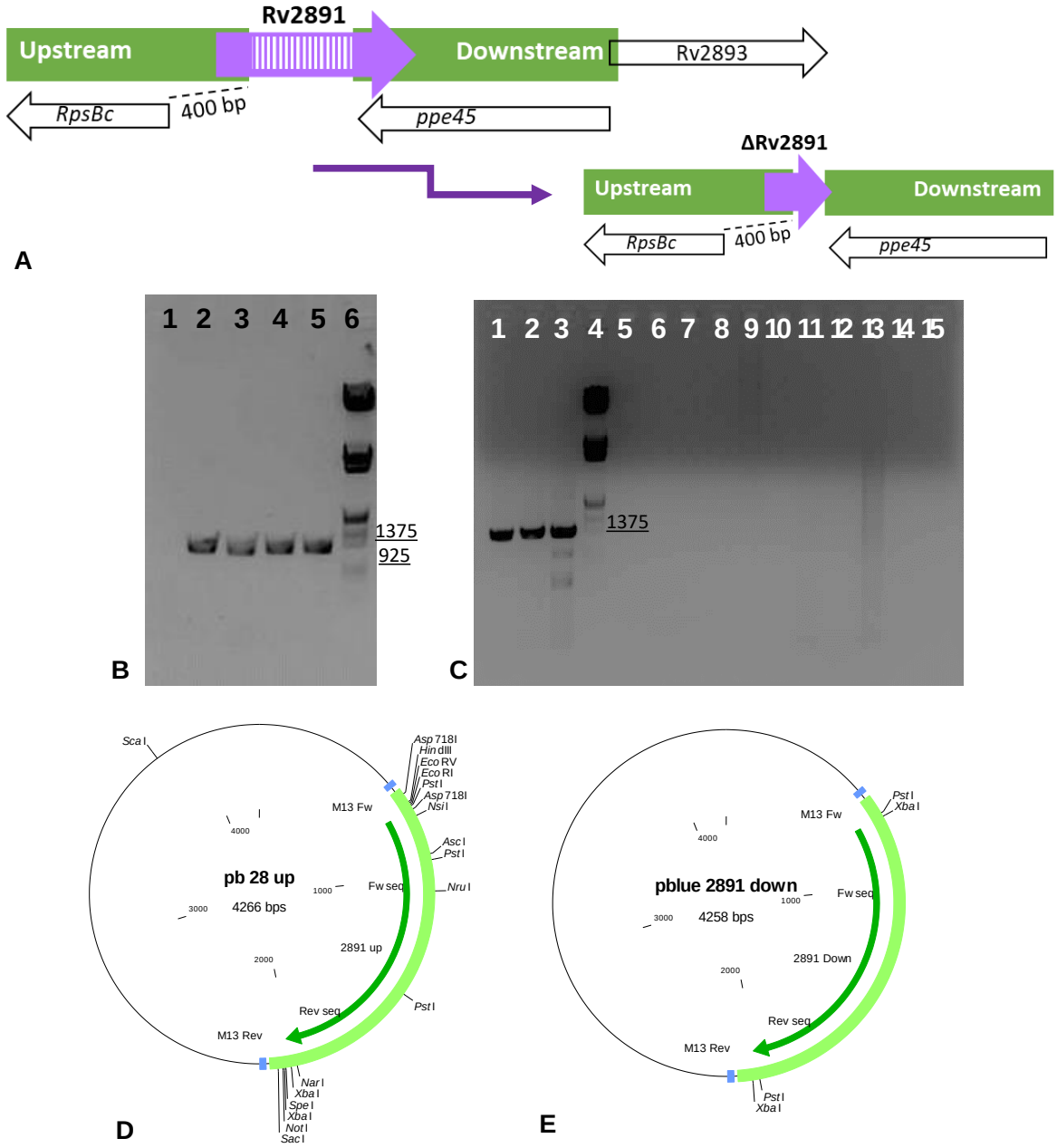

Figure 3.3.1 Rv2891 suicide vector construction.
A) Schematic diagram of the genetic neighbourhood of Rv2891 showing proposed M23-domain deletion. Purple: Rv2891 locus; hatched bars: M23 domain-encoding region; green: homology arms which were fused for Rv2891 disruption; white: neighbouring genes with putative promoters indicated. B) PCR amplification of the upstream homology arm (1305 bp). 1) NTC, 2-5) the 1305 bp upstream (US) arm amplicon, 6) MWM III. C) Gradient PCR to optimise annealing temperature for amplifying Rv2891 downstream (DS) region (1275 bp): 60°C (1,5,9,12), 66°C (2,7,10,13), 70°C (3,8,11,14). 1-3) all components, 4) molecular weight marker III, 5-8) excluding forward primer, 9-11) excluding reverse primer, 12-14) NTC. D) Vector map of pBlueScript::Rv2891 upstream. Light green: sequenced region. E) Vector map of pBlueScript::Rv2891 downstream. Light green: sequenced region. MWM: Lambda phage DNA marker (underlined).

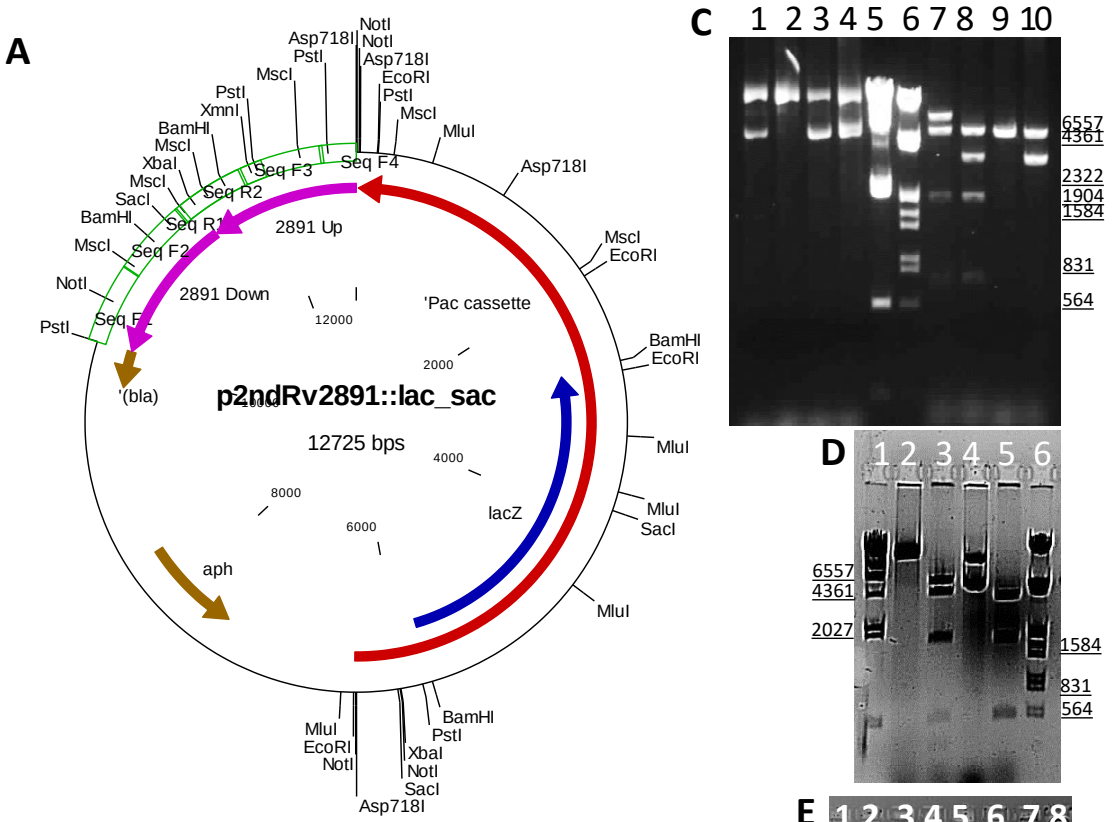

B

Restriction enzyme	Orientation A	Orientation B
*Eco*RI	**6501, 3594, 1863, 766**	9945, 1863, 766, 150
*Pst*I	**5690, 4298, 1810, 546, 374**	5696, 3933, 1810, 739, 546
*BamH*I	**5240, 3735, 3072, 677**	
*Mlu*I	**6800*, 2700*, 1987, 780, 425**	
*Msc*I	**8000*, 1600*, 750, 555**	
*Not*I	**6010, 4114, 2251, 333, 16**	
*Xmn*I + *Sac*I	**5148, 4657, 2195, 724**	

Figure 3.3.2 Rv2891 knockout vector.
A) Vector map: Green blocks indicate overlapping sequenced regions of the upstream and downstream homology arms for correct recombination. B) Expected restriction fragments. C) Following *lac-sac* ligation, 2 blue colonies (1-2) were screened by *Eco*RI digestion (7-8) alongside 2 vector controls (uncut: 3-4; cut: 9-10). The 2nd colony was taken forward 5) MWM II; 6) MWM III. D) *Pst*I digestion: 1) MWM II; 2) undigested clone; 3) digested clone; 4) undigested vector control; 5) digested vector control; 6) MWM III. E) Further mapping of the clone with 2) *BamH*I, 3) *Mlu*I, 4) *Msc*I, 5) *Not*I, 6) *Xmn*I and *Sac*I double-digestion. 7) undigested; 1) MWM III; 8) MWM IV. MWM: Lambda phage DNA marker (underlined).

Use of the upstream and downstream primers F1 and R1 identified SCOs which display both the larger wild-type and the smaller mutant allele in SCOs (Fig. 3.3.3d, odd lanes). Smaller products appeared brighter as faster rate of amplifying smaller PCR products means these products are in greater abundance than the larger products after the same

number of PCR cycles. The presence of the WT allele was confirmed using just primers F1 and R2 (Fig. 3.3.3.d, even lanes).

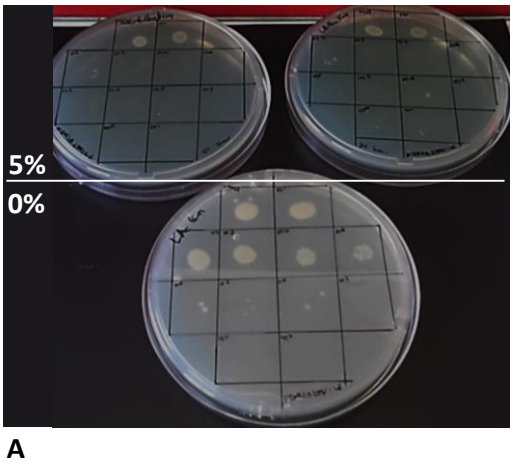

B

Dil. Factor (10^{-x})	0% sucrose	5% sucrose
0	TNTC	TNTC
1	TNTC	TNTC
2	TNTC	7
3	TNTC	0
4	TNTC	0
5	17	0
6	2	0
7	2	0
8	1	0
9-11	0	0

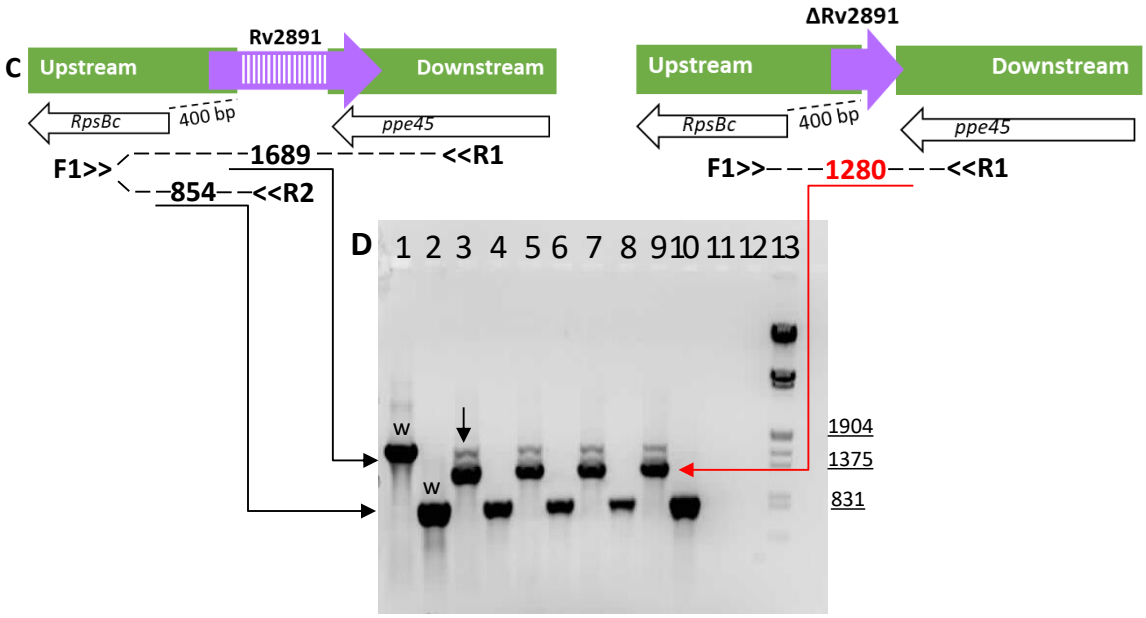

Figure 3.3.3 Screening for single-cross overs in *M. tuberculosis* transformed with the Rv2891 suicide vector.
A and B) Sucrose sensitivity of the Rv2891 deletion suicide construct tested in *E. coli*. A) Serial dilutions spotted on LA kanamycin (50 µg/ml), 0% OR 5% sucrose. B) Colony forming units of respective spots were quantified showing 5-log sucrose sensitivity of the construct. C and D) PCR genotyping of SCOs: C) Schematic diagram of amplicon size shifts for F1-R1 and F1-R2 primer combinations. D) 1-2: wild-type *M. tuberculosis* 1689 and 854 bp (w); 3-10: PCR products obtained from blue colonies indicating the presence of both wild-type and deletion alleles (down arrow, 1280 bp) expected for single cross over events. 11-12) no template controls. 1,3,5,9,11: Primers F1 and R1; 2, 4, 6, 8, 10: Primers F1 and R2. 13) MWM III. MWM: Lambda phage DNA marker.

3.3.2.3 Confirmation of double cross over events by PCR, Southern blotting and qPCR

Colonies confirmed as SCOs were propagated and sub-cultured into 7H9 without Km to screen for a double-cross over event before plating on sucrose and X-Gal to select for white, sucrose^{R} colonies as these would have lost the suicide vector backbone with the *lac_sac* cassette. To distinguish between DCOs which were successful Rv2891 deletion mutants, colonies were genotyped by PCR (Fig. 3.3.4a). ΔRv2891 DCOs were further confirmed by Southern blotting with DIG-labelled probes complementary to the upstream and downstream homology arms (Fig. 3.3.4b). Digestion of WT and ΔRv2891 genomic DNA with *Not*I for which fragments were probed with the upstream homology arm, as well as *Ale*I for which fragments were probed with the downstream homology arm generated distinctly-sized fragments for the respective strains, which matched what was observed after Southern blotting (Fig. 3.3.4b). The loss of Rv2891 gene expression was further confirmed in the deletion strain using RT-qPCR (Fig. 3.3.4.c). Confirming the loss of Rv2891 expression was particularly important since the deletion strategy only targeted the M23-domain, and not the entire Rv2891 locus.

3.3.3 Deletion of Rv2891 from the *M. tuberculosis* genome does not alter cell morphology

Given the evidence for the role of bacterial M23-endopeptidases in cell wall maintenance under various conditions in other organisms, SEM was used to study how deletion of Rv2891 affected the morphology of *M. tuberculosis* (Fig. 3.3.5). It was earlier observed that deletion of Rv0950c lead to cell shortening (section 3.2) while deletion of M23-endopeptidases required for cell division in *E. coli* (Uehara, Dinh & Bernhardt, 2009) and *M. smegmatis* (Shaku unpublished, 2017) for example expectedly causes cell chaining. Deletion of Rv2891 did not grossly alter rod morphology nor cause cell shortening (Fig. 3.3.5). As cell chaining was also not observed, a role for Rv2891 in cell division could not be determined herein, despite earlier observed phylogenetic clustering of Rv2891 with cell division endopeptidases.

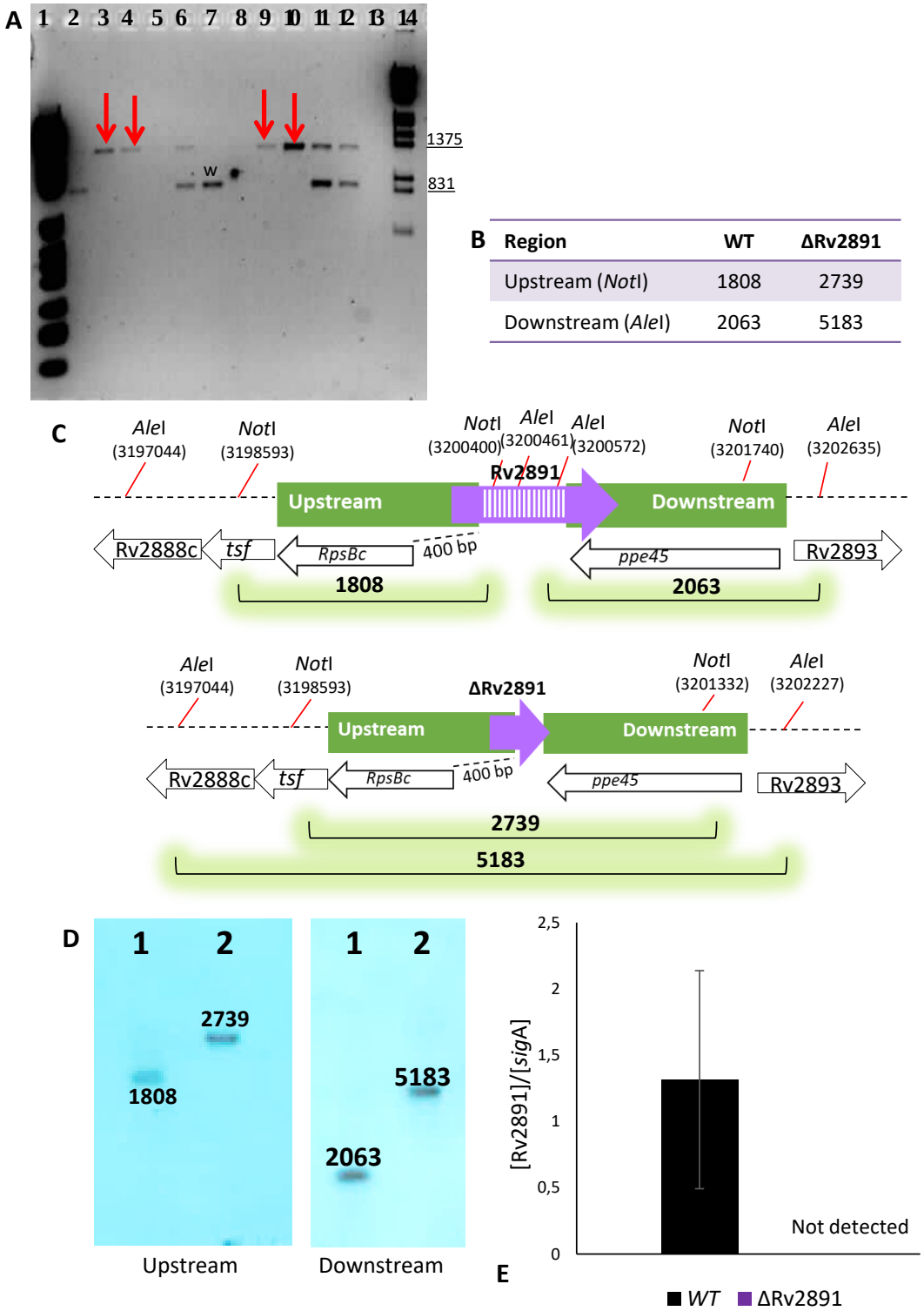

Figure 3.3.4 Genotyping of DCOs following sucrose selection of an ΔRv2891 SCO strain.
A) PCR screening for double-cross over Rv2891-deletion mutant strains of *M. tuberculosis*. 1) MWM VI, 2-11) template DNA obtained from white, sucrose-resistant colonies; 12) template DNA obtained from a blue, sucrose-sensitive colony (single cross-over); 13) no template control 14) MWM III. w: WT 854 bp; down arrows: Δ 1280 bp. B) Expected restriction fragments (bp) to be detected by Southern blotting with DIG-labelled probes either complementary to the upstream or downstream homology arms of Rv2891. C) Schematic diagram of upstream and downstream probe binding to *Not*I and *Ale*I fragments respectively. D) Southern blots: 1) WT allele; 2) ΔRv2891 allele. E) qPCR to confirm loss of Rv2891 expression in *M. tuberculosis* ΔRv2891. Expression normalised to *sigA*.

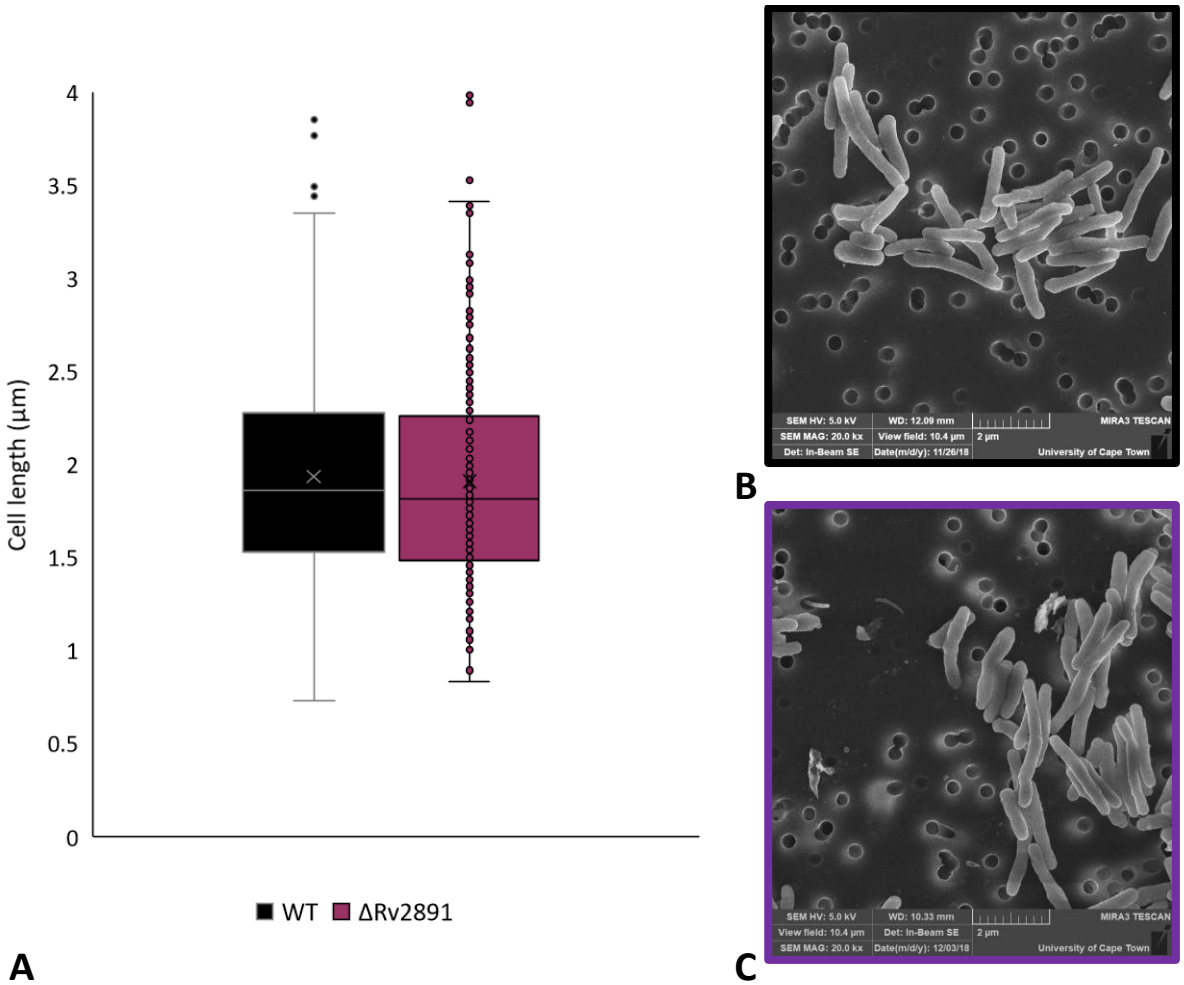

Figure 3.3.5 Scanning electron microscopy to study morphological changes to *M. tuberculosis* after Rv2891 deletion.
A) Box and whisker plot of cell lengths measured in ImageJ of 100 cells for each strain in triplicate. B, C) Representative micrographs of WT (B), ΔRv2891 (C), scale bar = 2 µm.

3.3.4 The effect of Rv2891 deletion on PG remodelling

As gross morphological defects as a result of Rv2891 deletion could not be identified by SEM, putative subtle changes to PG remodelling were studied using TADA incorporation and Van-FL labelling (described in section 3.2), with a particular focus on the process of cell division. As such, care was taken to label cultures during rapid cell division in exponential phase determined by OD_{600} between 0.6 and 0.8.

3.3.4.1 TADA incorporation

Although the role of Rv2891 was not clear, the subtle structural similarities to amidase activators was used as a basis to expect cell division aberrations. As before, heterogenous TADA labelling patterns were observed as expected for *M. tuberculosis* (Fig. 3.3.6). The proportions of TADA-incorporated sub-populations were the same between WT and ΔRv2891 strains and therefore did not point to a role for Rv2891 cell division (Fig.

3.3.6b). The normal, polar TADA incorporation suggests that Rv2891 deletion does not impact PG biosynthesis or elongation.

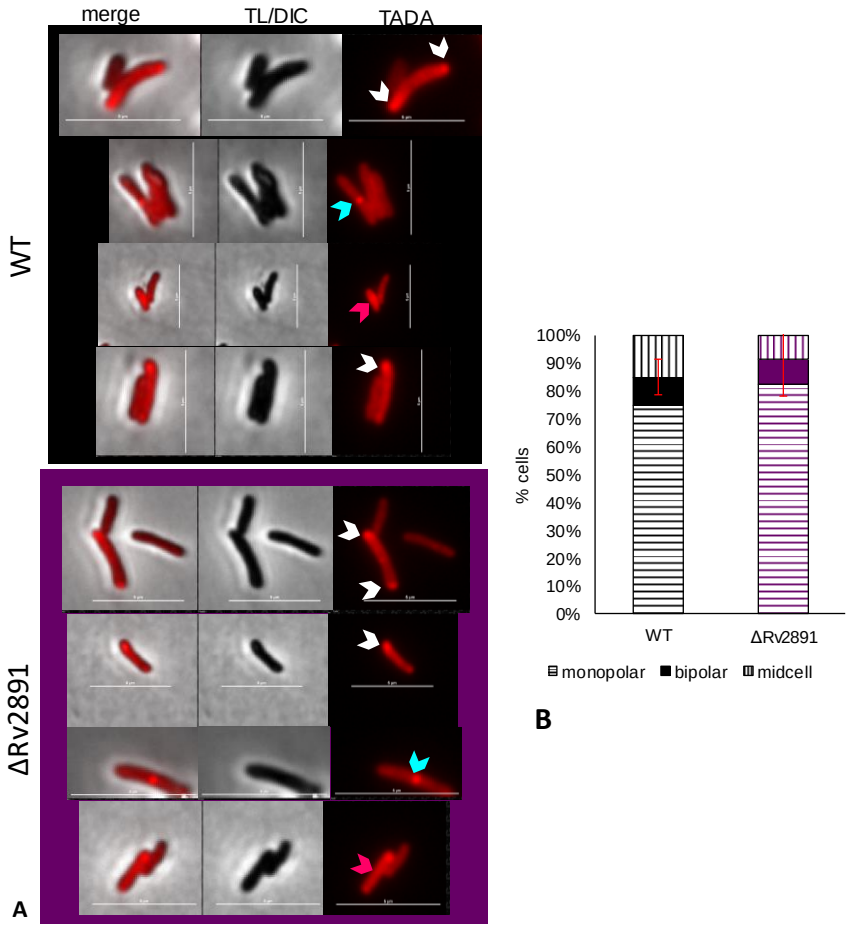

Figure 3.3.6 TADA-labelled *M. tuberculosis*.
A) Representative micrographs showing heterogenous incorporation of TADA in the *M. tuberculosis* cell wall. Arrows indicate sub-populations of interest: white: mono/bipolar, cyan: mid-cell, magenta: diffuse. B) Proportions of sub-populations as a percentage of the total number of polar and mid-cell incorporating cells.

FDAA incorporation is not just indicative of general cell processes like elongation or division but is sensitive to the PG compositional changes taking place during these processes. For example, comparing the levels of monopeptide TADA labelling and alkyne, di-peptide DADA labelling assisted in determining a role for Rv0950c in cross-link maturation in a manner which regulates cell length. Following Rv2891 deletion, a reduction in non-specific TADA fluorescence intensity (which includes laterally incorporated cells and non-incorporating cells) was observed (p = 4.5E-05; Fig. 3.3.7c), which was similar to Rv0950c deletion. Further, this trend was not observed in the polar-incorporated population (Fig. 3.3.7a) but was observed in the mid-cell population (p = 0.002; Fig. 3.3.7b).

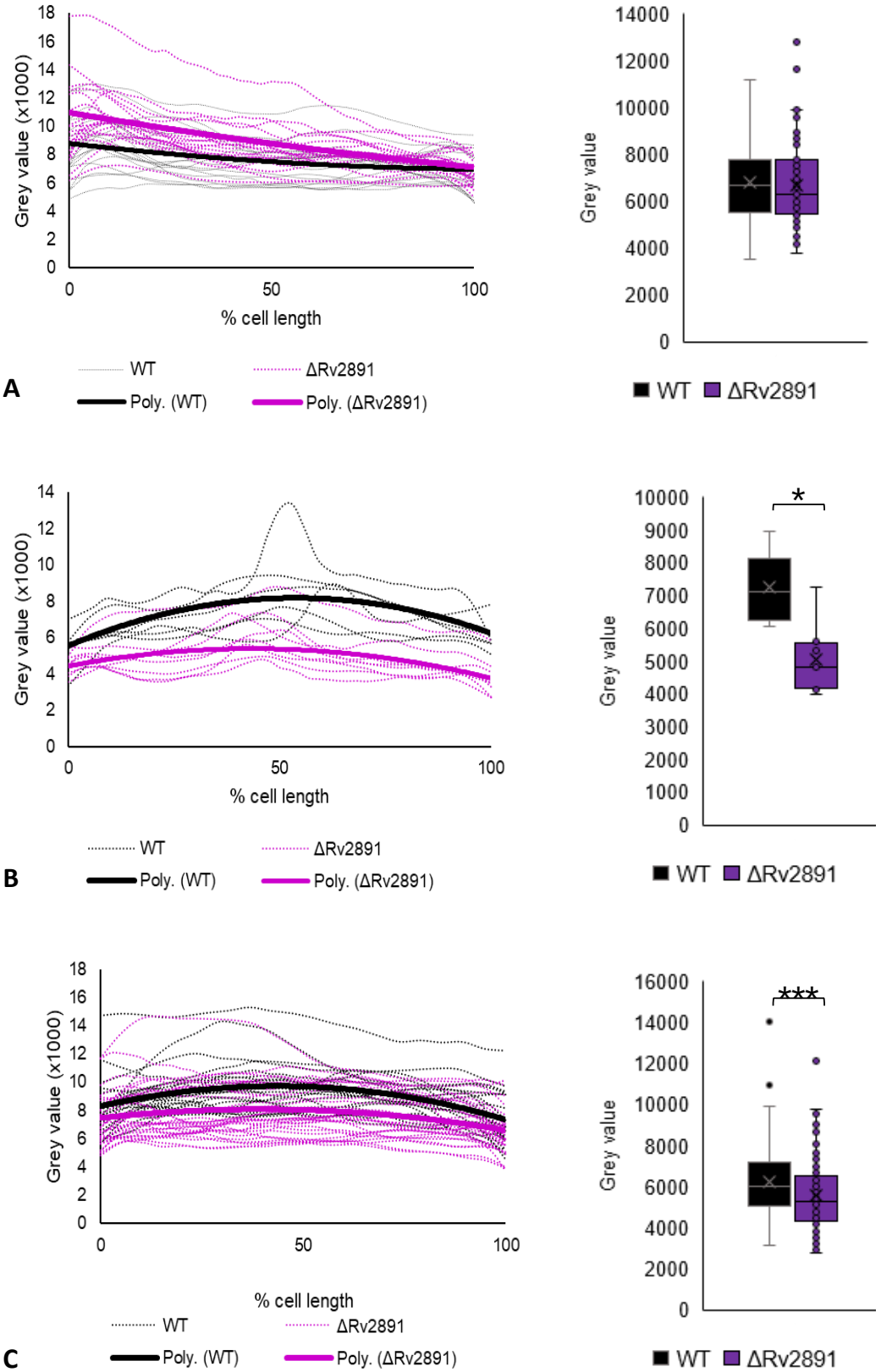

Figure 3.3.7 Fluorescence intensity of TADA-incorporating *M. tuberculosis*.
A) polar, B) midcell, C) diffuse. Left: fluorescence intensity profiles. Right: average fluorescence intensity per cell. *p = 0.002, ** p = 4.4E-05 for student's t-test.

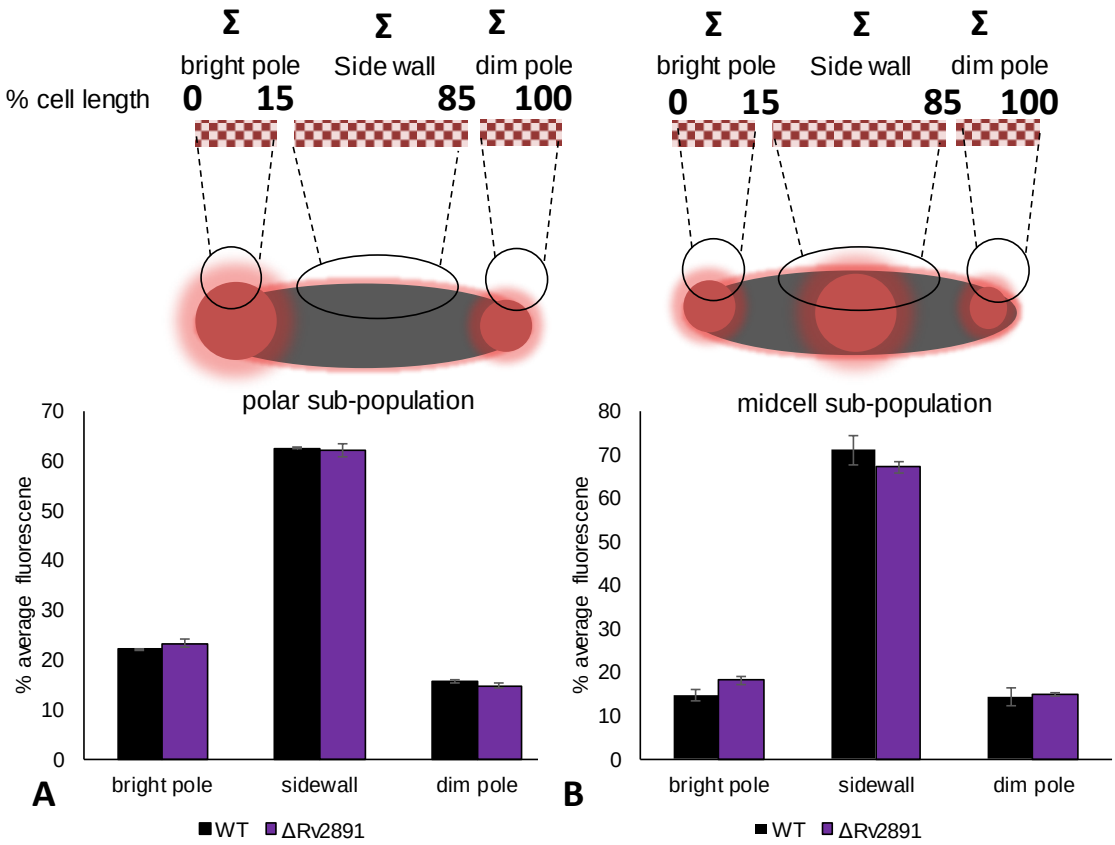

Figure 3.3.8 Characteristics of individual cells of TADA-incorporating *M. tuberculosis.*
A,B) distribution of fluorescence between the bright pole, side-wall and midcell of the polar (A) or midcell (B) sub-population.

Unlike Rv0950c, loss of ΔRv2891 did not change the spatial distribution of TADA between the poles and side-wall (Fig. 3.3.8). This is suggestive of a number of events: 1) Rv2891 may play a role in side-wall PG cross-linking as well as septum formation; 2) the shared reduction in side-wall TADA incorporation in Rv2891 or Rv0950c deletion mutant suggests that both enzymes are able to process PG in the same way but are not redundant as they are required for different processes: Rv0950c in cell length regulation, and Rv2891 not in cell length regulation, but possibly cell division. This also suggests that although Rv2891 does not have the same catalytic site as Rv0950c and other active M23-endopeptidases, the substitution of cysteine with the first Histidine may be inconsequential to zinc-binding. The distinct differences in the N-termini of the two homologues may provide the basis for specialisation of these enzymes. The signal-peptide of Rv2891 may allow export to the periplasm to process septal PG, a signal which is lacking in Rv0950c.

3.3.4.2 Fluorescent vancomycin incorporation

As with TADA staining, Vanc-FL labelling at sub-MIC concentration revealed the same sub-populations between WT and ΔRv2891 (Fig. 3.3.9b), agreeing with the TADA observation that Rv2891 does not appear to play a role in elongation. However, fluorescence intensity of polar-incorporated cells was higher following Rv2891 deletion, suggesting a higher level of uncross-linked PG ($p = 0.001$; Fig. 3.3.9c; Fig. 3.3.10a).

In WT cells 4-3 cross-links are formed once new PG is inserted. As the cell grows, these 4-3 cross-links are remodelled to 3-3 cross-links, characteristic of mature PG, mostly present along the side-wall. It is expected then, that if the loss of Rv2891 prevents cross-linking in new PG, side-wall PG may also not be cross-linked and should display a higher fluorescent intensity at the side-wall compared to WT. The opposite was observed whereby the bright sub-population, incorporating Vanc along the side-wall was higher in the WT, though not significantly (Fig. 3.3.9d; Fig. 3.3.10b). There was also no change in distribution of fluorescence between the poles and the side-wall after loss of Rv2891 (Fig. 3.3.10c).

The combined observations of TADA and Vanc-labelled ΔRv2891 cells suggest that reduced polar 4-3 cross-linking is compensated for perhaps by increased L,D-transpeptidase activity at the side-wall and at the septum as both these sites showed significant loss of TADA signal in the ΔRv2891 strain. Furthermore, the overall compositional changes were markedly different to what was observed for Rv0950c deletion.

The hypothetical role of Rv2891 in polar 4-3 cross-linking needs to be supported by studying fluorescent labelling of a genetic complement strain. Without demonstrating reintroduction of Rv2891 expression reverts the above phenotypes to WT, it cannot be concluded that the observed changes to PG remodelling are a direct result of the absence of Rv2891. A construct for genetic complementation was designed and cloned but is yet to be transformed into *M. tuberculosis* (Fig. 3.3.11). The Rv2891 locus along with 400 bp of upstream, putative promoter sequence was amplified and cloned into mycobacterial integrating vector, pMV306H (Andreu et al., 2010). The construct was confirmed using restriction digestion analysis and sequencing (Fig. 3.3.11) but has not yet been electroporated into *M. tuberculosis* ΔRv2891.

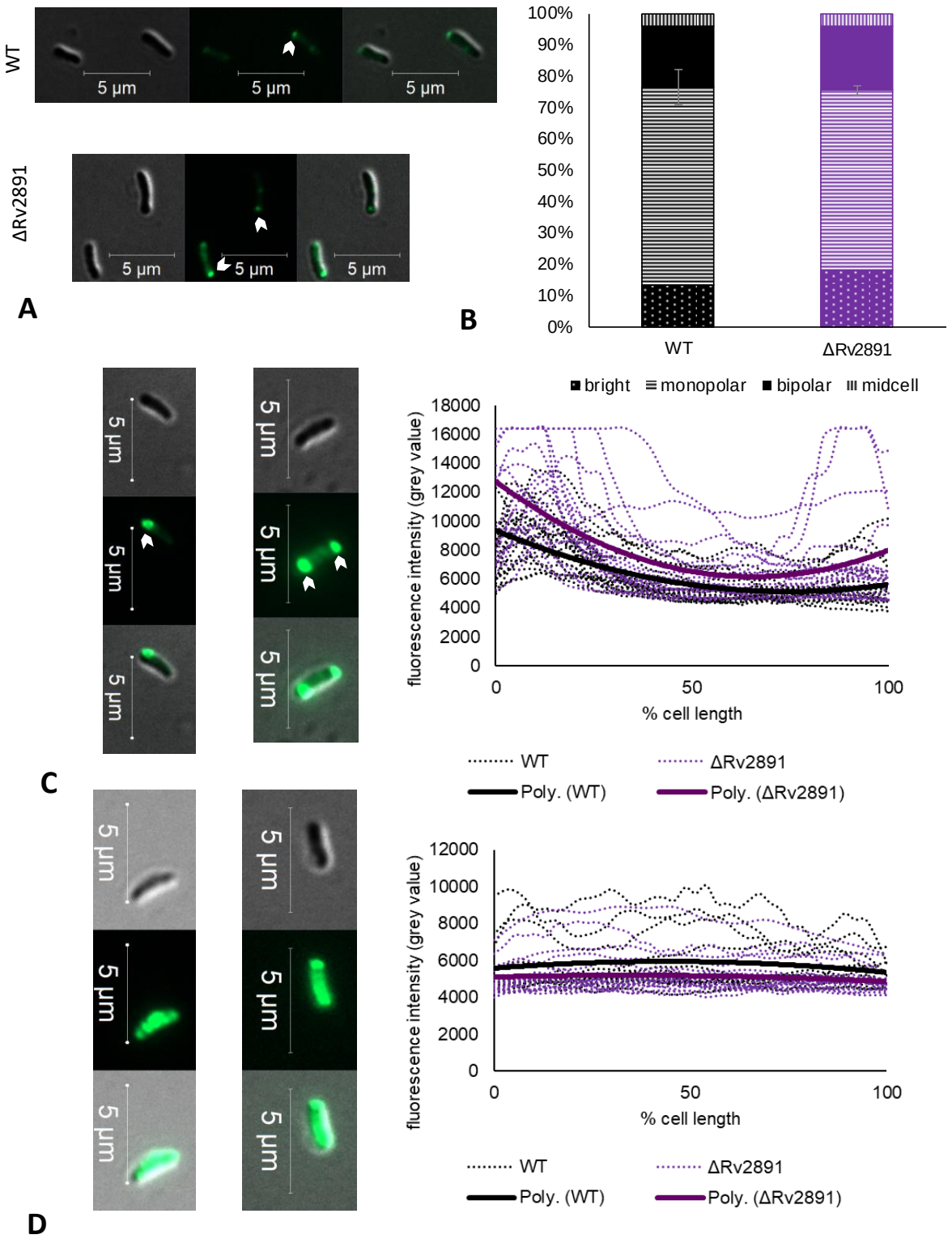

Figure 3.3.9 Vanc-FL-labelled *M. tuberculosis.*
A) micrographs representative of cells exhibiting common polar incorporation of Vanc-FL. B) sub-populations of Vanc-labelled *M. tuberculosis*. C, D) fluorescence intensity of polar (C) or side-wall incorporating cells (D). Left: representative micrographs, polar incorporation indicated by arrows. Right: fluorescence intensity across the cell length normalised to a %, 0% marks the bright pole.

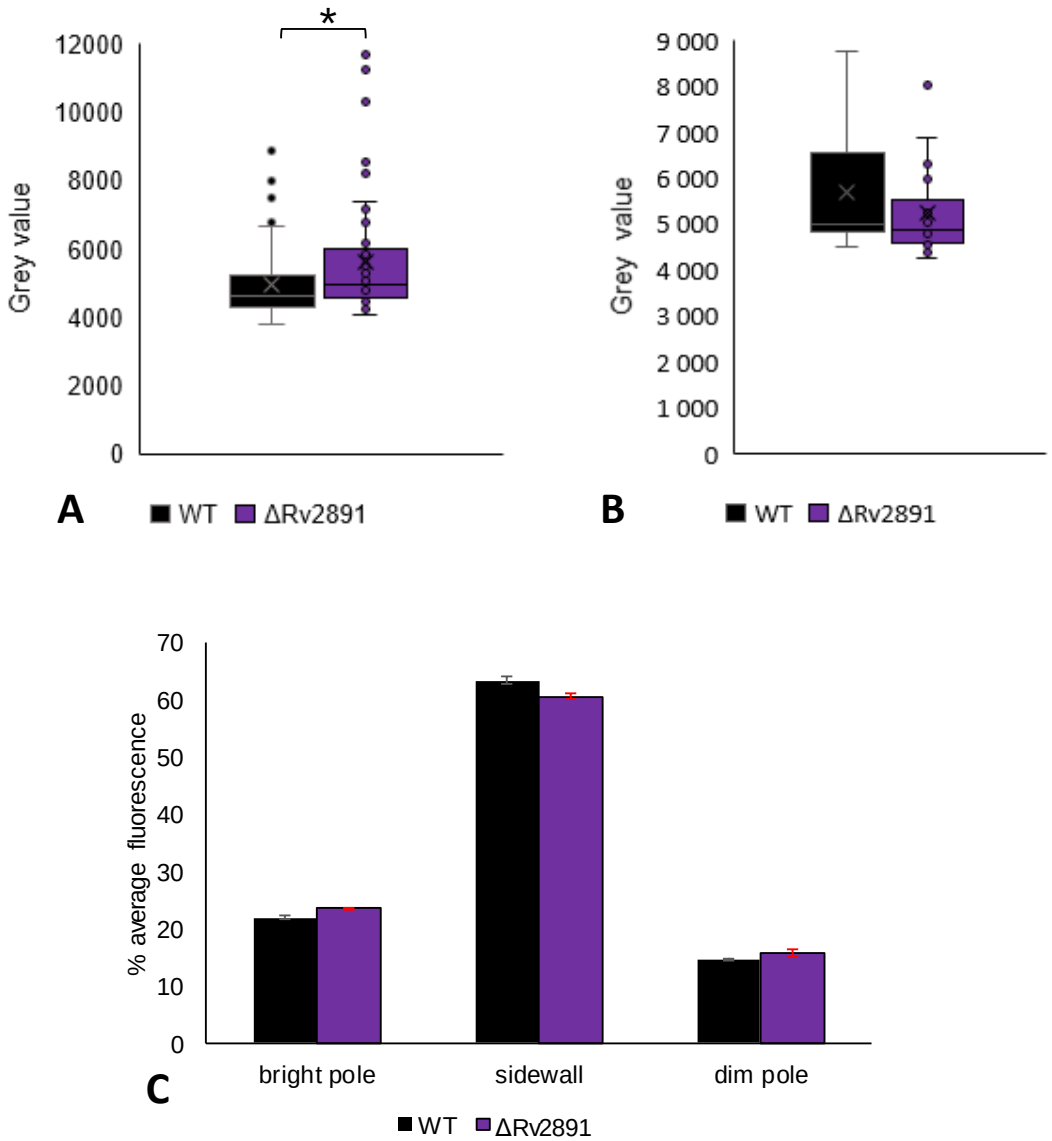

Figure 3.3.10 Characteristics of individual cells of Vanc-FL - labelled *M. tuberculosis.*
A,B) average fluorescence intensity: A) polar-labelled cells, **p* = 0.001; B) bright/side-wall labelled cells. C) Distribution of fluorescence between the poles and side-wall of Vanc-labelled cells.

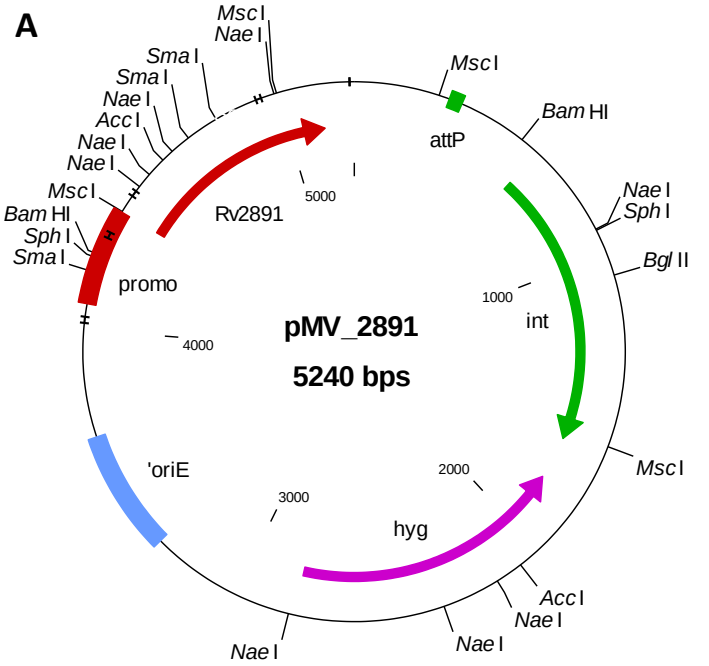

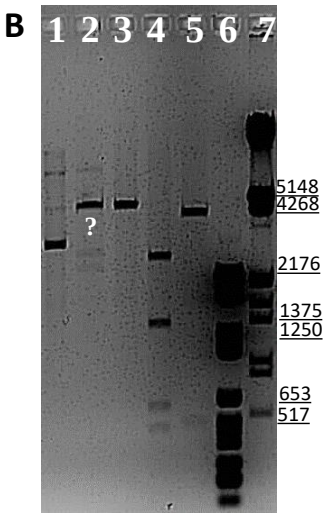

C

Enzyme	Expected fragments (bp)
*Acc*I	2721, 2519
*Bgl*II	5240
*Msc*I	2775, 1344, 613, 508
*Sma*I	4624, 513, 103

Figure 3.3.11 Rv2891 complementation vector construction.
A) pMV306H::Rv2891 vector map, B) Mapping of the construct with *Acc*I (2), *Bgl*II (3), *Msc*I (4) and *Sma*I (5), 1) uncut, 6) MVI, 7) MIII. C) Expected fragments for restriction mapping of the construct. MWM: Lambda phage DNA marker (underlined).

3.3.5 Rv2891 is not required for growth

Fluorescent probing of PG suggests that Rv2891 is required for polar PG biosynthesis. It was expected then that loss of Rv2891 would lead to a growth defect however this was not observed by optical density or CFU formation (Figure 3.3.12).

3.3.6 The loss of Rv2891 does not lead to cell wall vulnerability

PG labelling showed a disruption to the homeostasis between pre-mature and mature PG upon Rv2891 deletion. It was expected that this would change the susceptibility to cell-wall targeting antibiotics and cell wall permeability. Microbroth dilution measurement of MICs of various cell-wall targeting antibiotics was unchanged (Table 3.3.1), as was permeability to EtBtr (Fig. 3.3.13).

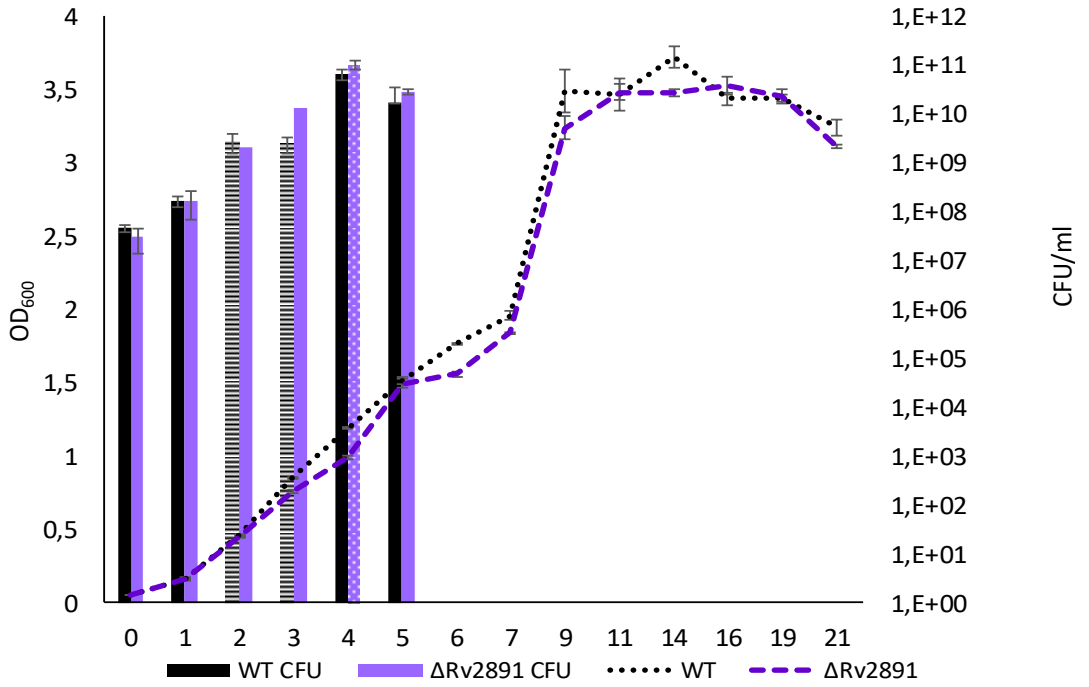

Figure 3.3.12 Growth kinetics of *M. tuberculosis* WT compared to ΔRv2891.
Growth curve in triplicate, monitored over 21 days measured by OD_{600} and colony forming units (CFU) of serially-diluted cultures. Hatched and spotted bars indicate time-points at which only duplicate or a single replicate of CFUs respectively, due to loss of the other replicates to contamination.

Table 3.3.1 Minimum inhibitory concentrations (MIC) of various antibiotics comparing wild-type *M. tuberculosis* to the ΔRv2891 deletion strain.

Antibiotic	**WT**	**ΔRv2891**
cycloserine	6.25	6.25
ethambutol	1.6-3.2	1.6-3.2
vancomycin	8	8
meropenem	2	2
ofloxacin	2.4	2.4
amoxicillin	40	40

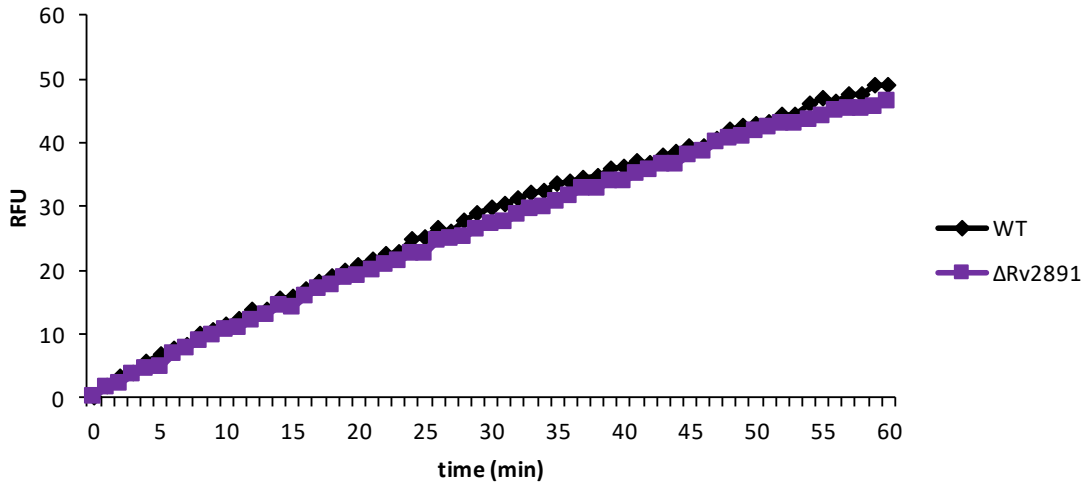

Figure 3.3.13 Permeability of *M. tuberculosis* to ethidium bromide.
Plate-based fluorescence readout over 60 min incubation of *M. tuberculosis* WT and ΔRv2891 with EtBr (0.25 µg/ml).

3.3.7 Summary of limited characterisation of *M. tuberculosis* Rv2891

Deletion of Rv2891 led to non-significant changes to TADA and Vancomycin incorporation, pointing to a putative role for Rv2891 in 4-3 cross-link remodelling (Section 3.3). However, these results are preliminary and require further validation. Still, two distinct M23-endopeptidases were identified for cell-wall modulation in *M. tuberculosis* for which Rv2891 possibly acts at the poles while Rv0950c is likely required for PG maturation.

As single deletions of these genes did not inhibit growth, it would be highly insightful in terms of drug-target identification to study the consequences of loss of both these genes. Towards this, the ΔRv2891 deletion vector was transformed into the ΔRv0950c background and a single SCO was identified, however initial attempts at DCO induction all lead to reversion to WT (Appendix C).

4 Discussion

Current treatment of TB takes at least six months, during which some patients will develop drug resistant disease and availability of drugs to treat MDR and XDR TB is greatly limited. Drugs currently available for drug-susceptible and multiple drug resistant TB are also very difficult to adhere to, both as a result of the extended treatment period and the side-effects experienced. The challenges of TB treatment coinciding with the HIV pandemic results in TB being one of the leading causes of mortality globally and the leading cause of death in South Africa. Urgent interventions are required to shorten the treatment duration required to cure DS TB and to produce novel treatments for DR TB. The aim of this research was to study the cell wall of *M. tuberculosis*, towards identifying novel drug targets. The core of the *M. tuberculosis* cell wall, PG, is a structure unique to bacteria and some plant species. As a result, drugs targeting PG are promising candidates and should result in reduced human cytotoxicity. As such, the study of how PG is synthesised and degraded is an important and growing field.

4.1 Structural conservation vs functional divergence of *M. tuberculosis* M23 endopeptidases

PG degradation is well-characterised in the rapid-growing and model firmicutes, *E. coli* (Priyadarshini, De Pedro & Young, 2007; Uehara et al., 2010; Hugonnet et al., 2016; Peters Kannan et al., 2016) and *B. subtilis* (Ishikawa et al., 1998; Fukushima et al., 2008; Sudiarta, Fukushima & Sekiguchi, 2010; Lebar et al., 2014). Recent advances in mycobacteriology, however, has revealed stark differences in the modes of cell wall expansion between the firmicutes and actinomycetes (Randich & Brun, 2015). This has highlighted the need to specifically study mycobacterial PG and cell wall maintenance as much of what is known in the firmicutes is not translatable in actinomycetes.

Study of the rapid-growing, non-pathogenic mycobacterium, *M. smegmatis* has helped advance characterisation of numerous PG remodelling enzymes, including lytic-transglycosylases (Hett, Chao & Rubin, 2010), *N*-acetyl muramyl L-alanine amidases (Boutte et al., 2016; Senzani et al., 2017), and numerous penicillin binding proteins (Bansal et al., 2015; Kieser et al., 2015; Pandey et al., 2018; Ealand et al., 2019). When some of these enzymes were further characterised in *M. tuberculosis*, their functions were not the same (Kumar et al., 2013; Senzani et al., 2017). Only 37% of the genome of non-pathogenic mycobacteria, such as *M. smegmatis*, share direct orthologues with pathogenic

bacteria (Prasanna & Mehra, 2013), and may explain why the ultrastructure of *M. smegmatis* is more similar to *E. coli* than *M. tuberculosis* (Yamada et al., 2018). Characterised genes associated with the mycobacterial cell wall are the least-conserved gene class comparing pathogenic and non-pathogenic mycobacteria (Prasanna & Mehra, 2013). This highlights the importance of studying potential drug targets directly in *M. tuberculosis*.

The focus on the M23-endopeptidases initially arose from the importance of these genes in cell division and PG remodelling in numerous other bacteria. What were initially identified as orthologues to the well-characterised cell-division factors, *E. coli* EnvC and NlpD (Uehara, Dinh & Bernhardt, 2009; Uehara et al., 2010), instead emerged as three M23-endopeptidases encoded at Rv0950c, Rv2891 and Rv3786c. The *M. tuberculosis* M23-endopeptidases are phylogenetically divergent from cell separation and other M23 endopeptidases, and instead, are closely related to *E. coli* stem-peptide remodelling, L,D-transpeptidases and other stem-peptide remodelling enzymes. It became clear from multiple *in silico* analyses that *M. tuberculosis* lacks cell-separation M23-endopeptidases, commonly known as degenerate LytM factors (dLytM).

Rv0950c is the most-conserved *M. tuberculosis* M23-endopeptidase, with direct orthologues encoded by multiple mycobacteria, and the only M23-endopeptidase encoded by *M. leprae*. *M. leprae* has the most reduced genome among the mycobacteria and therefore serves as a template for the minimum consortium of genes necessary for mycobacterial growth and survival (Vissa & Brennan, 2001), which includes the Rv0950c orthologue, ML0154c. Only 34% of the gene content of *M. tuberculosis* is conserved in *M. leprae* (Prasanna & Mehra, 2013). Within this margin, the genetic neighbourhoods of Rv0950c and ML0154c exist as an entire region of homology between the two pathogens. Synteny is evidence of a lack of genetic recombination during microevolution, which suggests that recombination events within Rv0950c and neighbouring genes would have been detrimental for survival of *M. tuberculosis* and *M. leprae*.

The minimal *M. leprae* genome bears a significant number of pseudogenes, many of which have functional orthologues required for lipid metabolism, a process readily occurring in macrophage hosts (Avni et al., 2018). Most of the non-pseudogenes encoded in *M. leprae*

are associated with the cell wall and cell wall processes (Avni et al., 2018), highlighting the critical importance of cell wall-maintenance for intracellular-pathogenic mycobacteria.

The neighbouring genes of Rv0950c are part of a number of "core orthologues" shared between pathogenic and non-pathogenic mycobacteria, although Rv0950c itself was not considered (Prasanna & Mehra, 2013). A pan-genome synteny study showed that both *M. tuberculosis* and *M. leprae* exhibit considerable syntenic rearrangement, wherein the Rv0950c and ML_0154c neighbourhoods were both reversed with respect to other mycobacteria, occurring close to the start of the genome, opposite to *M. smegmatis* for example (Prasanna & Mehra, 2013). A narrower analysis of mycobacterial synteny, comparing either orthologues of *M. leprae* pseudogenes or non-pseudogenes emphasised high similarity between *M. leprae* and *M. tuberculosis* (Avni et al., 2018).

The patterns of genetic conservation of the three *M. tuberculosis* M23-endopeptidases opposed to just one *M. leprae* ML_0154c seemingly agrees with the respective growth phase transcription profiles. In keeping with a predicted importance for Rv0950c during mycobacterial growth, Rv0950c showed a growth phase dependent-transcription profile unmatched by Rv2891 and Rv3786c expression. Notably, Rv2891, which was significantly less abundant than Rv0950c, is a direct orthologue of the *M. leprae* pseudogene ML_1599. Rv3786c only has one direct orthologue in *M. marinum*, with a highly unique domain architecture. The reasons for this remain unclear.

The basic domain architecture of Rv0950c, ML_0154c and other direct mycobacterial orthologues appears to be more conserved among mycobacterial M23-endopeptidases than that of orthologues with accessory domains, such as Rv3786c or *M. smegmatis* MSMEG_1192. Given the highly conserved nature of Rv0950c, clustering with other M23-endopeptidases was expected. Instead, Rv0950c and the other mycobacterial endopeptidases formed a cluster mainly with other PG remodelling enzymes and *E. coli* YgeR, highlighting that mycobacteria are functionally divergent within the M23 endopeptidase protein family. Still, secondary-structure homology modelling supports the annotation of Rv2891 and Rv3786c as M23-endopeptidases, as these proteins were modelled to *H. pylori* Csd3 and *S. simulans* lysostaphin respectively.

Homology-modelling of the *M. tuberculosis* M23 endopeptidases was limited to the respective M23 domains, even at the input of the full-length protein sequences. Rather than a limitation, this provided a crucial suggestion that although all three genes encode an M23 domain with characteristic β-sheets, the M23 endopeptidase domain of Rv0950c and Rv2891 best modelled to two different endopeptidases. It was determined here that Rv0950c and Rv2891 do not have the same zinc co-ordinating residues. In addition to different catalytic residues, Rv0950c and Rv2891 may exhibit different M23 endopeptidase substrate binding pockets. This explains the subtle differences in fluorescent D-amino acid (FDAA) probe incorporation in the PG of *M. tuberculosis* ΔRv0950c and ΔRv2891 (Section 3.3).

4.2 Fluorescent D-amino acid probes report on mycobacterial PG composition

Within the highly complex, rigid PG core, the terminal D-Alanines of the PG stem-peptide are the most commonly remodelled portion of PG. The terminal D-Alanines provide substrates for PG cross links which can be added and broken down to allow for strengthening and for loosening of the cell wall that is required during various stages in the cell cycle. Fluorescent D-amino acids (FDAA) are synthetic derivatives of D-Alanine or D-Lysine which are inherently fluorescent (Kuru et al., 2015) or are conjugated to a reactive amine (Shieh et al., 2014). Recent advances in D-amino acid fluorescent probe design has permitted tracking the fate of the D-Alanines inside and outside the mycobacterial cell, revealing insights into how mycobacterial PG is synthesised and remodelled, as well as the regulation of these two processes at different stages in the cell cycle and under environmental stress (Botella, Yang, et al., 2017; Baranowski et al., 2018; García-Heredia et al., 2018; Pidgeon et al., 2019). Importantly, FDAA incorporation only occurs in actively growing cells, relying on active PG synthetic and degrading machinery (Botella, Yang, et al., 2017). FDAA localisation observed here after 30 - 60 min incubation of *M. tuberculosis* was comparable to 30 min of tetra-peptide labelling (Pidgeon et al., 2019). Longer incubation periods of *M. tuberculosis* with probes display diffuse staining (Pidgeon et al., 2019), expected for mature PG but making it difficult to dissect out spatial PG remodelling in mycobacteria, for which the body of evidence, including this research, is growing. This work represents the first instance of a M23 endopeptidase dependent pathway for FDAA incorporation in *M. tuberculosis*.

4.2.1 Polar FDAA incorporation reports on nascent PG

When added to bacterial media, FDAAs are taken up by the cells, either intracellularly or extracellularly (García-Heredia et al., 2018). Intracellular FDAA incorporation takes place when a di-peptide FDAA is added to *m*-Dap of the PG stem peptide during PG synthesis (Sarkar et al., 2016; García-Heredia et al., 2018). Since vancomycin and di-peptide FDAAs label via MurF intracellularly, they are more sensitive to detecting uncross-linked PG than monopeptide FDAAs (García-Heredia et al., 2018). Extracellular FDAA incorporation, however, involves the addition of a mono-peptide FDAA to cross-linked PG from which the fifth, terminal D-Alanine was cleaved to facilitate 4-3 or 3-3 cross-linking (Baranowski et al., 2018; García-Heredia et al., 2018). In 4-3 cross-linked PG, the terminal D-alanine is cleaved from the receptor stem-peptide, possibly by D,D carboxypeptidase activity. This leaves a position onto which the FDAA can be incorporated, making new PG the brightest. Polar mono-peptide incorporation, therefore, reports on the presence of tetra-peptide substrate of nascent PG (Baranowski et al., 2018; García-Heredia et al., 2018).

In *E. coli* and *B. subtilis*, inhibiting cross-link degradation by depleting D,D carboxypeptidases caused an accumulation in intact cross-links which lead to enhanced fluorescence of cell wall probes (Lebar et al., 2014; Sarkar et al., 2016). The loss of Rv2891 had no effect on polar, TADA mono-peptide incorporation but increased fluorescent vancomycin staining showed that most of the polar PG is not cross-linked. Rv0950c deletion on the other hand was more effectual to side-wall FDAA incorporation, during maturation of PG rather than remodelling of nascent PG.

4.2.2 Side-wall incorporation reports primarily on PG maturation

Unlike *E. coli* and *B. subtilis*, actinomycetes have a characteristically high proportion of 3-3 cross linkage (Hugonnet et al., 2014). As PG ages, some but not all of the PG is remodelled to 3-3 cross-links from which the incorporated FDAA is cleaved, reducing the fluorescence intensity at the side-wall but not ablating it entirely (Baranowski et al., 2018). Mono-peptide incorporation at the side-wall reports on L,D-transpeptidase activity (Baranowski et al., 2018; García-Heredia et al., 2018). When all six *M. smegmatis* LDTs were deleted, FDAA incorporation was ablated (Baranowski et al., 2018). In a pulse-chase experiment, HADA monopeptide fluorescence at the *M. smegmatis* side-wall was almost entirely replaced by NADA incorporation after 16 hours (Botella, Vaubourgeix, et al.,

2017). At the *M. smegmatis* side-wall, tetra-peptide fluorescence was uniform, but penta-peptide fluorescence exhibited a polar gradient much like canonical DADA staining (Pidgeon et al., 2019). Pan-cell fluorescence intensity of *M. tuberculosis* was higher when labelling with the tetra-peptide probe than the penta-peptide (Pidgeon et al., 2019). At this point in time, a tri-peptide to further study 3-3 cross-linking has not yet been demonstrated in the literature.

Meropenem-treated *M. smegmatis* lost penta-peptide probe signal altogether but had a lesser effect on tetra-peptide incorporation (Pidgeon et al., 2019) while meropenem-treated *M. tuberculosis* exhibits reduced FDAA incorporation in a manner more consequential to pole formation than PG maturation (Botella, Yang, et al., 2017). Loss of Rv0950c did not affect *M. tuberculosis* Meropenem susceptibility, implying that Rv0950c acts downstream of penta-peptide remodelling. It is likely that Rv0950c acts on aged PG based on the observations that Vancomycin and di-peptide labelling revealed the same abundance of cross-linking at the poles. The increased di-peptide incorporation at the side walls of Rv0950c-depleted cells demonstrates that Rv0950c-depleted cells have 4-3 cross linked PG which is unable to mature to 3-3 cross-linked PG from which di-peptide signal would have been cleaved. In agreement, side-wall incorporation of di-peptide probes increased after labelling WT *M. smegmatis* treated with lysozyme and mutanolysin (García-Heredia et al., 2018) representing nascent, immature PG re-inserted at sites of damaged cell wall.

In this study, lysozyme-mutanolsyin treated *M. tuberculosis* WT cells recapitulated the pattern of di-peptide incorporation observed in *M. smegmatis* (García-Heredia et al., 2018). Co-treated Rv0950c-depleted cells, however, displayed the opposite effect, whereby di-peptide incorporation decreased with increasing muramidase concentration. It is possible that Rv0950c is an endopeptidase which cleaves the 4-3 cross-links of native PG for 3-3 cross-link formation. If this is the case, this hypothesised 4-3 degradation activity against neighbouring intact PG may be required for re-insertion of nascent PG at sites of muramidase damage, explaining the lack of nascent PG re-insertion in the *M. tuberculosis* ΔRv0950c cell wall. Unexpectedly then, loss of Rv0950c did not cause a population-level enhanced susceptibility to lysozyme-mediated cell lysis. The susceptibility of *M. tuberculosis* to cell-wall targeted antibiotics was also not changed at the loss of Rv0950c or Rv2891. It is possible that ΔRv0950c compensates for loss of rigidity in the cell wall by

maintaining shorter cells, decreasing the cell surface area exposed to cell wall insults. Another possibility is the upregulation of 4-3 cross-link machinery as Ldt-deletion caused conditional essentiality for carboxypeptidases in *M. smegmatis* (Baranowski et al., 2018).

4.2.3 FDAA incorporation at mid-cell reports on nascent PG of the cell division septum

It is expected that mature side-wall PG should be more rigid than septal PG. Septal PG needs to be rapidly degraded to allow daughter cell separation, whereas side-wall PG must supply a rigid protective barrier around the cell. A novel tetra-peptide fluorescent probe co-localised with the DADA di-peptide at the septum of *M. smegmatis* (Pidgeon et al., 2019) indicating 4-3 cross-linked PG. Individual peptide probes showed either tetra- or penta- probes at the poles and septa (Pidgeon et al., 2019). Meropenem-treated *M. smegmatis* exhibited differential mono-peptide incorporation comparing the poles to the septum due to incomplete septum formation (Botella, Yang, et al., 2017). The inverse manner in which Rv2891-depleted cells remodel polar and septal PG supports growing evidence that the septum and poles are differentially aged. Previously HADA-labelled, old septa, which were not degraded in the absence of the MarP protease, could re-incorporate, overlapping fresh NADA (Botella, Vaubourgeix, et al., 2017). This demonstrates that prevention of septal PG backbone degradation also prevents septal stem-peptide degradation, and that these activities are tightly co-regulated. This builds a hypothesis that Rv2891, required during septum remodelling, should be differentially regulated to Rv0950c. Upregulation of Rv2891 has been observed upon inhibition of FtsZ polymerisation, which in turn inhibits septum formation (Respicio et al., 2008). Changes to Rv0950c expression were not reported under the same conditions (Respicio et al., 2008).

Comparing D-Alanine probe fate between *M. tuberculosis* and *M. smegmatis* has also unmasked the differences in growth and cell-division regulation between the two mycobacterial species (Botella, Vaubourgeix, et al., 2017; García-Heredia et al., 2018), which may be the reason the growth rates of these organisms are drastically different. Septum FDAA incorporation revealed greater heterogeneity in the rate of septum degradation in *M. tuberculosis* compared to *M. smegmatis* (Botella, Vaubourgeix, et al., 2017). *M. tuberculosis* also displayed a greater propensity to incorporate mono-peptide probes at the side-wall than *M, smegmatis* (García-Heredia et al., 2018). This has implications for attempting to replicate cell wall maintenance phenotypes in both

organisms and may be associated with the lack of *M. tuberculosis* dLytM cell division factors present in *M. smegmatis.*

4.3 The relationship between PG remodelling and cell length

The Shy M23-endopepidases of *V. cholerae* enhance tolerance to β-lactamases by changing the shape of the cells (Dörr, Davis & Waldor, 2015). The significant cell-shortening phenotype of *M. tuberculosis* ΔRv0950c suggests an association between cell length maintenance and PG maturation. L,D transpeptidases required for 3-3 cross linkage in *M. smegmatis* are also required for cell shape maintenance (Baranowski et al., 2018). Purified *M. tuberculosis* LDTs exhibit 3-3 cross-link formation *in vitro* (Cordillot et al., 2013). Baranowski et al., (2018) also reported increased bleb formation due to reduced cell wall rigidity in the absence of Ldt-mediated PG maturation. The length of cells in the *M. smegmatis* sextuple mutant, lacking *ldtAEBCGF* was not reported (Baranowski et al., 2018). Remarkably, the Baranowski study also reported cell to cell heterogeneity within the morphological changes brought about by LDT deletion (Baranowski et al., 2018). Further, when D,D endopeptidase activity is lost, less blebbing occurs indicating that PG maturation by 3-3 cross-linkage is necessary for mycobacterial rod shape (Baranowski et al., 2018) and supports the hypothesis that changes to FDAA incorporation in the absence of Rv0950c is associated with PG maturation which maintains cell length.

There is further evidence for a relationship between cell length and PG synthesis and remodeling. *M. smegmatis* FhA interactory protein is required for elongation and a loss of *fhA* leads to cell shortening (Viswanathan et al., 2017). PG biosynthetic PBPa is an interaction partner of *M. smegmatis* FhA (Viswanathan et al., 2017). The *M. tuberculosis* PBP, Rv0050, interacts with the PG hydrolase RipA to regulate PG synthesis and degradation in a manner which maintains *M. tuberculosis* cell length (Gao et al., 2019). Protein kinase A (PknA) phospho-regulates PG synthesis and cell division, and PknA depletion causes cell shortening in *M. tuberculosis* (Nagarajan et al., 2015). Perturbation of FtsQ leads to cell length disregulation in *M. tuberculosis* (Jain et al., 2018). DivIVA, which acts as molecular Velcro by mediating formation of the mycobacterial elongasome complex, is required for rod-shape maintenance of *M. smegmatis* as DivIVA-depleted cells are spherical (Melzer et al., 2018).

Cell shape maintenance is also an important stress response in mycobacteria (Vijay et al., 2017). In a latency model, *M. tuberculosis* exhibited cell shortening and even loss of the cell wall (Velayati et al., 2016) also observed in other mycobacteria (Ramijan et al., 2018). Under stress conditions, metabolism of cell signaling molecules regulated elongation and cell division, thus maintaining cell shape (Gupta et al., 2016). Loss of Rv2891, although playing a role in nascent PG cross-linking, did not alter the cell length of *M. tuberculosis* under axenic conditions. Instead, it is possible that Rv2891 deletion may be more consequential under stress conditions. In transcriptome studies, Rv2891 is upregulated under nutrient-starved conditions or post-forty day stationary phase (Bacon et al., 2014); or steadily upregulated along the course of chronic mouse infection compared to active infection or axenic culture (Talaat et al., 2007). Rv2891 was also expressed at relatively low levels during axenic growth in this study. Alternatively, host-derived reactive nitrogen species caused Rv0950c repression (Ohno et al., 2003). This appears to contradict the observed upregulation of Rv0950c under nutrient-limited stress as well as a study for which Rv0950c expression was unchanged during active mouse infection, and downregulated during immune suppression-induced *M. tuberculosis* reactivation (Talaat et al., 2007). Still, the transcription responses of Rv0950c and Rv2891 did not appear to overlap in this or above-mentioned studies, further delineating differential functions for the *M. tuberculosis* M23 endopeptidases, a common trend in bacteria encoding multiple M23 endopeptidases.

4.4 Functional diversity within the M23-endopeptidase protein family

The M23 endopeptidases represent a highly versatile family of similar structured endopeptidases utilised for multiple facets of PG remodelling. The cell-shape determining M23-endopeptidase homologues of *H. pylori* act with differential cell-wall maintenance capabilities to collectively maintain the overall helical shape of the cells (Sycuro et al., 2010). HPLC analysis revealed the endopeptidases have both overlapping and differential stem-peptide remodelling capabilities (Sycuro et al., 2010). All three endopeptidases were required for 4-3 cross-link relaxation, but Csd1 was associated with additional cross-link degradation at dipeptides (Sycuro et al., 2010). Csd2 was associated with penta-peptide monomer release (Sycuro et al., 2010) while Csd3 is a dual function D,D carboxy and D,D endopeptidase (Bonis, Ecobichon, Guadagnini, Prévost, et al., 2010).

H. influenzae encodes three M23-endopeptidases. YebA, an active PG hydrolase localised to the outer membrane, and NlpD, a degenerate endopeptidase present at the surface of cell division sites, are both required for different aspects of cell separation (Ercoli et al., 2015). *H. influenzae* EnvC has subtle hydrolytic activity but a unique hypothesised role at the periplasm in stabilising outer membrane protein chaperones (Ercoli et al., 2015). EnvC and NlpD, of *E. coli* on the other hand are degenerate endopeptidases required for cell division (Uehara et al., 2010), and YebA is an active D,D endopeptidase collectively required for growth alongside NlpC/p60 endopeptidases (Singh et al., 2012).

In a single organism, differentially-structured or differentially-regulated M23 endopeptidases are utilised as a dynamic tool set for PG remodelling across a spectrum of physiological requirements. This is mirrored in the hypothesised roles of differentially regulated and functional Rv0950c and Rv2891 for PG remodelling during growth and cell division, which potentially act alongside the myriad of multi-family peptidoglycanses required for *M. tuberculosis* cell wall maintenance (Machowski et al., 2014).

4.5 Conclusions and proposed model for Rv0950c and Rv2891 remodelling of *M. tuberculosis* PG

The slow-growing pathogen, *M. tuberculosis*, has persisted throughout the course of human existence until today, likely with the aid of the intricate, complex cell wall. This research explored a previously unknown role for cell wall M23 endopeptidases in remodelling and maintenance of the PG core of the *M. tuberculosis* cell wall, during axenic growth and cell division. Both processes of cell elongation and division require a tightly-regulated interplay between PG biosynthesis and degradation as PG is remodelled along the cell wall. Two M23-endopeptidases of *M. tuberculosis*, Rv2891 and Rv0950c with homology to other M23 and non-M23 Peptidoglycanases were characterised here: Rv2891 plays a subtle role in PG cross-link formation at sites of nascent PG: elongation poles and cell division septum (Fig. 4.1). D,D-endopeptidase activity has been demonstrated by other M23 endopeptidases but have not yet been identified in mycobacteria (Baranowski et al., 2018). Rv2891 may be a novel D,D-endopeptidase, possibly playing an auxiliary role under axenic conditions evident by low axenic transcription levels, and not required for axenic population growth, as opposed to other gene expression studies pointing to an increased requirement for Rv2891 under stressors specific to *M. tuberculosis* pathogenesis. This may explain why Rv2891 is not as well-

conserved in other mycobacteria as Rv0950c. Rv0950c appears to be important for PG maturation at the side-wall (Fig. 4.1). Since L,D transpeptidases are well characterised for 3-3 cross-link formation (Pidgeon et al., 2019), it may be that Rv0950c is a L,D endopeptidase that acts to cleave existing 4-3 cross-links prior to 3-3 cross-link formation for PG maturation. The maturation status of side-wall PG may indirectly regulate the relationship between elongation and cell division since loss of Rv0950c causes cell shortening but no defect in population growth. The observed cell shortening may in turn be a compensatory mechanism for the potential loss of PG rigidity enabled by Rv0950c. The highly conserved nature of Rv0950c highlights the importance of PG remodelling and maturation for mycobacterial survival. The low-relatedness of the *M. tuberculosis* M23 endopeptidases to orthologues of other bacterial families is in line with the unique composition of mycobacterial PG.

In terms of identifying novel drug targets of the *M. tuberculosis* cell wall, a favourable outcome could be assumed to be the identification of genes indispensable for growth. Although Rv0950c and Rv2891 are individually dispensable for axenic growth, this cannot be assumed to be the case under *in vivo* conditions. Collective indispensability also cannot be ruled out based on the work presented here. Furthermore, if *M. tuberculosis* circumvented the loss of Rv0950c to continue growing without increased vulnerability to cell wall damaging agents, it is possible that overwhelming the system with exogenous Rv0950c may not be as easily circumvented, given the instances of conditional Rv0950c downregulation presented in the literature. The manipulation and utilisation of exogenous M23 endopeptidases for treatment is best exemplified in the production of Lysostaphin, a modified, recombinant version of the *S. simulans* LytM hydrolase (Sabala et al., 2012). Not only is PG a unique structure to bacteria but the hypothesised side-wall PG substrate of Rv0950c appears to be highly specific. This raises the possibility of developing a highly specific anti-tubercular hydrolase therapeutic. Many other ideas can be built upon this basic research of two previously conserved hypothetical genes which now appear to be important for PG remodelling. The work presented is of a novel nature, as there are no existing publications focusing on the functional characterisation of *M. tuberculosis* Rv0950c and Rv2891.

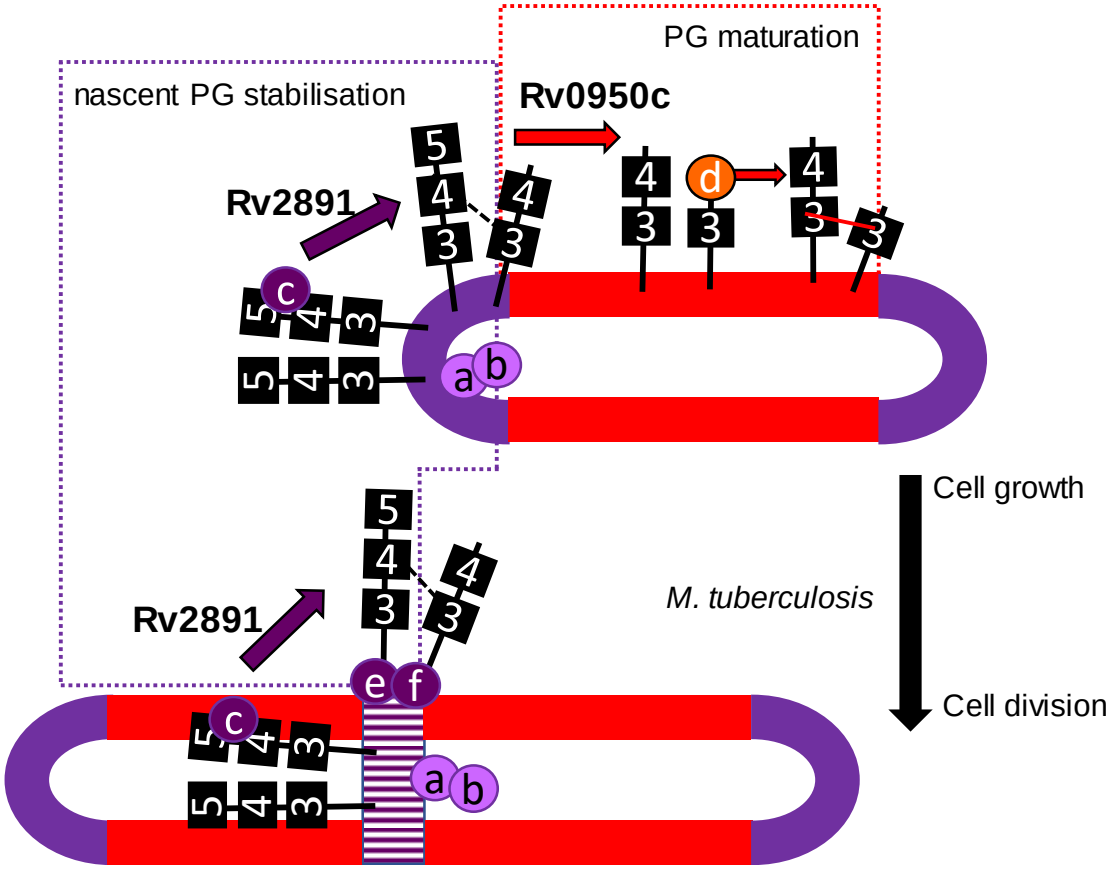

Figure 4.1 Model of hypothetical functions of Rv0950c and Rv2891 in PG remodelling of *M. tuberculosis* (red and purple cylinders) during growth and cell division.
During cell elongation, DivIVA (a) tethers elongasome proteins (b) at the poles where PG biosynthesis takes place inside the cytoplasm. Nascent PG (purple) residues are flipped across the cell membrane uncross-linked. At the poles, D,D carboxypeptidases cleave the terminal D-Alanine to regulate 4-3 cross-link formation to stabilise new PG, in which Rv2891 appears to play a role. A similar process is expected for synthesis of septal PG (hatched, purple), which is later degraded for cell separation by interacting RipA (e) and RpfB (f). Mycobacteria have characteristic 3-3 cross-linked PG, mostly occurring at the side-wall (red) as this consists of aged PG. Rv0950c is hypothesised to have D,D endopeptidase activity which cleaves 4-3 cross-links of nascent PG so that it can mature via 3-3 cross-link formation mediated by L,D transpeptidases (d). Numbers represent amino-acid positions of the PG stem-peptide. Dashed lines: 4-3 cross-links; Red solid line: 3-3 cross-links.

4.6 Limitations

A major limitation to elucidating the activity of Rv0950c and Rv2891 is the lack of HPLC-mass spectrometry data on PG extracted from the *M. tuberculosis* ΔRv0950c and ΔRv2891 cell walls and compared to wild-type to identify substrates and products of hydrolysis. The FDAA probes used here however, have been shown to produce incorporation patterns directly comparable to HPLC data in other studies (Baranowski et al., 2018). Alternative methods to study the hydrolytic activity of Rv0950c via protein expression or heterologous expression were attempted but were unsuccessful.

In addition to the single-cell fluorescence analyses performed here, population level study using flow cytometry might have enhanced analyses, especially in terms of the limited penetration of fluorescence probes in *M. tuberculosis*. Flow cytometry-based assays are also limited, however, as it provides a single fluorescence readout for an entire cell, making it difficult to identify localised signal changes such as that observed for polar acting Rv2891 and side-wall acting Rv0950c. Fluorescence studies would be further enhanced with access to super-resolution microscopy. For example, super resolution microscopy was used to resolve sub-polar, rather than polar, synthesis of PG in *M. smegmatis* (Meniche et al., 2014). This may have also been useful to distinguish true side-wall labelling from background TADA signal, which were classed together here as the "undefined population". Mono-peptide FDAAs can interact with the fixative, glutaraldehyde (Kuru et al., 2015) which was used here for biosafety purposes to view *M. tuberculosis.*

This study mainly focused on Rv0950c characterisation following on from the promising bioinformatics analyses highlighting the highly conserved nature of Rv0950c and the predicted active-site residues conserved in the Rv0950c endopeptidase domain. As a result, there was insufficient time completion of the Rv2891 complement strain. This is needed to confirm that the FDAA incorporation phenotypes are a true reflection of loss of Rv2891. While there are no publications focusing on Rv2891 and Rv0950, the Rv2891 findings of potential cell division involvement did corroborate well with a transcription analysis of septum inhibition (Respicio et al., 2008). In a similar respect, knock-out of the third M23-endopeptidase, Rv3786c and completion of the ΔRv0950c,ΔRv2891 double mutant strain fell outside the scope of this study.

4.7 Recommendations and future perspectives

Two M23-endopeptidases of *M. tuberculosis*, Rv2891 and Rv0950c appear to sequentially remodel PG. Numerous steps can be taken to study the impact of these proteins on mycobacterial physiology. A ΔRv0950c,ΔRv2891 double mutant strain would be useful in ascertaining if these two proteins may serve as a dual drug target against the *M. tuberculosis* cell wall. Targeting 4-3 and 3-3 cross-link formation by treating *M. tuberculosis* with both Amoxicillin and Meropenem enhanced killing (Baranowski et al.,

2018). Characterisation of Rv3786c, which also carries a unique glycosyl transferase might present a complete picture of coupling PG remodelling to overall cell wall maintenance. The available mutants can be phenotyped further *in vivo* in macrophage or mouse infections, to add to previously published transcriptional responses of Rv2891 and Rv0950c under such conditions. It is expected that Rv2891 deletion would lead to more drastic phenotypes than observed under axenic conditions. Similarly, *in vitro* studies can be taken further studying various stress conditions and late stationary phase. Overexpression of Rv0950c under these conditions might be detrimental to the *M. tuberculosis* cell.

Expression and purification of Rv0950c and Rv2891 would be useful both to assay the PG hydrolase activity of these endopeptidases but also to test potential lytic activity of exogenous addition of these proteins as an anti-tubercular therapeutic as with Lysostaphin M23-endopeptidase treatment of *S. aureus* (Sabala et al., 2012). Similarly, HPLC-mass spectrometry analyses should be done on cell wall material extracted from the available mutants to determine substrate and products of hydrolysis.

Localisation of Rv0950c and Rv2891 has not been reported here or in other publications. This would be a useful complement to the proposed differentially localised activity of the sequential acting M23 endopeptidases. In *M. smegmatis*, PBPs required for PG stabilisation localised at sites of nascent PG, while Ldts required for PG maturation localised to the cell wall (Baranowski et al., 2018). Given the proposed model, it is expected that Rv2891 would localise to the poles and septum of *M. tuberculosis* while Rv0950c likely spans the cell. In addition, localisation of cell elongation and cell division machinery can be studied in the available mutants to better understand the elongation rate dynamics causing cell shortening in the absence of Rv0950c or to better elucidate the function of Rv2891 at the poles and septum.

5 References

Abidi, S., Achar, J., Mohamed, M., Neino, A., Bang, D., Benedetti, A., Brode, S., Campbell, J.R., et al. 2019. Standardised shorter regimens versus individualised longer regimens for multidrug-resistant TB. *European Respiratory Journal*. In Press. DOI: 10.1183/13993003.01467-2019.

Ahmad, N., Ahuja, S.D., Akkerman, O.W., Alffenaar, J.W.C., Anderson, L.F., Baghaei, P., Bang, D., Barry, P.M., et al. 2018. Treatment correlates of successful outcomes in pulmonary multidrug-resistant tuberculosis: an individual patient data meta-analysis. *The Lancet*. 392(10150):821–834. DOI: 10.1016/S0140-6736(18)31644-1.

Ahmad Khan, F., Salim, M.A.H., du Cros, P., Casas, E.C., Khamraev, A., Sikhondze, W., Benedetti, A., Bastos, M., et al. 2017. Effectiveness and safety of standardised shorter regimens for multidrug-resistant tuberculosis: individual patient data and aggregate data meta-analyses. *The European respiratory journal*. 50(1). DOI: 10.1183/13993003.00061-2017.

Alix, B., Boubacar, D.A. & Vladimir, M. 2012. T-REX: A web server for inferring, validating and visualizing phylogenetic trees and networks. *Nucleic Acids Research*. 40(W1). DOI: 10.1093/nar/gks485.

Alting-Mees, M.A. & Short, J.M. 1989. pBluescript II: gene mapping vectors. *Nucleic acids research.* 17(22):9494. DOI: 10.1093/nar/17.22.9494.

Altschul, S.F., Gish, W., Miller, W., Myers, E.W. & Lipman, D.J. 1990. Basic local alignment search tool. *Journal of Molecular Biology*. 215(3):403–410. DOI: 10.1016/S0022-2836(05)80360-2.

Ammerman, N.C., Swanson, R. V, Bautista, E.M., Almeida, D. V, Saini, V., Omansen, T.F., Guo, H., Chang, Y.S., et al. 2018. Impact of Clofazimine Dosing on Treatment Shortening of the First-Line Regimen in a Mouse Model of Tuberculosis. *Antimicrobial agents and chemotherapy*. 62(7). DOI: 10.1128/AAC.00636-18.

An, D.R., Kim, H.S., Kim, J., Im, H.N., Yoon, H.J., Yoon, J.Y., Jang, J.Y., Hesek, D., et al. 2015. Structure of Csd3 from *Helicobacter pylori*, a cell shape-determining metallopeptidase. Acta crystallographica. Section D, Biological crystallography. 71(Pt 3):675–686. DOI: 10.1107/S1399004715000152.

An, D.R., Im, H.N., Jang, J.Y., Kim, H.S., Kim, J., Yoon, H.J., Hesek, D., Lee, M., et al. 2016. Structural basis of the heterodimer formation between cell shape-determining proteins Csd1 and Csd2 from *Helicobacter pylori*. *PLoS ONE*. 11(10):1–24. DOI: 10.1371/journal.pone.0164243.

Andreu, N., Zelmer, A., Fletcher, T., Elkington, P.T., Ward, T.H., Ripoll, J., Parish, T., Bancroft, G.J., et al. 2010. Optimisation of bioluminescent reporters for use with mycobacteria. *PLoS ONE*. 5(5). DOI: 10.1371/journal.pone.0010777.

Anthony, K.G., Strych, U., Yeung, K.R., Shoen, C.S., Perez, O., Krause, K.L., Cynamon, M.H., Aristoff, P.A., et al. 2011. New classes of alanine racemase inhibitors identified by high-throughput screening show antimicrobial activity against *Mycobacterium tuberculosis*. *PloS one*. 6(5):e20374. DOI: 10.1371/journal.pone.0020374.

Anuradha, C.M., Mulakayala, C., Babajan, B., Naveen, M., Rajasekhar, C. & Kumar, C.S. 2010. Probing ligand binding modes of *Mycobacterium tuberculosis* MurC ligase by molecular modeling, dynamics simulation and docking. *Journal of Molecular Modeling*. 16(1):77–85. DOI: 10.1007/s00894-009-0521-2.

Arvind, A., Kumar, V., Saravanan, P. & Mohan, C.G. 2012. Homology modeling, molecular dynamics and inhibitor binding study on MurD ligase of *Mycobacterium tuberculosis*. *Interdisciplinary Sciences: Computational Life Sciences*. 4(3):223–238. DOI: 10.1007/s12539-012-0133-x.

Auld, S.C., Shah, N.S., Mathema, B., Brown, T.S., Ismail, N., Omar, S.V., Brust, J.C.M., Nelson, K.N., et al. 2018. Extensively drug-resistant tuberculosis in South Africa: genomic evidence supporting transmission in communities. *The European respiratory journal*. 52(4). DOI: 10.1183/13993003.00246-2018.

Avni, E., Montoya, D., Lopez, D., Modlin, R., Pellegrini, M. & Snir, S. 2018. A phylogenomic study quantifies competing mechanisms for pseudogenization in prokaryotes-*The Mycobacterium leprae* case. *PLoS ONE*. 13(11):1–17. DOI: 10.1371/journal.pone.0204322.

Awasthy, D., Bharath, S., Subbulakshmi, V. & Sharma, U. 2012. Alanine racemase mutants of *Mycobacterium tuberculosis* require D-alanine for growth and are defective for survival in macrophages and mice. *Microbiology*. 158(2):319–327. DOI: 10.1099/mic.0.054064-0.

Babajan, B., Chaitanya, M., Rajsekhar, C., Gowsia, D., Madhusudhana, P., Naveen, M., Chitta, S.K. & Anuradha, C.M. 2011. Comprehensive structural and functional characterization of *Mycobacterium tuberculosis* UDP-NAG enolpyruvyl transferase (Mtb-MurA) and prediction of its accurate binding affinities with inhibitors. *Interdisciplinary Sciences: Computational Life Sciences*. 3(3):204–216. DOI: 10.1007/s12539-011-0100-y.

Bacon, J., Alderwick, L.J., Allnutt, J.A., Gabasova, E., Watson, R., Hatch, K.A., Clark, S.O., Jeeves, R.E., et al. 2014. Non-replicating *Mycobacterium tuberculosis* elicits a reduced infectivity profile with corresponding modifications to the cell wall and extracellular matrix. *PLoS ONE*. 9(2). DOI: 10.1371/journal.pone.0087329.

Bansal, A., Kar, D., Murugan, R.A., Mallick, S., Dutta, M., Pandey, S.D., Chowdhury, C. & Ghosh, A.S. 2015. A putative low-molecular-mass penicillin-binding protein (PBP) of *Mycobacterium smegmatis* exhibits prominent physiological characteristics of dd-carboxypeptidase and beta-lactamase. *Microbiology (United Kingdom)*. 161:1081–1091. DOI: 10.1099/mic.0.000074.

Baranowski, C., Welsh, M.A., Sham, L.T., Eskandarian, H.A., Lim, H.C., Kieser, K.J., Wagner, J.C., McKinney, J.D., et al. 2018. Maturing *Mycobacterium smegmatis* peptidoglycan requires non-canonical crosslinks to maintain shape. *eLife*. 7:1–24. DOI: 10.7554/eLife.37516.

Bardelang, P., Vankemmelbeke, M., Zhang, Y., Jarvis, H., Antoniadou, E., Rochette, S., Thomas, N.R., Penfold, C.N., et al. 2009. Design of a polypeptide FRET substrate that facilitates study of the antimicrobial protease lysostaphin. *Biochemical Journal*. 418(3):615–624. DOI: 10.1042/BJ20081765.

Basavannacharya, C., Robertson, G., Munshi, T., Keep, N.H. & Bhakta, S. 2010. ATP-dependent MurE ligase in *Mycobacterium tuberculosis*: Biochemical and structural characterisation. *Tuberculosis*. 90(1):16–24. DOI: 10.1016/j.tube.2009.10.007.

Bateman, A., Martin, M.J., O'Donovan, C., Magrane, M., Apweiler, R., Alpi, E., Antunes, R., Arganiska, J., et al. 2015. UniProt: A hub for protein information. *Nucleic Acids Research*. 43(D1):D204–D212. DOI: 10.1093/nar/gku989.

Becerra, M.C., Huang, C.C., Lecca, L., Bayona, J., Contreras, C., Calderon, R., Yataco, R., Galea, J., et al. 2019. Transmissibility and potential for disease progression of drug resistant *Mycobacterium tuberculosis*: Prospective cohort study. *The BMJ*. 367(l5894). DOI: 10.1136/bmj.l5894.

Bendtsen, J.D., Nielsen, H., Von Heijne, G. & Brunak, S. 2004. Improved prediction of signal peptides: SignalP 3.0. *Journal of Molecular Biology*. 340(4):783–795. DOI: 10.1016/j.jmb.2004.05.028.

Benson, T.E., Marquardt, J.L., Marquardt, A.C., Etzkorn, F.A. & Walsh, C.T. 1993. Overexpression, purification, and mechanistic study of UDP-N-acetylenolpyruvylglucosamine reductase. *Biochemistry*. 32(8):2024–2030. DOI: 10.1021/bi00059a019.

Van Den Berg, S., Koedijk, D.G.A.M., Back, J.W., Neef, J., Dreisbach, A., Van Dijl, J.M., Bakker-Woudenberg, I.A.J.M. & Buist, G. 2015. Active immunization with an octa-valent *Staphylococcus aureus* antigen mixture in models of *S. aureus* bacteremia and skin infection in mice. *PLoS ONE*. 10(2):1–20. DOI: 10.1371/journal.pone.0116847.

Bernhardt, T.G. & De Boer, P.A.J. 2003. The *Escherichia coli* amidase AmiC is a periplasmic septal ring component exported via the twin-arginine transport pathway. *Molecular Microbiology*. 48(5):1171–1182. DOI: 10.1046/j.1365-2958.2003.03511.x.

Bernhardt, T.G. & De Boer, P.A.J. 2004. Screening for synthetic lethal mutants in *Escherichia coli* and identification of EnvC (YibP) as a periplasmic septal ring factor with murein hydrolase activity. *Molecular Microbiology*. 52(5):1255–1269. DOI: 10.1111/j.1365-2958.2004.04063.x.

Bertoni, M., Kiefer, F., Biasini, M., Bordoli, L. & Schwede, T. 2017. Modeling protein quaternary structure of homo- and hetero-oligomers beyond binary interactions by homology. *Scientific Reports*. 7(1):10480. DOI: 10.1038/s41598-017-09654-8.

Bhamidi, S., Scherman, M.S., Jones, V., Crick, D.C., Belisle, J.T., Brennan, P.J. & McNeil, M.R. 2011. Detailed structural and quantitative analysis reveals the spatial organization of the cell walls of *in vivo* grown *Mycobacterium leprae* and *in vitro* grown *Mycobacterium tuberculosis*. *The Journal of biological chemistry*. 286(26):23168–23177. DOI: 10.1074/jbc.M110.210534.

Bhat, Z.S., Rather, M.A., Maqbool, M., Lah, H.U., Yousuf, S.K. & Ahmad, Z. 2017. Cell wall: A versatile fountain of drug targets in *Mycobacterium tuberculosis*. *Biomedicine and Pharmacotherapy*. 95:1520–1534. DOI: 10.1016/j.biopha.2017.09.036.

Bienert, S., Waterhouse, A., de Beer, T.A.P., Tauriello, G., Studer, G., Bordoli, L. & Schwede, T. 2017. The SWISS-MODEL Repository—new features and functionality. *Nucleic Acids Research*. 45(D1):D313–D319. DOI: 10.1093/nar/gkw1132.

Billones, J.B., Carrillo, M.C.O., Organo, V.G., Macalino, S.J.Y., Sy, J.B.A., Emnacen, I.A., Clavio, N.A.B. & Concepcion, G.P. 2016. Toward antituberculosis drugs: *in silico* screening of synthetic compounds against *Mycobacterium tuberculosis* l,d-transpeptidase 2. *Drug design, development and therapy*. 10:1147–1157. DOI: 10.2147/DDDT.S97043.

Bochtler, M., Odintsov, S.G., Marcyjaniak, M. & Sabała, I. 2004. Similar active sites in lysostaphins and D-Ala-D-Ala metallopeptidases. *Protein Science*. 13(4):854–861. DOI: 10.1110/ps.03515704.

Bonis, M., Ecobichon, C., Guadagnini, S., Prévost, M.C. & Boneca, I.G. 2010. A M23B family metallopeptidase of *Helicobacter pylori* required for cell shape, pole formation and virulence. *Molecular Microbiology*. 78(4):809–819. DOI: 10.1111/j.1365-2958.2010.07383.x.

Botella, H., Yang, G., Ouerfelli, O., Ehrt, S., Nathan, C.F. & Vaubourgeix, J. 2017. Distinct spatiotemporal dynamics of peptidoglycan synthesis between *Mycobacterium smegmatis* and *Mycobacterium tuberculosis*. *mBio*. 8(5):12–14. DOI: 10.1128/mBio.01183-17.

Botella, H., Vaubourgeix, J., Lee, M.H., Song, N., Xu, W., Makinoshima, H., Glickman, M.S. & Ehrt, S. 2017. *Mycobacterium tuberculosis* protease MarP activates a peptidoglycan hydrolase during acid stress. *The EMBO Journal*. 36(4):536–548. DOI: 10.15252/embj.201695028.

Bourai, N., Jacobs, W.R. & Narayanan, S. 2012. Deletion and overexpression studies on DacB2, a putative low molecular mass penicillin binding protein from *Mycobacterium tuberculosis* H 37Rv. *Microbial Pathogenesis*. 52(2):109–116. DOI: 10.1016/j.micpath.2011.11.003.

Boutte, C.C., Baer, C.E., Papavinasasundaram, K., Liu, W., Chase, M.R., Meniche, X., Fortune, S.M., Sassetti, C.M., et al. 2016. A cytoplasmic peptidoglycan amidase homologue controls mycobacterial cell wall synthesis. *eLife*. 5(JUN2016). DOI: 10.7554/eLife.14590.

Brammer Basta, L.A., Ghosh, A., Pan, Y., Jakoncic, J., Lloyd, E.P., Townsend, C.A., Lamichhane, G. & Bianchet, M.A. 2015. Loss of a Functionally and Structurally Distinct ld-Transpeptidase, LdtMt5, Compromises Cell Wall Integrity in *Mycobacterium tuberculosis*. *The Journal of biological chemistry*. 290(42):25670–25685. DOI: 10.1074/jbc.M115.660753.

Brindha, S., Sundaramurthi, J.C., Velmurugan, D., Vincent, S. & Gnanadoss, J.J. 2016. Docking-based virtual screening of known drugs against murE of *Mycobacterium tuberculosis* towards repurposing for TB. *Bioinformation*. 12(8):359–367. DOI: 10.6026/97320630012368.

Campbell, L. Unpublished. 2020.

Chacon, O., Bermudez, L.E., Zinniel, D.K., Chahal, H.K., Fenton, R.J., Feng, Z., Hanford, K., Adams, L.G., et al. 2009. Impairment of D-Alanine biosynthesis in *Mycobacterium smegmatis* determines decreased intracellular survival in human macrophages. *Microbiology*. 155(5):1440–1450. DOI: 10.1099/mic.0.024901-0.

Chowdhury, C., Kar, D., Dutta, M., Kumar, A. & Ghosh, A.S. 2012. Moderate deacylation efficiency of DacD explains its ability to partially restore beta-lactam resistance in *Escherichia coli* PBP5 mutant. *FEMS Microbiology Letters*. 337(1):73–80. DOI: 10.1111/1574-6968.12009.

Colditz, G.A., Brewer, T.F., Berkey, C.S., Wilson, M.E., Burdick, E., Fineberg, H. V & Mosteller, F. 1994. Efficacy of BCG vaccine in the prevention of tuberculosis. Meta-analysis of the published literature. *JAMA*. 271(9):698–702.

Cordillot, M., Dubée, V., Triboulet, S., Dubost, L., Marie, A., Hugonnet, J.E., Arthur, M. & Mainardia, J.L. 2013. *In vitro* cross-linking of *Mycobacterium tuberculosis* peptidoglycan by L,D-transpeptidases and inactivation of these enzymes by carbapenems. *Antimicrobial Agents and Chemotherapy*. 57(12):5940–5945. DOI: 10.1128/AAC.01663-13.

Darrah, P.A., Bolton, D.L., Lackner, A.A., Kaushal, D., Aye, P.P., Mehra, S., Blanchard, J.L., Didier, P.J., et al. 2014. Aerosol Vaccination with AERAS-402 Elicits Robust Cellular Immune Responses in the Lungs of Rhesus Macaques but Fails To Protect against High-Dose *Mycobacterium tuberculosis* Challenge . *The Journal of Immunology*. 193(4):1799–1811. DOI: 10.4049/jimmunol.1400676.

Davids, M., Dheda, K., Pai, N.P., Cogill, D., Pai, M. & Engel, N. 2015. A survey on use of rapid tests and tuberculosis diagnostic practices by primary health care providers in South Africa: Implications for the development of new point-of-care tests. *PLoS ONE*. 10(10). DOI: 10.1371/journal.pone.0141453.

Dawson, R., Diacon, A.H., Everitt, D., van Niekerk, C., Donald, P.R., Burger, D.A., Schall, R., Spigelman, M., et al. 2015. Efficiency and safety of the combination of moxifloxacin, pretomanid (PA-824), and pyrazinamide during the first 8 weeks of antituberculosis treatment: a phase 2b, open-label, partly randomised trial in patients with drug-susceptible or drug-resistant pul. *Lancet (London, England)*. 385(9979):1738–1747. DOI: 10.1016/S0140-6736(14)62002-X.

Deng, L.L., Humphries, D.E., Arbeit, R.D., Carlton, L.E., Smole, S.C. & Carroll, J.D. 2005. Identification of a novel peptidoglycan hydrolase CwlM in *Mycobacterium tuberculosis*. *Biochimica et Biophysica Acta - Proteins and Proteomics*. 1747(1):57–66. DOI: 10.1016/j.bbapap.2004.09.021.

Dheda, K., Shean, K., Zumla, A., Badri, M., Streicher, E.M., Page-Shipp, L., Willcox, P., John, M.-A., et al. 2010. Early treatment outcomes and HIV status of patients with extensively drug-resistant tuberculosis in South Africa: a retrospective cohort study. *Lancet (London, England)*. 375(9728):1798–1807. DOI: 10.1016/S0140-6736(10)60492-8.

Diacon, A.H., Dawson, R., von Groote-Bidlingmaier, F., Symons, G., Venter, A., Donald, P.R., van Niekerk, C., Everitt, D., et al. 2015. Bactericidal activity of pyrazinamide and clofazimine alone and in combinations with pretomanid and bedaquiline. *American journal of respiratory and critical care medicine*. 191(8):943–953. DOI: 10.1164/rccm.201410-1801OC.

Doan, T., Marquis, K.A. & Rudner, D.Z. 2005. Subcellular localization of a sporulation membrane protein is achieved through a network of interactions along and across the septum. *Molecular Microbiology*. 55(6):1767–1781. DOI: 10.1111/j.1365-2958.2005.04501.x.

Dörr, T., Cava, F., Lam, H., Davis, B.M. & Waldor, M.K. 2013. Substrate specificity of an elongation-specific peptidoglycan endopeptidase and its implications for cell wall architecture and growth of *Vibrio cholerae*. *Molecular Microbiology*. 89(5):949–962. DOI: 10.1111/mmi.12323.

Dörr, T., Davis, B.M. & Waldor, M.K. 2015. Endopeptidase-Mediated Beta Lactam Tolerance. *PLoS Pathogens*. 11(4):1–16. DOI: 10.1371/journal.ppat.1004850.

Ealand, C., Rimal, B., Chang, J., Mashigo, L., Chengalroyen, M., Mapela, L., Beukes, G., Machowski, E., et al. 2018. Resuscitation-promoting factors are required for *Mycobacterium smegmatis* biofilm formation. *Applied and Environmental Microbiology*. 84(17). DOI: 10.1128/AEM.00687-18.

Ealand, C.S., Asmal, R., Mashigo, L., Campbell, L. & Kana, B.D. 2019. Characterization of putative DD-carboxypeptidase-encoding genes in *Mycobacterium smegmatis*. *Scientific Reports*. 9(1). DOI: 10.1038/s41598-019-41001-x.

Eddy, S.R. 1998. Profile hidden Markov models. *Bioinformatics*. 14(9):755–763. DOI: 10.1093/bioinformatics/14.9.755.

Emanuelsson, O., Brunak, S., von Heijne, G. & Nielsen, H. 2007. Locating proteins in the cell using TargetP, SignalP and related tools. *Nature Protocols*. 2(4):953–971. DOI: 10.1038/nprot.2007.131.

Eniyan, K., Rani, J., Ramachandran, S., Bhat, R., Khan, I.A. & Bajpai, U. 2020. Screening of Antitubercular Compound Library Identifies Inhibitors of Mur Enzymes in *Mycobacterium tuberculosis*. *SLAS discovery : advancing life sciences R & D*. 25(1):70–78. DOI: 10.1177/2472555219881148.

Ercoli, G., Tani, C., Pezzicoli, A., Vacca, I., Martinelli, M., Pecetta, S., Petracca, R., Rappuoli, R., et al. 2015. Lytm proteins play a crucial role in cell separation, outer membrane composition, and pathogenesis in nontypeable *Haemophilus influenzae*. *mBio*. 6(2):1–10. DOI: 10.1128/mBio.02575-14.

Eschenburg, S., Priestman, M. & Schönbrunn, E. 2005. Evidence that the fosfomycin target Cys115 in UDP-N-acetylglucosamine Enolpyruvyl Transferase (MurA) is essential for product release. *Journal of Biological Chemistry*. 280(5):3757–3763. DOI: 10.1074/jbc.M411325200.

Esposito, M., Szadocka, S., Degiacomi, G., Orena, B.S., Mori, G., Piano, V., Boldrin, F., Zemanová, J., et al. 2017. A Phenotypic Based Target Screening Approach Delivers New Antitubercular CTP Synthetase Inhibitors. *ACS Infectious Diseases*. 3(6):428–437. DOI: 10.1021/acsinfecdis.7b00006.

Falzon, D., Schünemann, H.J., Harausz, E., González-Angulo, L., Lienhardt, C., Jaramillo, E. & Weyer, K. 2017. World Health Organization treatment guidelines for drug-resistant tuberculosis, 2016 update. *European Respiratory Journal*. 49(3). DOI: 10.1183/13993003.02308-2016.

Ferlazzo, G., Mohr, E., Laxmeshwar, C., Hewison, C., Hughes, J., Jonckheere, S., Khachatryan, N., De Avezedo, V., et al. 2018. Early safety and efficacy of the combination of bedaquiline and delamanid for the treatment of patients with drug-resistant tuberculosis in Armenia, India, and South Africa: a retrospective cohort study. *The Lancet Infectious Diseases*. 18(5):536–544. DOI: 10.1016/S1473-3099(18)30100-2.

Fine, P.E.M. 1995. Variation in protection by BCG: implications of and for heterologous immunity. *The Lancet*. 346(8986):1339–1345. DOI: 10.1016/S0140-6736(95)92348-9.

Finn, R.D., Bateman, A., Clements, J., Coggill, P., Eberhardt, R.Y., Eddy, S.R., Heger, A., Hetherington, K., et al. 2014. Pfam: The protein families database. *Nucleic Acids Research*. 42(D1):D222-30. DOI: 10.1093/nar/gkt1223.

Firczuk, M., Mucha, A. & Bochtler, M. 2005. Crystal structures of active LytM. *Journal of Molecular Biology*. 354(3):578–590. DOI: 10.1016/j.jmb.2005.09.082.

Fukushima, T., Kitajima, T., Yamaguchi, H., Ouyang, Q., Furuhata, K., Yamamoto, H., Shida, T. & Sekiguchi, J. 2008. Identification and characterization of novel cell wall hydrolase CwlT: A two-domain autolysin exhibiting N-acetylmuramidase and DL-endopeptidase activities. *Journal of Biological Chemistry*. 283(17):11117–11125. DOI: 10.1074/jbc.M706626200.

Gaiwala Sharma, S.S., Kishore, V. & Raghunand, T.R. 2016. Identification and functional annotation of mycobacterial septum formation genes using cell division mutants of *Escherichia coli*. *Research in Microbiology*. 167(2):142–148. DOI: 10.1016/j.resmic.2015.10.008.

Gao, B., Wang, J., Huang, J., Huang, X., Sha, W. & Qin, L. 2019. The dynamic region of the peptidoglycan synthase gene, Rv0050, induces the growth rate and morphologic heterogeneity in Mycobacteria. *Infection, Genetics and Evolution*. 72(December):86–92. DOI: 10.1016/j.meegid.2018.12.012.

García-Heredia, A., Pohane, A.A., Melzer, E.S., Carr, C.R., Fiolek, T.J., Rundell, S.R., Lim, H.C., Wagner, J.C., et al. 2018. Peptidoglycan precursor synthesis along the sidewall of pole-growing mycobacteria. *eLife*. 7:1–22. DOI: 10.7554/eLife.37243.

Goley, E.D., Comolli, L.R., Fero, K.E., Downing, K.H. & Shapiro, L. 2010. DipM links peptidoglycan remodelling to outer membrane organization in Caulobacter. *Molecular Microbiology*. 77(1):56–73. DOI: 10.1111/j.1365-2958.2010.07222.x.

Gonzalez V Merchand, J.A., Colston, M.J. & Cox, R. 1999. Effects of growth conditions on expression of mycobacterial murA and tyrS genes and contributions of their transcripts to precursor rRNA synthesis. *International Journal of Leprosy and Other Mycobacterial Diseases*. 67(4 SUPPL.):523.

Grace, A.G., Mittal, A., Jain, S., Tripathy, J.P., Satyanarayana, S., Tharyan, P. & Kirubakaran, R. 2019. Shortened treatment regimens versus the standard regimen for drug-sensitive pulmonary tuberculosis. *The Cochrane database of systematic reviews*. 12:CD012918. DOI: 10.1002/14651858.CD012918.pub2.

Grote, A., Hiller, K., Scheer, M., Münch, R., Nörtemann, B., Hempel, D.C. & Jahn, D. 2005. JCat: A novel tool to adapt codon usage of a target gene to its potential expression host. *Nucleic Acids Research*. 33(SUPPL. 2):W526-31. DOI: 10.1093/nar/gki376.

Guex, N. & Peitsch, M.C. 1997. SWISS-MODEL and the Swiss-PdbViewer: an environment for comparative protein modeling. *Electrophoresis*. 18(15):2714–23. DOI: 10.1002/elps.1150181505.

Guex, N., Peitsch, M.C. & Schwede, T. 2009. Automated comparative protein structure modeling with SWISS-MODEL and Swiss-PdbViewer: A historical perspective. *ELECTROPHORESIS*. 30(S1):S162–S173. DOI: 10.1002/elps.200900140.

Guo, X. V., Monteleone, M., Klotzsche, M., Kamionka, A., Hillen, W., Braunstein, M., Ehrt, S. & Schnappinger, D. 2007. Silencing essential protein secretion in *Mycobacterium smegmatis* by using tetracycline repressors. *Journal of Bacteriology*. 189(13):4614–4623. DOI: 10.1128/JB.00216-07.

Gupta, K.R., Baloni, P., Indi, S.S. & Chatterji, D. 2016. Regulation of growth, cell shape, cell division, and gene expression by second messengers (p)ppGpp and cyclic Di-GMP in *Mycobacterium smegmatis*. *Journal of Bacteriology*. 198(9):1414–1422. DOI: 10.1128/JB.00126-16.

Gupta, R., Lavollay, M., Mainardi, J.-L., Arthur, M., Bishai, W.R. & Lamichhane, G. 2010. The *Mycobacterium tuberculosis* protein LdtMt2 is a nonclassical transpeptidase required for virulence and resistance to amoxicillin. *Nature medicine*. 16(4):466–9. DOI: 10.1038/nm.2120.

Gustine, J.N., Au, M.B., Haserick, J.R., Hett, E.C., Rubin, E.J., Gibson, F.C. 3rd & Deng, L.L. 2019. Cell Wall Hydrolytic Enzymes Enhance Antimicrobial Drug Activity Against Mycobacterium. *Current microbiology*. 76(4):398–409. DOI: 10.1007/s00284-018-1620-z.

Halouska, S., Chacon, O., Fenton, R.J., Zinniel, D.K., Raul, G. & Powers, R. 2007. Use of NMR Metabolomics to Analyze the Targets of D-cycloserine in Mycobacteria: Role of D-Alanine Racemase. 6(12):4608–4614. DOI: 10.1021/pr0704332.Use.

Halouska, S., Fenton, R.J., Zinniel, D.K., Marshall, D.D., Powers, R., Barletta, R.G. & Powers, R. 2014. Metabolomics Analysis Identifies D-Alanine D-Alanine Ligase as the Primary Lethal Target of D-Cycloserine in Mycobacteria. *Journal of Proteome Research*. 13:1065–76.

Harausz, E.P., Garcia-Prats, A.J., Law, S., Schaaf, H.S., Kredo, T., Seddon, J.A., Menzies, D., Turkova, A., et al. 2018. Treatment and outcomes in children with multidrug-resistant tuberculosis: A systematic review and individual patient data meta-analysis. *PLoS Medicine*. 15(7):e1002591. DOI: 10.1371/journal.pmed.1002591.

Hatzios, S.K., Baer, C.E., Rustad, T.R., Siegrist, M.S., Pang, J.M., Ortega, C., Alber, T., Grundner, C., et al. 2013. Osmosensory signaling in *Mycobacterium tuberculosis* mediated by a eukaryotic-like Ser/Thr protein kinase. *Proceedings of the National Academy of Sciences of the United States of America*. 110(52):E5069-77. DOI: 10.1073/pnas.1321205110.

He, J., Fu, W., Zhao, S., Zhang, C., Sun, T. & Jiang, T. 2019. Lack of MSMEG_6281, a peptidoglycan amidase, affects cell wall integrity and virulence of *Mycobacterium smegmatis*. *Microbial Pathogenesis*. 128:405–413. DOI: 10.1016/j.micpath.2019.01.013.

Heidrich, C., Templin, M.F., Ursinus, A., Merdanovic, M., Berger, J., Schwarz, H., De Pedro, M.A. & Höltje, J.V. 2001. Involvement of N-acetylmuramyl-L-alanine amidases in cell separation and antibiotic-induced autolysis of *Escherichia coli*. *Molecular Microbiology*. 41(1):167–178. DOI: 10.1046/j.1365-2958.2001.02499.x.

Heidrich, C., Ursinus, A., Berger, J., Schwarz, H. & Höltje, J.V. 2002. Effects of multiple deletions of murein hydrolases on viability, septum cleavage, and sensitivity to large toxic molecules in *Escherichia coli*. *Journal of Bacteriology*. 184(22):6093–6099. DOI: 10.1128/JB.184.22.6093-6099.2002.

Hett, E.C., Chao, M.C., Steyn, A.J., Fortune, S.M., Deng, L.L. & Rubin, E.J. 2007. A partner for the resuscitation-promoting factors of *Mycobacterium tuberculosis*. *Molecular Microbiology*. 66(3):658–668. DOI: 10.1111/j.1365-2958.2007.05945.x.

Hett, E.C., Chao, M.C., Deng, L.L. & Rubin, E.J. 2008. A mycobacterial enzyme essential for cell division synergizes with resuscitation-promoting factor. *PLoS Pathogens*. 4(2). DOI: 10.1371/journal.ppat.1000001.

Hett, E.C., Chao, M.C. & Rubin, E.J. 2010. Interaction and modulation of two antagonistic cell wall enzymes of mycobacteria. *PLoS Pathogens*. 6(7):1–14. DOI: 10.1371/journal.ppat.1001020.

Heunis, J.C., Kigozi, N.G., Chikobvu, P., Botha, S. & Van Rensburg, H.D. 2017. Risk factors for mortality in TB patients: A 10-year electronic record review in a South African province. *BMC Public Health*. 17(38). DOI: 10.1186/s12889-016-3972-2.

Hu, Z., Jiang, W., Gu, L., Qiao, D., Shu, T., Lowrie, D.B., Lu, S.H. & Fan, X.Y. 2019. Heterologous prime-boost vaccination against tuberculosis with recombinant Sendai virus and DNA vaccines. *Journal of Molecular Medicine*. 97:1685–94. DOI: 10.1007/s00109-019-01844-3.

Hughes, J., Reuter, A., Chabalala, B., Isaakidis, P., Cox, H. & Mohr, E. 2019. Adverse events among people on delamanid for rifampicinresistant tuberculosis in a high HIV prevalence setting. *International Journal of Tuberculosis and Lung Disease*. 23(9):1017–1023. DOI: 10.5588/ijtld.18.0651.

Hugonnet, J.-E., Mengin-Lecreulx, D., Monton, A., den Blaauwen, T., Carbonnelle, E., Veckerle, C., Brun, Y. V, van Nieuwenhze, M., et al. 2016. Factors essential for L,D-transpeptidase-mediated peptidoglycan cross-linking and beta-lactam resistance in *Escherichia coli*. *eLife*. 5. DOI: 10.7554/eLife.19469.

Hugonnet, J.E., Haddache, N., Veckerlé, C., Dubost, L., Marie, A., Shikura, N., Mainardi, J.L., Rice, L.B., et al. 2014. Peptidoglycan cross-linking in glycopeptide-resistant Actinomycetales. *Antimicrobial Agents and Chemotherapy*. 58(3):1749–1756. DOI: 10.1128/AAC.02329-13.

Imperial, M.Z., Nahid, P., Phillips, P.P.J., Davies, G.R., Fielding, K., Hanna, D., Hermann, D., Wallis, R.S., et al. 2018. A patient-level pooled analysis of treatment-shortening regimens for drug-susceptible pulmonary tuberculosis. *Nature Medicine*. 24(11):1708–1715. DOI: 10.1038/s41591-018-0224-2.

Ishikawa, S., Hara, Y., Ohnishi, R. & Sekiguchi, J. 1998. Regulation of a new cell wall hydrolase gene, cwlF, which affects cell separation in *Bacillus subtilis*. *Journal of Bacteriology*. 180(9):2549–2555.

Jagielska, E., Chojnacka, O. & Sabała, I. 2016. LytM fusion with SH3b-like domain expands its activity to physiological conditions. *Microbial Drug Resistance*. 22(6):461–469. DOI: 10.1089/mdr.2016.0053.

Jain, P., Malakar, B., Khan, M.Z., Lochab, S., Singh, A. & Nandicoori, V.K. 2018. Delineating FtsQ-mediated regulation of cell division in *Mycobacterium tuberculosis*. *Journal of Biological Chemistry*. 293(32):12331–12349. DOI: 10.1074/jbc.RA118.003628.

Jang, J., Kim, R., Woo, M., Jeong, J., Park, D.E., Kim, G. & Delorme, V. 2017. Efflux attenuates the antibacterial activity of Q203 in *Mycobacterium tuberculosis*. *Antimicrobial Agents and Chemotherapy*. 61(7). DOI: 10.1128/AAC.02637-16.

Johnson, J.L., Hadad, D.J., Dietze, R., Maciel, E.L.N., Sewali, B., Gitta, P., Okwera, A., Mugerwa, R.D., et al. 2009. Shortening treatment in adults with noncavitary tuberculosis and 2-month culture conversion. *American journal of respiratory and critical care medicine*. 180(6):558–563. DOI: 10.1164/rccm.200904-0536OC.

Kalia, N.P., Hasenoehrl, E.J., Rahman, N.B.A., Koh, V.H., Ang, M.L.T., Sajorda, D.R., Hards, K., Grüber, G., et al. 2017. Exploiting the synthetic lethality between terminal respiratory oxidases to kill *Mycobacterium tuberculosis* and clear host infection. *Proceedings of the National Academy of Sciences of the United States of America*. 114(28):7426–7431. DOI: 10.1073/pnas.1706139114.

Kana, B.D., Gordhan, B.G., Downing, K.J., Sung, N., Vostroktunova, G., Machowski, E.E., Tsenova, L., Young, M., et al. 2008. The resuscitation-promoting factors of *Mycobacterium tuberculosis* are required for virulence and resuscitation from dormancy but are collectively dispensable for growth *in vitro*. *Molecular Microbiology*. 67(3):672–684. DOI: 10.1111/j.1365-2958.2007.06078.x.

Kapopoulou, A., Lew, J.M. & Cole, S.T. 2011. The MycoBrowser portal: A comprehensive and manually annotated resource for mycobacterial genomes. *Tuberculosis*. 91(1):8–13. DOI: 10.1016/j.tube.2010.09.006.

Kempker, R.R., Mikiashvili, L., Zhao, Y., Benkeser, D., Barbakadze, K., Bablishvili, N., Avaliani, Z., Peloquin, C.A., et al. 2019. Clinical Outcomes among Patients with Drug-resistant Tuberculosis receiving Bedaquiline or Delamanid Containing Regimens. *Clinical infectious diseases : an official publication of the Infectious Diseases Society of America*. (November). DOI: 10.1093/cid/ciz1107.

Kendall, S.L., Withers, M., Soffair, C.N., Moreland, N.J., Gurcha, S., Sidders, B., Frita, R., Ten Bokum, A., et al. 2007. A highly conserved transcriptional repressor controls a large regulon involved in lipid degradation in *Mycobacterium smegmatis* and *Mycobacterium tuberculosis*. *Molecular Microbiology*. 65(3):684–699. DOI: 10.1111/j.1365-2958.2007.05827.x.

Kerff, F., Petrella, S., Mercier, F., Sauvage, E., Herman, R., Pennartz, A., Zervosen, A., Luxen, A., et al. 2010. Specific Structural Features of the N-Acetylmuramoyl-l-Alanine Amidase AmiD from *Escherichia coli* and Mechanistic Implications for Enzymes of This Family. *Journal of Molecular Biology*. 397(1):249–259. DOI: 10.1016/j.jmb.2009.12.038.

Kiefer, F., Arnold, K., Künzli, M., Bordoli, L. & Schwede, T. 2009. The SWISS-MODEL Repository and associated resources. *Nucleic acids research*. 37(Database issue):D387-92. DOI: 10.1093/nar/gkn750.

Kieser, K.J., Boutte, C.C., Kester, J.C., Baer, C.E., Barczak, A.K., Meniche, X., Chao, M.C., Rego, E.H., et al. 2015. Phosphorylation of the Peptidoglycan Synthase PonA1 Governs the Rate of Polar Elongation in Mycobacteria. *PLoS Pathogens*. 11(6):1–28. DOI: 10.1371/journal.ppat.1005010.

Van Der Kooi-Pol, M.M., De Vogel, C.P., Westerhout-Pluister, G.N., Veenstra-Kyuchukova, Y.K., Duipmans, J.C., Glasner, C., Buist, G., Elsinga, G.S., et al. 2013. High anti-staphylococcal antibody titers in patients with epidermolysis bullosa relate to long-term colonization with alternating types of *Staphylococcus aureus*. *Journal of Investigative Dermatology*. 133(3):847–850. DOI: 10.1038/jid.2012.347.

Kumar, A., Sarkar, S.K., Ghosh, D. & Ghosh, A.S. 2012. Deletion of penicillin-binding protein 1b impairs biofilm formation and motility in *Escherichia coli*. *Research in microbiology*. 163(4):254–257. DOI: 10.1016/j.resmic.2012.01.006.

Kumar, A., Kumar, S., Kumar, D., Mishra, A., Dewangan, R.P., Shrivastava, P., Ramachandran, S. & Taneja, B. 2013. The structure of Rv3717 reveals a novel amidase from *Mycobacterium tuberculosis*. *Acta Crystallographica Section D: Biological Crystallography*. 69(12):2543–2554. DOI: 10.1107/S0907444913026371.

Kumar, V., Saravanan, P., Arvind, A. & Mohan, C.G. 2011. Identification of hotspot regions of MurB oxidoreductase enzyme using homology modeling, molecular dynamics and molecular docking techniques. *Journal of Molecular Modeling*. 17(5):939–953. DOI: 10.1007/s00894-010-0788-3.

Kuru, E., Tekkam, S., Hall, E., Brun, Y. V. & Van Nieuwenhze, M.S. 2015. Synthesis of fluorescent D-amino acids and their use for probing peptidoglycan synthesis and bacterial growth in situ. *Nature Protocols*. 10(1):33–52. DOI: 10.1038/nprot.2014.197.

Lamprecht, D.A., Finin, P.M., Rahman, M.A., Cumming, B.M., Russell, S.L., Jonnala, S.R., Adamson, J.H. & Steyn, A.J.C. 2016. Turning the respiratory flexibility of *Mycobacterium tuberculosis* against itself. *Nature Communications*. 7:12393. DOI: 10.1038/ncomms12393.

Lavollay, M., Arthur, M., Fourgeaud, M., Dubost, L., Marie, A., Veziris, N., Blanot, D., Gutmann, L., et al. 2008. The peptidoglycan of stationary-phase *Mycobacterium tuberculosis* predominantly contains cross-links generated by L,D-transpeptidation. *Journal of Bacteriology*. 190(12):4360–4366. DOI: 10.1128/JB.00239-08.

Lavollay, M., Arthur, M., Fourgeaud, M., Dubost, L., Marie, A., Riegel, P., Gutmann, L. & Mainardi, J.L. 2009. The β-lactam-sensitive D,D-carboxypeptidase activity of Pbp4 controls the L,D and D,D transpeptidation pathways in *Corynebacterium jeikeium*. *Molecular Microbiology*. 74(3):650–661. DOI: 10.1111/j.1365-2958.2009.06887.x.

Lebar, M.D., May, J.M., Meeske, A.J., Leiman, S.A., Lupoli, T.J., Tsukamoto, H., Losick, R., Rudner, D.Z., et al. 2014. Reconstitution of peptidoglycan cross-linking leads to improved fluorescent probes of cell wall synthesis. *Journal of the American Chemical Society*. 136(31):10874–10877. DOI: 10.1021/ja505668f.

Lechat, P., Hummel, L., Rousseau, S. & Moszer, I. 2008. GenoList: an integrated environment for comparative analysis of microbial genomes. *Nucleic acids research*. 36(Database issue):D469-74. DOI: 10.1093/nar/gkm1042.

Lee, Y., Mootien, S., Shoen, C., Destefano, M., Cirillo, P., Asojo, O.A., Yeung, K.R., Ledizet, M., et al. 2013. Inhibition of mycobacterial alanine racemase activity and growth by thiadiazolidinones. *Biochemical Pharmacology*. 86(2):222–230. DOI: 10.1016/j.bcp.2013.05.004.

Lenz, J.D., Stohl, E.A., Robertson, R.M., Hackett, K.T., Fisher, K., Xiong, K., Lee, M., Hesek, D., et al. 2016. Amidase activity of AmiC controls cell separation and stem peptide release and is enhanced by NlpD in *Neisseria gonorrhoeae*. *Journal of Biological Chemistry*. 291(20):10916–10933. DOI: 10.1074/jbc.M116.715573.

Li, G., Li, F., Zhao, H.M., Wen, H.L., Li, H.C., Li, C.L., Ji, P., Xu, P., et al. 2017. Evaluation of a new IFN-γ release assay for rapid diagnosis of active tuberculosis in a high-incidence setting. *Frontiers in Cellular and Infection Microbiology*. 7(APR). DOI: 10.3389/fcimb.2017.00117.

Li, Y., Mortuza, R., Milligan, D.L., Tran, S.L., Strych, U., Cook, G.M. & Krause, K.L. 2014. Investigation of the essentiality of glutamate racemase in *Mycobacterium smegmatis*. *Journal of Bacteriology*. 196(24):4239–4244. DOI: 10.1128/JB.02090-14.

Liechti, G.W., Kuru, E., Hall, E., Kalinda, A., Brun, Y. V., Vannieuwenhze, M. & Maurelli, A.T. 2014. A new metabolic cell-wall labelling method reveals peptidoglycan in *Chlamydia trachomatis*. *Nature*. 506(7489):507–510. DOI: 10.1038/nature12892.

Liew, Y.K., Hamat, R.A., Belkum, A. Van, Chong, P.P. & Neela, V. 2015. Comparative exoproteomics and host inflammatory response in *Staphylococcus aureus* skin and soft tissue infections, bacteremia, and subclinical colonization. *Clinical and Vaccine Immunology*. 22(5):593–603. DOI: 10.1128/CVI.00493-14.

Lioliou, E., Fechter, P., Caldelari, I., Jester, B.C., Dubrac, S., Helfer, A.C., Boisset, S., Vandenesch, F., et al. 2016. Various checkpoints prevent the synthesis of *Staphylococcus aureus* peptidoglycan hydrolase LytM in the stationary growth phase. *RNA Biology*. 13(4):427–440. DOI: 10.1080/15476286.2016.1153209.

Lukoye, D., Ssengooba, W., Musisi, K., Kasule, G.W., Cobelens, F.G.J., Joloba, M. & Gomez, G.B. 2015. Variation and risk factors of drug resistant tuberculosis in sub-Saharan Africa: A systematic review and meta-analysis. *BMC Public Health*. 15(1). DOI: 10.1186/s12889-015-1614-8.

Machowski, E.E., Senzani, S., Ealand, C. & Kana, B.D. 2014. Comparative genomics for mycobacterial peptidoglycan remodelling enzymes reveals extensive genetic multiplicity. *BMC Microbiology*. 14(1):1–12. DOI: 10.1186/1471-2180-14-75.

Mahapatra, S., Crick, D.C., McNeil, M.R. & Brennan, P.J. 2008. Unique structural features of the peptidoglycan of *Mycobacterium leprae*. *Journal of bacteriology*. 190(2):655–661. DOI: 10.1128/JB.00982-07.

Mahomed, S., Dlamini-Mvelase, N.R., Dlamini, M. & Mlisana, K. 2017. Failure of BACTEC ™ MGIT 960 ™ to detect *Mycobacterium tuberculosis* complex within a 42-day incubation period. *African Journal of Laboratory Medicine*. 6(1):2010–2012. DOI: 10.4102/ajlm.v6i1.537.

Mangtani, P., Abubakar, I., Ariti, C., Beynon, R., Pimpin, L., Fine, P.E.M., Rodrigues, L.C., Smith, P.G., et al. 2014. Protection by BCG vaccine against tuberculosis: a systematic review of randomized controlled trials. *Clinical infectious diseases : an official publication of the Infectious Diseases Society of America*. 58(4):470–480. DOI: 10.1093/cid/cit790.

Manjaly Thomas, Z.-R., Satti, I., Marshall, J.L., Harris, S.A., Lopez Ramon, R., Hamidi, A., Minhinnick, A., Riste, M., et al. 2019. Alternate aerosol and systemic immunisation with a recombinant viral vector for tuberculosis, MVA85A: A phase I randomised controlled trial. *PLoS medicine*. 16(4):e1002790. DOI: 10.1371/journal.pmed.1002790.

Van Der Meeren, O., Hatherill, M., Nduba, V., Wilkinson, R.J., Muyoyeta, M., Van Brakel, E., Ayles, H.M., Henostroza, G., et al. 2018. Phase 2b controlled trial of M72/AS01E vaccine to prevent tuberculosis. *New England Journal of Medicine*. 379(17):1621–1634. DOI: 10.1056/NEJMoa1803484.

Meisner, J. & Moran, C.P. 2011. A LytM domain dictates the localization of proteins to the mother cell-forespore interface during bacterial endospore formation. *Journal of Bacteriology*. 193(3):591–598. DOI: 10.1128/JB.01270-10.

Meisner, J., Maehigashi, T., André, I., Dunham, C.M. & Moran, C.P. 2012. Structure of the basal components of a bacterial transporter. *Proceedings of the National Academy of Sciences of the United States of America*. 109(14):5446–5451. DOI: 10.1073/pnas.1120113109.

Melzer, E.S., Sein, C.E., Chambers, J.J. & Sloan Siegrist, M. 2018. DivIVA concentrates mycobacterial cell envelope assembly for initiation and stabilization of polar growth. *Cytoskeleton*. 75(12):498–507. DOI: 10.1002/cm.21490.

Meniche, X., Otten, R., Siegrist, M.S., Baer, C.E., Murphy, K.C., Bertozzi, C.R. & Sassetti, C.M. 2014. Subpolar addition of new cell wall is directed by DivIVA in mycobacteria. *Proceedings of the National Academy of Sciences of the United States of America*. 111(31). DOI: 10.1073/pnas.1402158111.

Milligan, D.L., Tran, S.L., Strych, U., Cook, G.M. & Krause, K.L. 2007. The alanine racemase of *Mycobacterium smegmatis* is essential for growth in the absence of D-alanine. *Journal of Bacteriology*. 189(22):8381–8386. DOI: 10.1128/JB.01201-07.

Minasov, G., Shuvalova, L., Pshenychnyi, S., Satchell, K.J.F. & Joachimiak, A. 2018. 1.93 Angstrom Resolution Crystal Structure of Peptidase M23 from *Neisseria gonorrhoeae*. Unpublished.

Mohr, E., Hughes, J., Reuter, A., Duran, L.T., Ferlazzo, G., Daniels, J., De Azevedo, V., Kock, Y., et al. 2018. Delamanid for rifampicin-resistant tuberculosis: A retrospective study from South Africa. *European Respiratory Journal*. 51(6):1–11. DOI: 10.1183/13993003.00017-2018.

Möll, A., Dörr, T., Alvarez, L., Chao, M.C., Davis, B.M., Cava, F. & Waldor, M.K. 2014. Cell separation in *Vibrio cholerae* is mediated by a single amidase whose action is modulated by two nonredundant activators. *Journal of Bacteriology*. 196(22):3937–3948. DOI: 10.1128/JB.02094-14.

Moraes, G.L., Gomes, G.C., Monteiro De Sousa, P.R., Alves, C.N., Govender, T., Kruger, H.G., Maguire, G.E.M., Lamichhane, G., et al. 2015. Structural and functional features of enzymes of *Mycobacterium tuberculosis* peptidoglycan biosynthesis as targets for drug development. *Tuberculosis*. 95(2):95–111. DOI: 10.1016/j.tube.2015.01.006.

Morayya, S., Awasthy, D., Yadav, R., Ambady, A. & Sharma, U. 2015. Revisiting the essentiality of glutamate racemase in *Mycobacterium tuberculosis*. *Gene*. 555(2):269–276. DOI: 10.1016/j.gene.2014.11.017.

Morè, N., Martorana, A.M., Biboy, J., Otten, C., Winkle, M., Serrano, C.K.G., Montón Silva, A., Atkinson, L., et al. 2019. Peptidoglycan remodeling enables *Escherichia coli* to survive severe outer membrane assembly defect. *mBio*. DOI: 10.1128/mBio.02729-18.

Mori, G., Chiarelli, L.R., Esposito, M., Makarov, V., Bellinzoni, M., Hartkoorn, R.C., Degiacomi, G., Boldrin, F., et al. 2015. Thiophenecarboxamide Derivatives Activated by EthA Kill *Mycobacterium tuberculosis* by Inhibiting the CTP Synthetase PyrG. *Chemistry & biology*. 22(7):917–27. DOI: 10.1016/j.chembiol.2015.05.016.

Mukamolova, G. V., Murzin, A.G., Salina, E.G., Demina, G.R., Kell, D.B., Kaprelyants, A.S. & Young, M. 2006. Muralytic activity of *Micrococcus luteus* Rpf and its relationship to physiological activity in promoting bacterial growth and resuscitation. *Molecular Microbiology*. 59(1):84–98. DOI: 10.1111/j.1365-2958.2005.04930.x.

Munshi, T., Gupta, A., Evangelopoulos, D., Guzman, J.D., Gibbons, S., Keep, N.H. & Bhakta, S. 2013. Characterisation of ATP-Dependent Mur Ligases Involved in the Biogenesis of Cell Wall Peptidoglycan in *Mycobacterium tuberculosis*. *PLoS ONE*. 8(3):1–12. DOI: 10.1371/journal.pone.0060143.

Murphy, S.G., Alvarez, L., Adams, M.C., Liu, S., Chappie, J.S., Cava, F. & Dörra, T. 2019. Endopeptidase regulation as a novel function of the zur-dependent zinc starvation response. *mBio*. 10(1):1–15. DOI: 10.1128/mBio.02620-18.

Nagarajan, S.N., Upadhyay, S., Chawla, Y., Khan, S., Naz, S., Subramanian, J., Gandotra, S. & Nandicoori, V.K. 2015. Protein Kinase a (PknA) of *Mycobacterium tuberculosis* is independently activated and is critical for growth *in vitro* and survival of the pathogen in the host. *Journal of Biological Chemistry*. 290(15):9626–9645. DOI: 10.1074/jbc.M114.611822.

Nelson, D.E. & Young, K.D. 2000. Penicillin binding protein 5 affects cell diameter, contour, and morphology of *Escherichia coli*. *Journal of bacteriology*. 182(6):1714–21. DOI: 10.1128/jb.182.6.1714-1721.2000.

Nelson, D.E. & Young, K.D. 2001. Contributions of PBP 5 and DD-carboxypeptidase penicillin binding proteins to maintenance of cell shape in *Escherichia coli*. *Journal of Bacteriology*. 183(10):3055–3064. DOI: 10.1128/JB.183.10.3055-3064.2001.

Nemes, E., Geldenhuys, H., Rozot, V., Rutkowski, K.T., Ratangee, F., Bilek, N., Mabwe, S., Makhethe, L., et al. 2018. Prevention of *M. tuberculosis* infection with H4:IC31 vaccine or BCG revaccination. *New England Journal of Medicine*. 379(2):138–149. DOI: 10.1056/NEJMoa1714021.

Nkurunziza, J., Karstaedt, A.S., Louw, R. & Padanilam, X. 2018. Treatment outcomes of pre- and extensively drug-resistant tuberculosis in Johannesburg , South Africa. 22(March):1469–1474.

Odintsov, S.G., Sabala, I., Marcyjaniak, M. & Bochtler, M. 2004. Latent LytM at 1.3 Å resolution. *Journal of Molecular Biology*. 335(3):775–785. DOI: 10.1016/j.jmb.2003.11.009.

Ohno, H., Zhu, G., Mohan, V.P., Chu, D., Kohno, S., Jacobs, W.R. & Chan, J. 2003. The effects of reactive nitrogen intermediates on gene expression in *Mycobacterium tuberculosis*. *Cellular Microbiology*. 5(9):637–648. DOI: 10.1046/j.1462-5822.2003.00307.x.

Olayanju, O., Esmail, A., Limberis, J. & Dheda, K. 2019. A regimen containing bedaquiline and delamanid compared to bedaquiline in patients with drug resistant tuberculosis. *The European respiratory journal*. In press. DOI: 10.1183/13993003.01181-2019.

Osipovitch, D.C. & Griswold, K.E. 2015. Fusion with a Cell Wall Binding Domain Renders Autolysin LytM a Potent Anti-*Staphylococcus aureus* Agent. *FEMS microbiology letters*. 362(2):1–7. DOI: 10.1093/femsle/fnu035.

Osman, K., Evangelopoulos, D., Basavannacharya, C., Gupta, A., McHugh, T.D., Bhakta, S. & Gibbons, S. 2012. An antibacterial from Hypericum acmosepalum inhibits ATP-dependent MurE ligase from *Mycobacterium tuberculosis*. *International Journal of Antimicrobial Agents*. 39(2):124–129. DOI: 10.1016/j.ijantimicag.2011.09.018.

Pandey, S.D., Pal, S., N, G.K., Bansal, A., Mallick, S. & Ghosh, A.S. 2018. Two DD-carboxypeptidases from *Mycobacterium smegmatis* affect cell surface properties through regulation of peptidoglycan cross-linking and glycopeptidolipids. *Journal of Bacteriology*. 200(14). DOI: 10.1128/JB.00760-17.

Parish, T. & Stoker, N.G. 2000. Use of a flexible cassette method to generate a double unmarked *Mycobacterium tuberculosis* tlyA plcABC mutant by gene replacement. *Microbiology*. 146:1969–1975. DOI: 10.1099/00221287-146-8-1969.

Park, S.W., Tasneen, R., Converse, P.J. & Nuermberger, E.L. 2017. Immunodeficiency and intermittent dosing promote acquired rifamycin monoresistance in murine tuberculosis. *Antimicrobial Agents and Chemotherapy*. 61(11). DOI: 10.1128/AAC.01502-17.

Pawar, A., Jha, P., Konwar, C., Chaudhry, U., Chopra, M. & Saluja, D. 2019. Ethambutol targets the glutamate racemase of *Mycobacterium tuberculosis*-an enzyme involved in peptidoglycan biosynthesis. *Applied microbiology and biotechnology*. 103(2):843–851. DOI: 10.1007/s00253-018-9518-z.

Peng, H., Hu, Q., Shang, W., Yuan, J., Zhang, X., Liu, H., Zheng, Y., Hu, Z., et al. 2017. WalK(S221P), a naturally occurring mutation, confers vancomycin resistance in VISA strain XN108. *Journal of Antimicrobial Chemotherapy*. 72(4):1006–1013. DOI: 10.1093/jac/dkw518.

Peters, N.T., Dinh, T. & Bernhardt, T.G. 2011. A Fail-safe mechanism in the septal ring assembly pathway generated by the sequential recruitment of cell separation amidases and their activators. *Journal of Bacteriology*. 193(18):4973–4983. DOI: 10.1128/JB.00316-11.

Peters, N.T., Morlot, C., Yang, D.C., Uehara, T., Vernet, T. & Bernhardt, T.G. 2013. Structure-function analysis of the LytM domain of EnvC, an activator of cell wall remodeling at the *Escherichia coli* division site. 89(4):690–701. DOI: 10.1111/mmi.12304.

Peters Kannan, S., Rao, V.A., Biboy, J., Vollmer, D., Erickson, S.W., Lewis, R.J., Young, K.D. & Vollmer, W., K. 2016. The Redundancy of Peptidoglycan Carboxypeptidases Ensures Robust Cell Shape Maintenance in *Escherichia coli*. *mBIO*. 7(3):e00819-16. DOI: 10.1128/mBio.00819-16.Editor.

Peterson, M.L., Gandhi, N.R., Clennon, J., Nelson, K.N., Morris, N., Ismail, N., Allana, S., Campbell, A., et al. 2019. Extensively drug-resistant tuberculosis "hotspots" and sociodemographic associations in Durban, South Africa. *The international journal of tuberculosis and lung disease : the official journal of the International Union against Tuberculosis and Lung Disease*. 23(6):720–727. DOI: 10.5588/ijtld.18.0575.

Pethe, K., Bifani, P., Jang, J., Kang, S., Park, S., Ahn, S., Jiricek, J., Jung, J., et al. 2013. Discovery of Q203, a potent clinical candidate for the treatment of tuberculosis. *Nature Medicine*. 19(9):1157–1160. DOI: 10.1038/nm.3262.

Pham, T.T., Jacobs-Sera, D., Pedulla, M.L., Hendrix, R.W. & Hatfull, G.F. 2007. Comparative genomic analysis of mycobacteriophage Tweety: Evolutionary insights and construction of compatible site-specific integration vectors for mycobacteria. *Microbiology*. 153(8):2711–2723. DOI: 10.1099/mic.0.2007/008904-0.

Picconi, P., Jeeves, R., Moon, C.W., Jamshidi, S., Nahar, K.S., Laws, M., Bacon, J. & Rahman, K.M. 2019. Noncytotoxic Pyrrolobenzodiazepine-Ciprofloxacin Conjugate with Activity against *Mycobacterium tuberculosis*. *ACS Omega*. 4(25):20873–20881. DOI: 10.1021/acsomega.9b00834.

Pidgeon, S.E., Apostolos, A.J., Nelson, J.M., Shaku, M., Rimal, B., Islam, M.N., Crick, D.C., Kim, S.J., et al. 2019. L,D-Transpeptidase Specific Probe Reveals Spatial Activity of Peptidoglycan Cross-Linking. *ACS Chemical Biology*. (September, 16). DOI: 10.1021/acschembio.9b00427.

Pietersen, E., Ignatius, E., Streicher, E.M., Mastrapa, B., Padanilam, X., Pooran, A., Badri, M., Lesosky, M., et al. 2014. Long-term outcomes of patients with extensively drug-resistant tuberculosis in South Africa: a cohort study. *Lancet (London, England)*. 383(9924):1230–1239. DOI: 10.1016/S0140-6736(13)62675-6.

Polsfuss, S., Hofmann-Thiel, S., Merker, M., Krieger, D., Niemann, S., Rüssmann, H., Schönfeld, N., Hoffmann, H., et al. 2019. Emergence of Low-level Delamanid and Bedaquiline Resistance during Extremely Drug-resistant Tuberculosis Treatment. *Clinical Infectious Diseases*. 69(7):1229–1231. DOI: 10.1093/cid/ciz074.

Pontali, E., Sotgiu, G., Tiberi, S., Tadolini, M., Visca, D., D'Ambrosio, L., Centis, R., Spanevello, A., et al. 2018. Combined treatment of drug-resistant tuberculosis with bedaquiline and delamanid: A systematic review. *European Respiratory Journal*. 52(1). DOI: 10.1183/13993003.00934-2018.

Poupel, O., Proux, C., Jagla, B., Msadek, T. & Dubrac, S. 2018. *SpdC, a novel virulence factor, controls histidine kinase activity in Staphylococcus aureus*. V. 14. DOI: 10.1371/journal.ppat.1006917.

Prasanna, A.N. & Mehra, S. 2013. Comparative Phylogenomics of Pathogenic and Non-Pathogenic Mycobacterium. *PLoS ONE*. 8(8). DOI: 10.1371/journal.pone.0071248.

Prigozhin, D.M., Mavrici, D., Huizar, J.P., Vansell, H.J. & Alber, T. 2013. Structural and Biochemical Analyses of *Mycobacterium tuberculosis* N-Acetylmuramyl-L-alanine Amidase Rv3717 Point to a Role in Peptidoglycan Fragment Recycling. *Journal of Biological Chemistry*. 288(44):31549–31555. DOI: 10.1074/jbc.M113.510792.

Priyadarshini, R., De Pedro, M.A. & Young, K.D. 2007. Role of peptidoglycan amidases in the development and morphology of the division septum in *Escherichia coli*. *Journal of Bacteriology*. 189(14):5334–5347. DOI: 10.1128/JB.00415-07.

Ragumani, S., Kumaran, D., Burley, S.K. & Subramanyam, S. 2008. Crystal structure of a putative lysostaphin peptidase from *Vibrio cholerae*. *Proteins*. 72(3):1096–1103. DOI: 10.1002/prot.22095.

Rahman, K.M., Jackson, P.J.M., James, C.H., Basu, B.P., Hartley, J.A., de la Fuente, M., Schatzlein, A., Robson, M., et al. 2013. GC-targeted C8-linked pyrrolobenzodiazepine-biaryl conjugates with femtomolar *in vitro* cytotoxicity and *in vivo* antitumor activity in mouse models. *Journal of medicinal chemistry*. 56(7):2911–35. DOI: 10.1021/jm301882a.

Ramijan, K., Ultee, E., Willemse, J., Zhang, Z., Wondergem, J.A.J., van der Meij, A., Heinrich, D., Briegel, A., et al. 2018. Stress-induced formation of cell wall-deficient cells in filamentous actinomycetes. *Nature Communications*. 9(1). DOI: 10.1038/s41467-018-07560-9.

Randich, A.M. & Brun, Y. V. 2015. Molecular mechanisms for the evolution of bacterial morphologies and growth modes. *Frontiers in Microbiology*. 6:e580. DOI: 10.3389/fmicb.2015.00580.

Raulinaitis, V., Tossavainen, H., Aitio, O., Juuti, J.T., Hiramatsu, K., Kontinen, V. & Permi, P. 2017. Identification and structural characterization of LytU, a unique peptidoglycan endopeptidase from the lysostaphin family. *Scientific Reports*. 7(1):1–14. DOI: 10.1038/s41598-017-06135-w.

Den Reijer, P.M., Haisma, E.M., Lemmens-Den Toom, N.A., Willemse, J., Koning, R.A., Demmers, J.A.A., Dekkers, D.H.W., Rijkers, E., et al. 2016. Detection of alpha-toxin and other virulence factors in biofilms of *Staphylococcus aureus* on polystyrene and a human epidermalmodel. *PLoS ONE*. 11(1):1–19. DOI: 10.1371/journal.pone.0145722.

Respicio, L., Nair, P.A., Huang, Q., Anil, B., Tracz, S., Truglio, J.J., Kisker, C., Raleigh, D.P., et al. 2008. Characterizing septum inhibition in *Mycobacterium tuberculosis* for novel drug discovery. *Tuberculosis*. 88(5):420–429. DOI: 10.1016/j.tube.2008.03.001.

Rivera, I., Molina, R., Lee, M., Mobashery, S. & Hermoso, J.A. 2016. Orthologous and paralogous AmpD peptidoglycan amidases from gram-negative bacteria. In *Microbial Drug Resistance*. V. 22. Mary Ann Liebert Inc. 470–476. DOI: 10.1089/mdr.2016.0083.

Rocaboy, M., Herman, R., Sauvage, E., Remaut, H., Moonens, K., Terrak, M., Charlier, P. & Kerff, F. 2013. The crystal structure of the cell division amidase amic reveals the fold of the AMIN domain, a new peptidoglycan binding domain. *Molecular Microbiology*. 90(2):267–277. DOI: 10.1111/mmi.12361.

Rodriguez-Rivera, F.P., Zhou, X., Theriot, J.A. & Bertozzi, C.R. 2018. Acute Modulation of Mycobacterial Cell Envelope Biogenesis by Front-Line Tuberculosis Drugs. *Angewandte Chemie (International ed. in English)*. 57(19):5267–5272. DOI: 10.1002/anie.201712020.

Sabala, I., Jonsson, I.M., Tarkowski, A. & Bochtler, M. 2012. Anti-staphylococcal activities of lysostaphin and LytM catalytic domain. *BMC Microbiology*. 12. DOI: 10.1186/1471-2180-12-97.

Sabala, I., Jagielska, E., Bardelang, P.T., Czapinska, H., Dahms, S.O., Sharpe, J.A., James, R., Than, M.E., et al. 2014. Crystal structure of the antimicrobial peptidase lysostaphin from Staphylococcus simulans. *The FEBS journal*. 281(18):4112–4122. DOI: 10.1111/febs.12929.

Sarkar, S., Libby, E.A., Pidgeon, S.E., Dworkin, J. & Pires, M.M. 2016. *In vivo* Probe of Lipid II-Interacting Proteins. *Angewandte Chemie (International ed. in English)*. 55(29):8401–4. DOI: 10.1002/anie.201603441.

Schneider, C.Z., Parish, T., Basso, L.A. & Santos, D.S. 2008. The two chorismate mutases from both *Mycobacterium tuberculosis* and *Mycobacterium smegmatis*: Biochemical analysis and limited regulation of promoter activity by aromatic amino acids. *Journal of Bacteriology*. 190(1):122–134. DOI: 10.1128/JB.01332-07.

Schoonmaker, M.K., Bishai, W.R. & Lamichhane, G. 2014. Nonclassical transpeptidases of *Mycobacterium tuberculosis* alter cell size, morphology, the cytosolic matrix, protein localization, virulence, and resistance to beta-lactams. *Journal of bacteriology*. 196(7):1394–1402. DOI: 10.1128/JB.01396-13.

Senzani, S., Li, D., Bhaskar, A., Ealand, C., Chang, J., Rimal, B., Liu, C., Joon Kim, S., et al. 2017. An Amidase-3 domain-containing N-acetylmuramyl-L-alanine amidase is required for mycobacterial cell division. *Scientific Reports*. 7(1). DOI: 10.1038/s41598-017-01184-7.

Seung, K.J., Khan, P., Franke, M.F., Ahmed, S., Aiylchiev, S., Alam, M., Putri, F.A., Bastard, M., et al. (in press). Culture conversion at six months in patients receiving delamanid-containing regimens for the treatment of multidrug-resistant tuberculosis. *Clinical Infectious Diseases*. ciz1084:ahead-of-print. DOI: 10.1093/cid/ciz1084.

Shaku, M.T. Unpublished 2017.

Shaku, M.T. & Kana, B.D. 2018. Breaking down walls. *eLife*. 7. DOI: 10.7554/eLife.42033.

Sharma, A., Hill, A., Kurbatova, E., van der Walt, M., Kvasnovsky, C., Tupasi, T.E., Caoili, J.C., Gler, M.T., et al. 2017. Estimating the future burden of multidrug-resistant and extensively drug-resistant tuberculosis in India, the Philippines, Russia, and South Africa: a mathematical modelling study. *The Lancet. Infectious diseases*. 17(7):707–715. DOI: 10.1016/S1473-3099(17)30247-5.

Shean, K., Streicher, E., Pieterson, E., Symons, G., van Zyl Smit, R., Theron, G., Lehloenya, R., Padanilam, X., et al. 2013. Drug-associated adverse events and their relationship with outcomes in patients receiving treatment for extensively drug-resistant tuberculosis in South Africa. *PloS one*. 8(5):e63057. DOI: 10.1371/journal.pone.0063057.

Sheehan, S., Harris, S.A., Satti, I., Hokey, D.A., Dheenadhayalan, V., Stockdale, L., Manjaly Thomas, Z.R., Minhinnick, A., et al. 2015. A phase I, open-label trial, evaluating the safety and immunogenicity of candidate tuberculosis vaccines AERAS-402 and MVA85A, administered by prime-boost regime in BCG-vaccinated healthy adults. *PLoS ONE*. 10(11). DOI: 10.1371/journal.pone.0141687.

Shieh, P., Siegrist, M.S., Cullen, A.J. & Bertozzi, C.R. 2014. Imaging bacterial peptidoglycan with near-infrared fluorogenic azide probes. *Proceedings of the National Academy of Sciences of the United States of America*. 111(15):5456–5461. DOI: 10.1073/pnas.1322727111.

Shin, J.-H., Sulpizio, A.G., Kelley, A., Alvarez, L., Murphy, S.G., Fan, L., Cava, F., Mao, Y., et al. (in press). Structural basis of peptidoglycan endopeptidase regulation. *Proceedings of the National Academy of Sciences*. 117(21):11692 LP – 11702. DOI: 10.1073/pnas.2001661117.

Siegrist, M.S., Whiteside, S., Jewett, J.C., Aditham, A., Cava, F. & Bertozzi, C.R. 2013. (D)-Amino acid chemical reporters reveal peptidoglycan dynamics of an intracellular pathogen. *ACS chemical biology*. 8(3):500–505. DOI: 10.1021/cb3004995.

Sievers, F., Wilm, A., Dineen, D., Gibson, T.J., Karplus, K., Li, W., Lopez, R., McWilliam, H., et al. 2011. Fast, scalable generation of high-quality protein multiple sequence alignments using Clustal Omega. *Molecular Systems Biology*. 7. DOI: 10.1038/msb.2011.75.

Singh, A., Mai, D., Kumar, A. & Steyn, A.J.C. 2006. Dissecting virulence pathways of *Mycobacterium tuberculosis* through protein-protein association. *Proceedings of the National Academy of Sciences of the United States of America*. 103(30):11346–11351. DOI: 10.1073/pnas.0602817103.

Singh, S.K., Saisree, L., Amrutha, R.N. & Reddy, M. 2012. Three redundant murein endopeptidases catalyse an essential cleavage step in peptidoglycan synthesis of *Escherichia coli* K12. *Molecular Microbiology*. 86(5):1036–1051. DOI: 10.1111/mmi.12058.

De Smet, K.A.L., Kempsell, K.E., Gallagher, A., Duncan, K. & Young, D.B. 1999. Alteration of a single amino acid residue reverses fosfomycin resistance of recombinant MurA from *Mycobacterium tuberculosis*. *Microbiology*. 145(11):3177–3184. DOI: 10.1099/00221287-145-11-3177.

Stohl, E.A., Chan, Y.A., Hackett, K.T., Kohler, P.L., Dillard, J.P. & Seifert, H.S. 2012. *Neisseria gonorrhoeae* virulence factor NG1686 is a bifunctional M23B family metallopeptidase that influences resistance to hydrogen peroxide and colony morphology. *Journal of Biological Chemistry*. 287(14):11222–11233. DOI: 10.1074/jbc.M111.338830.

Stohl, E.A., Dale, E.M., Criss, A.K. & Seifert, H.S. 2013. *Neisseria gonorrhoeae* Metalloprotease NGO1686 Is Required for Full Piliation, and Piliation Is Required for Resistance to H_2O_2 and Neutrophil-Mediated Killing. *mBio*. 4(4):00399–13. DOI: 10.1128/mBio.00399-13.

Stohl, E.A., Lenz, J.D., Dillard, J.P. & Seifert, H.S. 2016. The gonococcal NlpD protein facilitates cell separation by activating peptidoglycan cleavage by AmiC. *Journal of Bacteriology*. 198(4):615–622. DOI: 10.1128/JB.00540-15.

Studer, G., Rempfer, C., Waterhouse, A.M., Gumienny, R., Haas, J. & Schwede, T. 2020. QMEANDisCo—distance constraints applied on model quality estimation. *Bioinformatics*. 36(6):1765–1771. DOI: 10.1093/bioinformatics/btz828.

Sudiarta, I.P., Fukushima, T. & Sekiguchi, J. 2010. *Bacillus subtilis* CwlP of the Sp-β prophage has two novel peptidoglycan hydrolase domains, muramidase and cross-linkage digesting DD-endopeptidase. *Journal of Biological Chemistry*. 285(53):41232–41243. DOI: 10.1074/jbc.M110.156273.

Sycuro, L.K., Pincus, Z., Gutierrez, K.D., Biboy, J., Stern, C.A., Vollmer, W. & Salama, N.R. 2010. Peptidoglycan crosslinking relaxation promotes *Helicobacter pylori*'s helical shape and stomach colonization. *Cell*. 141(5):822–833. DOI: 10.1016/j.cell.2010.03.046.

Tait, D.R., Hatherill, M., Van Der Meeren, O., Ginsberg, A.M., Van Brakel, E., Salaun, B., Scriba, T.J., Akite, E.J., et al. 2019. Final Analysis of a Trial of M72/AS01 E Vaccine to Prevent Tuberculosis . *New England Journal of Medicine*. (October, 28). DOI: 10.1056/nejmoa1909953.

Talaat, A.M., Ward, S.K., Wu, C.W., Rondon, E., Tavano, C., Bannantine, J.P., Lyons, R. & Johnston, S.A. 2007. Mycobacterial bacilli are metabolically active during chronic tuberculosis in murine lungs: Insights from genome-wide transcriptional profiling. *Journal of Bacteriology*. 189(11):4265–4274. DOI: 10.1128/JB.00011-07.

Tameris, M., Geldenhuys, H., Luabeya, A.K.K., Smit, E., Hughes, J.E., Vermaak, S., Hanekom, W.A., Hatherill, M., et al. 2014. The candidate TB vaccine, MVA85A, induces highly durable Th1 responses. *PLoS ONE*. 9(2). DOI: 10.1371/journal.pone.0087340.

Telkov, M. V., Demina, G.R., Voloshin, S.A., Salina, E.G., Dudik, T. V., Stekhanova, T.N., Mukamolova, G. V., Kazaryan, K.A., et al. 2006. Proteins of the Rpf (resuscitation promoting factor) family are peptidoglycan hydrolases. *Biochemistry (Moscow)*. 71(4):414–422. DOI: 10.1134/S0006297906040092.

Tidhar, A., Flashner, Y., Cohen, S., Levi, Y., Zauberman, A., Gur, D., Aftalion, M., Elhanany, E., et al. 2009. The NIpD lipoprotein is a novel *Yersinia pestis* virulence factor essential for the development of plague. *PLoS ONE*. 4(9). DOI: 10.1371/journal.pone.0007023.

Tidhar, A., Levy, Y., Zauberman, A., Vagima, Y., Gur, D., Aftalion, M., Israeli, O., Chitlaru, T., et al. 2019. Disruption of the NlpD lipoprotein of the plague pathogen *Yersinia pestis* affects iron acquisition and the activity of the twin-arginine translocation system. *PLoS neglected tropical diseases*. 13(6):e0007449. DOI: 10.1371/journal.pntd.0007449.

Tiwari, K.B., Gatto, C., Walker, S. & Wilkinson, B.J. 2018. Exposure of *Staphylococcus aureus* to targocil blocks translocation of the major autolysin atl across the membrane, resulting in a significant decrease in autolysis. *Antimicrobial Agents and Chemotherapy*. 62(7):1–10. DOI: 10.1128/AAC.00323-18.

Tsang, M.J., Yakhnina, A.A. & Bernhardt, T.G. 2017. NlpD links cell wall remodeling and outer membrane invagination during cytokinesis in *Escherichia coli*. *PLoS Genetics*. 13(7). DOI: 10.1371/journal.pgen.1006888.

Tuckman, D., Donnelly, R.J., Zhao, F.X., Jacobs, W.R. & Connell, N.D. 1997. Interruption of the phosphoglucose isomerase gene results in glucose auxotrophy in *Mycobacterium smegmatis*. *Journal of Bacteriology*. 179(8):2724–2730. DOI: 10.1128/jb.179.8.2724-2730.1997.

Tufariello, J.A.M., Jacobs, W.R. & Chan, J. 2004. Individual *Mycobacterium tuberculosis* Resuscitation-Promoting Factor Homologues Are Dispensable for Growth *In vitro* and *In vivo*. *Infection and Immunity*. 72(1):515–526. DOI: 10.1128/IAI.72.1.515-526.2004.

Turapov, O., Forti, F., Kadhim, B., Ghisotti, D., Sassine, J., Straatman-Iwanowska, A., Bottrill, A.R., Moynihan, P.J., et al. 2018. Two Faces of CwlM, an Essential PknB Substrate, in *Mycobacterium tuberculosis*. *Cell Reports*. 25(1):57-67.e5. DOI: 10.1016/j.celrep.2018.09.004.

Tweed, C.D., Dawson, R., Burger, D.A., Conradie, A., Crook, A.M., Mendel, C.M., Conradie, F., Diacon, A.H., et al. 2019. Bedaquiline, moxifloxacin, pretomanid, and pyrazinamide during the first 8 weeks of treatment of patients with drug-susceptible or drug-resistant pulmonary tuberculosis: a multicentre, open-label, partially randomised, phase 2b trial. *The Lancet. Respiratory medicine*. 7(12):1048–1058. DOI: 10.1016/S2213-2600(19)30366-2.

Uehara, T. & Park, J.T. 2007. An anhydro-N-acetylmuramyl-L-alanine amidase with broad specificity tethered to the outer membrane of *Escherichia coli*. *Journal of Bacteriology*. 189(15):5634–5641. DOI: 10.1128/JB.00446-07.

Uehara, T., Dinh, T. & Bernhardt, T.G. 2009. LytM-domain factors are required for daughter cell separation and rapid ampicillin-induced lysis in *Escherichia coli*. *Journal of Bacteriology*. 191(16):5094–5107. DOI: 10.1128/JB.00505-09.

Uehara, T., Parzych, K.R., Dinh, T. & Bernhardt, T.G. 2010. Daughter cell separation is controlled by cytokinetic ring-activated cell wall hydrolysis. *EMBO Journal*. 29(8):1412–1422. DOI: 10.1038/emboj.2010.36.

Velayati, A.A., Abeel, T., Shea, T., Konstantinovich Zhavnerko, G., Birren, B., Cassell, G.H., Earl, A.M., Hoffner, S., et al. 2016. Populations of latent *Mycobacterium tuberculosis* lack a cell wall: Isolation, visualization, and whole-genome characterization. *International Journal of Mycobacteriology*. 5(1):66–73. DOI: 10.1016/j.ijmyco.2015.12.001.

Verreck, F.A.W., Vervenne, R.A.W., Kondova, I., van Kralingen, K.W., Remarque, E.J., Braskamp, G., van der Werff, N.M., Kersbergen, A., et al. 2009. MVA.85A boosting of BCG and an attenuated, phoP deficient *M. tuberculosis* vaccine both show protective efficacy against tuberculosis in rhesus macaques. *PloS one*. 4(4):e5264. DOI: 10.1371/journal.pone.0005264.

Vijay, S., Vinh, D.N., Hai, H.T., Ha, V.T.N., Dung, V.T.M., Dinh, T.D., Nhung, H.N., Tram, T.T.B., et al. 2017. Influence of stress and antibiotic resistance on cell-length distribution in *Mycobacterium tuberculosis* clinical isolates. *Frontiers in Microbiology*. 8(NOV):1–12. DOI: 10.3389/fmicb.2017.02296.

Vissa, V.D. & Brennan, P.J. 2001. The genome of *Mycobacterium leprae*: A minimal mycobacterial gene set. *Genome Biology*. 2(8):1–8.

Viswanathan, G., Yadav, S., Joshi, S. V. & Raghunand, T.R. 2017. Insights into the function of FhaA, a cell division-associated protein in mycobacteria. *FEMS Microbiology Letters*. 364(2):1–9. DOI: 10.1093/femsle/fnw294.

Waterhouse, A., Bertoni, M., Bienert, S., Studer, G., Tauriello, G., Gumienny, R., Heer, F.T., de Beer, T.A.P., et al. 2018. SWISS-MODEL: homology modelling of protein structures and complexes. *Nucleic Acids Research*. 46(W1):W296–W303. DOI: 10.1093/nar/gky427.

White, A.D., Sibley, L., Dennis, M.J., Gooch, K., Betts, G., Edwards, N., Reyes-Sandoval, A., Carroll, M.W., et al. 2013. Evaluation of the safety and immunogenicity of a candidate tuberculosis vaccine, MVA85A, delivered by aerosol to the lungs of macaques. *Clinical and vaccine immunology : CVI*. 20(5):663–672. DOI: 10.1128/CVI.00690-12.

WHO. 2018a. *Global Health TB Report*. DOI: ISBN 978-92-4-156564-6.

WHO. 2018b. BCG vaccine: WHO position paper, February 2018 - Recommendations. *Vaccine*. 36(24):3408–3410. DOI: 10.1016/j.vaccine.2018.03.009.

WHO. 2019. *Global Tuberculosis report 2019*. Geneva: World Health Organization. DOI: ISBN 978-92-4-156571-4.

Wu, J.A., Kusuma, C., Mond, J.J. & Kokai-Kun, J.F. 2003. Lysostaphin Disrupts *Staphylococcus aureus* and *Staphylococcus epidermidis* Biofilms on Artificial Surfaces. *Antimicrobial Agents and Chemotherapy*. 47(11):3407–3414. DOI: 10.1128/AAC.47.11.3407–3414.2003.

Wu, K.J., Boutte, C.C., Ioerger, T.R. & Rubin, E.J. 2019. *Mycobacterium smegmatis* HtrA Blocks the Toxic Activity of a Putative Cell Wall Amidase. *Cell Reports*. 27(8):2468-2479.e3. DOI: 10.1016/j.celrep.2018.12.063.

Xu, L., Wu, D., Liu, L., Zheng, Q., Song, Y., Ye, L., Sha, S., Kang, J., et al. 2014. Characterization of mycobacterial UDP-N-acetylglucosamine enolpyruvyle transferase (MurA). *Research in Microbiology*. 165(2):91–101. DOI: 10.1016/j.resmic.2014.01.004.

Yamada, H., Yamaguchi, M., Igarashi, Y., Chikamatsu, K., Aono, A., Murase, Y., Morishige, Y., Takaki, A., et al. 2018. *Mycolicibacterium smegmatis*, Basonym *Mycobacterium smegmatis*, Expresses Morphological Phenotypes Much More Similar to *Escherichia coli* Than *Mycobacterium tuberculosis* in Quantitative Structome Analysis and CryoTEM Examination. *Frontiers in Microbiology*. 9(SEP). DOI: 10.3389/fmicb.2018.01992.

Yang, D.C., Peters, N.T., Parzych, K.R., Uehara, T., Markovski, M. & Bernhardt, T.G. 2011. An ATP-binding cassette transporter-like complex governs cell-wall hydrolysis at the bacterial cytokinetic ring. *Proceedings of the National Academy of Sciences of the United States of America*. 108(45). DOI: 10.1073/pnas.1107780108.

Yuen, C.M., Kurbatova, E. V, Tupasi, T., Caoili, J.C., Van Der Walt, M., Kvasnovsky, C., Yagui, M., Bayona, J., et al. 2015. Association between Regimen Composition and Treatment Response in Patients with Multidrug-Resistant Tuberculosis: A Prospective Cohort Study. *PLoS Medicine*. 12(12). DOI: 10.1371/journal.pmed.1001932.

Zauberman, A., Vagima, Y., Tidhar, A., Aftalion, M., Gur, D., Rotem, S., Chitlaru, T., Levy, Y., et al. 2017. Host iron nutritional immunity induced by a live *Yersinia pestis* vaccine strain is associated with immediate protection against plague. *Frontiers in Cellular and Infection Microbiology*. 7(JUN):1–12. DOI: 10.3389/fcimb.2017.00277.

Zhang, W., Li, S., Ma, L., Ding, W. & Xu, Y. 2019. Identification of a novel carboxypeptidase encoded by Rv3627c that plays a potential role in mycobacteria morphology and cell division. *Enzyme and microbial technology*. 126:32–40. DOI: 10.1016/j.enzmictec.2019.03.003.

Appendix A: Supplementary information pertaining to Materials and Methods.

A1 Composition of media, solutions and buffers

A1.1 Media

Middlebrook 7H9 (BD) (4.7 g/l) Ammonium Sulphate (0.5 g), L-glutamic acid (0.5 g), Sodium Citrate (0.1 g), Pyridoxine (1 mg), Biotin (0.5 mg), Disodium Phosphate (2.5 g), Monopotassium Phosphate (1 g), Ferric Ammonium Citrate (40 mg), Magnesium Sulphate (50 mg), Calcium Chloride (0.5 mg), Zinc Sulphate (1 mg), Copper Sulphate (1 mg).

BBL 7H11 Agar (BD) (19 g/l) Pancreatic Digest of Casein (1 g), Monopotassium Phosphate (1.5 g), Disodium Phosphate (1.5 g), Monosodium Glutamate (0.5 g), Ammonium Sulphate (0.5 g), Sodium Citrate (0.4 g), Ferric Ammonium Citrate (40 mg), Magnesium Sulphate (50 mg), Zinc Sulphate (1 mg), Copper Sulphate (1 mg), Pyridoxine (1 mg), Agar (13.5 g), Biotin (0.5 mg), Calcium Chloride (0.5 mg), Malachite Green (0.25 mg).

Middlebrook 7H10 Agar (BD) (19 g/l) Ammonium Sulphate (0.5 g), Monopotassium Phosphate (1.5 g), Disodium Phosphate (1.5 g), Sodium Citrate (0.4 g), Magnesium Sulphate (25 mg), Calcium Chloride (0.5 mg), Zinc Sulphate (1 mg), Copper Sulphate (1 mg), L-glutamic acid (0.5 g), Ferric Ammonium Citrate (40 mg), Pyridoxine hydrochloride (1 mg), Agar (15 g), Biotin (0.5 mg), Malachite Green (0.25 mg).

25% Tween-80 Tween-80 (Sigma) (12.5 ml), dH_2O (37.5 ml) heated and mixed. Filter sterilised.

100X Glucose Salts Glucose (Sigma) (20 g), NaCl (Merck) (8.5 g), dH_2O (100 ml). Autoclaved.

Luria Bertani (LB) Tryptone (Merck) (10 g), Yeast Extract (Sigma) (5 g), NaCl (Merck) (10 g), dH_2O (1 l). Autoclaved.

Luria Bertani Agar (LA) Tryptone (Merck) (10 g), Yeast Extract (Sigma) (5 g), NaCl (Merck) (5 g), Agar (Sigma) (15 g) dH_2O (1 l). Autoclaved.

2% X-Gal X-Gal (Melford) (0.5 g), deionised Dimethyl Formamide (25 ml). Stored at -20°C

2XTY Tryptone (Merck) (20 g), Yeast Extract (Sigma) (10 g), NaCl (Merck) (10 g), dH_2O (1 l). Autoclaved.

Sauton's minimal media Ferric Ammonium Citrate (Sigma) (0.05 g), Asparagine (Sigma) (4 g), Magnesium Sulphate (Sigma) (0.5 g), Citric Acid (Merck) (2 g), Potassium Dihydrogen OrthoPhosphate (AnalaR) (0.5 g), Glycerol (Sigma) (60 ml), 1% Zinc Sulphate (0.1 ml), dH_2O (800 ml – 1l) pH to 7.2 with ammonia. Autoclaved.

A1.2 DNA isolation solutions

10X Tris-EDTA (TE) 1M Tris-HCl (5 ml), 0.5M EDTA (1 ml), dH_2O (44 ml). Autoclaved.

1M Tris-HCl Tris-HCl (12.1 g), dH_2O (80-100 ml), pH to 8.0 with concentrated HCl. Autoclaved.

0.5M EDTA EDTA (Merck) (46.5 g), dH_2O (200-250 ml), pH to 8.0 with NaOH. Autoclaved.

10% Sodium Dodecyl Sulphate (SDS) SDS (Merck) (10 g), dH_2O (100 ml).

5M NaCl NaCl (Merck) (29.22 g), dH_2O (100 ml). Dissolved before autoclaving.

CTAB/NaCl NaCl (Merck) (0.41 g), dH_2O (8-10 ml), CTAB (Merck) (1 g). Heat to dissolve. Filter Sterilise.

Solution I 1 M Tris-HCl (2.5 ml), 0.5M EDTA (0.5 ml), 0.5M Glucose (10 ml), dH_2O (87 ml). Autoclave. Stored at 4°C.

0.5M Glucose Glucose (Sigma) (9.01 g), dH_2O (100 ml). Autoclave.

Solution II 10% SDS (1 ml), 10M NaOH (200 µl), dH_2O (9.88 ml). Prepared for immediate use.

10M NaOH NaOH (Merck) (40 g), dH_2O (100 ml).

Solution III 5M Potassium acetate (60 ml), Glacial Acetic Acid (Sigma) (11.5 ml), dH_2O (28.5 ml).
5M Potassium Acetate Potassium Acetate (Melford) (29.5 g), dH_2O (60 ml). Autoclave.

3M Sodium Acetate Sodium Acetate (Sigma) (102.25 g), dH_2O (150-250 ml). pH to 5.2 with Glacial Acetic Acid.

A1.3 Transformation and Electroporation

100 mM $CaCl_2$ $CaCl_2$ (Merck) (1.47 g), dH_2O (100 ml). Autoclave.
30% Glycine Glycine (Sigma) (30 g), dH_2O (100 ml). Autoclave.

10% Glycerol Glycerol (Sigma) (100 ml), dH_2O (1 l). Autoclave. Store at 4°C.

A1.4 DNA electrophoresis

1% agarose gel Agarose (Lonza) (0.35 g), 1X TAE (35 ml), heat dissolved. 10 mg/ml EtBr (Sigma) (1.5 µl).

50X TAE Tris (Melford) (242 g), Glacial Acetic Acid (Sigma) (57.1 ml), 0.5M EDTA (100 ml), dH_2O (842.9 ml).

6X Loading Dye Bromophenol Blue (Sigma) (40 mg), Glycerol (Sigma) (4.5 ml), dH_2O (10.5 ml). Filter sterilised.

A1.5 Southern Blotting

Depurination solution 0.25M HCl.

Denaturation solution 0.5M NaOH, 1.5M NaCl.

Solution 1 20X SSC (10 ml), 10% SDS (1 ml)
20X SSC TriSodium Citrate (Sigma) (88.2 g), NaCl (175.3 g), dH_2O (0.9-1 l), pH to 7 with NaOH or HCl. Autoclave.
Solution 2 20X SSC (2.5 ml), 10% SDS (1 ml)

Wash buffer 1X Maleic Acid buffer (130 ml), Tween-20 (Sigma) (390 µl).
10X Maleic Acid buffer 1M Maleic Acid (Sigma), 1.5M NaCl.
Blocking buffer 1X Maleic Acid buffer (67.5 ml), 1X Blocking Solution (Roche) (7.5 ml).

Detection buffer 1M $MgCl_2$ (Sigma) (1.25 ml), 1M Tris-HCl (2.5 ml), 5M NaCl (5 ml), dH_2O (16.25 ml).
1M $MgCl_2$ $MgCl_2$ (Sigma) (20.3 g), dH_2O (100 ml). Autoclave.

A1.6 Protein Electrophoresis and Western Blotting

Running buffer Tris (Melford) (303 g), Glycine (Sigma) (144 g), SDS (Merck) (10g), dH_2O (1 l).

Coomasie Blue Stain Coomasie Blue (Sigma) (1 g), Methanol (Kemikal) (500 ml), Glacial Acetic Acid (Sigma) (100 ml), dH_2O (400 ml).

Destain Methanol (Kemikal) (400 ml), Glacial Acetic Acid (Sigma) (100 ml), dH_2O (500 ml).

Transfer buffer Tris (Melford) (6 g), Glycine (Sigma) (28.8 g), SDS (Merck) (2 g), Methanol (Kemical) (400 ml), dH_2O (1600 ml).

TBST 1X TBS, 0.1% Tween20, dH_2O.
10X TBS pH 7.6 Tris (Melford) (24.2 g), NaCl (Merck) (80 g), dH_2O (1 l).
Blocking buffer 5% Nonfat Dry Milk (Cell Signal), 1X TBST.

A2 Restriction maps of plasmid backbones

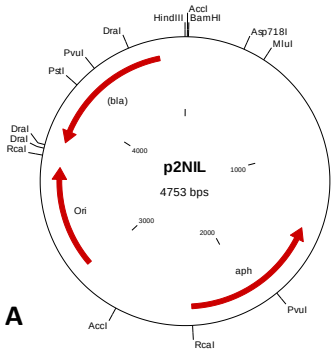

A

Enzyme	Expected fragment (bp)
***Acc*I**	2741, 2012
***BspH*I (*Rca*I)**	3388, 1365
***Dra*I**	4042, 692, 19
***Mlu*I**	4735
***Pvu*I**	2384, 2369

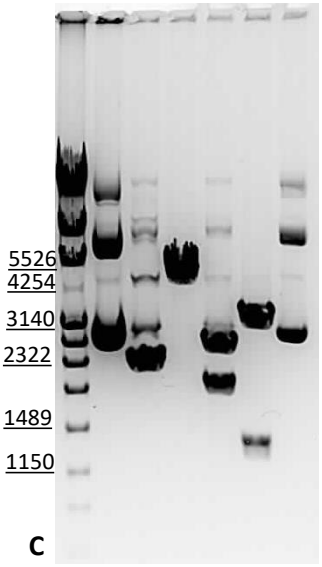

C

Figure A2.1 Restriction map of p2Nil.
A) Vector map. B) Expected fragment sizes. C) 1) MWM IV, 2) uncut, 3) *Pvu*I, 4) *Mlu*I, 5) *Acc*I, 6) *BspH*I, 7) *Dra*I.

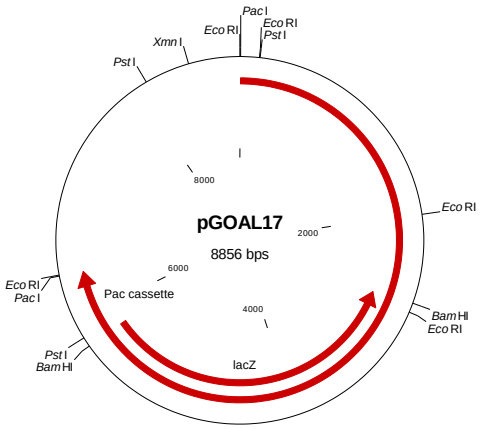

A

Enzyme	Expected fragment (bp)
***BamH*I**	5784, 3072
***EcoR*I + *Pac*I**	3590, 2482, 1864, 766, 140, 10, 4
***Pst*I**	5697, 2251, 908
***Xmn*I**	8856

B

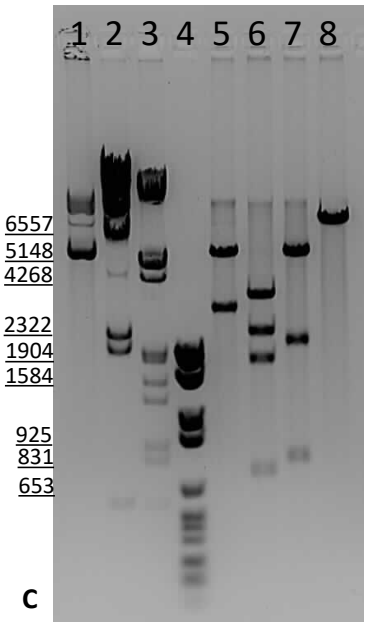

C

Figure A2.2 Restriction map of pGOAL17
A) Vector map. B) Expected fragment sizes. C) 1) uncut, 2) MWM II, 3) MWM III 4) MWM IV 5) *BamH*I, 6) *EcoR*I and *Pac*I, 7) *Pst*I, 8) *Xmn*I.

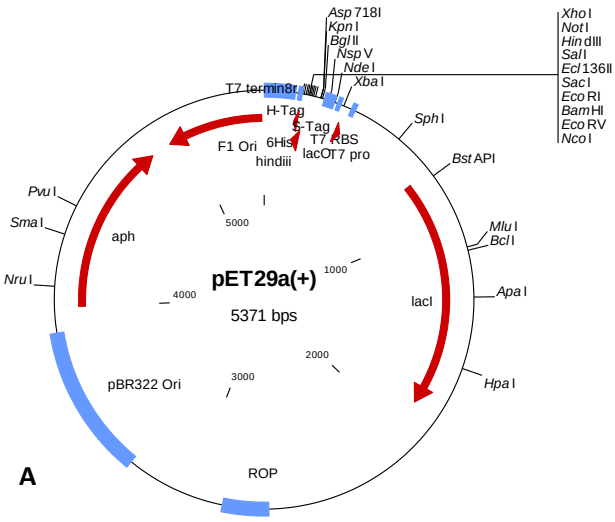

Restriction enzyme	Expected fragments (bp)
*Xho*I	5371
*Xmn*I	3338, 2033
*BspH*I	3423, 1073, 875
*Mlu*I	5371
*Nde*I	5371

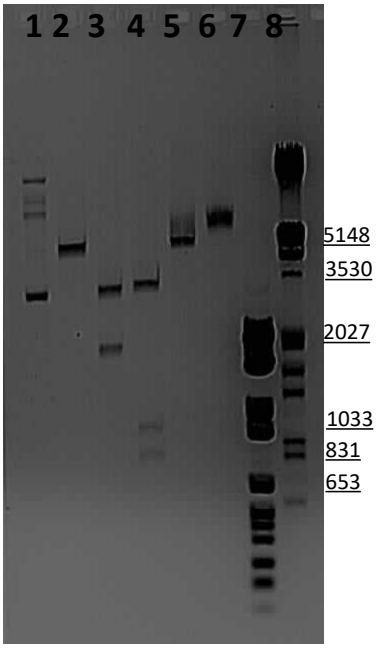

Figure A2.3 Restriction mapping of pET29a His-Tag expression vector
A) Vector map. B) Expected fragments of restriction mapping. C) Restriction digestion fragments obtained: 1) undigested 2) *Xho*I; 3) *Xmn*I; 4) *BspH*I; 5) *Mlu*I; 6) *Nde*I; 7) MWM VI; 8) MWM III.

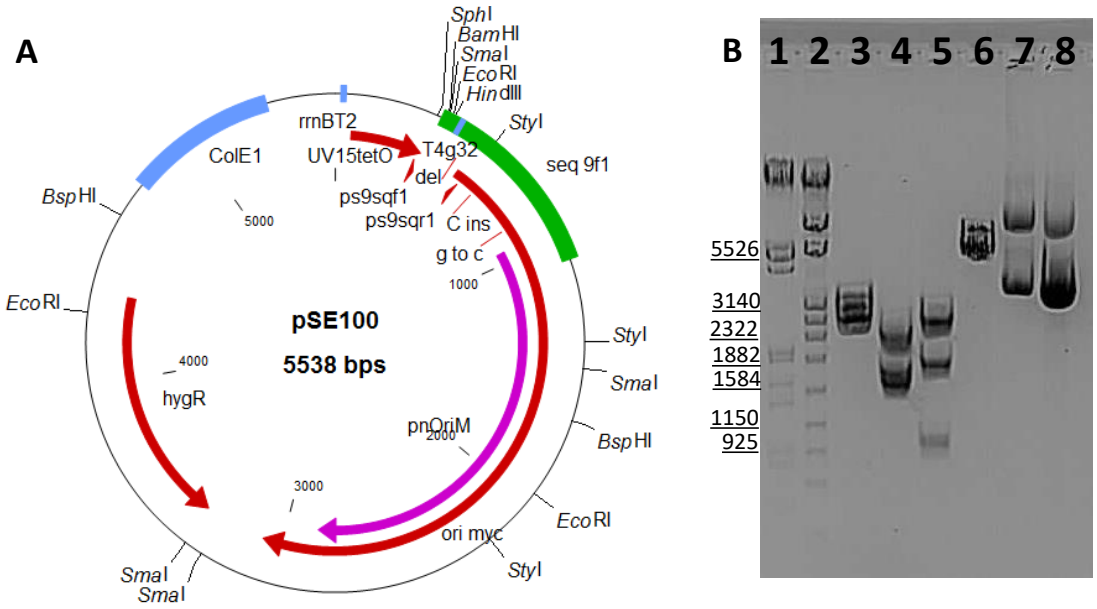

C	Enzyme	Expected fragments (bp)
	*BspH*I	2961, 2577
	*EcoR*I	2306, 1694, 1538
	*Sma*I	2609, 1792, 1071, 66
	*Sph*I	5538
	*Sty*I	3950, 803, 785

Figure A2.4 pSE100 restriction profiling and sequencing.
A) Vector map showing sequenced region in green. Three point mutations (red lines) were identified in the mycobacterial origin of replication (ori myc) but alignment with the pNit mycobacterial origin of replication (magenta) located the point mutations outside of the conserved origin. B) Restriction profiling: 1) MWMIII; 2) MWM IV; 3) *BspH*I; 4) *EcoR*I; 5) *Sma*I; 6) *Sph*I; 7) *Sty*I; 8) undigested. C) Expected restriction fragments. MWM: Lambda phage DNA marker (underlined).

A

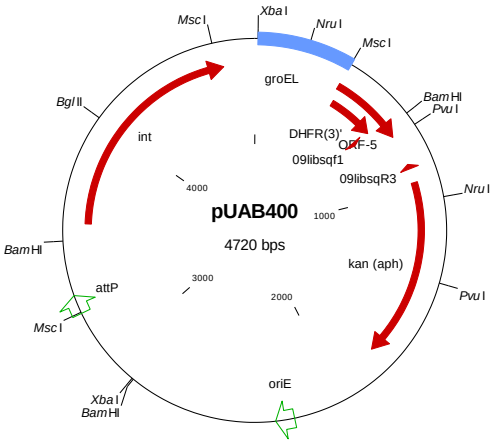

B

Restriction enzyme	Expected fragments (bp)
*BamH*I	2188, 1908, 624
*Bgl*II	4720
*Msc*I	2814, 1342, 564
*Nru*I	3889, 831
*Pvu*I	4071, 641
*Xba*I	2867, 1853

C

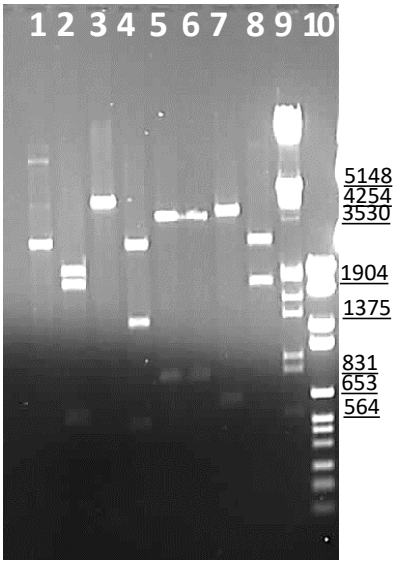

Figure A2.5 pUAB400 restriction profiling and sequencing.
A) Vector map. B) Expected restriction fragments. C) 1) uncut, 2) *BamH*I, 3) *Bgl*II, 4) *Msc*I, 5-6) *Nru*I, 7) *Pvu*I, 8) *Xba*I, 9) MWM III, 10) MWM VI.

A3 Lambda Phage Molecular Weight Markers (Roche Biosciences)

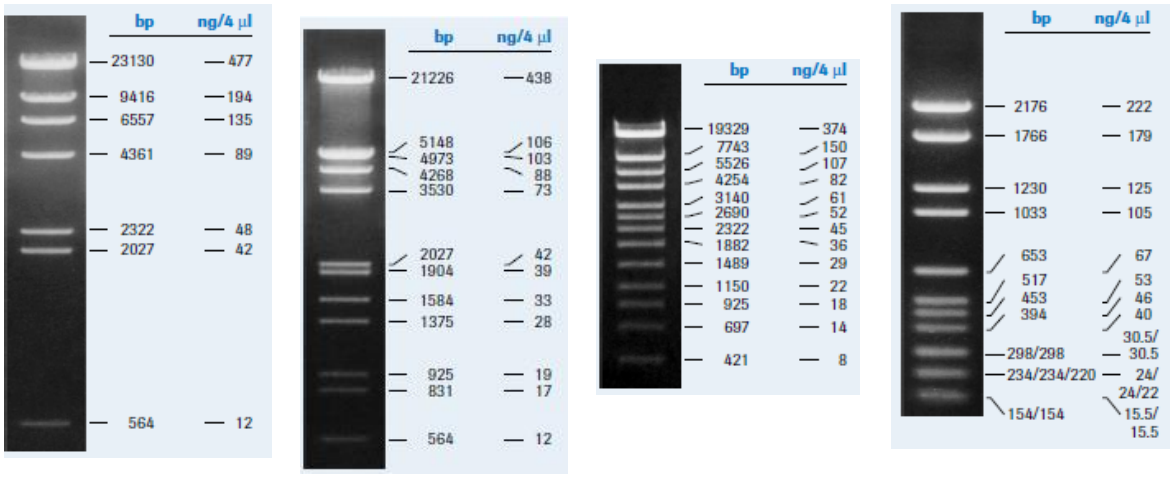

II III IV VI

A4 PAGE Ruler (A) and PAGE Ruler Plus (B) protein molecular weight markers (Thermo Scientific)

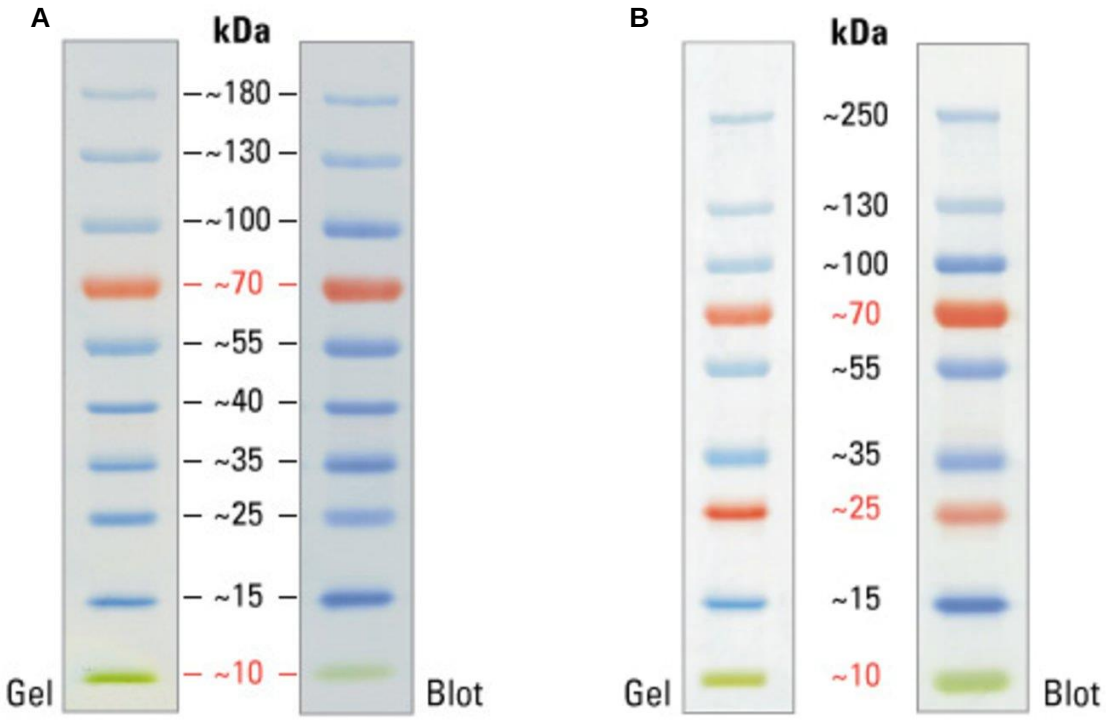

A5 Rv0950c His-tag construct translated using CloneManager to predict correct, co-translation of the C-terminal His-tag

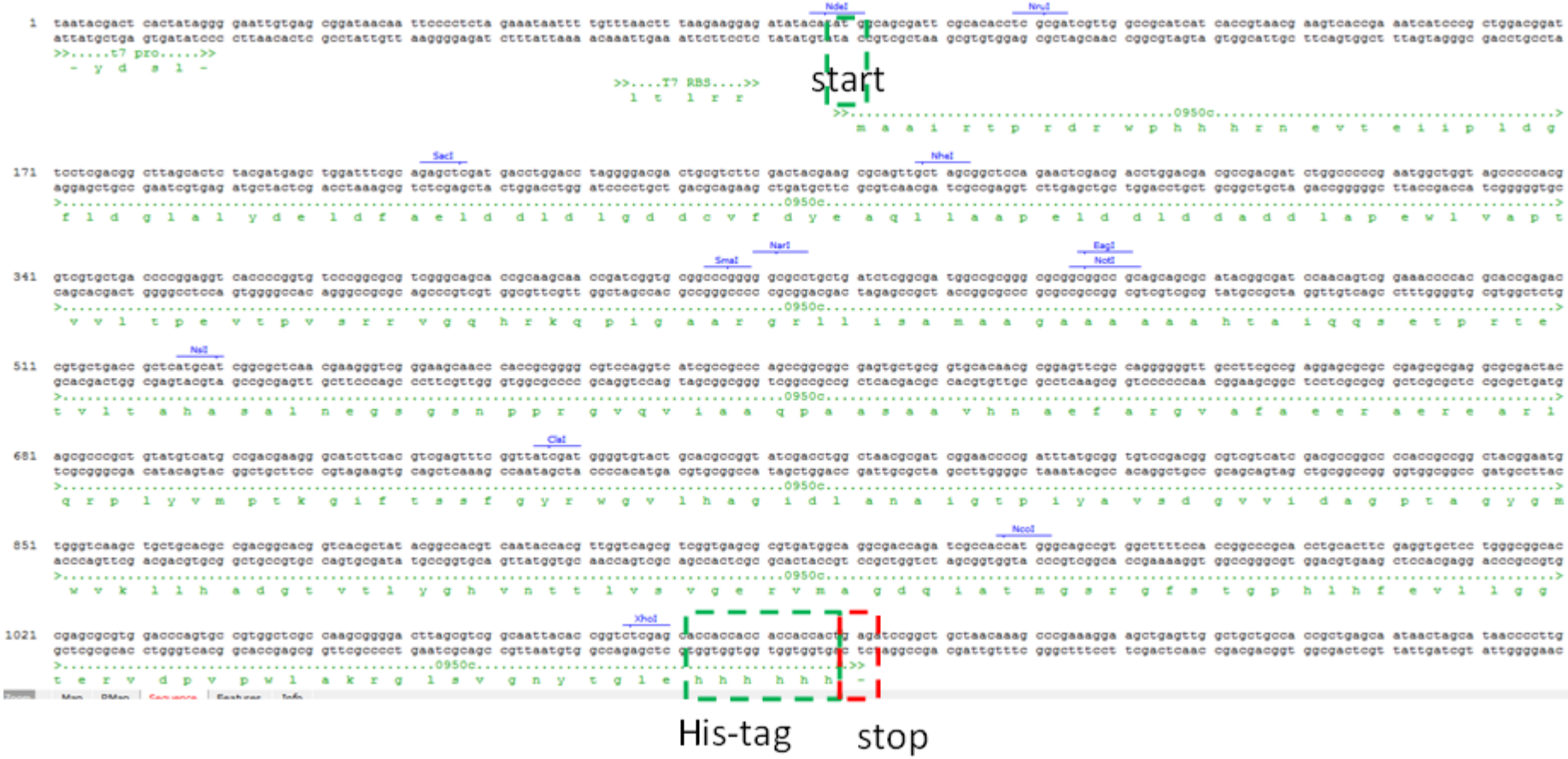

Appendix B: Additional data supporting Rv0950c characterisation.

B1 Proteins included in phylogenetic analysis in order of tree appearance.

Species	Protein/locus	pFAM 32.0 domain architecture
C.glutamicum	2497	SP, low complexity, M23
C.glutamicum	0858	TM, M23
C.glutamicum	2027	SP, M23
M. avium para K10	1928c	SP, 2x coiled-coil, low complexity, NlpC/p60
M. avium para K10	0980	random N-term, NlpC/p60
M. marinum	3448	SP, M23
M. marinum	1818	SP, M23
M. abscessus	1055c	random N-term, M23
M. smegmatis	2518	SP, M23
M. smegmatis	5526	low complexity/disorder, active M23
M. smegmatis	1192 or MepB2	SP, low complexity, M23
M. tuberculosis	Rv2891	SP, M23
M. tuberculosis	Rv0950c	low complexity, M23
M. leprae	0154	low complexity, M23
M. tuberculosis	Rv3786c	GT2_4, M23
M. marinum	5347	GT2_4, M23
M. marinum	4551	low complexity, M23
E. coli	YcbB	SP, random, PG binding1, YkuD (a type of L,D endopeptidase domain)
E. coli	AmpH	SP, B-lactamase domain
E. coli	LdtD	random, PG binding1, YkuD
E. coli	YgeR	SP, LysM, low complexity, M23 domain
E. coli	PBP1b or mrcB	PBP1TM-TM, U2BH (bifunctional transglycosylase second domain)+transgly, transpeptidase domain, low complexity
E. coli	PBP6 or *dacC*	SP, S11, PBP5_C
E. coli	DacD	SP, S11, PBP5_C
E. coli	PBP1a	SP, tansglyosylase, PCB_OB (PBP OB-like domain), transpeptidase
M. avium para	0036	disorder, low complexity, Nlpc/p60
M. abscessus	3197	random N-term, partial M23
MAP	2957	SP, M23
Streptomyces	Mitrecin A	undefined N-term, peptidase M15_4
Corynebacterium jeikeium	PBP4	TM, 2x partial SP13
E. coli	PBP2 or MrdA	TM, PBP dimer, transpeptidase
E. coli	PBP5 or *dacA*	SP, S11, PBP5_C
M. smegmatis	MSM_2432	SP, peptidase S11
M. tuberculosis	Rv3627c	SP, 2x partial SP13 peptidase domains
M. smegmatis	2433	SP, S11 peptidase domain
M. smegmatis	1661	SP, disorder, S11, disorder
M. tuberculosis	Rv2911 or DacB2	S11
M. smegmatis	6113 or DacB	SP, 2x partial SP13
P. aeruginosa	PBP4 or DacB	Peptidase S13
M. avium paratuberculosis	MAP_1203	SP, 2x coiled-coils, NlpC/p60 potentially active
M. avium paratuberculosis	MAP_1204	SP, low complexity, active NlpC/p60
S. aureus	CwlT	lysozyme-like, NlpC/p60
B. subtilis	CwlT or YddH	lysozyme-like, nlpc/p60
B. subtilis	CwlF/papQ/LytE	SP, 3xLysM, NlpC/p60 could be active

Y. Pestis	nlpD or YPO3356	SP, LysM, M23 no zinc
Caulobacter sp K31	3112 or DipM	SP, 4x LysM, M23 no zinc
C. diptheriae	1509	SP, M23 domain no zinc
C. diptheriae	0836	SP, active m23
P. aeruginosa	PA3787	SP, M23-N, active M23 domain
P. aeruginosa	PA0667 or MepM	OapA-LysM, active M23
H. influenza	LppB or NlpD	SP, disorder, LysM, M23 domain no zinc
H. influenzae	0756 or EnvC	SP, 2x coiled-coil, M23 domain
H. influenza	0409 or YebA	TM, OapA-LysM like, active M23
V. cholerae	A1043	TM, coiled coil, active M23
V. cholerae	0843 or TagE	TM, 1x coiled coil, M23 domain active
V. cholerae	A0079 or ShyA	SP, OapA LysM-like domain, active M23
V. cholerae	0630 or ShyC	OapA N-like, active M23
P. aeruginosa	5551	SP, partial active M23
P. aeruginosa	5363	SP, DUF4124, partial active M23
S. simulans	Lysostaphin	undefined N-term, partial M23, shb3 domain
H. pylori	Csd1 or TagE	TM, low complexity, active M23
H. pylori	Csd2	TM, inactive M23
P. aeruginosa	NlpD or 3623	LysM, low complexity, peptidase M23
P. aeruginosa	PA4404	TM, 2x coiled-coil, active M23
P. aeruginosa	5551	SP, partial active M23
N. gohnorrea	NGO1686/*mpg*	SP, low complexity, active M23
Pseudoalteromonas sp.CF6-2	Pseudoalterin	Random N-term, Partial C-term M23
E. coli	MepS/Spr	SP, disorder, NlpC-P60 with active sites
P. aeruginosa	RlpA	Random N-term, Lytic transglycosylase, Sporulation related domain.
P. aeruginosa	LasA	SP, random, low complexity, M23 active
E. coli	EnvC	SP-3xcoiled-coils and M23 domain
B. subtilis	SpollQ	disorder, TM, disorder, low complexity, M23 domain, disorder, low complexity
B. subtilis	YOM1/CwlP	coiled-coils, Phage minor tail, TM, TM, more coiled coils, SLT and active M23 domain, more coiled-coils.
S. aureus	LytM	SP, disorder, metal-binding disorder, active M23 domain.
P. aeruginosa	EnvC (5133)	SP, 3x coiled-coils, M23 domain (no zinc residues)
P. aeruiginosa	NlcS or 4924	SP, lysM, M23 domain no zinc
E. coli	MepH (YdhO)	SP, low complexity, NlpC-p60
P. aeruginosa	NlpD	random N-terminus, LysM, low complexity, M23 domain no zinc
E. coli	Spr	SP, NlpC-p60
E. coli	MepM/YebA	Opacity associated protein A N-term, LysM, zinc-binding M23 domain
V. cholerae	0355	SP, 3x coiled coli, M23 no zinc
E. coli	NlpD	SP, low complexity, LysM, low complexity
V. cholerae	NlpD or 0533	SP, LysM, low complexity, M23 domain no zinc
Lactobacillus salivarius REN	CbpA	random N-term, partial M23 domain at C-term.
S. aureus	LytU	TM domain and active M23-domain at C-term.
helicobacter pylori	HdpA/ Csd3	TM, Zn-binding “Csd3 N domain”, C-term M23 active,

		coiled-coil.
M. tuberculosis	RipA/Rv1477	SP, 3x coiled-coils, NlpC/p60
Listeria monocytogenes	P60	LysM, SH3, LysM, random C term
M. tuberculosis	Rv0024/RipE?	low complexity N-terminus, NlpC/p60 C term
C. glutamicum	CGR_1596	Undefined N-term, NlpC/p60 C-term
M. tuberculosis	RipB/Rv1478	SP, low complexity, active NlpC/p60
C. glutamicum	CGR_2070	undefined N-term, possibly inactive Nlpc/p60
C. glutamicum	CGR_0802	undetermined N-terminus, partial NlpC/p60
C. glutamicum	CGR_2069	unkown N-term, partial NlpC/p60
M. tuberculosis	Rv2190c/RipC	SP, coiled-coil, low complexity, C-term NlpC/p60
M. tuberculosis	Rv1566c/RipD	SP, Nlpc/p60 possibly inactive, low complexity C-term
C. diptheriae	DIP1621	SP, low complexity, coiled-coil, NlpC/p60
C. diptheriae	DIP1281	SP, 3x coiled coil, NlpC/p60
Neisseria meningitidis ATCC 13091	0018	undetermined N-term
N. meningitidis serogroup B	NMB0315	SP, active M23
M. avium paratuberculosis	MAP1272c	disorder, TM, Nlpc/p60

B2 Appending data for Swiss homology modelling

All data represented below are extracts from the modelling reports provided by the Swiss Model PDB (http://swissmodel.expasy.org/repository/) (Guex, Peitsch & Schwede, 2009; Bertoni et al., 2017; Bienert et al., 2017; Waterhouse et al., 2018; Studer et al., 2020).

B2.1 Alignments for homology modelling

Zinc binding sites are highlighted in yellow.

```
Rv0950c   MAAIRTPRDRWPHHHRNEVTEIIPLDGFLDGLALYDELDFAELDDLDLGDDCVFDYEAQLLAAPELDDLDDADDLAPEWL
6muk.1.A  ------------------------------------------------------------------------------
Rv0950c   VAPTVVLTPEVTPVSRRVGQHRKQPIGAARGRLLISAMAAGAAAAAAHTAIQQSETPRTETVLTAHASALNEGSGSNPPR
6muk.1.A  ------------------------------------------------------------------------------
Rv0950c   GVQVIAAQPAASAAVHNAEFARGVAFAEERAEREARLQRPLYVMPTK-GIFTSSFGYRWG------VLHAGIDLANAIGT
6muk.1.A  ------------------------------------GFNIEPLVYTRISSPFGYRMHPILHTWRLHTGIDYAAPQGT

Rv0950c   PIYAVSDGVVIDAGPTAGYGMWVKLLHADGTVTLYGHVNTTLVSVGERVMAGDQIATMGSRGFSTGPHLHFEVLLGGTER
6muk.1.A  PVRASADGVITFKGRKGGYGNAVMIRHANGVETLYAHLSAF-SQAQGNVRGGEVIGFVGSTGRSTGPHLHYEARING-QP

Rv0950c   VDPVPWLAKRGLSVGNYTG
6muk.1.A  VNPVSVALPT---------

Rv0950c   MAAIRTPRDRWPHHHRNEVTEIIPLDGFLDGLALYDELDFAELDDLDLGDDCVFDYEAQLLAAPELDDLDDADDLAPEWL
6u2a.1.A  ------------------------------------------------------------------------------
Rv0950c   VAPTVVLTPEVTPVSRRVGQHRKQPIGAARGRLLISAMAAGAAAAAAHTAIQQSETPRTETVLTAHASALNEGSGSNPPR
6u2a.1.A  ------------------------------------------------------------------------------
Rv0950c   GVQVIAAQPAASAAVHNAEFARGVAFAEERAEREARLQRPLYVMPTKGI--FTSSFG-YRW------GVLHAGIDLANAI
6u2a.1.A  ------------------------------------RAFQRYPVDSKWRISSNFDPRRLHPVTKRVAPHNGTDFAMPI

Rv0950c   GTPIYAVSDGVVIDAGPTAGYGMWVKLLHADGTVTLYGHVNTTLVSVGERVMAGDQIATMGSRGFSTGPHLHFEVLLGGT
6u2a.1.A  GTPVYTSGDGVVVMTRNHPYAGNYVVIQHGNTYMTRYLHLSKILVKKGQKVSRGQRIGLSGNTGRVTGPHLHYELIVRG-

Rv0950c   ERVDPVPWLAKRGLSVGNYTG
6u2a.1.A  RPVNAMKANIPMASSV-----


Rv2891    MAKSPARRCTAKVRRVLSRSVLILCWSLLGAAPAHADDSRLGWPLRPPPAVVRQFDAAS----PNWNPGHRGVDLAGRPG
4rny.1.A  ------------------------------------FLLETPVKY-TRISSPFSYGRFHPVLKVRRPHYGVDYAAKHG

Rv2891    QPVYAAGSATVVFAGLLAGR-PVVSLAHPGGLRTSYEPVV-AQ--VRVGQPVSAPTVIGALAAGHPGCQAAACLHWGAMW
4rny.1.A  SLIHSASDGRVGFMGVKAGYGKVVEI-HLNELRLVYAHMSAFANGLKKGSFVKKGQIIGRV--GSTGLSTGPHLHFGVYK

Rv2891    GPASGANYVDPLGLLKSTPIRLKPLSSEGRTLHYRQAEPVFVNEAAAGALAGAGHRKSPKQGVFRGAAQGGDIVARQPPG
4rny.1.A  ----NSRPINPLGYIRTAK---SKLHGKQREVFLEKAQRSKQKLEELLKTHS----------------------------

Rv2891    RWVCPSSAGGPIGWHRQ
4rny.1.A  -----------------


Rv3786c   MRILAMTRAHNAGRTLAATLDSLAVFSDDIYVIDDRSTDDTAEILANHPAVTNVVRARPDLPPTPWLIPESAGLELLYRM
4lxc.4.A  ------------------------------------------------------------------------------
Rv3786c   ADFCRPDWVMMVDADWLVETDIDLRAVLARTPDDIVALMCPMVSRWDDPEYPDLIPVMGTAEALRGPLWRWYPGLRAGGK
4lxc.4.A  ------------------------------------------------------------------------------
Rv3786c   LMHNPHWPANITDHGRIGQLPGVRLVHSGWSTLAERILRVEHYLRLDPDYRFNFGVAYDRSLLFGYALDEVDLLKADYRR
4lxc.4.A  ------------------------------------------------------------------------------
Rv3786c   RIRGDFDPLEPGGRLPIDREPRAIGRGYGPHAG------GFHPGVDFATDPGTPVYAVASGAVSAIDEVD-GLV-SLTIA
4lxc.4.A  ----------HEHSAQWLN---NYKKGYGYGPYPLGINGGMHYGVDFFMNIGTPVKAISSGKIVEAGWSNYGGGNQIGLI

Rv3786c   RCELD-VVYVFRPGDEGRLVLGDRIAAGAQLGTIGAQGESADGYLHFEVRTQ----DGHVNPVRYLANMGLRPWPPPGRL
4lxc.4.A  END-GVHRQWYMHLSKYNVKVGDYVKAGQIIGWSGSTGYSTAPHLHFQRMVNSFSNSTAQDPMPFLKSAGYG--------

Rv3786c   RAVSGSYPPATPCTITAEDR
4lxc.4.A  --------------------


Rv3786c   MRILAMTRAHNAGRTLAATLDSLAVFSDDIYVIDDRSTDDTAEILANHPAVTNVVRARPDLPPTPWLIPESAGLELLYRM
2b0p.1.A  ------------------------------------------------------------------------------
Rv3786c   ADFCRPDWVMMVDADWLVETDIDLRAVLARTPDDIVALMCPMVSRWDDPEYPDLIPVMGTAEALRGPLWRWYPGLRAGGK
2b0p.1.A  ------------------------------------------------------------------------------
Rv3786c   LMHNPHWPANITDHGRIGQLPGVRLVHSGWSTLAERILRVEHYLRLDPDYRFNFGVAYDRSLLFGYALDEVDLLKADYRR
2b0p.1.A  ------------------------------------------------------------------------------
```

```
Rv3786c  RIRGDFDPLEPGGRLPIDREPRAIGRGYGPHA-GGFHPGVDFATDPGTPVYAVASGAVSAIDEVD-GLV-SLTIARCELD
2b0p.1.A -----------AKDASWLTS-RKQLQPYGQYHGGGAHYGVDYAMPENSPVYSLTDGTVVQAGWSNYGGGNQVTIKEANSN

Rv3786c  VVYVFRPGDEGRLVLGDRIAAGAQLGTIGAQGESADGYLHFEVRTQD----GHVNPVRYLANMGLRPWPPPGRLRAVSGS
2b0p.1.A NYQWYMHNNRLTVSAGDKVKAGDQIAYSGSTGNSTAPHVHFQRMSGGIGNQYAVDPTSYLQSR-----------------

Rv3786c  YPPATPCTITAEDR
2b0p.1.A --------------
```

B2.2 Truncated Swiss homology model reports

Rv0950c

Model #01	File	Built with	Oligo-State	Ligands	GMQE	QMEAN
	PDB	ProMod3 3.1.1	monomer	None	0.27	-1.68

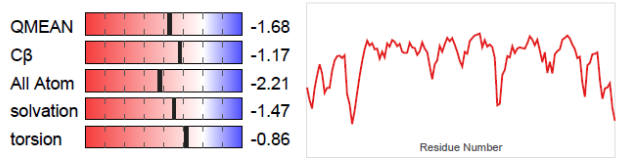

Template	Seq Identity	Oligo-state	QSQE	Found by	Method	Resolution	Seq Similarity	Range	Coverage	Description
6muk.1.A	40.16	monomer	0.00	HHblits	X-ray	1.93Å	0.39	200 - 323	0.37	Peptidase M23

Excluded ligands

Ligand Name.Number	Reason for Exclusion	Description
ZN.1	Not in contact with model.	ZINC ION

Model #02	File	Built with	Oligo-State	Ligands	GMQE	QMEAN
	PDB	ProMod3 3.1.1	monomer	1 x ZN: ZINC ION;	0.26	-2.84

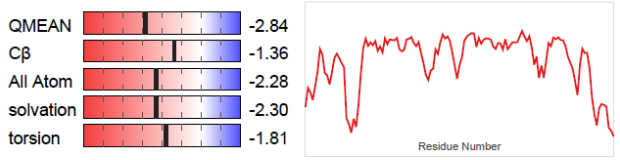

Template	Seq Identity	Oligo-state	QSQE	Found by	Method	Resolution	Seq Similarity	Range	Coverage	Description
6u2a.1.A	33.59	monomer	0.00	HHblits	X-ray	2.30Å	0.36	199 - 327	0.39	ShyA endopeptidase

Included Ligands

Ligand	Description
1 x ZN	ZINC ION

Rv2891

Model #01	File	Built with	Oligo-State	Ligands	GMQE	QMEAN
	PDB	ProMod3 3.1.1	monomer	None	0.41	-3.71

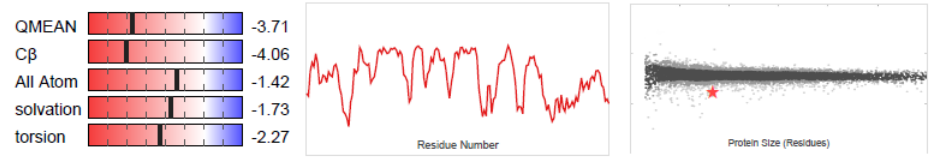

Template	Seq Identity	Oligo-state	QSQE	Found by	Method	Resolution	Seq Similarity	Range	Coverage	Description
4rny.1.A	23.23	monomer	0.00	HHblits	X-ray	2.00Å	0.32	39 - 204	0.62	Conserved hypothetical secreted protein

Excluded ligands

Ligand Name.Number	Reason for Exclusion	Description
GOL.6	Not biologically relevant.	GLYCEROL
GOL.7	Not biologically relevant.	GLYCEROL
GOL.8	Not biologically relevant.	GLYCEROL
GOL.9	Not biologically relevant.	GLYCEROL
SO4.2	Not biologically relevant.	SULFATE ION
SO4.3	Not biologically relevant.	SULFATE ION
SO4.4	Not biologically relevant.	SULFATE ION
SO4.5	Not biologically relevant.	SULFATE ION
ZN.1	Binding site not conserved.	ZINC ION

Rv3786c

	PDB	ProMod3 3.1.1	monomer	None	0.17	-2.19

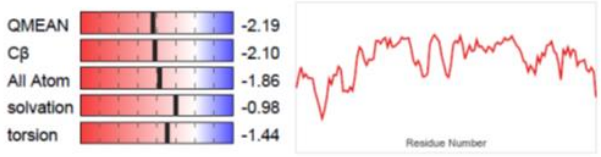

Template	Seq Identity	Oligo-state	QSQE	Found by	Method	Resolution	Seq Similarity	Range	Coverage	Description
4lxc.4.A	24.80	monomer	0.00	HHblits	X-ray	3.50Å	0.32	251 - 379	0.31	Lysostaphin

Excluded ligands

Ligand Name.Number	Reason for Exclusion	Description
SO4.2	Not biologically relevant.	SULFATE ION
SO4.3	Not biologically relevant.	SULFATE ION
SO4.4	Not biologically relevant.	SULFATE ION
SO4.5	Not biologically relevant.	SULFATE ION
ZN.1	Binding site not conserved.	ZINC ION

Model #03	File	Built with	Oligo-State	Ligands	GMQE	QMEAN
	PDB	ProMod3 3.1.1	monomer	1 x ZN: ZINC ION;	0.17	-2.02

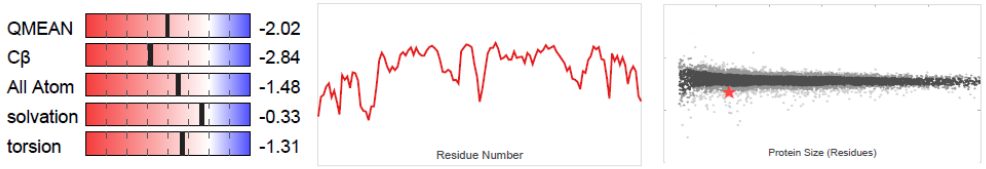

Template	Seq Identity	Oligo-state	QSQE	Found by	Method	Resolution	Seq Similarity	Range	Coverage	Description
2b0p.1.A	25.81	monomer	0.00	HHblits	X-ray	1.50Å	0.33	254 - 376	0.30	Glycyl-glycine endopeptidase lytM

Included Ligands

Ligand	Description
1 x ZN	ZINC ION

B2.3 Details of proposed templates for homology modelling (showing first ten)

Rv0950c

Template	Seq Identity	Oligo-state	QSQE	Found by	Method	Resolution	Seq Similarity	Coverage	Description
6muk.1.A	40.16	monomer	-	HHblits	X-ray	1.93Å	0.39	0.37	Peptidase M23
6jn1.1.A	35.20	monomer	-	HHblits	X-ray	2.38Å	0.37	0.38	Peptidase M23
4rny.1.A	33.59	monomer	-	HHblits	X-ray	2.00Å	0.36	0.39	Conserved hypothetical secreted protein
4rnz.1.A	33.59	monomer	-	HHblits	X-ray	1.98Å	0.36	0.39	Conserved hypothetical secreted protein
6u2a.1.A	33.59	monomer	-	HHblits	X-ray	2.30Å	0.36	0.39	ShyA endopeptidase
5kvp.1.A	36.51	monomer	-	HHblits	NMR	NA	0.36	0.38	Zoocin A endopeptidase
6ue4.1.A	33.59	homo-dimer	-	HHblits	X-ray	2.08Å	0.36	0.39	ShyA endopeptidase
6ue4.1.B	33.59	homo-dimer	-	HHblits	X-ray	2.08Å	0.36	0.39	ShyA endopeptidase
6jmz.1.A	35.20	monomer	-	HHblits	X-ray	1.92Å	0.37	0.38	Peptidase M23
6jn0.1.A	35.20	monomer	-	HHblits	X-ray	2.16Å	0.37	0.38	Peptidase M23

Rv2891

Template	Seq Identity	Oligo-state	QSQE	Found by	Method	Resolution	Seq Similarity	Coverage	Description
4rny.1.A	23.23	monomer	-	HHblits	X-ray	2.00Å	0.32	0.62	Conserved hypothetical secreted protein
6muk.1.A	24.16	monomer	-	HHblits	X-ray	1.93Å	0.31	0.60	Peptidase M23
4rnz.1.A	23.23	monomer	-	HHblits	X-ray	1.98Å	0.32	0.62	Conserved hypothetical secreted protein
6u2a.1.A	20.39	monomer	-	HHblits	X-ray	2.30Å	0.29	0.61	ShyA endopeptidase
6ue4.1.A	20.39	homo-dimer	0.00	HHblits	X-ray	2.08Å	0.29	0.61	ShyA endopeptidase
6ue4.1.B	20.39	homo-dimer	0.00	HHblits	X-ray	2.08Å	0.29	0.61	ShyA endopeptidase
3slu.1.A	24.16	monomer	-	HHblits	X-ray	2.41Å	0.31	0.60	M23 peptidase domain protein
3slu.2.A	24.16	monomer	-	HHblits	X-ray	2.41Å	0.31	0.60	M23 peptidase domain protein
5j1l.2.A	22.60	monomer	-	HHblits	X-ray	2.27Å	0.31	0.59	ToxR-activated gene (TagE)
5j1m.1.A	22.60	monomer	-	HHblits	X-ray	2.35Å	0.31	0.59	ToxR-activated gene (TagE)

Rv3786c

Template	Seq Identity	Oligo-state	QSQE	Found by	Method	Resolution	Seq Similarity	Coverage	Description
4lxc.4.A	24.80	monomer	-	HHblits	X-ray	3.50Å	0.32	0.31	Lysostaphin
4lxc.1.A	24.80	monomer	-	HHblits	X-ray	3.50Å	0.32	0.31	Lysostaphin
4lxc.3.A	24.80	monomer	-	HHblits	X-ray	3.50Å	0.32	0.31	Lysostaphin
6jmz.1.A	23.62	monomer	-	HHblits	X-ray	1.92Å	0.32	0.31	Peptidase M23
5j1k.1.A	28.46	homo-dimer	-	HHblits	X-ray	1.81Å	0.32	0.30	ToxR-activated gene (TagE)
4lxc.2.A	24.80	monomer	-	HHblits	X-ray	3.50Å	0.32	0.31	Lysostaphin
4rnz.1.A	20.93	monomer	-	HHblits	X-ray	1.98Å	0.30	0.32	Conserved hypothetical secreted protein
4rny.1.A	20.93	monomer	-	HHblits	X-ray	2.00Å	0.30	0.32	Conserved hypothetical secreted protein
5j1l.2.A	25.60	monomer	-	HHblits	X-ray	2.27Å	0.33	0.31	ToxR-activated gene (TagE)
5j1m.1.A	25.60	monomer	-	HHblits	X-ray	2.35Å	0.33	0.31	ToxR-activated gene (TagE)

B3 Sequencing data of important constructs

Sequence alignments for p2NilΔRv0950c, p2NilΔRv2891 and pTT1b::Rv0950c are provided below. The reference sequence is highlighted (light turquoise: downstream homlogy, dark turquoise: upstream homology, dark grey: Rv0950c, light grey: 337 bp promotor region) and aligned with sequencing products from overlapping primers numbered by letters.

B3.1 p2NilΔRv0950c

```
Ref  3980   aaccagccagccggaagggccgagcgcagaagtggtcctgcaactttatccgcctccatc
G06_p2nd09                                 agtggt-ctgc-actttatccgcctccatc
Ref  4040   cagtctattaattgttgccgggaagctagagtaagtagttcgccagttaatagtttgcgc
G06_p2nd09 cagtctattaattgttgccgggaagctagagtaagtagttcgccagttaatagtttgcgc
Ref  4100   aacgttgttgccattgctgcaggctatgtcgccgacaacgagcacgacgaggcccggttc
G06_p2nd09 aacgttgttgccattgctgcaggctatgtcgccgacaacgagcacgacgaggcccggttc
Ref  4160   gtggccgaggagatcgatgcgctcgccgagggtagcgagatcacctacaacgatgtcgcc
G06_p2nd09 gtggccgaggagatcgatgcgctcgccgagggtagcgagatcacctacaacgatgtcgcc
Ref  4220   gtcttctaccgcaccaacaactcgtcgcggtcactggaagaggtgctgatccgcgccggt
G06_p2nd09 gtcttctaccgcaccaacaactcgtcgcggtcactggaagaggtgctgatccgcgccggt
Ref  4280   attccgtacaaggtcgttgggggagtgcgcttttacgagcgcaaggagattcgcgacatc
G06_p2nd09 attccgtacaaggtcgttgggggagtgcgcttttacgagcgcaaggagattcgcgacatc
Ref  4340   gttgcctacctgcgcgtgctggacaacccgggcgacgcggtcagcctacggcgcatcctt
G06_p2nd09 gttgcctacctgcgcgtgctggacaacccgggcgacgcggtcagcctacggcgcatcctt
Ref  4400   aacaccccgcgccgcggtatcggggatcgtgccgaggcgtgtgtggcggtgtacgccgag
G06_p2nd09 aacaccccgcgccgcggtatcggggatcgtgccgaggcgtgtgtggcggtgtacgccgag
Ref  4460   aacaccggcgtcggcttcggtgacgcgctcgtcgccgcggcccaaggcaaagtaccgatg
G06_p2nd09 aacaccggcgtcggcttcggtgacgcgctcgtcgccgcggcccaaggcaaagtaccgatg
H06_p2nd09                             cgctcgtcgccgcggtc--aggc-aagtaccgatg
Ref  4520   ctgaatacccgggcggagaaggcgatcgcgggtttcgtcgagatgttcgacgagctgcgg
G06_p2nd09 ctgaatacccgggcggagaaggcgatcgcgggtttcgtcgagatgttcgacgagctgcgg
H06_p2nd09 ctgaatacccgggcggagaaggcgatcgcgggtttcgtcgagatgttcgacgagctgcgg
Ref  4580   ggccgcctcgatgacgacctgggggagctggtcgaggcggtgctggaacgcaccggatac
G06_p2nd09 ggccgcctcgatgacgacctgggggagctggtcgaggcggtgctggaacgcaccggatac
H06_p2nd09 ggccgcctcgatgacgacctgggggagctggtcgaggcggtgctggaacgcaccggatac
Ref  4640   cgccgcgagctggaagcgtccaccgatccacaggaattggcccgcctggacaacctcaac
G06_p2nd09 cgccgcgagctggaagcgtccaccgatccacaggaattggcccgcctggacaacctcaac
H06_p2nd09 cgccgcgagctggaagcgtccaccgatccacaggaattggcccgcctggacaacctcaac
Ref  4700   gaattagtcagcgtcgcacacgaattcagtaccgaccgggagaatgccgccgcacttggc
G06_p2nd09 gaattagtcagcgtcgcacacgaattcagtaccgaccgggagaatgccgccgcacttggc
H06_p2nd09 gaattagtcagcgtcgcacacgaattcagtaccgaccgggagaatgccgccgcacttggc
Ref  4760   ccagacgacgaagacgtccccgacaccggtgtgctggcggattttctggaacgggtgtcg
G06_p2nd09 ccagacgacgaagacgtccccgacaccggtgtgctggcggattttctggaacgggtgtcg
H06_p2nd09 ccagacgacgaagacgtccccgacaccggtgtgctggcggattttctggaacgggtgtcg
Ref  4820   ctggtcgccgacgccgatgagatcccggagcatggcgcgggtgtggttaccttgatgacc
G06_p2nd09 ctggtcgccgacgccgatgagatcccggagcatggcgcgggtgtggttaccttgatgacc
H06_p2nd09 ctggtcgccgacgccgatgagatcccggagcatggcgcgggtgtggttaccttgatgacc
Ref  4880   ttgcacaccgccaagggtttggagttcccggtggtgtttgtgaccggctgggaggacggg
G06_p2nd09 ttgcacaccgccaagggtttggagttcccggtggtgtttgtgaccggctgggaggacggg
H06_p2nd09 ttgcacaccgccaagggtttggagttcccggtggtgtttgtgaccggctgggaggacggg
Ref  4940   atgttcccgcacatgcgggcgttggacaacccgaccgagttgtccgaggagcggcggctg
G06_p2nd09 atgttcccgcacatgc-ggcgttggacaacccgaycgagttgtccgaggagcggcggctg
H06_p2nd09 atgttcccgcacatgcgggcgttggacaacccgaccgagttgtccgaggagcggcggctg
A07_p2nd09                                                 cggcggctg
Ref  5000   gcctatgtcggcatcacccgcgcccggcagcggttgtacgtgagccgggcgatcgtgcg
G06_p2nd09 gtctatgtcggcatcacycgcgcycggcagcggtgtacgtgagcccggcgatcgtgcg
H06_p2nd09 gcctatgtcggcatcacccgcgcccggcagcggttgtacgtgagccgggcgatcgtgcg
A07_p2nd09 gcctatgtcggcatcacccgcgcccggcagcggttgtacgtgagccgggcgatcgtgcg
```

```
Ref  5059   ttcgtcttggggccagccgatgctcaacccggagtcgcggtttctgcgggaaatcccgc
G06_p2nd09 tttcgtctgggg--cagccgatgctcaacyc-gagtcgcgg-ttctgcggg-aatcccgc
H06_p2nd09 ttcgtcttggggccagccgatgctcaacccggagtcgcggtttctgcgggaaatcccgc
A07_p2nd09 ttcgtcttggggccagccgatgctcaacccggagtcgcggtttctgcgggaaatcccgc
Ref  5118   aggagctcatcgactggcggcgcaccgccccgaagccgtcgttcagtgccccggtgagt
G06_p2nd09 a-ga-ctcatcgactgggcgggccaccg-ctcgaag
H06_p2nd09 aggagctcatcgactggcggcgcaccgccccgaagccgtcgttcagtgccccggtgagt
A07_p2nd09 aggagctcatcgactggcggcgcaccgccccgaagccgtcgttcagtgccccggtgagt
Ref  5177   ggcgccggtcggttcggtagcgcgcgtccatcaccgacccgctcgggggcgagcaggcgc
H06_p2nd09 ggcgccggtcggttcggtagcgcgcgtccatcaccgacccgctcgggggcgagcaggcgc
A07_p2nd09 ggcgccggtcggttcggtagcgcgcgtccatcaccgacccgctcgggggcgagcaggcgc
Ref  5237   ccgctgctggtgcttcaggtcggcgaccgcgtgacccatgacaaatacggcctgggccgt
H06_p2nd09 ccgctgctggtgcttcaggtcggcgaccgcgtgacccatgacaaatacggcctgggccgt
A07_p2nd09 ccgctgctggtgcttcaggtcggcgaccgcgtgacccatgacaaatacggcctgggccgt
Ref  5297   gtcgaggaggtctccggtgtcggcgaatcggcgatgtcgctgatcgacttcggtagctcg
H06_p2nd09 gtcgaggaggtctccggtgtcggcgaatcggcgatgtcgctgatcgacttcggtagctcg
A07_p2nd09 gtcgaggaggtctccggtgtcggcgaatcggcgatgtcgctgatcgacttcggtagctcg
C07_p2nd09                                         tcgctgatcgac-tc-gtagctc-
Ref  5357   gggcgggtgaagctgatgcacaaccacgcccctgtcaccaagctctgagatttcgcgccg
H06_p2nd09 gggcgggtgaagctgatgcacaaccacgccyctgtcaccaagctctgagatttcgcgccg
A07_p2nd09 gggcgggtgaagctgatgcacaaccacgcccctgtcaccaagctctgagatttcgcgccg
C07_p2nd09 gggcgrgkg-agctgatgcac-atcmc-sccctgtcac--agctctgagatttcgcsccg
Ref  5417   agcgtgaagtcacggcggctatttcgcggatttctcgccctgagaacacgttcggcgt
H06_p2nd09 agcgtgaagtcacggcggctatttcgcggatttctcgccctgagaacacgttcggcgt
A07_p2nd09 agcgtgaagtcacggcggctatttcgcggatttctcgccctgagaacacgttcggcgt
C07_p2nd09 aggcgkgaagtcacggcggctatttcgcggatttytcgccctgagaacacgttcggcgt
B07_p2nd09                                                       gt
Ref  5475   cgttgccgggtcaaccggtgtaattgccgacgctaagtccccgcttagatctatc
H06_p2nd09 cgttgcc-ggtcaaycggtgtaattgccgackctaagtcccycgcttagatyttatc
A07_p2nd09 cgttgccgggtcaaccggtgtaattgccgacgctaagtccccgcttagatctatc
C07_p2nd09 cgttgcccgggttcaacccggtgtaattgccgacgctaagtccc-cgcttagat-ctatc
B07_p2nd09 cgttgccgggtc-accggtgtaattgccgacgctaagtccccgcttagatctatc
Ref  5530   gcgaggtgtgcgaatcgctgccatggcagcagaacgggcgatacggtgctgggacaaatc
H06_p2nd09 gcga-gtgkgcg-atcgctg-cattgcagccgaac-ggcgawccggtgctgg--catatc
A07_p2nd09 gcgaggtgtgcgaatcgctgccatggcagcagaacgggcgatacggtgctgggacaaatc
C07_p2nd09 gcgaggtgtgcgaatcgctgccatggcagcagaacgggcgatacggtgctgggacaaatc
B07_p2nd09 gcgaggtgtgcgaatcgctgccatggcagcagaacgggcgatacggtgctgggacaaatc
Ref  5590   tgaaatgtcctcggatcgtgaccataacgttatctggaccctgagacgttatccgcaacc
H06_p2nd09 tg-aatgtcttcggatcg-kaccat-acgttatct
A07_p2nd09 tgaaatgtcctcggatcgtgaccataacgttatctggaccctgagacgttatccgcaacc
C07_p2nd09 tgaaatgtcctcggatcgtgaccataacgttatctgga-cctgagacgttatccgcaacc
B07_p2nd09 tgaaatgtcctcggatcgtgaccataacgttatctggaccctgagacgttatccgcaacc
Ref  5650   ggatggtagtggcaacttcagcgcggaattcggctgtgattgtgagttggatcacgtttc
A07_p2nd09 ggatggtagtggcaacttcagcgcggaattcggctgtgattgtgagttggatcacgtttc
C07_p2nd09 ggatggtagtggcaacttcagcgcggaattcggctgtgattgtgagttggatcacgtttc
B07_p2nd09 ggatggtagtggcaacttcagcgcggaattcggctgtgattgtgagttggatcacgtttc
Ref  5710   ggctggacaaacatatcggtgagctgtgccacaccgggtggatgcggccgcggagttaat
A07_p2nd09 ggctggacaaacatatcggtgagctgtgccacaccgggtggatgcggccgcggagttaat
C07_p2nd09 ggctggacaaacatatcggtgagctgtgccacaccgggtggatgcggccgcggagttaat
B07_p2nd09 ggctggacaaacatatcggtgagctgtgccacaccgggtggatgcggccgcggagttaat
Ref  5770   cggcggtctcgatacagttctccgtgcgagtcgccgatttcggcaccgcctacctattgg
A07_p2nd09 cggcggtctcgatacagttctccgtgcgagtcgccgatttcggcaccgcctacctattgg
C07_p2nd09 cggcggtctcgatacagttctccgtgcgagtcgccgatttcggcaccgcctacctattgg
B07_p2nd09 cggcggtctcgatacagttctccgtgcgagtcgccgatttcggcaccgcctacctattgg
D07_p2nd09                                                 ctaccta-tgg
Ref  5830   tcgagcagtaagccgagcgaagacggtgagcccatggatcttttcgagtatcaagccaa
A07_p2nd09 tcgagcagtaagccgagcgaagacggtgagcccatggatcttttcgagtatcaagccaa
C07_p2nd09 tcgagcagtaagccgagcgaagacggtgagcccatggatcttttcgagtatcaagccaa
B07_p2nd09 tcgagcagtaagccgagcga-agacggtgagcccatggatcttttcgagtatcaagccaa
D07_p2nd09 tcgagcagttagtcgagcgagrtccggtgagtccatgaatc-tttcgagtatcaagccca
```

```
Ref 5889    ggagttattcgccaagcacaacgtgcccagcacgccgggtcgggtgaccgacacagccga
A07_p2nd09 ggagttattcgccaagcacaacgtgcycagcacgccgggtcgggtgaccgacacagccga
C07_p2nd09 ggagttattcgccaagcacaacgtgcccagcacgccgggtcgggtgaccgacacagccga
B07_p2nd09 ggagttattcgccaagcacaacgtgcccagcacgccgggtcgggtgaccgacacagccga
D07_p2nd09 cgagtta-tcgccaagcac-acgtgcccagcacgccgggtcgggtgaccgacacagccga
Ref 5949    gggtgccaaggctatcgccacggagatcgggcgtccggtgatggtcaaagcgcaggtcaa
A07_p2nd09 gggtgccaaggctatcgccacggagatcgggcgtcc-gtgatggtc-aagcgcaggtc-a
C07_p2nd09 gggtgccaaggctatcgccacggagatcgggcgtccggtgatggtcaaagcgcaggtcaa
B07_p2nd09 gggtgccaaggctatcgccacggagatcgggcgtccggtgatggtcaaagcgcaggtcaa
D07_p2nd09 gggtgccaaggctatcgccacggagatcgggcgtccggtgatggtcaaagcgcaggtcaa
Ref 6009    gatcggcggccggggcaaggccggtggcgtcaaatacgccgcgaccccacaagacgcg
A07_p2nd09 gatc-gcg--tggggcaaggycggtggcgtc-aatacgtckcgacccycac-agackcg
C07_p2nd09 gatcggcggccggggcaaggccggtggcgtcaaatacgccgcgaccccacaagacgcg
B07_p2nd09 gatcggcggccggggcaaggccggtggcgtcaaatacgccgcgaccccacaagacgcg
D07_p2nd09 gatcggcggccggggcaaggccggtggcgtcaaatacgccgcgaccccacaagacgcg
Ref 6067    tacgagcacgccaagaacatcctcggcctggacatcaaaggacacatcgtcaagaaactg
A07_p2nd09 tacgagcayggcaagawcatcctc-gcctggacatcaagg---acatcgtc-ag-ac--k
C07_p2nd09 tacgagcacgccaagaacatcctcggcctggacatcaaaggacacatcgtcaagaaactg
B07_p2nd09 tacgagcacgccaagaacatcctcggcctggacatcaaaggacacatcgtcaagaaactg
D07_p2nd09 tacgagcacgccaagaacatcctcggcctggacatcaaaggacacatcgtcaagaaactg
Ref 6127    ctggtcgctgaggctagcgatatcgccgaggagtactacctatccttcctgctcgaccgg
A07_p2nd09 ctggtcgctgagtctagc
C07_p2nd09 ctggtcgctgaggctagcgatatcgccgaggagtactacctatccttcctgctcgaccgg
B07_p2nd09 ctggtcgctgaggctagcgatatcgccgaggagtactacctatccttcctgctcgaccgg
D07_p2nd09 ctggtcgctgaggctagcgatatcgccgaggagtactacctatccttcctgctcgaccgg
Ref 6187    gccaaccgcacctacctggcgatgtgctcggtggagggcggcatggagatcgaagaggta
C07_p2nd09 gccaaccgcacctacctggcgatgtgctcggtggagggcggcatggagatcgaagaggta
B07_p2nd09 gccaaccgcacctacctggcgatgtgctcggtggagggcggcatggagatcgaagaggta
D07_p2nd09 gccaaccgcacctacctggcgatgtgctcggtggagggcggcatggagatcgaagaggta
Ref 6247    gcggccaccaaacccgagcggctcgccaaagtcccggtgaatgccgtcaagggcgttgac
C07_p2nd09 gcggccaccaaacccgagcggctcgccaaagtcccggtgaatgccgtcaagggcgttgac
B07_p2nd09 gcggccaccaaacccgagcggctcgccaaagtcccggtgaatgccgtcaagggcgttgac
D07_p2nd09 gcggccaccaaacccgagcggctcgccaaagtcccggtgaatgccgtcaagggcgttgac
Ref 6307    ctagatttcgcgcggtccatcgccgaacagggtcatcttccggccgaggtgctcgacacc
C07_p2nd09 ctagatttcgcgcggtccatcgccgaacagggtcatcttccggccgaggtgctcgacacc
B07_p2nd09 ctagatttcgcgcggtccatcgccgaacagggtcatcttccggccgaggtgctcgacacc
D07_p2nd09 ctagatttcgcgcggtccatcgccgaacagggtcatcttccggccgaggtgctcgacacc
Ref 6367    gcagcggtcaccatcgccaagctgtgggagctcttcgtcgccgaggacgcgacgctggtt
C07_p2nd09 gcagcggtcaccatcgccaagctgtgggagctcttcgtcgccgaggacgcgacgctggtt
B07_p2nd09 gcagcggtcaccatcgccaagctgtgggagctcttcgtcgccgaggacgcgacgctggtt
D07_p2nd09 gcagcggtcaccatcgccaagctgtgggagctcttcgtcgccgaggacgcgacgctggtt
Ref 6427    gaggtcaacccgttggtgcggacgcctg-accacaagatcctcgcgctggatgccaagat
C07_p2nd09 gaggtcaacccgttggtgcggacgcc
B07_p2nd09 gaggtcaacccgttggtgcggacgcctgaaccac-agatcctcgcgctggatgccaagat
D07_p2nd09 gaggtcaacccgttggtgcggacgcctg-accacaagatcctcgcgctggatgccaagat
Ref 6486    caccctcgacggcaacgccgatttccgtcagcctggccatgccgagttcgaggatcgagc
B07_p2nd09 caccctcgacggccacg-cga-ttccgtcagcctg--catg-cgag-tcgaggatcgagc
D07_p2nd09 caccctcgacggcaacgccgatttccgtcagcctggccatgccgagttcgaggatcgagc
Ref 6546    tgccaccgatccactggagttgaaggccaaggagcacg-acctcaactacgtcaagctgg
B07_p2nd09 tg-catcgatccactgaag-tgaagg-caagg-rcacgaacctcaactacgtc-agctgg
D07_p2nd09 tgccaccgatccactggagttgaaggccaaggagcacg-acctcaactacgtcaagctgg
Ref 6605    acggtcaggtggggatcatcggcaatggcgcgggcttggtgatgtcgactctcgacgtcg
B07_p2nd09 acg
D07_p2nd09 acggtcaggtggggatcatcggcaatggcgcgggcttggtgatgtcgactctcgacgtcg
Ref 6665    tcgcgtatgccggtgagaagcacggcggagtcaagccggccaacttcctggatatcggcg
D07_p2nd09 tcgcgtatgccggtgagaagcacggcggagtcaagccggccaacttcctggatatcggcg
Ref 6725    gcggcgcttcggccgaggtgatggccgcgggtctggacgtggtgctgggcgaccagcagg
D07_p2nd09 gcggcgcttcggccgaggtgatggccgcgggtctggacgtggtgctgggcgaccagcagg
Ref 6785    tcaagagcgtgttcgtcaaa
D07_p2nd09 tcaagagcgtgttcgtcaaa
```

B3.2 p2NilΔRv2891

```
Ref 3781      gcaacgttgttgccattgctgcaggtaaccacgccgtgatcccggccggctagggaggga
G06_P2nd2891                  ttgctgcaggtaaccacgccgtgatcccggccggctagggaggga
Ref 3841      tgggcgttggactttggggtgttgccgcccgagatcaactccggtcgaatgtacgcaggt
G06_P2nd2891 tgggcgttggactttggggtgttgccgcccgagatcaactccggtcgaatgtacgcaggt
Ref 3901      ccgggatcggggcccatgatggccgccgcggcggcctgggatagtttggcggctgaattg
G06_P2nd2891 ccgggatcggggcccatgatggccgccgcggcggcctgggatagtttggcggctgaattg
Ref 3961      ggcttggccgccggcggctaccggttggctatctcggagctgaccggtgcgtactgggcg
G06_P2nd2891 ggcttggccgccggcggctaccggttggctatctcggagctgaccggtgcgtactgggcg
Ref 4021      gggcccgcagcggcgtcgatggtggccgcggtcacgccttatgtggcgtggctcagcgcc
G06_P2nd2891 gggcccgcagcggcgtcgatggtggccgcggtcacgccttatgtggcgtggctcagcgcc
Ref 4081      accgccggtcaggctgaacaggcgggcatgcaggccagagcggccgcggcagcctatgag
G06_P2nd2891 accgccggtcaggctgaacaggcgggcatgcaggccagagcggccgcggcagcctatgag
Ref 4141      ctggcgtttgcgatgacggtgcccccgccggtggtcgttgccaaccgcgcgctgttggtg
G06_P2nd2891 ctggcgtttgcgatgacggtgcccccgccggtggtcgttgccaaccgcgcgctgttggtg
Ref 4201      gcgctggtcgcgaccaacttttttcgggcagaacaccccggcgatcgcggccaccgaggcc
G06_P2nd2891 gcgctggtcgcgaccaacttttttcgggcagaacaccccggcgatcgcggccaccgaggcc
Ref 4261      caatacgccgagatgtgggcccaagacgctgccgccatgtacgcctatgcgggctccgcg
G06_P2nd2891 caatacgccgagatgtgggcccaagacgctgccgccatgtacgcctatgcgggctccgcg
Ref 4321      gcaatcgccacggagttgaccccgttcaccgcggcgccagtgactaccagccctgccgcg
G06_P2nd2891 gcaatcgccacggagttgaccccgttcaccgcggcgccagtgactaccagccctgccgcg
H06_P2nd2891                                                          g
Ref 4381      ctggccggccaggcggcggcgacggtatcgtcgacggtcccaccgctggccaccaccgcc
G06_P2nd2891 ctggccgg
H06_P2nd2891 ctggccggccaggcggcggcgacggtatcgtcgacggtcccaccgctggccaccaccgcc
Ref 4441      gcggtgccccaactgttgcagcaactctcgtcgacgtcactgatcccgtggtactcggca
H06_P2nd2891 gcggtgccccaactgttgcagcaactctcgtcgacgtcactgatcccgtggtactcggca
Ref 4501      ttgcagcaatggctcgcggagaatcttctcggtctcacgcctgacaacaggatgacgatc
H06_P2nd2891 ttgcagcaatggctcgcggagaatcttctcggtctcacgcctgacaacaggatgacgatc
Ref 4561      gttcggttgctgggcatcagctacttcgacgaagggctactgcaattcgaggcttcgctc
H06_P2nd2891 gttcggttgctgggcatcagctacttcgacgaagggctactgcaattcgaggcttcgctc
Ref 4621      gcccagcaagcgatcccgggcaccccgggcggcgccggtgactcgggatcctcggtgctt
H06_P2nd2891 gcccagcaagcgatcccgggcaccccgggcggcgccggtgactcgggatcctcggtgctt
Ref 4681      gacagctggggtccaaccatcttcgccggcccgcgggcgagcccaagtgtggcaggcggc
H06_P2nd2891 gacagctggggtccaaccatcttcgccggcccgcgggcgagcccaagtgtggcaggcggc
Ref 4741      ggtgctgttggcggggttcagacgccccagccgtactggtactgggcactagaccgagaa
H06_P2nd2891 ggtgctgttggcggggttcagacgccccagccgtactggtactgggcactagaccgagaa
Ref 4801      agcattggcggatcggtatcggccgctttggggaaggggagctcggctggttcattgtcg
H06_P2nd2891 agcattggcggatcggtatcggccgctttggggaaggggagctcggctggttcattgtcg
Ref 4861      gtgccacccgattgggccgcccgcgctcgatgggcaaacccagcggcctggcggttgccg
H06_P2nd2891 gtgccacccgattgggccgcccgcgctcgatgggcaaacccagcggcctggcggttgccg
Ref 4921      ggcgacgatgtcaccgccctgcgcggcaccgcggaaaacgccctgcttcggggatttccg
H06_P2nd2891 ggcgacgatgtcaccgccctgcgcggcaccgcgg
B11_P2nd2891                        tgcgcggcaccgcggaaaacgccctgcttcggggatttccg
Ref 4981      atggccagcgccggccagagcaccggcggcggcttcgttcacaaatacgggttccgcttg
B11_P2nd2891 atggccagcgccggccagagcaccggcggcggcttcgttcacaaatacgggttccgcttg
Ref 5041      gcggtaatgcagcgtccgcccttcgctggatagcggctctagagagtcgtcggcatgggc
B11_P2nd2891 gcggtaatgcagcgtccgcccttcgctggatagcggctctagagagtcgtcggcatgggc
Ref 5101      cggcgccgcaccaagcagcgaccagcaaaggatcagtacgctgcggctcagaaccctccg
B11_P2nd2891 cggcgccgcaccaagcagcgaccagcaaaggatcagtacgctgcggctcagaaccctccg
Ref 5161      tacctttgcagtgcagcgccgcgcgggcgatttggccaatcgccgccgcccgttttgtgg
B11_P2nd2891 tacctttgcagtgcagcgccgcgcgggcgatttggccaatcgccgccgcccgttttgtgg
Ref 5221      acaatgtcgtcgctgtggattccgctgccgggaaaatcaccagctgggtcggtgtaaact
B11_P2nd2891 acaatgtcgtcgctgtggattccgctgccgggaaaatcaccagctgggtcggtgtaaact
Ref 5281      actcggcgcagctcgcatcggcgggctgacttcgcgtgtctgcaccgcggcccgcctttc
B11_P2nd2891 actcggcgcagctcgcatcggcgggctgacttcgcgtgtctgcaccgcggcccgcctttc
Ref 5341      cgggatccgcaacagcatgccggggcggtcccgcggcggttcccttcggggatttcctcc
B11_P2nd2891 cgggatccgcaacagcatgccggggcggtcccgcggcggttcccttcggggatttcctcc
Ref 5401      cgggtccggcatcgcggcagacgccagggcccggcttcagccgatgccgggcgaacaacc
B11_P2nd2891 cgggtccggcatcgcggcagacgccagggcccggcttcagccgatgccgggcgaacaacc
```

```
Ref 5461      gacacatgagtaaggcataggtatggccgtagtcaccatgaagcagctgcttgacagcgg
B11_P2nd2891 gacacatgagtaaggcataggta
H10_P2nd2891                                                gaagcagctgcttgacagcgg
Ref 5521      cacccacttcgggcatcagacccgtcgctggaatcccaagatgaagcgtttcatcttcac
H10_P2nd2891 cacccacttcgggcatcagacccgtcgctggaatcccaagatgaagcgtttcatcttcac
Ref 5581      cgaccgcaacggcatctacatcatcgacctgcagcagacgttgaccttcatcgataaggc
H10_P2nd2891 cgaccgcaacggcatctacatcatcgacctgcagcagacgttgaccttcatcgataaggc
Ref 5641      gtacgagttcgtgaaagagaccgtcgctcacggtgggtcggtgctcttcgtcggcacaaa
H10_P2nd2891 gtacgagttcgtgaaagagaccgtcgctcacggtgggtcggtgctcttcgtcggcacaaa
Ref 5701      gaagcaggcgcaggagtcggtggccgccgaagccacccgggtcggcatgccgtatgtgaa
H10_P2nd2891 gaagcaggcgcaggagtcggtggccgccgaagccacccgggtcggcatgccgtatgtgaa
Ref 5761      ccagcgctggctgggaggcatgctcaccaacttctccaccgtgcataagcggctgcaacg
H10_P2nd2891 ccagcgctggctgggaggcatgctcaccaacttctccaccgtgcataagcggctgcaacg
Ref 5821      cctcaaggagcttgaggcgatggagcagaccggtggcttcgagggccgcaccaagaagga
H10_P2nd2891 cctcaaggagcttgaggcgatggagcagaccggtggcttcgagggccgcaccaagaagga
Ref 5881      aatcttgggattgacccgcgagaagaacaagctcgagcgcagcctcggcggcatccgcga
H10_P2nd2891 aatcttgggattgacccgcgagaagaacaagctcgagcgcagcctcggcggcatccgcga
Ref 5941      catggccaaggtgccgtcggcgatctgggtcgtcgacacgaacaaagagcacattgccgt
H10_P2nd2891 catggccaaggtgccgtcggcgatctgggtcgtcgacacgaacaaagagcacattgccgt
Ref 6001      cggtgaggcccgcaaactgggcatcccggtcatcgcgatccttgacacgaactgcgaccc
H10_P2nd2891 cggtgaggcccgcaaactgggcatcccggtcatcgcgatccttgacacgaactgcgaccc
Ref 6061      cgacgaggtcgactacccaatcccaggcaacgacgacgcgatccgctcggccgcgctgct
H10_P2nd2891 cgacgaggtcgactacccaatcccaggcaacgacgacgcgatccgctcggccgcgc
A11_P2nd2891                                    acgacgcgatccgctcggccgcgctgct
Ref 6121      gactagggtgatcgcttccgcggtcgccgagggcctgcaggcccgtgccggactggggcg
A11_P2nd2891 gactagggtgatcgcttccgcggtcgccgagggcctgcaggcccgtgccggactggggcg
Ref 6181      cgccgacggcaagccggaggccgaagccgccgagccgctggccgaatgggagcaagagct
A11_P2nd2891 cgccgacggcaagccggaggccgaagccgccgagccgctggccgaatgggagcaagagct
Ref 6241      gctggcctcggcgacagcttcggcaacgccatcagcaaccgcgtcaacaactgccctcac
A11_P2nd2891 gctggcctcggcgacagcttcggcaacgccatcagcaaccgcgtcaacaactgccctcac
Ref 6301      cgacgccccgcaggcgcaaccgaaccaaccacagatgcatcctaggaaaggctgatatg
A11_P2nd2891 cgacgccccgcaggcgcaaccgaaccaaccacagatgcatcctaggaaaggctgatatg
Ref 6361      gcgag
A11_P2nd2891 gcgag
```

B3.3 pTT1b::Rv0950c (pT09)

```
Ref 901   cacgttcggcgtcgttgccgggtcaaccggtgtaattgccgacgctaagtccccgcttgg
A11_pT09                                cggtgt-attgccgacgct-agtccccgcttgg
Ref 961   cgagccacggcactgggtccacgcgctcggtgccgcccaggagcacctcgaagtgcaggt
A11_pT09 cgagccacggcactgggtccacgcgctcggtgccgcccaggagcacctcgaagtgcaggt
Ref 1021  gcgggccggtggaaaagccacggctgcccatggtggcgatctggtcgcctgccatcacgc
A11_pT09 gcgggccggtggaaaagccacggctgcccatggtggcgatctggtcgcctgccatcacgc
Ref 1081  gctcaccgacgctgaccaacgtggtattgacgtggccgtatagcgtgaccgtgccgtcg
A11_pT09 gctcaccgacgctgaccaacgtggtattgacgtggccgtatagcgtgaccgtgccgtcg
D11_pT09                              gtattgacgkggccgtawaagcgtgaccgtgcsktcg
Ref 1140  gcgtgcagcagcttgacccacattccgtagccggcggtggggccggcgtcgatgacg
A11_pT09 gcgtgcagcagcttgacccacattccgtagccggcggtggggccggcgtcgatgacg
D11_pT09 gckkgcagcagcyttracccammattccgtagccggcggtggggccggcktcgatgacg
B11_pT09                                      ggcggtgggg-cggcgtcgatgacg
Ref 1197  acgccgtcggacaccgcataaatcggggttccgatcgcgttagccaggtcgataccggc
A11_pT09 acgccgtcggacaccgcataaatcggggttccgatcgcgttagccaggtcgataccggc
D11_pT09 acgccgtcggacaccgcataaatcggggttccgatcgcgttagccaggtcgawaccgggc
B11_pT09 acgccgtcggacaccgcataaatcggggttccgatcgcgttagccaggtcgataccggc
Ref 1256  gtgcagtacaccccatcgataaccgaaactcgacgtgaagatgcccttcgtcggcatgac
A11_pT09 gtgcagtacaccccatcgataaccgaaactcgacgtgaagatgcccttcgtcggcatgac
D11_pT09 gtgcagtacaccccatcsataaccgaaactcgacgtgaagatgcccttcgtcggcatgac
B11_pT09 gtgcagtacaccccatcgataaccgaaactcgacgtgaagatgcccttcgtcggcatgac
Ref 1316  atacagcgggcgctgtagtcgcgcctcgcgctcggcgcgctcctcggcgaaggcaacccc
A11_pT09 atacagcgggcgctgtagtcgcgcctcgcgctcggcgcgctcctcggcgaaggcaacccc
D11_pT09 atacagcgggcgctgtagtcgcgcctcgcgctcggcgcgctcctcggcgaaggcaacccc
```

```
B11_pT09 atacagcgggcgctgtagtcgcgcctcgcgctcggcgcgctcctcggcgaaggcaacccc
Ref 1376 cctggcgaactccgcgttgtgcaccgcagcactcgccgccggctgggcggcgatgacctg
A11_pT09 cctggcgaactccgcgttgtgcaccgcagcactcgccgccggctgggcggcgatgacctg
D11_pT09 cctggcgaactccgcgttgtgcaccgcagcactcgccgccggctgggcggcgatgacctg
B11_pT09 cctggcgaactccgcgttgtgcaccgcagcactcgccgccggctgggcggcgatgacctg
Ref 1436 gacgccccgcggtgggttgcttcccgacccttcgttgagcgccgatgcatgagcggtcag
A11_pT09 gacgccccgcggtgggttgcttcccgacccttcgttgagcgccgatgcatgagcggtcag
D11_pT09 gacgccccgcggtgggttgcttcccgacccttcgttgagcgccgatgcatgagcggtcag
B11_pT09 gacgccccgcggtgggttgcttcccgacccttcgttgagcgccgatgcatgagcggtcag
Ref 1496 cacggtctcggtgcgtggggtttccgactgttggatcgccgtatgcgctgctgcggccgc
A11_pT09 cacggtctcggtgcgtggggtttccgactgttggatcgccgtatgcgctgctgcggccgc
D11_pT09 cacggtctcggtgcgtggggtttccgactgttggatcgccgtatgcgctgctgcggccgc
B11_pT09 cacggtctcggtgcgtggggtttccgactgttggatcgccgtatgcgctgctgcggccgc
Ref 1556 cgcgcccgcggccatcgccgagatcagcaggcgcccccgggccgcaccgatcggttgctt
A11_pT09 cgcgcccgcggccatcgccgagatcagcaggcgcccccgggccgcaccgatcggttgctt
D11_pT09 cgcgcccgcggccatcgccgagatcagcaggcgcccccgggccgcaccgatcggttgctt
B11_pT09 cgcgcccgcggccatcgccgagatcagcaggcgcccccgggccgcaccgatcggttgctt
Ref 1616 gcggtgctgcccgacgcgccgggacaccggggtgacctccggggtcagcacgaccgtggg
A11_pT09 gcggtgctgcccgacgcgccgggacaccggggtgacctccggggtcagcacgaccgtggg
D11_pT09 gcggtgctgcccgacgcgccgggacaccggggtgacctccggggtcagcacgaccgtggg
B11_pT09 gcggtgctgcccgacgcgccgggacaccggggtgacctccggggtcagcacgaccgtggg
Ref 1676 ggctaccagccattcgggggccagatcgtcggcgtcgtccaggtcgtcgagttctggagc
A11_pT09 ggctaccagccattcgggggccagatcgtcggcgtcgtccaggtcgtcgagttctggagc
D11_pT09 ggctaccagccattcgggggccagatcgtcggcgtcgtccaggtcgtcgagttctggagc
B11_pT09 ggctaccagccattcgggggccagatcgtcggcgtcgtccaggtcgtcgagttctggagc
C11_pT09             ttcgggggcagatcgtcggcgtcgtccaggtcgtcgagttctggagc
Ref 1736 cgctagcaactgcgcttcgtagtcgaagacgcagtcgtcccctaggtccaggtcatcgag
A11_pT09 cgctagcaactgcgcttcgtagtcgaagacgcagtcgtcccctaggtccaggtcatcgag
D11_pT09 cgctagcaactgcgcttcgtagtcgaagacgcagtcgtcccctaggtccaggtcatcgag
B11_pT09 cgctagcaactgcgcttcgtagtcgaagacgcagtcgtcccctaggtccaggtcatcgag
C11_pT09 cgctagcaactgcgcttcgtagtcgaagacgcagtcgtcccctaggtccaggtcatcgag
Ref 1796 ctctgcgaaatccagctcatcgtagagtgctaagccgtcgaggaatccgtccagcgggat
A11_pT09 ctctgcgaaatccagctcatcgtagagtgctaagccgtcgaggaatccgtccagcgggat
D11_pT09 ctctgcgaaatccagctcatcgtagarwrmtaagccgtcgaggaatccgtccagcgggat
B11_pT09 ctctgcgaaatccagctcatcgtagagtgctaagccgtcgaggaatccgtccagcgggat
C11_pT09 ctctgcgaaatccagctcatcgtagagtgctaagccgtcgaggaatccgtccagcgggat
Ref 1856 gatttcggtgacttcgttacggtgatgatgcggccaacgatcgcgaggtgtgcgaatcgc
A11_pT09 gatttcggtgacttcgttac-gtgatgatgcggccaacgatcgcgaggtgtgcgaatcgc
D11_pT09 gatttcggtgacttcgttacggtgatgatgcggccaacgatcgcgaggtgtgcgaatcgc
B11_pT09 gatttcggtgacttcgttacggtgatgatgcggccaacgatcgcgaggtgtgcgaatcgc
C11_pT09 gatttcggtgacttcgttacggtgatgatgcggccaacgatcgcgaggtgtgcgaatcgc
Ref 1916 tgccatggcagcagaacgggcgatacggtgctgggacaaatctgaaatgtcctcggatcg
A11_pT09 tgccatggcagcagaacgggcgatac-gtgctgggacaaatctgaaatgtcctcggatcg
D11_pT09 tgccatggcagcagaacgggcgatacggtgctgggacaaatctgaaatgtcctcggatcg
B11_pT09 tgccatggcagcagaacgggcgatacggtgctgggacaaatctgaaatgtcctcggatcg
C11_pT09 tgccatggcagcagaacgggcgatacggtgctgggacaaatctgaaatgtcctcggatcg
Ref 1976 tgaccataacgttatctggaccctgagacgttatccgcaaccggatggtagtggcaactt
A11_pT09 tga-cat-acgttatctggaccctgagacg-tat-cgcaa-cggatggtag-kgc-acct
D11_pT09 tgaccataacgttatctggaccctgagacgttatccgcaaccggatggtagtggcaactt
B11_pT09 tgaccataacgttatctggaccctgagacgttatccgcaaccggatggtagtggcaactt
C11_pT09 tgaccataacgttatctggaccctgagacgttatccgcaaccggatggtagtggcaactt
Ref 2036 cagcgcggaattcggctgtgattgtgagttgg-atcacgtttcggctggacaaacatatc
A11_pT09 cagcgcgta--tc-gctgtga-tgt-arttggaatcacgttccgyctgg-caaacat-tc
D11_pT09 cagcgcggaattcggctgtgattgtgagttgg-atcacgtttcggctggacaaacatatc
B11_pT09 cagcgcggaattcggctgtgattgtgagttgg-atcacgtttcggctggacaaacatatc
C11_pT09 cagcgcggaattcggctgtgattgtgagttgg-atcacgtttcggctggacaaacatatc
Ref 2095 ggtgagctgtgccacaccgggtggatgcggccgcggagttaatcggcggtctcgatacag
A11_pT09 -gcgryctgtg-c-maccgggtgtatgcggccgc
D11_pT09 ggtgagctgtgccacaccgggtggatgcggccgcggagttaatcggcggtctcgatacag
B11_pT09 ggtgagctgtgccacaccgggtggatgcggccgcggagttaatcggcggtctcgatacag
C11_pT09 ggtgagctgtgccacaccgggtggatgcggccgcggagttaatcggcggtctcgatacag
```

```
Ref 2155 ttctccgtgcgagtcgccgatttcggcaccgcctacctattggtcgagcagtaagccgag
D11_pT09 ttctccgtgcgagtcgccgatttcggcaccgcctacctattggtcgagcagtaagccgag
B11_pT09 ttctccgtgcgagtcgccga-ttcgc--mcgcctacctatt-gtcgagcagt-agccgag
C11_pT09 ttctccgtgcgagtcgccgatttcggcaccgcctacctattggtcgagcagtaagccgag
Ref 2215 cgaagactctagagtcgagatttacagtcggtcgcctacgcaaacgtcgatgggagcagt
D11_pT09 cgaagactctagagtcgagat
B11_pT09 cgaagactctagagtcgagatttacagtc-gtcgcttacgc-aacgtcgatgggagcag-
C11_pT09 cgaagactctagagtcgagatttacagtcggtcgcctacgcaaacgtcgatgggagcagt
```

B4 qPCR products amplified from ΔRv0950c cDNA produce a C_q value but are non-specific for Rv0950c expression.

Signal was obtained in two of three replicates of the deletion strain, but the curves were atypical compared to signal from genomic standards, the WT and complement strain. One replicate of ΔRv0950c did not produce any signal (flat red line) along with the No Template Control (flat purple line) or 10^1 genomic equivalents (flat green line) (Fig. B4). However, inspection of the melting temperature revealed a completely different amplification product to that expressed in *M. tuberculosis* WT ΔRv0950c::Rv0950c (Fig. B4d,e). The observed product is likely a result of mis-priming, whereby the lack of Rv0950c-specific cDNA in the deletion strains leads to primer binding at other sites.

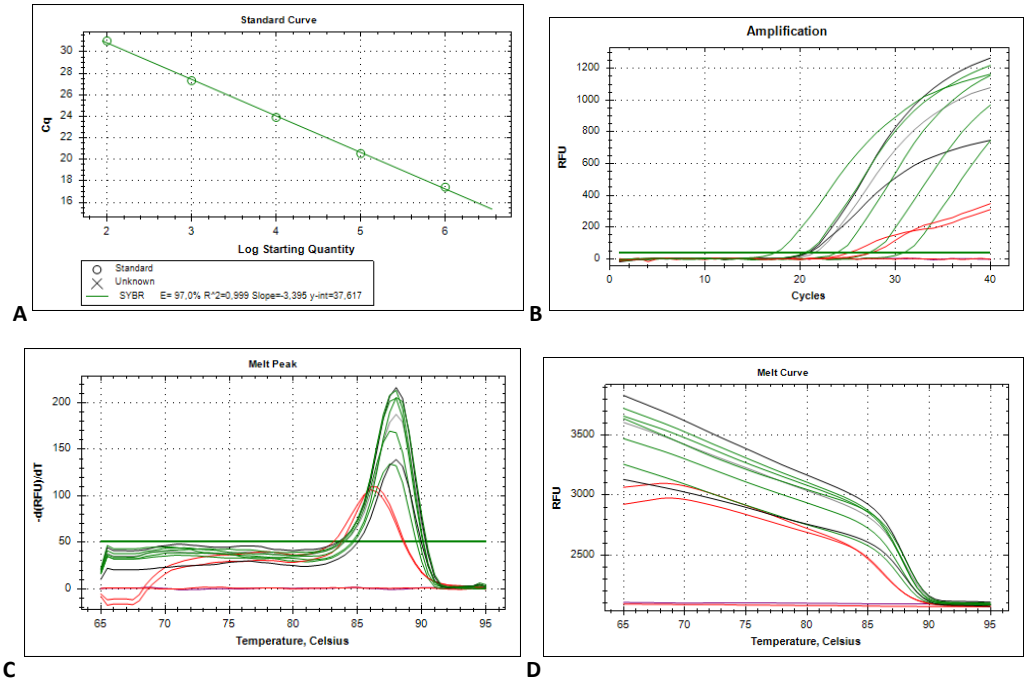

E

Target	Content	Sample	Melt Temp
0950	Std		88,00
0950	Std		88,00
0950	Unkn	WT	88,00
0950	Std		88,00
0950	Unkn	WT	88,00
0950	Std		87,50
0950	Unkn	d09	86,50
0950	Std		87,50
0950	Unkn	d09	None
0950	Unkn	d09	86,00
0950	Unkn	comp09	88,00
0950	NTC		None

Std. curve
WT
ΔRv0950c
ΔRv0950c::Rv0950c
NTC

Figure B4 qPCR to confirm deletion of Rv0950c in the *M. tuberculosis* ΔRv0950c strain.
A) Standard curve of Rv0950c amplified from gDNA at genomic equivalents from 10^1-10^6. B) Amplification curves for Rv0950c. C, D, E) Melting temperature of products amplified with Rv0950c targeted primers. Products amplified from the ΔRv0950c strain did not match WT and complement.

B5 Determining putative *in vitro* hydrolytic activity of Rv0950c

B5.1 Expression of recombinant Rv0950c

Earlier, the predicted secondary structure of Rv0950c displayed a putatively active, zinc-coordinating catalytic site (section 3.1), much like the active M23 endopeptidases reported in the literature to remodel the PG stem peptide. To test the activity, attempts were made to purify recombinant Rv0950c. A c-terminal His-tagged, Rv0950c construct was designed for the pET29a backbone using an N-terminal *Nde*I site, which incorporates the Rv0950c ATG-start codon, and replacing the stop codon with an *Xho*I site flanking the pET29a His-tag. The Rv0950c expression cassette was PCR amplified from a pBlueScript clone and cloned into pET29a (Fig. B5.1.1). Induction at 18°C or 30°C at various time-points did not result in overexpression of a 36.5 KDa protein (Fig. B5.1.2). Induction at 37°C also did not result in Rv0950c expression.

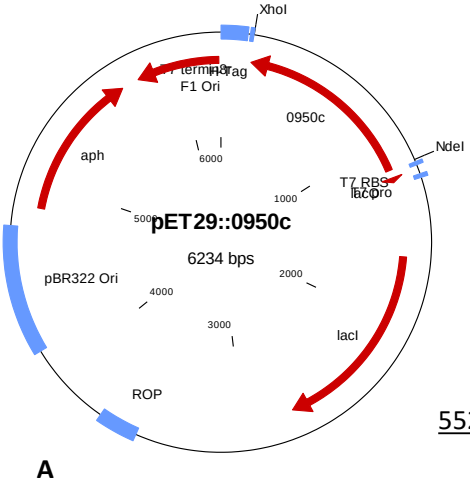

B

Restriction enzyme	Expected fragments (bp)
*Nco*I	6234
*Nhe*I	6234
*Pvu*I	4157, 1412, 375, 290
*Nar*I	4434, 1182, 487, 114, 21
*Sma*I	4434, 1900

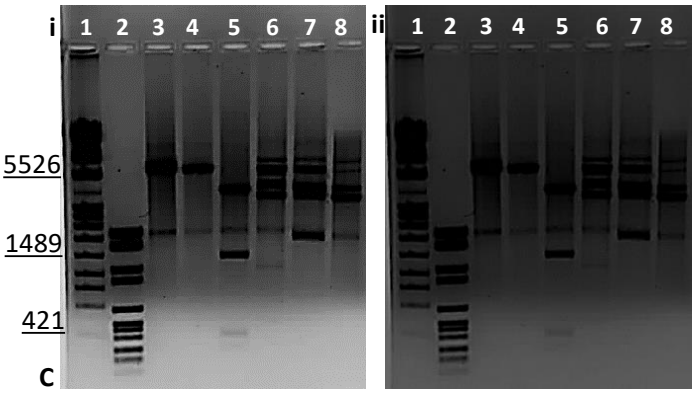

Figure B5.1.1 Vector map of pET29a::Rv0950c for C-terminal His-tagged expression
A) pET29a Rv0950c vector map. B) Expected restriction fragments. C) Fragments obtained by restriction digestion with 3) *Nco*I, 4) *Nhe*I, 5) *Pvu*I, 6) *Nar*I and 7) *Sma*I. 1) MWM IV, 2) MWM VI. 8) undigested. MWM: Lambda phage DNA molecular weight marker (underlined). i,ii: Duplicate gels at different exposures.

To try improving Rv0950c expression in *E. coli*, the Rv0950c ORF was codon-harmonised for *E. coli* using the JCat online tool (Grote et al., 2005), synthesised and cloned by GenScript into the pET24a expression vector. Codon harmonisation converts the nucleotide sequence of a gene to match the abundance of specific codons to that available

to the host expression organism. The sequence of the pET24aRv0950c vector was validated by restriction digestion (Fig. B5.1.3) and transformed into *E. coli* DH5α for propagation followed by transformation into *E. coli* BL21* expression strain. Cultures (5 ml) were sampled at various time-points following addition of 1 mM IPTG at 30°C. Whole lysate was extracted using Bacterial Protein Extraction Reagent (B-PER), lysed in a ribolyser and analysed on a PAGE gel. A small band approximating the expected size of 36.45 KDa appeared in the 2 hr-induction sample that was not present in the uninduced control (Fig. B5.1.4). However, background proteins were not repressed (Fig. B5.1.4).

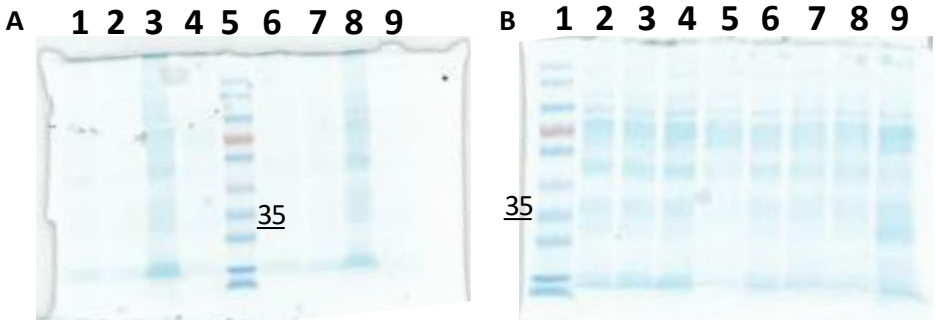

Figure B5.1.2 PAGE for crude detection of Rv0950c expression in *E. coli* whole cell lysate
A) soluble fraction. 1-4) 18°C, 6-9) 30°C, 1,6) uninduced, 2,7) 1 hr, 3,8) 2 hr, 4,9) overnight, 5) PAGE Ruler. B) insoluble fraction 1) PAGE Ruler 2-5) 18°C, 6-9) 30°C, 2,6) uninduced, 3,7) 1 hr, 4,8) 3 hr, 5,9) overnight. 35: 35 KDa band of the PAGE Ruler.

Different concentrations of IPTG were tested for induction (Fig. B5.1.5). 0.8 mM and 1 mM IPTG produced prominent bands near the expected size of 36kDa (Fig. B5.1.5) however the PAGE procedure was problematic with samples overflowing between wells. Nonetheless, 30°C 2-hour induction was attempted again (Fig. B5.1.6), and gel-loading was normalised according to protein concentrations determined by Bradford Assay (Table B5.1.1,2). Although a faint band could be seen (Fig. B5.1.6, red arrow), parallel Western blot with an anti-Histidine antibody, at different concentrations did not produce any signal (Fig. B5.1.7). To assist in troubleshooting, PAGE was repeated for *E. coli* pET24a-Rv0950c protein extracts alongside a successful *M. tuberculosis* RipA expression system (Campbell *et al.,* 2020, unpublished) (Fig. B5.1.8). The expected RipA bands were observed, but not for Rv0950c (Fig. B5.1.8), suggesting that the general process of IPTG induction, whole cell protein extraction and PAGE protein electrophoresis were successful but this was to be further optimised for specific expression and detection of Rv0950c beyond the time constraints of this study.

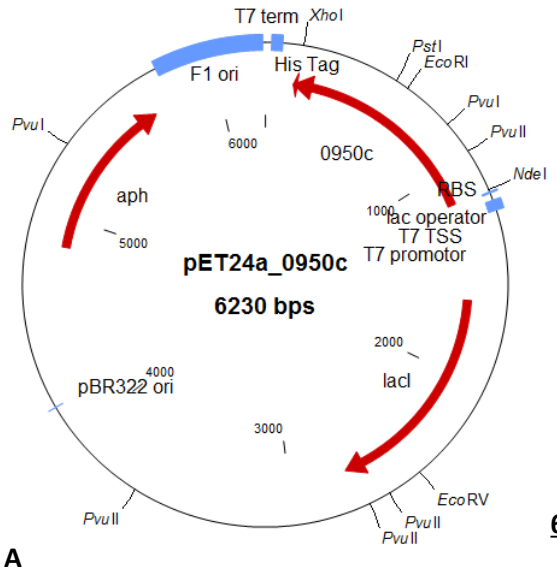

B

Enzyme	Expected fragments (bp)
*EcoR*I	6230
*EcoR*V	6230
*Pst*I	6230
*Pvu*I	4443, 1787
*Pvu*II	3536, 1602, 999, 93
*Nde*I+*Xho*I	5230, 1000

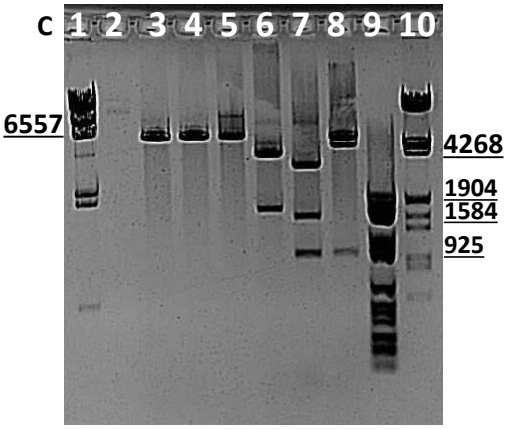

Figure B5.1.3 Restriction profiling of pET24a::Rv0950c expression vector.
A) Expression vector map. B) Expected restriction fragments. C) 1) MWM II; 2) undigested vector; 3) *EcoR*I; 4) *EcoR*V 5) *Pst*I; 6) *Pvu*I; 7) *Pvu*II; 8) *Nde*I and *Xho*I double digestion; 9) MWM VI; 10) MWM III. MWM: digested Lambda phage DNA marker (underlined).

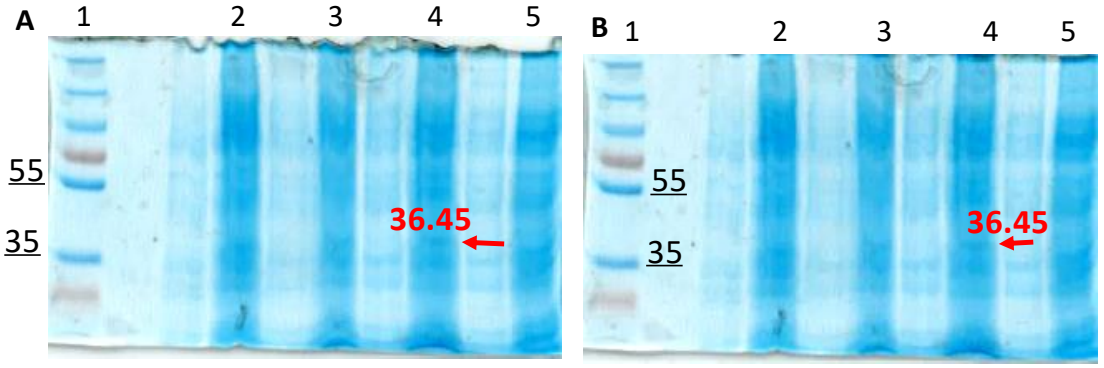

Figure B5.1.4 PAGE electrophoretogram for optimising Rv0950c expression and purification from *E. coli*.
A and B) PAGE gel at different scanner exposures. 1) MWM, 2) Overnight, 3) 3 hours, 4) 2 hours, 5) uninduced. Arrow indicates expected band for Rv0950cMWM: PAGE Ruler Plus (underlined, KDa).

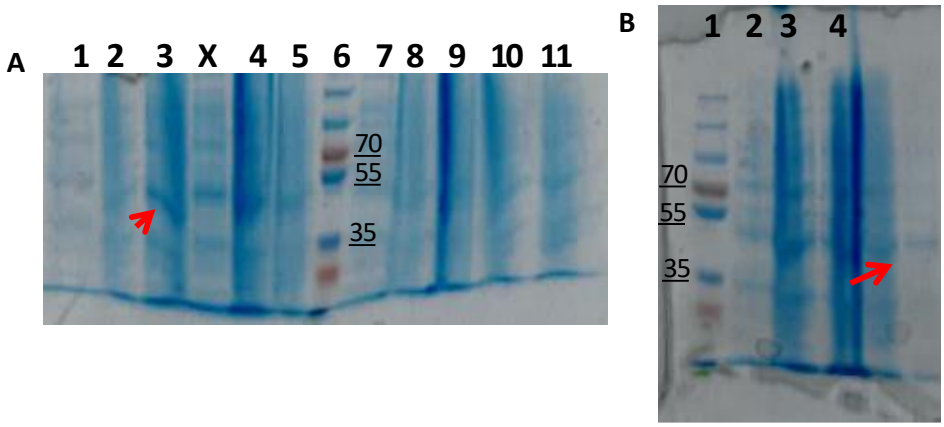

Figure B5.1.5 Induction optimisation of Rv0950c-His expression in *E. coli*.
A) Induction at 30°C with 1 mM IPTG (1-5) and 1.2 mM IPTG, 6) MWM, (7-11): 1,7) uninduced; 2,8) 1 hr; 3,9) 2 hr; 4,10) 3 hr, 5,11) overnight; B) induction at 30°C with 0.8 mM IPTG: 1) MWM, 2) uninduced, 3) 2 hr, 4) 3 hr, 5) overnight. MWM: PAGE Ruler plus (KDa, underlined); X: excluded due to overflow. Arrows indicate putative Rv0950c-His. Whole cell extract prepared by resuspending cell pellet in 5X loading dye and incubating at 70°C for 20 min. 10 µl supernatant loaded after centrifugation of the lysate for 20 min.

Table B5.1.1 Protein extracted from frozen culture and quantified by Bradford assay against BSA

Fraction	Uninduced (µg/ml)	Induced (µg/ml)
Soluble	695.7	1111
Soluble x 10^{-1}	69.15	285.7
Insoluble	225.2	349
Insoluble x 10^{-1}	54.6	156.8

Table B5.1.2 Protein (µg/ml) extracted from fresh culture and quantified by Bradford assay against BSA

Fraction	Uninduced (µg/ml)	Induced (µg/ml)
Soluble	1488	1076
Soluble x 10^{-1}	589.4	879.9
Insoluble	647	633
Insoluble x 10^{-1}	-57.20	216.5

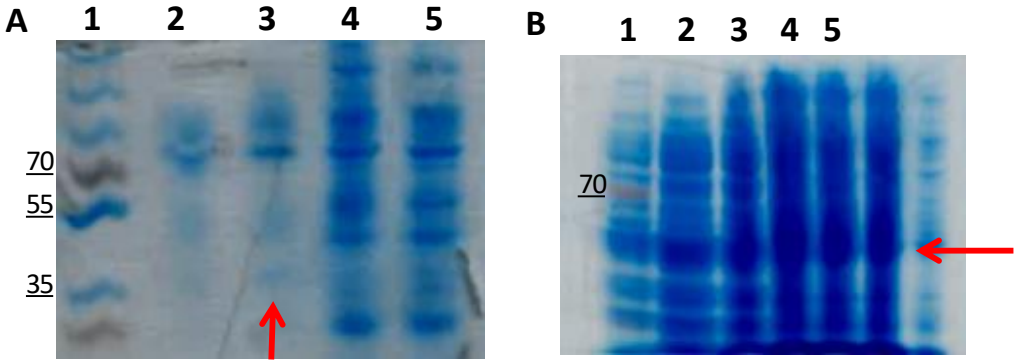

Figure B5.1.6 PAGE following induction of Rv0950c with 0.8 mM IPTG for 2 hours at 30°C.
M: Pre-stained PAGE-ruler Plus (5 µl), 1) MWM, 2) uninduced, soluble; 3) induced, soluble; 4) induced, insoluble; 5) uninduced, insoluble. Arrows indicate putative bands pertaining to Rv0950c-His. A) Protein extracted from frozen culture, ~200 µg protein/well; B) Protein extracted from fresh culture, ~60 µg protein/well. Loaded 20 µl 1:1 protein sample: 5x loading dye. Protein was extracted by centrifuging 20 ml of cells in bacterial protein extraction reagent (BPER) spiked with protease inhibitor cocktail, incubated at ambient temperature for 10 min. Soluble and insoluble fractions were separated by centrifugation for 20 min. and quantified by Bradford assay prior to loading. MWM: PAGE Ruler Plus (KDa, underlined).

Figure B5.1.7 Lack of induction of Rv0950c.
Western blotting with various concentration of anti-His Ab following attempted induction of Rv0950c at 30°C.

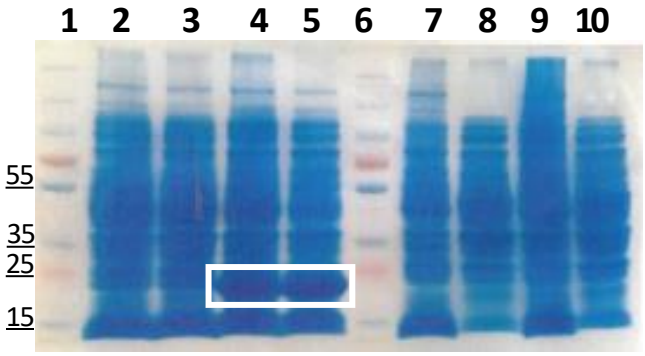

Figure B5.1.8 Control *M. tuberculosis* RipA expression
Protein extracts of *E. coli* expressing *M. tuberculosis* RipA (2-5) were loaded alongside the pET24aRv0950c expression system (7-10). 1,6) MWM, 2,7) uninduced, insoluble, 3,8) uninduced, soluble, 4,9) induced, insoluble, 5,10) induced, soluble. White rectangle: expected bands for RipA overexpression. MWM: PAGE Ruler Plus (KDa, underlined).

B5.2 Heterologous complementation of *E. coli* Δ*envC*,Δ*nlpD* with *M. tuberculosis* Rv0950c

The capacity of Rv0950c to degrade septal PG of the *E. coli* M23-endopeptidase mutant, Δ*envC*,Δ*nlpD* which forms chains of cells, in which septum-degrading amidases cannot be activated, was studied (Uehara *et al.*, 2009, 2010). Rv0950c episomal expression was performed by cloning the Rv0950c ORF into replicating vector, pse100 under the control of a tetracycline-repressible promoter (Fig. B5.2.1). The *E. coli* double-mutant was transformed with pse100 expressing full-length Rv0950c or empty pse100 backbone, selected by hygromycin resistance and screened again by restriction digestion analysis to ensure vector integrity (Fig.B5.2.2).

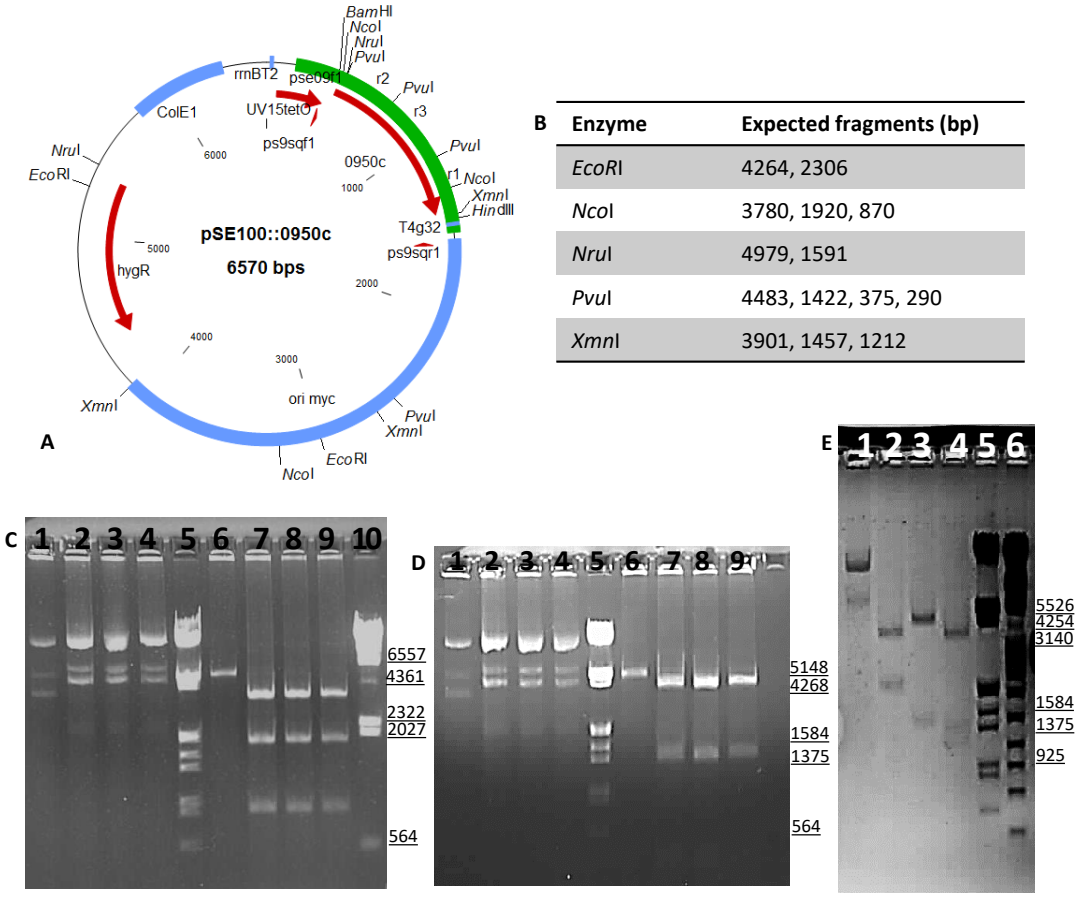

Enzyme	Expected fragments (bp)
*Eco*RI	4264, 2306
*Nco*I	3780, 1920, 870
*Nru*I	4979, 1591
*Pvu*I	4483, 1422, 375, 290
*Xmn*I	3901, 1457, 1212

Figure B5.2.1 Construct for overexpression of Rv0950c in *M. smegmatis*.
A) Vector map showing sequenced region in green. B) Expected restriction digestion fragments. C) Putative clones were identified by *Nco*I digestion: 1) undigested empty vector; 2-4) undigested clones; 5) MWM III; 6) digested empty vector; 7-9) digested clones all displaying the expected fragments; 10) MWM II. D) Putative clones were identified by *Pvu*I digestion: 1) undigested empty vector; 2-4) undigested clones; 5) MWM III; 6) digested empty vector; 7-9) digested clones all displaying the expected fragments. E) Further restriction profiling with *Eco*RI (2); *Nru*I (3) and *Xmn*I (4); 1) undigested; 5) MWM III; 6) MWM IV. MWM: digested Lambda phage DNA marker (underlined).

Strain	*Nco*I fragments (bp)
E. coli Δ*envC*,Δ*nlpD*::pSE100	5538
E. coli Δ*envC*,Δ*nlpD*::pSE100-Rv0950c	3780, 1920, 870

A

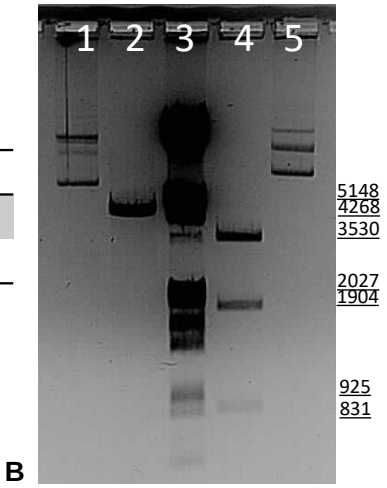

Figure B5.2.2 Confirmation of complementation of *E. coli* Δ*envC*,Δ*nlpD* with pse100 and pse100-Rv0950c by *Nco*I restriction mapping.
A) Expected restriction fragments. B) 1) Uncut *E. coli* Δ*envC*,Δ*nlpD*::pse100; 2) *Nco*I-digested *E. coli* Δ*envC*,Δ*nlpD*::pse100; 3) MWM III; 4) *E. coli* Δ*envC*,Δ*nlpD*::pse100-Rv0950c; 5) Uncut *E. coli* Δ*envC*,Δ*nlpD*::pse100-Rv0950c. MWM: Lambda phage DNA marker (underlined).

Transformants were grown to mid-log phase alongside the double-mutant parent strain and labelled briefly with FM-464 membrane stain. *E. coli* Δ*envC,*Δ*nlpD* formed previously reported chains of cells (Fig. B5.2.3). Expression of *M. tuberculosis* Rv0950c did not resolve chains but large bulging was observed at the end of a few chains (Fig. B5.2.3). This may however be a polar effect of pse100, since small bulges were also observed in the empty vector strain (Fig. B5.2.3). Expression of Rv0950c in *E. coli* did not confirm or contradict the putative hydrolytic activity of Rv0950c. Confirming the expression of Rv0950c in the pSE100 system may assist in troubleshooting the lack of observations here.

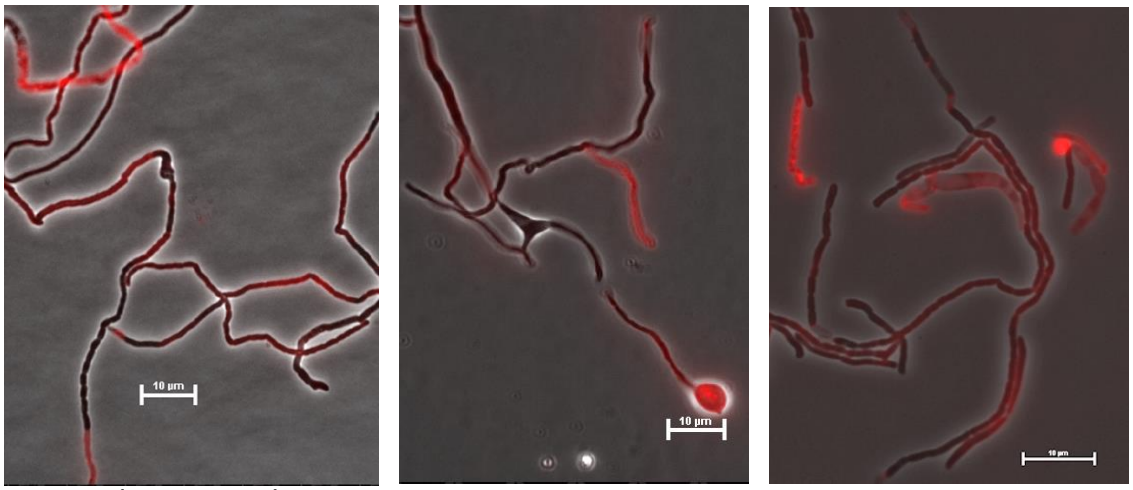

Figure B5.2.3 *E. coli* Δ*envC,*Δ*nlpD* complementation with *M. tuberculosis* Rv0950c. Fluorescence micrographs showing *E. coli* chains defecttive for cell seperation due to loss of amidase activators, *envC* and *nlpD* stained with FM-464. Scale bar = 10 µm.

B5.3 Heterologous expression of *M. tuberculosis* Rv0950c in *M. smegmatis* reveals a role in stress tolerance

Putative PG hydrolase activity was investigated in two heterologous systems: *E. coli* Δ*envC,*Δ*nlpD* and WT *M. smegmatis*. In *M. smegmatis*, full length, N' terminal (M23-domain truncation) and C' terminal (M23 domain alone) derivatives of Rv0950c were expressed from the mycobacterial integrating vector backbone, pUAB400. The pUAB400 vector backbone was developed for MPFC assays and therefore was designed for overexpression via an *hsp*60 promoter (Singh *et al*., 2006). The pUAB400 transformants are grown on agar in the presence of glucose alone, and not conventional glucose-salt supplementation (Singh *et al*, 2006) to prevent toxicity of proteins expressed heterologously. It was hypothesised that the putative hydrolytic M23 domain of Rv0950c may confer toxicity to *M. smegmatis* due to unregulated hydrolytic activity. Full length Rv0950c as well as N' and C' terminus truncations were cloned into the pUAB400 and electroporated into *M. smegmatis*. The pUAB400 constructs were confirmed by restriction

endonuclease mapping (Fig. B5.3.1) and sequencing (data not shown) and electroporated into *M. smegmatis*, selected for by kanamycin resistance on 7H11 supplemented with glucose-salt. Km^R colonies were genotyped by PCR to confirm integration of pUAB400 (Fig. B5.3.2).

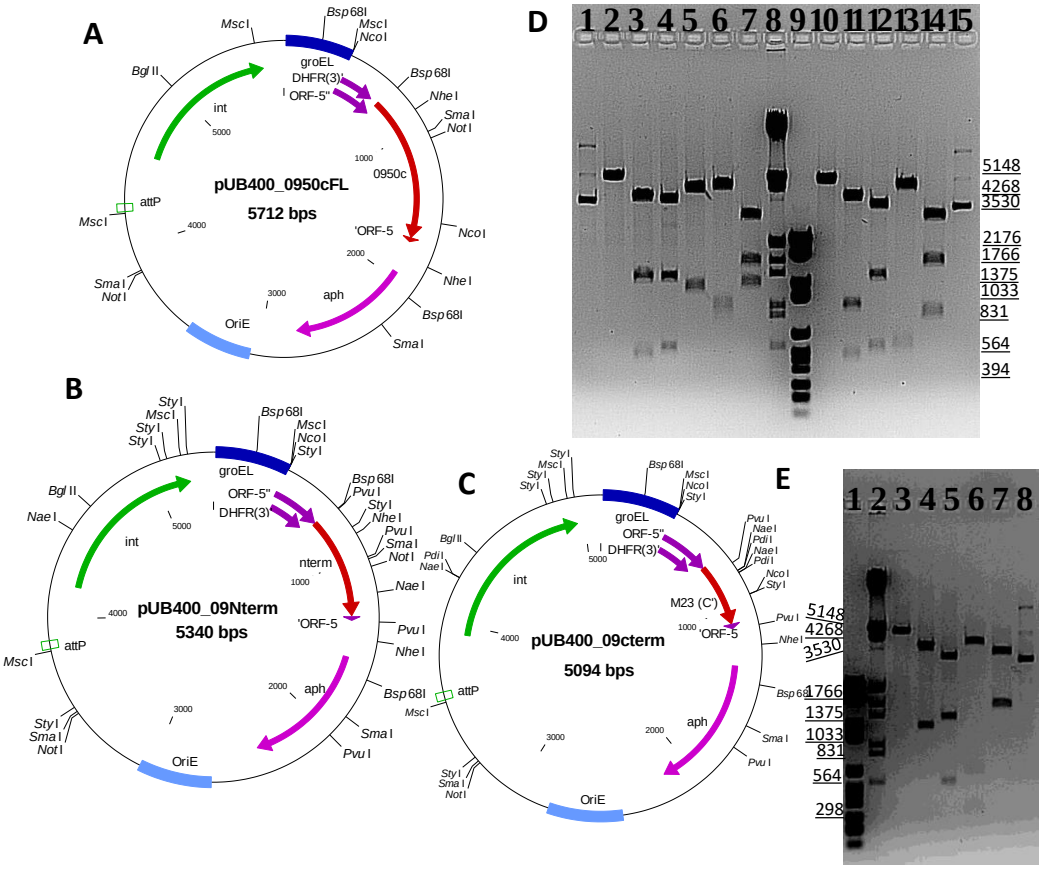

F

	Expected fragments (bp)		
Enz.	Full length	N' term	C' term
*Bgl*II	5712	5340	5094
*Bsp*68I	3889, 1316, 507	3889, 944, 507	3889, 1205
*Msc*I	3806, 1342, 564	3434, 1342, 564	3188, 1342, 564
*Nco*I	4539, 1173		
*Nhe*I	4761, 951	4761, 579	
*Pvu*I			4104, 649, 341
*Sma*I	2879, 1605, 1228	2879, 1605, 856	3489, 1605

Figure B5.3.1 Restriction digestion mapping of pUB400::Rv0950c constructs heterologous overexpression.
Vector maps of A) pUB400::Rv0950c full length (red, FL), B) pUB400::Rv0950c N' truncation (N' red), and C) pUB400::Rv0950c C' truncation (M23, red). Respective Rv0950c cassettes were fused to the C'terminus of the DHFR 3' domain (purple). D) 'FL map: 1) uncut, 2) *Bgl*II, 3) *Bsp*68I, 4) *Msc*I, 5) *Nco*I, 6) *Nhe*I, 7) *Sma*I. 8) MWM III, 9) MWM VI; N' mapping: 9) *Bgl*II, 10) *Bsp*68I, 11) *Msc*I, 12) *Nhe*I, 13) *Sma*I 14) uncut. E) C' map:1) MVI, 2) MWM III, 3) *Bgl*II, 4) *Bsp*68I, 5) *Msc*I, 6) *Pvu*I, 7) *Sma*I F) Acquired restriction fragments for respective constructs matched all the expected fragments. MWM: digested Lambda phage DNA marker (underlined).

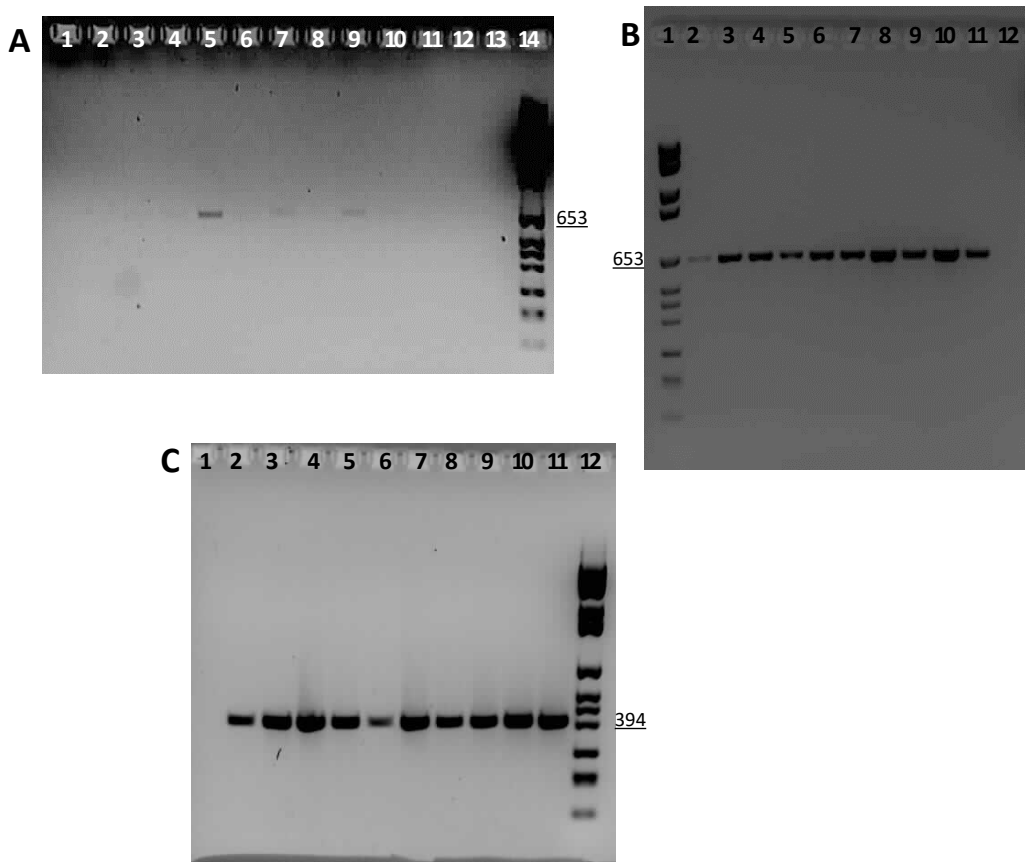

Figure B5.3.2 Genotyping *M. smegmatis* pUAB400 strains by PCR.
A) Full length Rv0950c screened with primers for cloning the N'terminus 1) no template control; 2-13) putative strains; 14) MWM VI. B) N' terminal Rv0950c screened with primers for cloning the N'terminus 1) MWM VI; 2-11) putative strains; 12) no template control. C) C'terminal Rv0950c screened with primers for cloning the C'terminus 1) no template control; 2-11) putative strains; 12) MWM VI. MWM: digested Lambda phage DNA marker (underlined).

Comparing CFUs of *M. smegmatis* pUB400 transformants in the presence of glucose and glucose-salt supplemented 7H11, pUB400-transformed carrying full-length Rv0950c (F) or the only the M23 domain (C) grew poorly on excess salt compared to 7H11 supplemented with glucose alone, whereas the derivative lacking the M23 domain (N) was unaffected (Fig. B5.3.3). Although the pUAB400-empty vector strain also grew poorly in excess salt, the phenotype was not reversed with glucose alone (Fig. B5.3.3). Although, a pSE100-Rv0950c strain grew better than the pUAB400 strains, growth was still lower on excess salt (Fig. B5.3.3) suggesting Rv0950c may confer subtle toxicity although this should be confirmed with more replicates and correlated with expression of Rv0950c in each of the strains.

As Rv0950c exhibited transient toxicity in *M. smegmatis* under salt-stress and cell wall stress required for electrocompetency, the role of Rv0950c was studied in *M. tuberculosis* osmolarity sensing in the deletion mutant. A study which identified a serine-threonine protein kinase involved in regulating the cell wall response to osmolarity changes also observed upregulation of Rv0950c upon NaCl treatment (140 mM) of cultures grown in Sauton's minimal media (Hatzios et al., 2013). Therefore, expression of Rv0950c was also measured in 7H9 cultures, untreated or treated with 280 mM NaCl (Fig. B5.3.4).

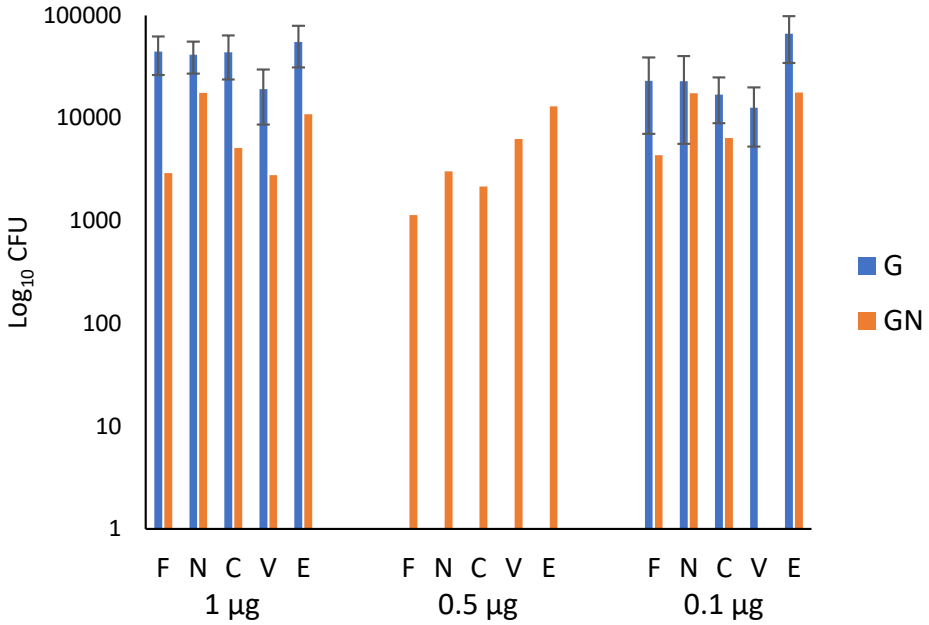

Figure B5.3.3 Domain-dependent osmo-toxicity of Rv0950c expressed in *M. smegmatis*.
M. smegmatis CFUs comparing the Rv0950c-expressing derivatives plated on 7H11 supplemented with glucose (G, n = 3) or glucose+salt.(GN, n = 1). F, N, and C: *M. smegmatis* transformed with pUAB400 carrying either full length, the N' terminus without the M23 domain or the C' terminal M23 domain of Rv0950c respectively. V: *M. smegmatis* transformed with empty pUB400; E: *M. smegmatis* transformed with pSE100-Rv0950c. Amounts of vector used for transformation indicated below graph. For 0.5 µg, only the glucose+salt experiment was performed. G: average of 3 experiments each averaged over 3 dilutions. GN: one experiment averaged over 3 dilutions.

A non-significant increase in Rv0950c expression was observed under osmolarity stress (Fig. B5.3.4). To further study if the published observation of Rv0950c upregulation was perhaps due to nutrient limitation stress after growth in Sauton's media, untreated Sauton's and 7H9 expression levels were compared (Fig. B5.3.4). Rv0950c was expressed significantly more (p=0.027) in exponentially growing Sauton's culture compared to the equivalent growth period in 7H9 (Fig. B5.3.4), suggesting that Rv0950c is required for cell wall modelling under nutrient limiting conditions. This supports the hypothesis that Rv0950c is involved in PG maturation via 3-3 cross-link formation as an increased abundance of 3-3 cross-links has been previously reported for stationary phase *M.*

tuberculosis cells (Lavollay et al., 2008). Further experiments should be performed on the ΔRv0950c mutant strain under nutrient starvation conditions, for which a growth defect is expected or the upregulation of compensatory genes.

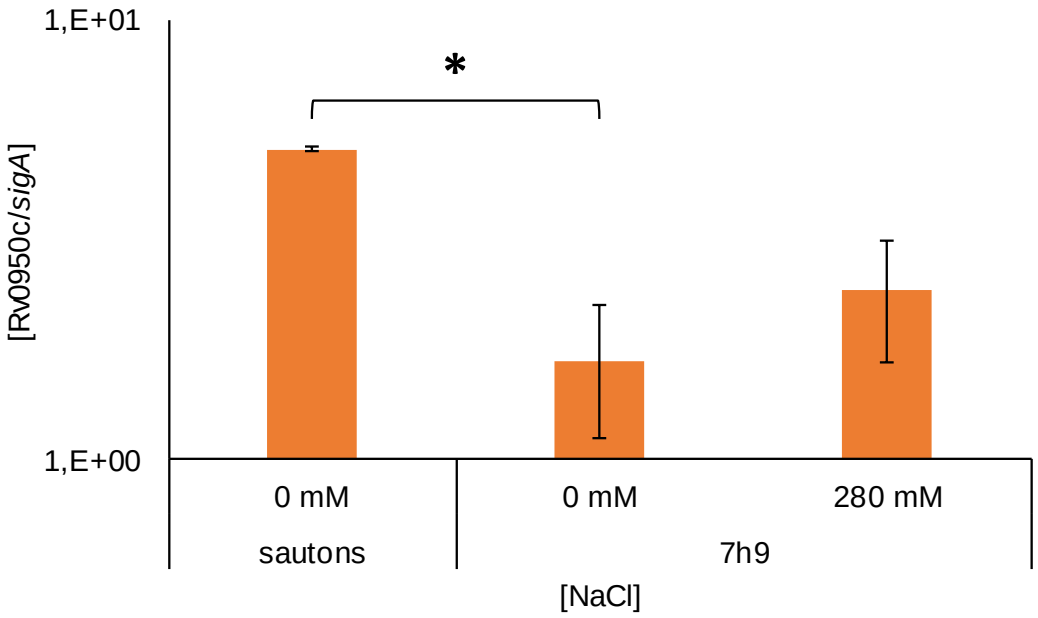

Figure B5.3.4 Expression levels of Rv0950c determined by RT qPCR compared in cultures of *M. tuberculosis* grown in Sauton's, 7H9 media, or 7H9 treated for 60 min with 280 mM NaCl.
RNA was extracted from triplicate (untreated) or duplicate (treated) cultures. *p = 0.027 for student's t-test comparing untreated Sauton's and 7H9.

Appendix C: Attempts to generate *M. tuberculosis* ΔRv2891, ΔRv0950c.

Biochemical characterisation of Rv2891 and Rv0950c suggest that both these M23-endopeptidases have overlapping, non-redundant functions in cell wall remodelling (Chapter three) but are individually dispensable for cell growth. To test whether simultaneous loss of both endopeptidases inhibits growth of *M. tuberculosis* towards predicting the possibility of dual-target of these similar enzymes by a single drug, the ΔRv2891 deletion construct was electroporated into the *M. tuberculosis* ΔRv0950c background. The ΔRv0950c background was chosen as single mutant DCOs were achieved at a very low frequency for this strain, particularly 1:10 sucrose resistant colonies. It was assumed, therefore that Rv2891 deletion would be more successful. A single SCO was obtained for ΔRv0950c,ΔRv2891 (Fig. C1c), but all subsequent DCOs reverted to single ΔRv0950c background strain (Fig. C1d).

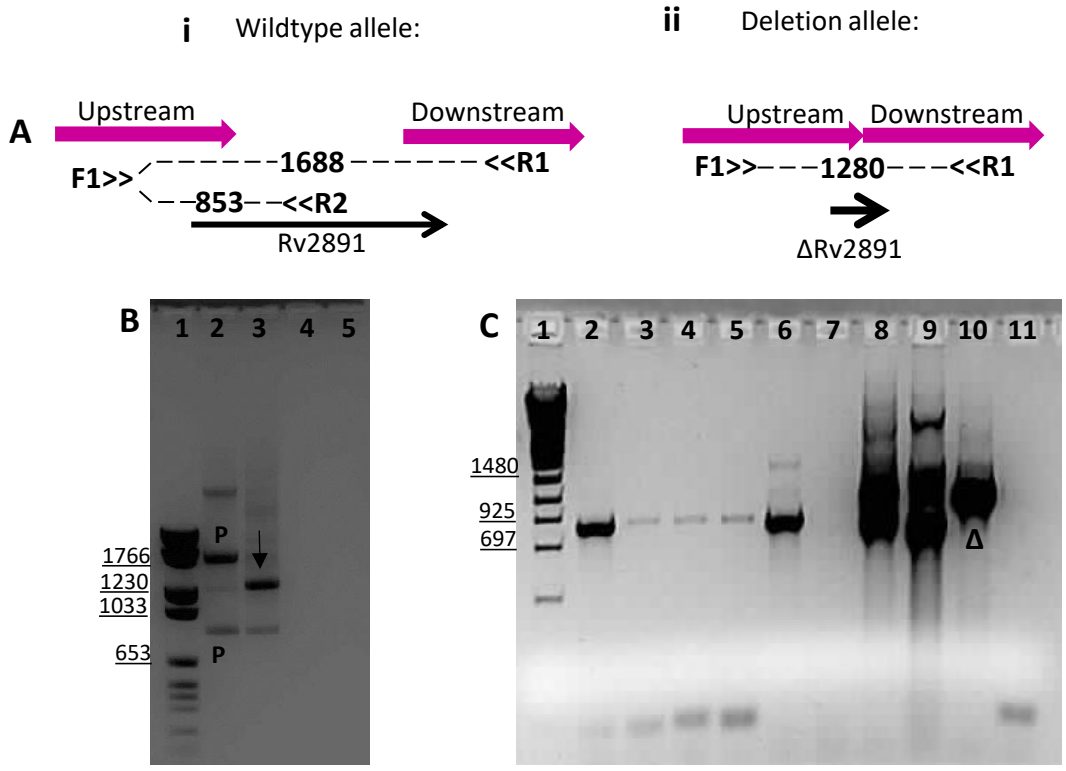

Figure C1 Genotyping of *M. tuberculosis* ΔRv2891,ΔRv0950c.
A) Expected amplicon sizes for WT (i) and mutant Rv2891 (ii) alleles. B) 1) MWM VI; 2) ΔRv0950c parent strain (P, 1688 and 853 bp); 3) single blue colony confirmed to be a SCO (down arrow, additional 1280 bp); 4) ΔRv2891 control? 5) NTC. C) Initial screening of sucrose colonies for DCO are all wild-type Rv2891. 1) MWM IV; 2-7) sucrose colonies; 8) ΔΔ SCO control (see B); 9) ΔRv0950c parent strain; 10) ΔRv2891 control (Δ); 11) NTC.

Appendix D: Human ethics waiver (W-CJ-160208-3)

Human Research Ethics Committee (Medical)

Research Office Secretariat: Senate House Room SH10005, 10th floor. Tel +27 (0)11-717-1252
Medical School Secretariat: Tobias Health Sciences Building, 2nd floor Tel +27 (0)11-717-2700
Private Bag 3, Wits 2050, www.wits.ac.za. Fax +27 (0)11-717-1265

Ref: W-CJ-160208-3 08/02/2016

TO WHOM IT MAY CONCERN:

Waiver: This certifies that the following research does not require clearance from the Human Research Ethics Committee (Medical).

Investigator: **Ms A O Papadopoulos (Student no 0713551A).**

Project title: **Characterisation of M 23-domain activators of peptidoglycan degrading amidases in *Mycobacteria tuberculosis*.**

Reason: This is a laboratory study using bacterial cultures of *Mycobacterium tuberculosis*. The study will be done in biosafety level III laboratories, clearance from the Wits Biosafety Committee has been granted. There are no human participants.

Professor Peter Cleaton-Jones

Chair: Human Research Ethics Committee (Medical)

UNIVERSITY OF THE WITWATERSRAND
OFFICE OF THE DEPUTY VICE CHANCELLOR RESEARCH
08 FEB 2016
RESEARCH OFFICE HREC (Medical)
JOHANNESBURG

Copy – HREC (Medical) Secretariat: Zanele Ndlovu, Rhulani Mkansi.